Dynamic Modelling and Simulation of Biocatalytic Reactions

by

MOHAMAD HEKARL UZIR

March 2005

A thesis submitted to the
University of London in the fulfilment of the requirement for the degree of
DOCTOR OF PHILOSOPHY

Department of Biochemical Engineering
University College London
Torrington Place
London, WC1E 7JE.

ProQuest LLC
789 East Eisenhower Parkway
P.O. Box 1346
Ann Arbor, MI 48106-1346

Abstract

Enzyme catalysis is of key importance in the synthesis of new fine chemicals. The use of enzymes to undertake chemical conversion has become commonplace among pharmaceutical companies alongside conventional catalysis. This is mainly due to the working conditions of enzyme-catalysed reactions, the specificity as well as stereo– and regio– selectivity of enzymes as biocatalysts. Many novel techniques have been developed to carry out such catalysis ranging from a simple batch reactor to a complex fluidised bed reactor. Evaluating these techniques requires experimental work and repeat experiments and through these, optimised conditions could be achieved for better yield and productivity. Experimental work is costly and the only cost-effective method is to introduce computer-based experiments via mathematical modelling.

For this purpose, a complete kinetic study based on mechanisms of general enzyme-catalysed reactions was established and the Michaelis-Menten type kinetics has been used as the basis of the steady-state analysis. Prior to the steady-state kinetics, dynamic analyses of enzyme-catalysed reactions were also undertaken and this has led to the understanding of the quasi steady-state assumption that governed the model. New conditions were proposed for the validity of this assumption and the stability of enzyme-catalysed reactions.

In this work, Baeyer-Villiger monooxygenase enzyme-catalysed synthesis of optically pure lactone was used as a model system. A complete model of the rate expression of Baeyer-Villiger reaction was devised. This provided the foundation of the fed-batch whole cell process model carried out as the main part of this work. The effect of substrate and product inhibitions was integrated into this model system and an outcome comparable to that of the experimental data was achieved.

The whole cell process system has been found to be affected by membrane diffusivity during

the course of reaction. This has led to the introduction of diffusion coefficients for both substrate and product into the process model. A simple enzyme-catalysed reaction-diffusion system was successfully modelled and numerically solved. Finally, stability analysis was carried out in order to prove and understand the particular biocatalytic process system.

Acknowledgements

First and foremost, I would like to thank Professor John M. Woodley for his enthusiastic supervision on modelling of enzyme-catalysed systems, his many valuable ideas and his understanding of when encouragement was required so that I always felt that the work was worthwhile and important. I would also like to thank my advisor, Professor Nigel Titchener-Hooker for his guidance and advice especially at the start of my PhD.

I am greatly indebted to Professor Steve R. Bishop from the Department of Mathematics, UCL, for showing me the "beauty" of nonlinear dynamics and chaos; areas which I greatly enjoyed working in. His constant tutorials and interesting demonstrations especially the one on the Lorenz system are highly appreciated.

I would also like to thank Professor David C. Stuckey from the Department of Chemical Engineering and Chemical Technology, Imperial College London, for introducing me to this department and for keeping in touch throughout my years at UCL.

I have greatly benefited from a number of useful discussions with Dr. Jean P. Aucamp, particularly with regard to the issues of biochemistry and molecular biology which were totally new to me when I first started this work.

Not to forget, members of Foster Court for their friendship and constant persuasion just to get me off my desk for lunch and coffee break. Similar goes to all my friends at Imperial College London without whom I would not have enjoyed those three-year period.

Last but not least, I would like to thank my family for their love and support for almost eight years of my studies in the United Kingdom.

"Curiously, the unexpected complexity that has been discovered in Nature has not led to a slowdown in the progress of science, but on the contrary to the emergence of new conceptual structures that now appear as essential to our understanding of the physical world; the world that includes us".
(Order Out of Chaos, 1985).

Ilya Prigogine
(1917–2003)

Contents

List of Figures

List of Tables

Abbreviation

	Definition
Abs	Absorbance
ADH	Alcohol dehydrogenase enzyme
ADP	Adenosine 5'–diphosphate
ANN	Artificial neural network
ATP	Adenosine 5'–triphosphate
BVMO	Baeyer-Villiger monooxygenase enzyme
CHMO	Cyclohexanone monooxygenase enzyme
CPR	Carbon dioxide production rate
CSTR	Continuous stirred tank reactor
CSTBR	Continuous stirred tank bioreactor
DOT	Dissolved oxygen tension
FAD	Flavin adenine dinucleotide
GC	Gas chromatography
ISPR	*In situ* product removal
NAD^+	Oxidised nicotinamide adenine dinucleotide
NADH	Reduced nicotinamide adenine dinucleotide
$NADP^+$	Oxidised nicotinamide adenine dinucleotide phosphate
NADPH	Reduced nicotinamide adenine dinucleotide phosphate
NMR	Nuclear magnetic resonance
OD_{670}	Optical density at wavelength, $\lambda = 670$nm
OUR	Oxygen uptake rate
PAMO	Phenylacetone monooxygenase
PEP	Phosphoenolpyruvate
PTS	Phosfotransferase
RO	Reverse osmosis
r.p.m	Rotation per minute
sQSSA	Standard quasi steady-state approximation
tQSSA	Total quasi steady-state approximation
U	Unit activity of enzyme ($\mu M \cdot min^{-1}$)
vvm	Volume of gas per volume of liquid per minute
Subscript b	Boundary limit

	Definition
Subscript *co*	Cofactor
Subscript *dcw*	Dry cell weight
Subscript *dha*	Dihydroxyacetone
Subscript *gly*	Glycerol
Subscript *i*	Inhibition constant
Subscript inh	Inhibition
Subscript *irr*	Irreversible
Subscript *m*	Michaelis constant
Subscript *max*	Maximum
Subscript *p*	Product
Subscript *rev*	Reversible
Subscript *s*	Substrate
Superscript $\top$	Transpose
Superscript *app*	Apparent

Nomenclature

		Units
A_c	Total area of membrane/cell	m^2
a	Effective area of porin structure	m^2
a_0	Total cross–sectional area of all porin structures available	m^2
C_p	Product concentration	mM
C_s	Substrate concentration	mM
C_p^*	Dimensionless product concentration	–
C_s^*	Dimensionless substrate concentration	–
$C_{p,b}$	Bulk product concentration	mM
$C_{s,b}$	Bulk substrate concentration	mM
$\mathscr{D}$	Diffusivity of component i, $(i = s, p)$	$m^2 \cdot s^{-1}$
Da_n	Damköler number of component n, $(n = 1, 2)$	–
D	Discriminant of characteristic equations or *dilution rate* in *Chapter 4*	$-/(min^{-1})$
$\mathscr{D}_{e,i}$	Effective diffusivity of component i, $(i = s, p)$	$m^2 \cdot s^{-1}$
$\mathscr{D}_{\mathcal{K}}$	Diffusivity value of ketone	$m^2 \cdot s^{-1}$
$\mathscr{D}_{\mathcal{L}}$	Diffusivity value of lactone	$m^2 \cdot s^{-1}$
det	Determinant of a matrix	–
d_K	Diameter of bicyclo[3.2.0]hept-2-en-6-one molecule	Å (10^{-10}m)
$d_{L,1}$	Diameter of (-)1(S)5(R)2-oxabicyclo[3.3.0]oct-6-en-3-one molecule	Å (10^{-10}m)
$d_{L,2}$	Diameter of (-)1(R)5(S)3-oxabicyclo[3.3.0]oct-6-en-2-one molecule	Å (10^{-10}m)
$\mathbf{e}$	Eigenvectors	–
E^c	Centre eigenspace	–
E^s	Stable eigenspace	–
E^u	Unstable eigenspace	–
[E]	Arbitrary enzyme concentration	mM
[EP]	Arbitrary enzyme-product complex concentration	mM
[ES]	Arbitrary enzyme-substrate complex concentration	mM
$[ES]_{ss}$	Enzyme-substrate complex concentration at steady-state	mM
[ESS]	Arbitrary ternary enzyme-substrate complex concentration	mM

		Units
$[E]_T$	Total enzyme concentration	mM
$F_{j,in}$	Inlet flowrate of component j, $(j = s,p)$	$m^3 \cdot min^{-1}$
I	Identity matrix	–
J_m	Jacobian of a matrix system, m	–
$J_{x,y,z}$	Diffusional flux in x or y or z–direction	–
K	Van-Slyke-Cullen constant	–
K_{i_j}	Inhibition constant for component j, $(j = s,p)$	mM
$K^*_{i_j}$	Dimensionless inhibition constant for component j, $(j = s,p)$	–
K_{m_j}	Michaelis constant of component j, $(j = s,p)$	mM
$K^*_{m_j}$	Dimensionless Michaelis constant for component j, $(j = s,p)$	–
k_n	Rate constants of enzyme mechanism, n, $(n = \mathbb{R}^+,\ 0 > n > 0)$	s^{-1}, $mol \cdot s^{-1}$, etc.
k_B	Boltzmann's constant (1.3807×10^{-23})	$J \cdot K^{-1}$
ΔL	Change of total length per unit volume	$m \cdot m^3$
l	Thickness of cell membrane	m
M	Relative molecular mass	$g \cdot mol^{-1}$
[P]	Arbitrary product concentration	mM
$[P]_{ss}$	Product concentration at steady-state	mM
$[P_{OxaBicyclo}]$	Average concentration of (-)1(S)5(R)2-oxabicyclo[3.3.0]oct-6-en-3-one and (-)1(R)5(S)3-oxabicyclo[3.3.0]oct-6-en-2-one	mM
P_{theory}	Theoretical permeability	$m \cdot s^{-1}$
r_{ADH}	Rate of biotransformation of ADH system	$mM \cdot min^{-1}$
$\mathbf{r_c}$	Arbitrary rate of biotransformation for a single cell	$mM \cdot min^{-1}$
r_{CHMO}	Rate of biotransformation of CHMO system	$mM \cdot min^{-1}$
r_{sol}	Radius of solute	m
$r_{s,p}$	Rate of biotransformation as a function of substrate and product	$mM \cdot min^{-1}$
R_c	Cell radius	m
R_p	Porin radius	m
$\mathbb{R}^m$	Real space of dimension m, $(m = 1, 2, \ldots, n)$	–
[S]	Arbitrary substrate concentration	mM
$[S]_{ss}$	Substrate concentration at steady-state	mM
$[S]_0$	Arbitrary initial substrate concentration	mM
$[S_{Bicyclo}]$	Concentration of bicyclo[3.2.0]hept-2-en-6-one	mM
T	Absolute temperature	Kelvin (K)
t	Time	min
t^*	Dimensionless time	–
tr	Trace of a matrix	–
v	*Velocity* of enzyme-catalysed reaction	$mM \cdot min^{-1}$

		Units
V_0	Initial volume of reactor	m^3
V_c	Cell volume	m^3
$\bar{v}$	Average molecular velocity	$m \cdot s^{-1}$
V_g	Void volume per gram of cell	$m^3 \cdot g^{-1}$
V_m	Volumetric mass	$m^3 \cdot g^{-1}$
V_{max}	Maximum velocity	$mM \cdot min^{-1}$
V_r	Reactor volume	m^3
V_T	Total reactor volume	m^3
$\mathbf{V}$	Vector field of a flow	–
y	Cellular radius at time, t	m
y^*	Dimensionless cellular radius at dimensionless time, t^*	–
∇	Grad	–
∇^2	Laplacian operator	–

Greek letters

		Units
ϕ_i	Apparent Thiele modulus for component i before the integration	–
Φ_i	Thiele modulus of component i	–
ρ_c	Single cell density	$g \cdot m^{-3}$
ρ_p	Density of porous cell	$g \cdot m^{-3}$
η	Effectiveness factor	–
ε_p	Fractional free space of porin, (porosity)	–
τ	Dimensionless time	–
τ_p	Tortuosity of porin structure	–
μ	Enzyme to substrate ratio	–
μ_0	Solute's viscosity	$Ns \cdot m^{-2}$
χ	Interaction parameter between solutes (= 2.26)	–
λ_m	Eigenvalues m, $(m = 1, 2, \ldots, N)$	–
λ_p	Molecular mean free path	–
$\mathbf{\Lambda}$	A vector of eigenvalues	–
κ_{i_j}	Dimensionless inhibition constant of component j	–
κ_{m_j}	Dimensionless Michaelis constant of component j	–
θ	Angle	°

Chapter 1

Introduction

Mathematical modelling, that describes the dynamic behaviour of a system has become popular in many practical applications especially in process design and operations (Asprey and Macchietto, 2000; Asprey, 2001). It is actually the first step towards closely understanding any (bio)process systems and, with the help of computer simulations, prediction and *virtual* experiments can be easily carried out (Dunn *et al.*, 1992). In addition, based on such simulations, individual components can be verified separately by physical experiment if necessary. This however does not aim to replace physical tests completely, but it can act as a guide to reduce experimental costs.

In the area of biological sciences, mathematical modelling has started to be of use in describing the growth of bacterial cell (Dunn and Mor, 1975; Chen *et al.*, 1976; Keller and Dunn, 1978*a*,*b*). However, not so long ago it was thought by some that the complexity of biological systems would forever defeat any attempt to describe their behaviour in neat mathematical terms (Villadsen, 1989). Consequently, most biochemists and microbiologists shield away from modelling their experimental results, preferring a long, wordy qualitative description to the quantitative description. This formal, algebraic approach using differential calculus was in a way thought to be a game of no inherent value in understanding the reality of the system. This attitude has actually given an unfortunate impact to this field by leaving it far behind other scientific fields when it comes to exploiting the experimental results in industrial processes. This statement however, does not describe every individual in the biological field, especially during this present time. The elucidation of DNA structure marked the beginning of the involvement

of these scientists into the realm of complex biological processes.

Nowadays, engineers as well as computer scientists have taken a step towards defining and describing biological systems in mathematical forms (Daniel *et al.*, 2003; Warshel, 2003). Such an involvement is highly important both in understanding the system as well as improving the available process if biochemical reaction systems are to be exploited.

1.1 Modelling Biological Reaction Systems

In order to understand the complex systems of living organisms, which, in this context is a bacterial cell, data that describes its growth kinetics should be gathered from a vast number of experiments. The growth of the cell is actually related to the metabolic reaction within the cellular ensemble (Ataai and Shuler, 1985*b*). The process involves a particular substrate used by the cell to produce energy which in turn produces another living cell, and the process continues as long as there is enough substrate to carry out the reaction. A simple generic system that describes a glycolytic process in a living cell is shown in *Figure 1.1.*

Each route of the bacterial glycolysis requires a specific enzyme, and connecting each of these enzyme-catalysed reactions will produce a highly complex model. With the available techniques of describing the kinetics of enzyme reactions, a mathematical model of each reaction catalysed by enzymes $[E]_1$ to $[E]_5$ could be formed. The only problem one might face is to analyse the individual reaction within the system which is confined within a cellular membrane. Such an analysis is vital in order to determine the parameters that become part of the construction of a kinetic model. The only way of obtaining these parameters is to develop an individual assay for each of the enzymes. A sufficient amount of data gathered from the assay can be fitted to each of the kinetic expressions in order to approximate the parameters.

Following the advancement in the area of molecular biology, one could exploit the route within the glycolysis system shown in *Figure 1.1.* If for instance, there is a specific enzyme catalyses a specific reaction in a slow growing bacterial cell which is highly sensitive to changes of temperature and pH, the genes that trigger the excretion or production of the enzyme from that particular cell can be expressed in another host in which the growth can be easily monitored and the production of the particular enzyme can be greatly increased. Hence, the new host is not

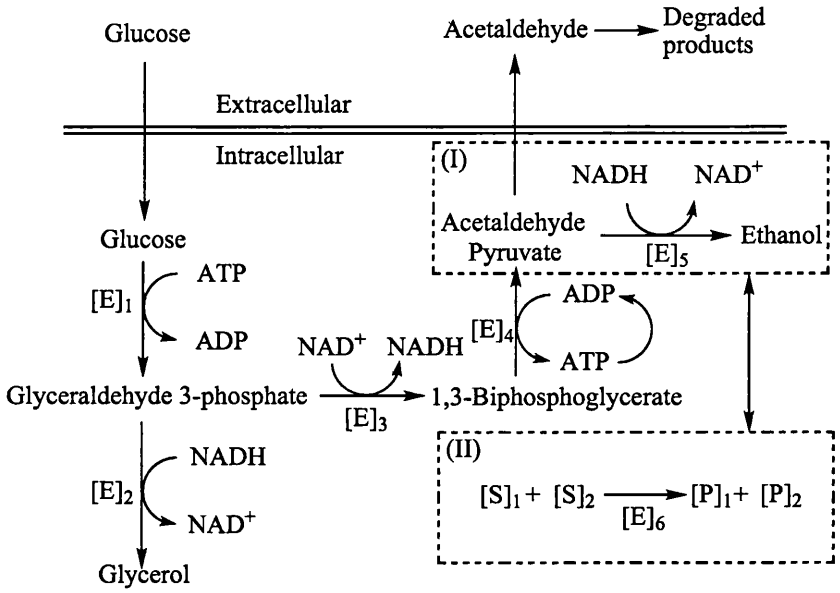

Figure 1.1: Simplified glycolytic pathways during cellular growth. Additional substrates, $[S]_1$ and $[S]_2$ and products, $[P]_1$ and $[P]_2$ travel through the intracellular and extracellular cell respectively in the same manner as glycerol and acetaldehyde. Adapted from Bailey and Ollis (1986).

just producing the normal enzymes for the glycolytic reaction, it is also expressing an additional enzyme, $[E]_6$ which can be used to catalyse an additional reaction such as converting substrates, $[S]_1$ and $[S]_2$ forming products, $[P]_1$ and $[P]_2$ simultaneously during its growth. Often, most of these additional reactions cannot function independently; they mainly rely on another reaction such as that given in *Figure 1.1.* Sub–system (I) which occurs naturally in a glycolysis system can interact with the additional reaction of sub-system (II) and produces a new system that catalyses the additional substrates. The technique described above is termed as the whole-cell biocatalysis (Cabral *et al.*, 1997; Rozzell, 1999). This technique is found to give many advantages compared to that of pure enzymes. One of them is the cofactor regeneration in the cellular system. This will provide a continuous supply of cofactor for those reactions that require such a component. A detailed description of different techniques of biocatalytic processes is given in *Figure 1.2*

Nonetheless, the new technique of utilising pure enzymes has recently been introduced (*Figure 1.2(c)*), and there are still major obstacles to such a method being applied in an industrial scale; lack of fast, efficient methods of extracting enzymes from the cells of biological organisms is one of them. The enzyme purification methods currently available are suitable for the production of enzymes on a small scale (lab-scale) for research applications. However, the isolation of large quantities of enzymes from microorganisms has not reached its full potential. Procedures for synthesising enzymes artificially are being investigated, but these are still in a preliminary research stage (Carbonell and Kostin, 1972). In the future, enzymes will continue to be of great interest to engineers because of their many applications to medicine, analytical chemistry and the chemical industry.

A question might arise in modelling a biocatalytic reaction, whether the study is actually a *true* modelling work or just a fitting procedure of experimental data to the model equation. Ocone and Kummer (2002) have tried to explain the differences between these two separate entities. Modelling of any reaction catalysed by an enzyme is basically dependent on a good assumption with a preliminary experimental observation. The kinetic mechanism of a reaction is entirely based on the given assumption, and the model should vary if a different assumption is chosen on the same reaction. The only method of confirming which model is appropriate is by fitting these equations with the kinetic experimental data. The model that gives the lowest

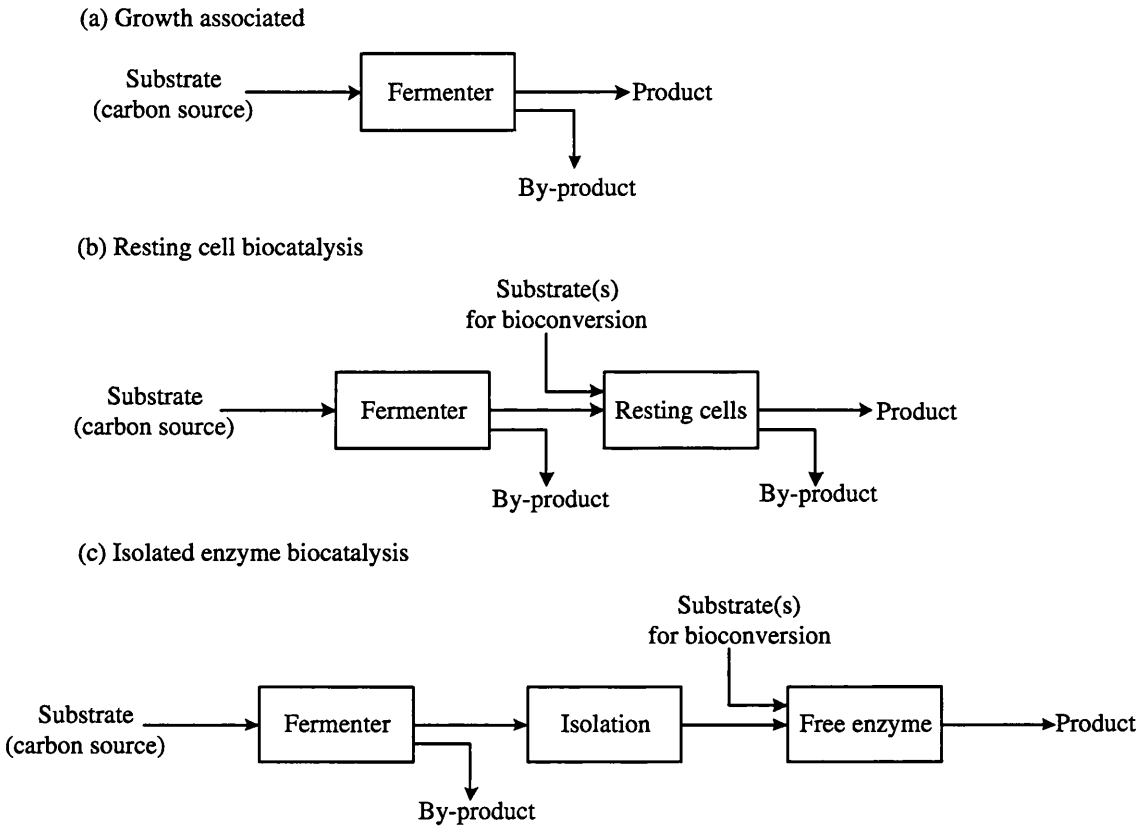

Figure 1.2: Different techniques for carrying out biocatalytic processes.

estimation error will describe the reaction and that with the highest error will definitely be ignored. There is also a possibility that more than one mechanism is consistent with the kinetic data, and the only solution is to carry out a deep and extensive study of the chemistry of the substrates as well as the binding mechanism of the enzyme. Often, such work is not possible. It is also interesting to note here that rarely does engineering design rely entirely on "theory" to predict the rate of reaction, simply because one cannot even guarantee the order of magnitude to be correct.

Therefore, it can be summarised that a biocatalytic modelling cannot stand on its own to accurately describe any enzyme-catalysed reaction or any biological system as a whole. This could even be hazardous if such a model involves the area of medical diagnostic.

1.2 Enzyme-Catalysed Reactions versus Conventional Chemical Reactions

Chemical catalysis has long been the method of choice in converting a reactant into varieties of useful products. However, there are some products that can barely be formed with ordinary chemical reactions. Frequently, if such a reaction does proceed, the product yield and its percentage enantiomeric excesses (e.e.)[1] would be unfeasibly low. This will result in lost of profit due to the lack of productivity as well as enormous capital investment in achieving the "extreme" conditions for the reaction.

Due to this reason, many major chemical and in particular, pharmaceutical companies have turned their attention towards biocatalytic reactions. There has been a significant growth in the area for the past decade as noted by Schmid *et al.* (2001). Enzyme-catalysed reactions have been known to give an effective result in producing fine chemicals; i.e chemicals with low molecular mass and with specific conformation. The main application apparently lies in the exploitation of its outstanding properties with respect to chemoselectivity, regioselectivity, and especially stereoselectivity for the production of enantiomerically pure compounds (Schulze and Wubbolts, 1999; Liese and Filho, 1999). The conditions used to carry out these reactions are comparatively mild; with temperature as low as 30 to 40°C and at atmospheric pressure. The

[1]For a mixture containing different proportions of enantiomers, the enantiomeric excess is given by, e.e. $= \frac{A-B}{A+B}$, where, A is the proportion of most abundant enantiomer and B is the proportion of least abundant enantiomer.

Biocatalytic reaction	Chemical-catalysed reaction
Long development time	Quick development time
Mild reaction conditions (Temperature, pressure and aqueous solution)	Poor operational stability (extreme conditions)
Highly stereo–, regio– and chemoselective but low volumetric productivity	High volumetric productivity but low product specificity
Unique and varied chemistry	Unwanted reaction with impure preparation
Environmentally friendly	High cost

Table 1.1: Advantages of biocatalytic reactions compared to conventional chemical reactions.

differences of the two type of reactions can be summarised in the *Table 1.1.*

The ability of enzymes to enhance the rate of chemical reactions by many order of magnitude at room temperature together with their specificity towards substrates make them an ideal type of catalyst for industrial use. In addition, they also provide a way of eliminating many of the operational difficulties of high pressures and temperatures often encountered in chemical catalytic processes (*Table 1.1*), while at the same time avoiding costly and time consuming product purifications.

1.3 The Kinetics of Enzyme-Catalysed Reactions and Modelling of Bioreactor Process Systems

1.3.1 Kinetic Modelling

At the heart of biocatalytic process systems are the biocatalytic properties of the enzymatic reaction, to which the kinetic model is key. This therefore, forms the basis of the biocatalytic process model. Biocatalytic reactions, operated as either isolated enzyme or whole–cell systems has become increasingly popular over the past two decades. The continued use of such systems has made the understanding of the kinetic of enzyme reactions rather important, this knowledge will indirectly link to the understanding of the operation of bioreactors.

The most important characteristics of an enzyme are the fundamental data about the kinetics of the catalysed process and knowledge about the factors that affect the kinetic properties. The two main kinetics constants; the Michaelis constant, K_m and the maximum velocity, V_{max} are particularly important information. They describe the nature of the relationship between the initial reaction rate and the substrate concentration. If substrate and/or product inhibition occur, the corresponding K_i values are also important.

The actual form of the intrinsic rate equation of an enzyme-catalysed reaction depends on the mechanism of the enzymatic bioconversion, which can be very complex. In order to carry out the characteristic study of an enzyme, it should be as pure as possible, preferably recrystallized several times, and in any case should be free from any other enzyme acting on similar substrates. The substrates as well should be as pure as possible and free from any other substances on which the enzyme may act. In carrying out the specificity study it is usual to select a reference substrate which generally is the most readily attacked biological substrate and to work out the optimum conditions for this substrate.

However, the used of pure enzyme and its natural substrate is technically impossible. The kinetic measurements of enzyme-catalysed reactions that exist in the literature are mainly concerned with the characterisation of the biocatalyst and not with its design problems. These measurements refer to conditions of pH, temperature, and substrate concentration required to characterise the enzymes. The use of such data in designing a reactor can be misleading because the investigations are mainly carried out in a concentration range which has no relation to the technical applications. In an industrial scale process, such a high concentration is desirable to avoid the design of large bioreactor vessel for a given productivity and thus, the kinetic measurements have to be carried out under conditions relevant to large-scale processes.

Finally, when a complete rate expression of an enzyme–catalysed reaction is obtained together with the appropriate kinetic experimental data, the nonlinear regression method can be used to determine the kinetic parameters. The procedure can be applied either from the initial rate data or from the actual plot of the progress curve. The nonlinear least–squares regression technique is often used incorporating any of the powerful optimisation algorithms such as the Levernberg-Marquardt (Marquardt, 1963), Nelder-Mead's simplex method (Nelder and Mead,

1965), Gauss–Newton and Rosenbrock method (Bard, 1974; Beck and Arnold, 1977). The estimated parameters serve as the values of initial estimates of the parameter determination through the fitting procedure to the overall reaction rate.

1.3.2 Bioreactor Process Modelling

When the kinetics of an enzyme-catalysed reaction is fully understood and all parameters involved in the rate expression are completely determined, a relationship between the kinetic rate expression and the bioreactor configuration can then be developed. This is done by doing a material balance on every component involved in the reaction. The bioreactor configuration can be either a simple batch or fed-batch or perhaps a continuous stirred-tank type bioreactor. The model can be easily swapped whenever a new system is preferred depending on the desired productivity.

In order to observe the result of a constructed model system, it needs to be numerically integrated. This is normally done with the fourth order Runge-Kutta algorithm (Dunn *et al.*, 1992). A complete solution of the system is then graphically simulated. To test the sensitivity of the system, different initial conditions can be imposed on the model, this refers to the concentration of substrates or perhaps the concentration of the enzyme, if only the amount is exactly known.

Validation of the model system can be done by comparing the experimental data with conditions similar to that imposed to the system under investigation. For a good model system, the simulated data by means of numerical integration should lie on the experimental data points.

1.4 Chemical Catalysis to Enzyme-Catalysed Baeyer-Villiger Reaction

The development of catalytic reaction in chemical transformation has led to the improvement of many reaction systems by increasing their yield and productivity. Such work may involve utilising different types of catalysts, changing various reaction conditions such as temperature and pressure and prolonging the period of reaction. Characterisation of catalysts for a particular reaction is considered to be the main approach in order to achieve a fast transformation at mild reaction conditions, and the only practical way is by means of formulating a highly reactive catalyst. However, one could compensate this by having a much less reactive catalyst, but the

reaction conditions need to be optimised either by conducting the reaction at a high pressure or temperature. This implies that the working environment is highly at risk and precaution should be taken while carrying out such reactions.

However, the whole scenario has completely changed over the recent decades. The introduction of biological catalysis has provided a new approach in carrying out chemical reactions. Reaction conditions should not be a major problem for systems that work under atmospheric pressure and temperature which usually does not exceed 40°C. Such a biocatalytic transformation with an enzyme as the main catalyst is less hazardous, produces less polluting side-products and requires low energy consumption compared to the conventional pure chemistry based methodologies (*Table 1.1*) (Schmid *et al.*, 2001).

To understand the differences between a reaction under conventional chemical transformation and that of biochemical transformation, both systems should be analysed separately. The systems may undergo different catalytic reactions, however, the catalytic route remains the same. This will be explained in the first two parts of this section.

1.4.1 The Chemistry of Baeyer-Villiger Reaction

Before analysing the detailed chemistry of the system, this historical reaction was first discovered by Adolf von Baeyer and Victor Villiger in 1899 by carrying out the chemical transformation of ketones into esters or cyclic ketones into lactones using peracids oxidant (Renz and Meunier, 1999). A few different reactants were used for the particular transformation such as, menthone, carvomenthone and camphor. An oxidising agent known as potassium monopersulphate ($KHSO_5$) was used to carry out the reaction at room temperature for 24 hours. The reaction resulted in the corresponding lactones with percentage yield shown in *Figure 1.3.*

The review by Renz and Meunier (1999) also described the preparation of the oxidising agent. The mixture consists mainly of concentrated sulphuric acid, potassium persulphate powder and finally after a thorough mixing of the first two reagents for 10 minutes, potassium sulphate was then added. A dry powder composed of $KHSO_5 \cdot 7KHSO_4 \cdot 2K_2SO_4$ was stable in the absence of humidity. Baeyer and Villiger also looked at other types of oxidising agents and preferably the organic peracids. The treatment of dibenzoyl peroxide with sodium ethoxide and sodium salt of perbenzoic acid was made and the mixture precipitated as a colourless powder. The free

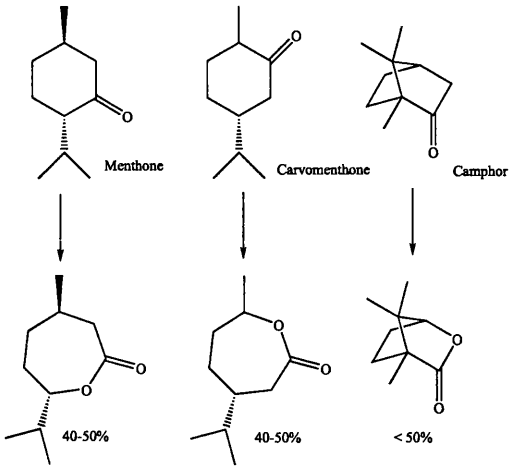

Figure 1.3: Chemical conversion of menthone, carvomenthone and camphor using potassium monopersulphate ($KHSO_5$) as the oxidising agent at room temperature for 24 hours.

perbenzoic acid could be generated by protonating the salt with the very weak proton donour, H_2CO_3.

The acid shows identical activity as H_2SO_5 when reaction with potassium iodide, (KI) immediately gave a black precipitation. This first discovery of the carbon–carbon bond formation by Baeyer and Villiger has led a few other researchers to optimise and improve the reaction. A summary of different type of oxidising agents catalysing different reactants at the given conditions can be referred to *Table 1.2.* A full list of other catalysts that have been developed to carry out the reaction can be obtained from Renz and Meunier (1999).

The success of steroid syntheses using Baeyer-Villiger reaction has led to systematic explorations of this reaction. This was originally due to the higher conversion of such reactions and a lower acidity of the reagent. The mechanism of the rearrangement of the main atoms participating in the reaction is clearly defined in the next section.

1.4.2 Baeyer-Villiger Reaction Mechanism

A reaction that proceeds in the presence of a catalyst should behave differently compared to that of a normal reaction. This dissimilarity is closely related to the mechanistic changes caused

Investigators	Oxidising agent and reaction conditions	Reactant (% yield)
Baeyer and Villiger[a,†]	H_2SO_5, room temperature, 24 hours	Menthone ($\sim$ 40–50%) Carvomenthone ($\sim$ 40–50%) Camphor (<50%) (*Figure 1.3*)
Ruzicka and Stoll (1928)	H_2SO_5, 65°C, in petroleum ether/glacial acetic acid	13– to 17–membered ring ketones, (N.A)
Dilthey *et al.* (1940)	Acidic solution of H_2O_2	Benzophenone (N.A) Cyclohexanone (N.A)
Witting and Pieper[a]	Ether H_2O_2 solution and P_2O_5	Fluorenone (N.A)
Criegee (1948)	$Pb(OAc)_4$	Fluorenone (25%)
Velluz, Amiard, Martel and Warnant[a]	H_2O_2 solution and P_2O_5 with acetic anhydride	Dihydroperoxy steroids (N.A)

[a]Renz and Meunier (1999)
[†]Although the reaction was named after Baeyer and Villiger when they documented the preparation in 1899, the first reaction was actually discovered by Caro in 1898 (Ruzicka and Stoll, 1928; Renz and Meunier, 1999).

Table 1.2: Different oxidising agents developed to carry out Baeyer-Villiger reactions, (N.A.; not available).

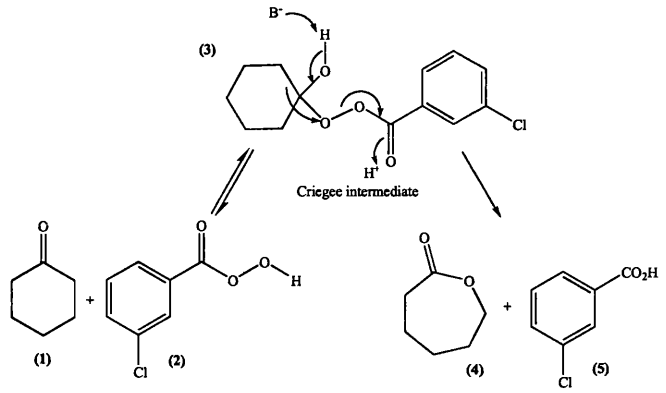

Figure 1.4: Atoms rearrangement proposed by Criegee on cyclohexanone structure (Stewart, 1998).

by the catalyst towards the rearrangement of the specific atoms. The mechanism of the well-established Baeyer-Villiger reaction was proposed by Doering and Speers (1950) and Doering and Dorfman (1953) whose work was mainly based on the rearrangement provided by Criegee on decalin peroxyester. It was postulated that there is a nucleophilic attack of the peracid onto the ketone compound in the Baeyer-Villiger oxidation to generate the so-called "Criegee intermediate". The schematic diagram of the reaction route was simplified by Stewart (1998) using cyclohexanone molecule as the reactant (*Figure 1.4*).

The addition of peracid (**2**) to the carbonyl compound (**1**) gives a reversible reaction forming the "Criegee intermediate", (**3**) which can undergo rearrangement, forming products. The compound (**2**) acts as a leaving group, and in a quasi-concerted fashion, the C=O bond is formed again and one substituent migrates from the carbonyl carbon atom to the partially positively charged oxygen atom. This produces compound (**4**) together with a carboxylic acid, (**5**). In addition, studies with conformationally locked systems have revealed that stereoelectronic control governs the rearrangement step where the C–C bond must be antiperiplanar with respect to the O–O bond and to one of the lone pair orbitals of the hydroxyl group.

1.4.3 The Kinetics of Enzyme-Catalysed Baeyer-Villiger Reaction

It was mentioned before that in either chemically catalysed or enzyme-based reactions, the mechanism of the reaction remains the same. This has been clearly shown by Ryerson *et al.*

(1982) where, in her work, an enzyme that catalyses the conversion of a cyclic ketone called cyclohexanone monooxygenase was used. The enzyme contains a tightly bound flavin adenine dinucleotide (FAD) cofactor that forms the basic oxygenating intermediate. The oxidised flavin found in the resting form of the enzyme is first reduced by hydride transfer from a reversibly bound nicotinamide adenine dinucleotide phosphate (NADPH), and the cyclic ketone binds to the enzyme. The molecular oxygen binding is then followed by the rapid formation of the flavin a4–hydroperoxide, one of the intermediates formed during the reaction. The terminal oxygen of this hydroperoxide is added to the carbonyl to form a tetrahedral species analogous to the "Criegee intermediate" shown by (**3**) in *Figure 1.4*. Rearrangement of the intermediate forms the product lactone and the 4a–hydroxyflavin. After the release of the product and the oxidised cofactor ($NADP^+$) from the arrangement, the 4a–hydroxyflavin is dehydrated to regenerate the oxidised flavin and prepare the enzyme for the next catalytic cycle. The mechanism clearly shows that the carbonyl group should be initially bound to the enzyme before the oxygenating intermediate can take place. This provides a unique characteristic to the monooxygenase type enzyme to carry out enantioselective reaction. The carbonyl molecule binds to the active site of the enzyme which directly influences the overall reaction rate by controlling the rate of formation of the flavin 4a–hydroperoxide.

Schwab and co-workers (Schwab, 1981; Schwab *et al.*, 1983) have found that the break–up of the "Criegee intermediate" leads to retention of configuration at the migrating carbon which allows the enzyme to give regio– and enantioselective ability by permitting only one of the two C–C bonds to be antiperiplanar with respect to the O–O bond in the tetrahedral intermediate. As the reaction proceeds, the flavin remains strongly bound to the enzyme and the stereochemistry of the formed product is believed to be controlled by the stearic interaction between the enzyme structure and the substrate.

A similar enzyme also catalyses conversion of bicyclic ketone which is shown in *Figure 1.5*. However the full kinetic study of this type of substrate remains incomplete. A comprehensive analysis on the mechanism and kinetics, based on the monooxygenase enzyme-catalysed bicyclic ketone reaction will be covered in *Chapter 3*.

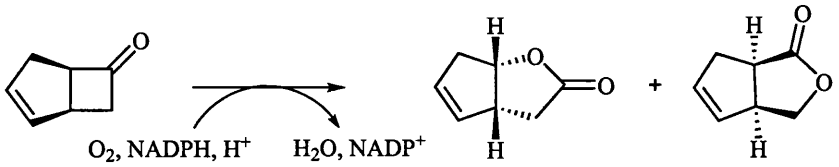

Figure 1.5: Bioconversion of bicyclo[3.2.0]hept-2-en-6-one to (-)1(S)5(R)2-oxabicyclo[3.3.0]oct-6-en-3-one and (-)1(R)5(S)3-oxabicyclo[3.3.0]oct-6-en-2-one.

1.5 Mathematical Analysis of Enzyme-Catalysed Systems

After a detailed explanation of the complex chemical and biochemical reactions which are governed by complex mechanistic routes, one might wonder how can this mechanism describe the dynamics of the whole reaction system. Experimental investigation is not the only means of understanding the mechanism of a reaction, putting the components into a system of mathematical equations proves to be another method of understanding how the system is likely to behave based on the knowledge of (bio)chemistry and physics. The most famous chemical reaction which has gained interest from chemists and surprisingly mathematicians bearing the name of Belousov-Zhabotinsky (Roux, 1993) is one example of system that has been actively theoretically studied. Epstein (1984) worked on a similar reaction and used the model describing the chemical components known as the Oregonator and had carried out numerous experimental works that confirmed some of the rich dynamic phenomena which arose in the numerical simulations; periodic oscillations were observed, which led to chaotic behaviour. Further discussion on systems exhibiting various dynamic behaviours is given in the last two subsections.

The success of understanding this complex behaviour of a simple chemical reaction has led others to explore a relatively complex biological system; the glycolytic pathways. The route resembling that of *Figure 1.1* has now become the centre of attention among biochemists as well as engineers (Lyberatos *et al.*, 1985*a*,*b*,*c*; Wolf and Heinrich, 2000; Brusch *et al.*, 2004). To obtain a complete glycolytic model system, each reaction route is separately analysed and individually defined by a rate expression; an expression that describes the mechanism of a reaction. Each expression is then combined, forming a system of ordinary differential equations. Solving such a system using the fourth order Runge-Kutta algorithm leads to observation of

sustained oscillations.

Detail studies of such a system perhaps requires an in depth knowledge of the metabolite interactions within the pathways and their initial amounts present at the start of the reaction. However, such complications can be reduced by taking into account only parts of the cycle where complete information regarding the amount of the components and relationship of the rate expressions between the two sub-systems (systems (I) and (II) in *Figure 1.1*) can be accurately derived.

With the given system and accurate mechanism of reaction, a complete relationship summarised by the "rate expression" can be directly obtained. The use of rate expression is fundamental in interconnecting one system to the other. Therefore, the method used to obtain these terms should be properly selected according to the condition of a reaction as well as their mechanistic arrangements. The latter being the most important rule in defining an enzyme–catalysed reaction. Schnell and Maini (2003) have thoroughly discussed the history behind its early work and the discrepancy that it held before a rigorous mathematical explanation was published to defend its validity based on a given assumption (Heineken *et al.*, 1967). This topic will be summarised in the first subsection.

1.5.1 Uniqueness of the Kinetic of Enzyme-Catalysed Reactions

The main objective of studying the kinetics of enzyme-catalysed reaction is to obtain the rate expression of that particular reaction. Mostly, in the study of reactions catalysed by enzymes, no matter how complex the mechanism of such reactions, the rate expression is always assumed to obey the simple Michaelis-Menten kinetics (Lee *et al.*, 1999; Zambianchi *et al.*, 2000). This is only true if the reaction proceeds in the presence of substrate at lower concentrations. If the substrate is increased to a higher concentration range, it will give rise to substrate inhibition. The simple expression however, becomes void if the enzyme gives a different curve to that of the simple Michaelis-Menten model. This type of curve requires a different form of rate expression. A detailed study of enzyme kinetics at high substrate concentration is particularly important when dealing with large scale processes when high productivity and yield are the main objectives.

Rate expression of an enzyme-catalysed reaction is basically a summary of the reaction mechanism of a particular reaction in a single equation. The expression should contain the

main properties of a reaction such as the speed, the effect of substrate and product and most importantly the route that it follows. Therefore, different enzymes will give different forms of rate expression in a given reaction.

The method of obtaining the equation however has it's own story. The first expression derived by Michaelis and Menten in 1913 was not based on any mathematical grounding until Briggs and Haldane proposed the rule of quasi steady-state approximation in 1925 upon deriving the model equation (Ainsworth, 1977; Segel, 1993; Cornish-Bowden, 1995). Yet, no rigorous mathematical proof was accompanied with the stated rule of Briggs-Haldane. The proposed mechanism describing the enzyme-catalysed reaction does not match the approximation of quasi steady-state! This inconsistency was finally revealed in 1967 when a rigorous mathematical proof was published explaining the new rules and conditions in dealing with enzyme catalysis. Mathematical analysis of enzyme-catalysed reaction from the work of Heineken *et al.* (1967) has provided a foundation of other important discoveries in this highly competitive area.

The system of equations that made up the model employing the quasi steady-state approximation can be observed using the theory of singular perturbation (Segel, 1988; Segel and Slemrod, 1989). The model which is closely related to the ratio of total amount of enzyme to total substrate concentration has been found to govern the validity of the assumption, failure to follow this particular condition will lead to an error in estimating the kinetic parameters. Further characterisation of this simple model equation and its uniqueness was also made by Schnell and Maini (2000, 2002).

This short summary of the kinetics of enzyme-catalysed reaction and the equation that describes the model system has shown that a simple equation could provide a vast information either experimentally or mathematically. However, there are still a number of problems that need to be addressed in certain areas of enzyme kinetic model. In the next chapter of this thesis, a new problem has been raised and suitable solutions have been proposed.

1.5.2 Dynamics of Linear and Nonlinear Systems

Mathematical modelling is concerned with describing, as well as explaining, any physical phenomena in terms of mathematical forms or equations. These phenomena can either be a *simple* system, a *complicated* system or perhaps a *complex* system (Amaral and Ottino, 2004). A *simple*

system consists of components which act according to well-understood laws such as a swinging pendulum. A *complicated* system, however, contains a considerably large number of components which may have well–defined roles and they are governed by well-understood rules. A flying aircraft is considered as a *complicated* system since its components are highly interconnected with one another in order to achieve a certain function. But, the knowledge of these components may not be needed if one only wishes to know the path taken during the flight. Finally, a *complex* system which contains typically of a large number of components that may act according to rules that may change over time and that may not be well-understood. They are many examples which can be correlated with *complex* system such as, the stock market and the human brain. These systems when they are mathematically modelled could result in equations which might be linear or nonlinear, and analysis of these equations highly depends on their nonlinearity. The study of nonlinear equations has been an integral part of science and engineering and it forms the basis of all dynamical model systems. The theoretical foundations of these systems are on firm mathematical footing (Villadsen, 1989; Amaral and Ottino, 2004).

For a model describing a reaction catalysed by biological cell, it is certainly classified as producing a complex nonlinear model due to the complexity given by the cellular system. A *complex* system that has been previously explained, is not well-understood and a complete mathematical terms could not be obtained to describe the phenomena. Therefore, assumptions are required to reduce such complexity where simple mathematical terms can be used to form a complete set of equations. Model reduction based on the given assumption however, does not mean producing a simple system with a linear model, it may still be a *simple* system, but the equations that governs the system may be of the nonlinear type.

Then, complex systems and complex dynamics need to be distinguished. These are two completely different criteria. In order to define complex dynamics, consider a physical system of simple pendulum i.e. *simple* system which is governed by a nonlinear equation (Bishop and Clifford, 1996);

$$\ddot{\theta} + c\dot{\theta} + (1 + p\cos\omega t)\sin\theta = 0$$

A forced pendulum, with gravity being a periodic function of time, t with angle of oscillation, θ and frequency, ω, generates complex dynamics with "erratic", undetermined oscillations. Other

similar systems that exhibit various dynamical phenomena can be referred to Verhulst (1985); Wiggins (1990) and Thompson and Stewart (2002).

On the other hand, the effect of simple dynamics can be observed in a simple enzymatic reaction described by Bruns *et al.* (1973). The reaction given by $aA + sS \rightarrow pP$ is simply governed by dimensionless coupled nonlinear equations with the rate expression $R(x_1, x_2)$ given by;

$$R(x_1, x_2) = \frac{x_1}{(\kappa_m + x_1)\left(1 + \frac{x_2}{\kappa_1} + \frac{\kappa_2}{x_2}\right)}$$

and

$$\dot{x}_1 = \alpha(\beta - x_1) - \gamma\phi R(x_1, x_2)$$

$$\dot{x}_2 = 1 - x_2 - \phi R(x_1, x_2)$$

Although the system exhibits simple dynamics, the steady-state solutions are highly unstable at different parameter values and yet a stable oscillatory state is observed for small perturbations of its initial conditions.

1.5.3 Introduction to the Method of Bifurcation Theory

Every model system consists of parameters that govern the behaviour of the model solutions. A good model system will always be such that the qualitative behaviour does not change when the parameters are varied about a small value for which the original design was made, i.e. the system is robust to any parameter changes.

Yet, the behaviour may change if a large variation of parameter values were subjected to the system and the change in the qualitative properties could mean a change in the stability of the original system. The value of these parameters that result in the change of the system's stability are known as "bifurcation values". The theory is particularly useful in investigating the stability of any dynamical systems.

For clarity, consider a similar system of the enzymatic reaction given in the previous section. The steady-state plot of component x_2 against the parameter, ϕ is given in *Figure 1.6.* It is clear that multiple steady-steady solutions exist in the first curve, (I), which means the system is highly unstable at the given range of parameters, ϕ. Putting these values in the "real" process

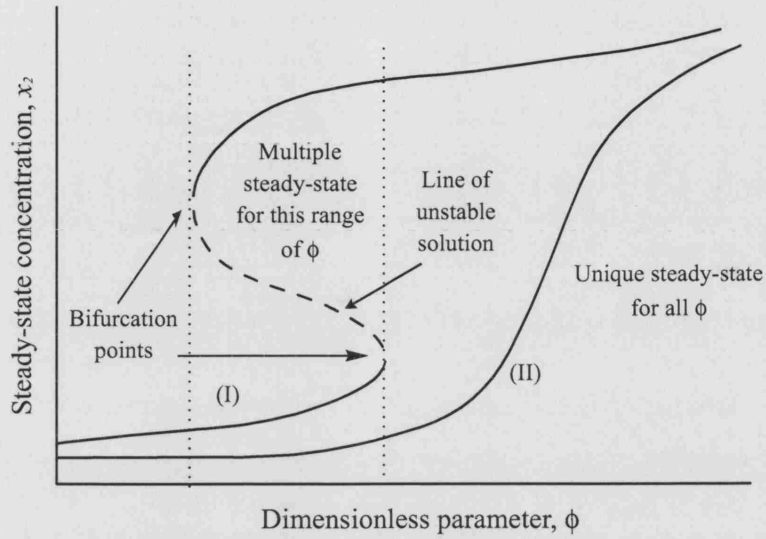

Figure 1.6: Bifurcation diagram of enzyme-catalysed reaction. Adapted from Bruns *et al.* (1973).

system could give an unpredictable result regarding the consumption of substrate [S]. However, on a different condition of the system, an asymptotically stable solution is found (curve (II)) that can be used to avoid instability of the system.

Local Bifurcations

The study of bifurcation phenomena can be divided into two main categories; the local analysis and the global analysis. The local analysis is used to described bifurcations and other phenomena whose effects are restricted to a neighbourhood of a point or cycle in phase space. On the other hand, the bifurcations which are not so restricted are termed global bifurcations. In the study of the dynamic of an enzyme-catalysed system, only the local bifurcation method will be applied.

A local bifurcation is observed on an equilibrium path of a *flow* as the real part of a linear eigenvalue passes through zero. If a real eigenvalue passes through zero, a *saddle-node bifurcation* is observed. Typically, this will be detected as a fold, at which the path of the folds smoothly back at a maximum or minimum value of the control parameter. However, in the presence of symmetry, or other constraints, the saddle-node can manifest itself as a sub– (unstable), super– (stable) or transcritical bifurcation in which a secondary equilibrium path bifurcates from the

monotonically increasing fundamental path. If the real part of a complex conjugate pair of flow eigenvalues passes through zero, the *Hopf bifurcation* will be observed in which stable (unstable) cycle emerge from the monotonic fundamental path at supercritical (subcritical) values of the control parameter.

The local bifurcation analysis can also be observed on a path of a fixed points of a *map*, representing for instance a path of cycles in a stroboscopically sampled flow. A loss of stability will now correspond to a mapping eigenvalue passing through the unit circle. If a real eigenvalue passes through +1, a saddle-node bifurcation is obtained, which typically manifests itself as a cyclic fold. If a real eigenvalue passes through -1, a flip bifurcation is observed at which a secondary stable (unstable) path of period-doubled fixed points bifurcates off the monotonically fundamental path at supercritical (subcritical) values of the control parameter. If a complex conjugate pair of eigenvalues penetrates the unit circle, the *Neimark-Sacker bifurcation* or the secondary Hopf bifurcation is observed. A complete definition of the types of bifurcation phenomena can be referred to Thompson and Stewart (2002); Guckenheimer and Holmes (2002) and a complete introductory review of bifurcation theory by Crawford (1991).

The terms discussed in this section will be largely used in the main chapters of this thesis pertaining the stability study of enzyme-catalysed reaction systems.

1.6 Reaction-Diffusion Model of Cellular Systems

One of the major effects of the whole-cell system is the transfer of material across the cell membrane. This has broadening the scope of investigation into a more complex diffusion problem (Keener and Sneyd, 1998; Plimpton and Slepoy, 2005). The movement across the cell membrane can occur in three different ways and it is not unexpected that for a single membrane, movement can occur at the same time by simple diffusion, active transport and exchange diffusion (Hogben, 1960). It should be apparent that there is no simple dichotomy between passive diffusion and active transport and these two terms alone do not serve to characterise movement through cell membranes (Tanojo *et al.*, 1997).

There has been an emphasis placed upon the temperature coefficient or activation energy of a process. Unfortunately, the activation energy does not distinguish between a *passive* and

active transport process. For a simple physical system involving a highly restricted diffusion, the activation energy may be of the same magnitude as those associated with a chemical reaction. On the other hand, in a complicated chain of chemical reactions, it is obvious that the overall process should have high activation energy. In fact, there is no reason why it should not have a negative temperature coefficient as it frequently does in biological systems. It should be emphasised here that the temperature coefficient does not give a reliable hint to the nature of a process and therefore any changes of the values would not provide any answer to the question whether a transport process is *passive* or *active.*

1.6.1 Transport Mechanisms Across Cell Membranes

In this introductory chapter, a summary of different transport phenomena through cell membrane mentioned in the first paragraph is given and their complications that should arise in modelling of such complex biological systems are highlighted. Previous attempts in modelling these phenomena are presented in the subsequent section in order to support the above discussion.

Simple Passive Diffusion

The concept of simple passive diffusion is reasonably easy and has been widely accepted. The transfer of a particle is basically due to the random movement caused by the thermal energy without a significant interaction with other molecules moving through the membrane; either of the same or of different species. A number of mathematical correlations have been constructed in order to quantitatively describe the transfer of such particles (Ussing, 1949; Renkin, 1954). It is worth noting that such correlations exactly define simple passive diffusion without making any *a priori* assumption regarding the nature of the membrane structure.

In order to describe this simple passive diffusion, Fick's law always being the first to be considered especially when explaining reaction-diffusion systems (Murray, 2002). However, there are two substantial restrictions to the application of the *Fickian* diffusion to describe the transfer of material through biological membranes. A difficulty should arise when making a stipulation on the boundary conditions that permit the use of the differential equation and secondly, the incorporation of the diffusion coefficient which is treated as a constant rather than a complex

function of other variables of the equation. Therefore, the use of *Fickian* diffusion does imply some *a priori* assumptions regarding the nature of the membrane.

Generally, in a physiological point of view, it is important to emphasise that simple passive diffusion through a membrane can occur by either of two quite dissimilar routes; aqueous porins and lipoid matrix (Hogben, 1960). A detailed discussion on the structure of porin and its transfer mechanism is given in *Chapter 5.*

Active Transport

The transfer of molecules via active transport can be simply defined as the net transfer of a molecular species from a lower to a higher electrochemical potential. It is basically the transfer of energy from the cell or membrane to the moving species. This can be further divided into two categories; firstly, the specific active transport where the movement of molecular species is mediated by "carriers" and characterised by structural specificity, saturation kinetics and analogue competition as well as being subject to metabolic poisoning and secondly, the nonspecific active transport where the movement of molecular species is not necessarily attributed to a fixed membrane carrier. Such examples can be seen in the transfer of weak electrolyte across the gastrointestinal epithelium and the transfer of water from a lower to a higher activity.

Exchange Diffusion

Exchange diffusion is a type of material transfer that provides a one-for-one exchange of isotopically distinguishable particles. In other words, it is a movement mediated by membrane carrier. Differ from that of active transport, membrane carrier in exchange diffusion produces a complex with the exchanging particle. At the membrane-solution interfaces, an exchanging particle can be displaced from the complex by a similar particle. If isotopically labelled particles are introduced into one solution bathing a membrane, they are able to pass into the solution on the other side of the membrane with the help of the complex formed with the exchange diffusion carrier. Since exchange diffusion does not contribute to the net movement of a molecule, when it is present, it does contribute equally to the magnitude of the two unidirectional fluxes across a membrane because they are measured by the use of isotopes. However, if there is simultaneously both simple and exchange diffusions, the flux ratio will be less than that predicted by Ussing's

flux ratio correlation (Ussing, 1949). There are instances where exchange diffusion is sensitive to metabolic inhibition and other instances where it is not.

The above discussion on exchange diffusion serves to outline the principle contribution to exchange across a membrane, a somewhat important circumstance should be noted. When a carrier, responsible for the exchange diffusion of a particle, complexes with closely related but chemically different species, it is possible that one of the chemical species may approximate being a tracer of the other. In such a situation, a gradient for one species would be capable of driving the movement of its close relative through the carrier.

1.6.2 Mathematical Model of Systems with Reaction-Diffusion Phenomena

Mathematical modelling can be considered as a useful technique of understanding any physical phenomena. The techniques used to describe such systems are closely related to the complexity of those systems themselves. Phair and Misteli (2001) have listed some of the techniques which can be applied especially in modelling biological systems, that include, statistical tools of time series analysis, analytical and computational tool of differential equations, computational tools of stochastic systems and the scaling and phase-space tools of fractal and chaos. For a specific application in cell biology, differential equations are often used because they are a natural mathematical language for cellular processes, such as biochemical kinetics, membrane transport and binding events.

Among other types of biological models, cellular modelling is considered as the most complex and challenging task at this present time. From a biology standpoint, the challenge is to represent cellular function with model inputs such as diffusion constants, lists of biochemical reactions within the cell and reaction rates which enable both qualitative and quantitative comparison of simulation results with experiment and which ultimately lead to biological insight (Plimpton and Slepoy, 2005). This is an incredibly difficult task, since model inputs are often not known to high fidelity. Algorithms are needed in order to accurately perform parameter estimation and testing various models for stability and robustness.

Currently, research in this area is actively undertaken both experimentally and theoretically. Experimental work is mainly focussed on determining a suitable and most accurate diffusion constant. Since the cell membrane constitutes of complex structure of Golgi-apparatus and

endoplasmic reticulum, therefore, experiments should be designed in such a way that these components are taken into account (Siggia *et al.*, 2000; Gerlich *et al.*, 2001). Even, the correlation used by Siggia and co-workers to estimate the diffusivity is still based on a number of assumptions imposed on the photobleach experimental technique (Gheber and Edidin, 1999; Peters and Kubitscheck, 1999). The value was calculated using;

$$\mathscr{D}_e = \langle \cos^2(\theta) \rangle = \frac{\mathscr{D}}{d}$$

with d as the dimension of porin tubes ($d = 2$ or $d = 3$) and θ is the angle between a tube and the plane that is imaged. On the other hand, Zhang *et al.* (1991) had estimated some values of $\mathscr{D}$ by simply using the Stoke-Einstein correlation and they were compared to the animal cells experimental data. Such methods given above have shown that there is no standard correlation which can be confidently used and the value can only be based upon estimations of the above equations or from experiments with a number of limitations.

The ability to simulate diffusion in a generally inhomogeneous but isotropic material is the first step in modelling diffusion in living cells. However, there are many complicating issues for which a general treatment is impossible and one must deploy biophysical methods in a way that optimises the prospects for quantitative analysis. Therefore, some intuitive guides have been proposed which taken into account the complexities of the cellular geometry, other dynamical processes and immobile fractions. Based upon these points, Howard and co-workers (Howard *et al.*, 2001) had gone a step ahead in modelling the proteins transfer between the cytoplasmic membrane to the cytoplasm in a single *E. coli* cell. The results had successfully led to the explanation of the mid-cell division and a natural oscillatory pattern of the *min* proteins in *E. coli*.

From the summary of the previous work and the work which are actively undertaken, it is clear that modelling of cellular systems is a complex and tedious tasks and it should be carried out independently. Apart from the theoretical study, experimental investigation should also play an important role especially when determining some biological constants such as diffusivity value of a particular molecule travelling across a particular cell membrane.

1.7 Summary

Process modelling of enzyme-catalysed reactions should be considered as one of the most important problems in biochemical engineering. The reason being that understanding of the process model can lead to a complete understanding of the process system ranging from the rate of reaction, bioreactor configuration and design, process control and finally the whole process operation. Information obtained from the model system can be used to improve and in some cases optimise the productivity of the available process. Practical work as well as computer simulation should work side-by-side so that knowledge on both sides can be exchanged for further improvement.

1.8 Research Objectives

The overall aim of this project was to obtain a complete process model of an established whole-cell system of cyclohexanone monooxygenase enzyme-catalysed reaction and simultaneously gain a greater understanding of the fundamental criteria in process/bioreactor design. In order to achieve the overall aim, several specific objectives were defined:

1. Theoretical study of enzyme-catalysed reaction based on different assumptions used to derive the rate expression and the range of validity of these assumptions.

2. Theoretical analysis of enzyme-catalysed reaction with inhibition and the dynamics of the system.

3. Develop a complete intrinsic rate expression of enzyme-catalysed Baeyer-Villiger reaction based on the proposed reaction mechanism.

4. Using an established Baeyer–Villiger type bioconversion of bicyclic ketone (bicyclo[3.2.0]-hept-2-en-6-one) forming chiral lactones ((-)1(S)5(R)2-oxabicyclo[3.3.0]oct-6-en-3-one and (-)1(R)5(S)3-oxabicyclo[3.3.0]oct-6-en-2-one) with cyclohexanone monooxygenase enzyme as the biocatalyst to obtain a set of kinetic parameters using appropriate experimental data.

5. Mathematically model the process system based on two bioreactor configurations (batch

and fed-batch reactor configurations) and carry out appropriate experimental work for model verification.

6. Develop a model system with the effect of membrane cell diffusion. Characterising the effect using Thiele modulus which later translated into graphical simulations.

7. Develop a model of coupled reactions based on cofactor regeneration of cyclohexanone monooxygenase enzyme (CHMO) and alcohol dehydrogenase enzyme (ADH) which later accompanied by appropriate experimental work.

1.9 Thesis Structure

Chapter 1 concludes with an overall project aims and a set of specific objectives. These objectives were defined from the desire to construct a complete biocatalytic process model and the shortcomings of the current model being developed. The rest of the thesis develops from these initial research objectives. In *Chapter 2* a detailed theoretical investigation of the uniqueness of enzyme-catalysed system is carried out. Work mainly based on the mathematical analysis of the derivation of biocatalytic rate expression following the two different assumptions. Validity of these two assumptions is clearly stated. This chapter also looks at the enzyme-catalysed system with substrate and product inhibitions. The differences between the dynamics of the two systems are carefully compared. *Chapter 3* begins with the derivation of the rate expression of cyclohexanone monooxygenase enzyme-catalysed reaction with appropriate assumptions to simplify the work. This chapter also concentrates on the determination of the kinetic rate constants defining the rate expression derived initially. Appropriate enzyme assay for data fitting procedure is clearly presented. In *Chapter 4*, two model systems describing batch and fed-batch bioreactor configurations are constructed. Separate simulations of both systems are presented with appropriate experimental data, verifying the work. Attempt to model a reaction with diffusion limitation is given in *Chapter 5*. The steps of carrying out the modelling work is carefully listed. The chapter concludes with 3 dimensional space-time simulations representing the effect of reaction and diffusion. One of the advantages of using the whole-cell biotransformation is exploiting the cofactor regeneration in the cellular system, *Chapter 6* carefully explains the method of coupling the two reaction systems and later verifies with the appropriate experimental

data. Finally, *Chapter 7* gives the overall conclusions, contribution of this research, comparison between results in a tabulated form and the fulfilment of the initial objectives. In addition, some avenues for further research are also suggested.

Chapter 2

General Mechanistic Analysis of Enzyme-Catalysed Systems

2.1 Introduction

The study of enzyme-catalysed reactions depends entirely on a mechanism that describe a particular reaction. A reaction mechanism actually refers to the route that the reaction takes during the conversion of a substrate to a particular product. Such information will lead to the understanding of the kinetics of a reaction under investigation. The method of analysing the kinetics based on the reaction mechanism has been applied to the enzyme catalysis following the celebrated work of Michaelis and Menten in 1913 (Michaelis and Menten, 1913). The expression was then further refined and mathematically explained by Briggs and Haldane incorporating the concept of steady-state enzyme kinetics (Ainsworth, 1977). The method differs from that of the recent work by Chen and Woodley (2002) and Chen *et al.* (2002) which was based on artificial neural network (ANN) to predict the formation of product during a reaction. Such method however, does not provide the parameters for which the substrate, cofactor or cell density could be controlled and varied. Despite of lacking of these parameters, ANN can still provide fast analysis of enzyme reaction especially when the network *polynomial* that described a system is fully "trained" with a sufficient amount of experimental data.

One of the areas that depends on the knowledge of enzyme kinetics is metabolic engineering. Reactions that occur inside a single cell during a growth period should be appropriately studied in order to connect one reaction to the other, forming a network between these reactions. As

an example, the identification of the relationship between ATP (adenosine 5'–triphosphate) and ADP (adenosine 5'–diphosphate) during the formation of pyruvate or the initial formation of pyruvate in the phosfotransferase (PTS) system (Hatzimanikatis and Bailey, 1997).

However, an enzyme-catalysed reaction is only a part of the metabolic network which can be exploited in biochemical reaction engineering. This can be observed when a mechanism that describes an enzyme-catalysed reaction interconnects with other cellular activities, for example, the consumption of cofactor, (NAD(P)H) in some reactions. Therefore, the knowledge of enzyme activity and stability in a cell is particularly important especially in understanding the reactions that occur in enzyme-catalysed reactors (Vasic-Racki *et al.*, 2003).

In the subsequent sections, a number of criteria required in analysing enzyme-catalysed reaction are described in detail. These include the original work of Michaelis and Menten in 1913 which was then continued by Briggs and Haldane in 1925 as described in Cornish-Bowden (1995). The work of the latter group on the proposed assumption according to Heineken *et al.* (1967) was inconsistent with the modelled system. This is theoretically re-examined and carefully re-formulated for further understanding. This is essential in order to understand the current work under investigation. The theoretical aspects of this study include the mathematical analysis of the enzyme mechanism, reformulation of rate expression when certain conditions failed and finally, computer simulations that support the analysis.

Before carrying out any mechanistic study of an enzyme reaction, one should bear in mind that an enzyme actually behaves as a catalyst. This is similar to the chemical catalysis, for example, a simple magnesium oxide-catalysed hydrogen peroxide decomposition forming water and oxygen. Without magnesium oxide, hydrogen peroxide can still decompose, but in a very slow rate and it might take weeks or months for the reaction to reach completion. A similar reaction can also be carried out with catalase, an enzyme secreted from the liver that gives out the same observation. From these two similar reactions, one should come to a conclusion that catalyst does speed up a reaction and the way it is doing this is by lowering the activation energy of a particular reaction. A schematic description of the activation energy and the effect of enzyme catalysis is given in *Figure 2.1.* Other characteristics of enzyme, such as its specificity and activity have been discussed previously in *Chapter 1* and further discussion of the active-

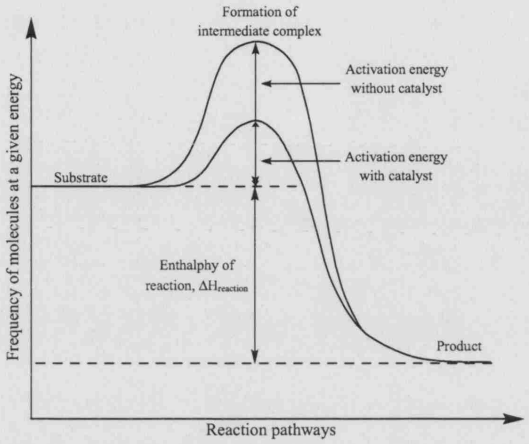

Figure 2.1: Activation energy of enzyme-catalysed reaction.

sites that give rise to the reaction specificity will be mentioned at the end of this chapter based on the cyclohexanone monooxygenase enzyme-catalysed reaction.

In order to describe any enzyme-catalysed reaction, one has to know the route that it follows in order to form the product(s). Consider a reaction of substrate [S] forming [P], catalysed by an enzyme [E], with [·] represents the concentration of a component. The mechanism of such reaction could be written as follows;

$$[E] + [S] \underset{k_{-1}}{\overset{k_1}{\rightleftharpoons}} [ES] \xrightarrow{k_2} [E] + [P]$$

Figure 2.2: Simple irreversible enzyme-catalysed reaction with single substrate and product.

Each term k_i, represents the rate constant of a particular pathway with units of mol·s^{-1} or s^{-1}, where i is the number of pathways observed in a mechanism and the positive and negative signs represent the forward and reverse reaction respectively. This is perhaps the simplest mechanism one could use to understand enzyme kinetics. However, in most of the enzyme-catalysed reactions, the mechanisms are much complicated then the one described above.

The mechanism can be divided into two main parts. Initially, the substrate, [S] is bound to the enzyme to form enzyme-substrate complex, [ES]. This conversion occurs reversibly with

the forward rate constant k_1 and that of k_{-1} for reverse reaction. Formation of [ES] is rather temporary, as it is being formed, it is immediately converted to product, [P] and enzyme, [E]. The formation of both products are governed by the rate constant k_2. This should be the basic mechanism of enzyme kinetics with irreversible product formation. There is another similar form of kinetics but with reversible product formation, this means that there is a negative i for the rate constant, k_{-2} acting reversibly and forcing the reaction to shift to the left, forming the enzyme-substrate complex, [ES]. This is clearly depicted in *Figure 2.3.*

$$[E] + [S] \underset{k_{-1}}{\overset{k_1}{\rightleftharpoons}} [ES] \underset{k_{-2}}{\overset{k_2}{\rightleftharpoons}} [E] + [P]$$

Figure 2.3: Simple reversible enzyme-catalysed reaction with single substrate and product.

The type of kinetics shown above normally occurs in most of the biological systems. Here, an equilibrium state will be established between the forward and reversed reaction as it proceeds. This will produce different forms of rate expression compared to that of the irreversible one and the differences will be discussed further in the next section.

2.1.1 Method of Deriving the Steady-State Michaelis-Menten Rate Expressions

The mechanism of enzyme-catalysed reaction devised previously should conform with the experimental data collected at suitable reaction conditions (temperature, pH, etc.). When both are agreed, the kinetic expression of mechanism shown in *Figure 2.2* can then be formulated. For further understanding of the main mechanism and the derivation of the kinetic expression related to this work, a detailed derivation of the simplified Michaelis-Menten kinetics is shown below. This can be obtained either by applying the equilibrium approximation or the quasi steady-state approximation. The formulation is based on the three assumptions; (1) there should be a formation of at least one enzyme intermediate complex, (e.g. [ES]) in the reaction mechanism, (2) the amount of substrate is such that greater than the amount of enzyme present in the reaction medium, ([S] $\gg$ [E]) so that the formation of enzyme intermediate complex, [ES] does not change the concentration of [S], (3) and the concentration of product, [P] is very small so

that it is valid only for the initial rate data. If the concentration of product, [P] in the reaction medium is very high, the reaction can be affected by product inhibition and the simple form of Michaelis-Menten expression will become invalid.

Mass balances of all species participated in the mechanism shown in *Figure 2.2* are given by a system of autonomous nonlinear differential equations;

$$\frac{d[E]}{dt} = -k_1[E][S] + (k_{-1} + k_2)[ES] \tag{2.1}$$

$$\frac{d[S]}{dt} = -k_1[E][S] + k_{-1}[ES] \tag{2.2}$$

$$\frac{d[ES]}{dt} = k_1[E][S] - (k_{-1} + k_2)[ES] \tag{2.3}$$

$$\frac{d[P]}{dt} = k_2[ES] \tag{2.4}$$

according to Briggs and Haldane and noted by Segel (1993), the total enzyme concentration can be expressed as an independent parameter, $[E]_T$. This can be achieved by adding equations (2.1) and (2.3) that leads to

$$\frac{d[E]}{dt} + \frac{d[ES]}{dt} = 0$$

hence,

$$\frac{d([E] + [ES])}{dt} = 0$$

and upon integration gives

$$[E]_T = [ES] + [E]$$

Upon substitution of this term into equations (2.2) and (2.3), the corresponding equations are obtained;

$$\frac{d[S]}{dt} = -k_1[E]_T[S] + (k_1[S] + k_{-1})[ES] \tag{2.5}$$

$$\frac{d[ES]}{dt} = k_1([E]_T - [ES])[S] - (k_{-1} + k_2)[ES] \tag{2.6}$$

with the above simplification, the rate of enzyme consumption $\frac{d[E]}{dt}$ is automatically incorporated in the coupled equations. Equations (2.5) and (2.6) can be combined and this requires an

assumption proposed again by Briggs and Haldane that,

$$\frac{d[ES]}{dt} \approx 0$$

provided that the amount of enzyme present in a reaction mixture is such that $[E]_T \ll [S]$, by putting [ES] in terms of [S] and substitution of this term into equation (2.6) results in a final rate expression given in terms of $\frac{d[S]}{dt}$;

$$\frac{d[S]}{dt} = -\frac{k_2[E]_T[S]}{\left(\frac{k_{-1}+k_2}{k_1}\right) + [S]}. \tag{2.7}$$

Further simplification of the above expression with $V_{max} = k_2[E]_T$ and $K_m = \left(\frac{k_{-1}+k_2}{k_1}\right)$ reduces equation (2.7) into;

$$v_{irr} = \frac{d[S]}{dt} = -\frac{d[P]}{dt} = -\frac{V_{max}[S]}{K_m + [S]} \tag{2.8}$$

Equation (2.8) is known as the Michaelis-Menten model that describes the kinetics of enzyme reaction, and this is true if the expression is put in terms of $\frac{d[P]}{dt}$ and plot the rate, v_{irr} against the substrate, [S]. A general plot generated is in the form given in *Figure 2.4*. With the simplification of equation (2.7), it is not possible to determine the individual rate constants k_i, and this is true for all rate expressions describing irreversible enzyme reactions.

On the other hand, if an enzyme-catalysed reaction follows the mechanism depicted in *Figure 2.3*, thus the balances now become;

$$\frac{d[S]}{dt} = -k_1[S][E] + k_{-1}[ES] \tag{2.9}$$

$$\frac{d[ES]}{dt} = k_1[S][E] - k_{-1}[ES] - k_2[ES] + k_{-2}[P][E] \tag{2.10}$$

$$\frac{d[P]}{dt} = k_2[ES] - k_{-2}[P][E] \tag{2.11}$$

Applying the similar assumption as that for the irreversible system leads to the final rate expression of the form;

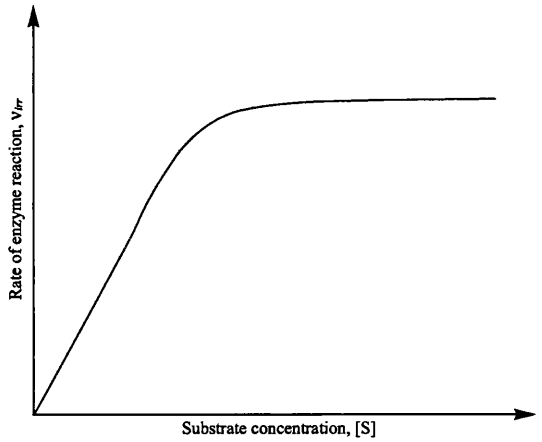

Figure 2.4: General plot of a simple Michaelis-Menten type kinetics.

$$v_{rev} = \frac{d[S]}{dt} = -\frac{d[P]}{dt} = -\frac{V_{max_f}\frac{[S]}{K_{m_{[S]}}} - V_{max_r}\frac{[P]}{K_{m_{[P]}}}}{1 + \frac{[S]}{K_{m_{[S]}}} + \frac{[P]}{K_{m_{[P]}}}} \tag{2.12}$$

with V_{max_f}, V_{max_r}, $K_{m_{[S]}}$ and $K_{m_{[P]}}$ defining $k_2[E]_T$, $k_{-1}[E]_T$, $\frac{k_2+k_{-1}}{k_1}$ and $\frac{k_2+k_{-1}}{k_{-2}}$ respectively. The terms V_{max_f} and V_{max_r} represent maximum velocity of forward and reverse reactions respectively while $K_{m_{[S]}}$ and $K_{m_{[P]}}$ represent Michaelis constants for substrate and product respectively. Equation (2.12) can be reduced into equation (2.8) whenever the product [P] is initially absent during the reaction.

The reversible rate expression can also allow one to determine the individual rate constant involved in the mechanism. These values are important for the analysis of how fast one species in the mechanism is converted to another as well as estimating the equilibrium constants provided by these forward and backward values. For the mechanism shown in *Figure 2.3*, the kinetic constants given previously can be rearranged in terms of rate constants k_i, given in *Table 2.1.*

Another advantage of dealing with reversible rate expression is that, it gives the ability to find the Haldane relationship (Cleland, 1982) by manipulating the kinetic constants given in *Table 2.1.* The terms avoid any redundancy between the kinetic constants obtained from the kinetic derivation. These redundancies are normally expressed in terms of K_{eq}. Following the method provided by the above citation, using equation (2.12) at equilibrium state;

Rate constant	Kinetic constant terms
k_1	$\frac{V_{max_f}+V_{max_r}}{K_{m_{[S]}}[E]_T}$
k_{-1}	$\frac{V_{max_r}}{[E]_T}$
k_2	$\frac{V_{max_f}}{[E]_T}$
k_{-2}	$\frac{V_{max_f}+V_{max_r}}{K_{m_{[P]}}[E]_T}$

Table 2.1: Individual rate constant determined from the kinetic parameters.

$$v_{rev}^{eq} = \frac{d[P]}{dt} = 0$$

hence,

$$\frac{V_{max_f}\frac{[S]}{K_{m_{[S]}}} - V_{max_r}\frac{[P]}{K_{m_{[P]}}}}{1 + \frac{[S]}{K_{m_{[S]}}} + \frac{[P]}{K_{m_{[P]}}}} = 0$$

upon simplification;

$$\frac{V_{max_f}[S]_{eq}}{K_{m_{[S]}}} = \frac{V_{max_r}[P]_{eq}}{K_{m_{[P]}}} \tag{2.13}$$

this can be further reduced into;

$$K_{eq} = \frac{V_{max_f}K_{m_{[P]}}}{V_{max_r}K_{m_{[S]}}} \tag{2.14}$$

where K_{eq} defines $\frac{[P]_{eq}}{[S]_{eq}}$ and the rate expression in terms of K_{eq} can be written as;

$$v_{rev}^{eq} = \frac{d[P]}{dt} = \frac{V_{max_f}\left([S] - \frac{[P]}{K_{eq}}\right)}{K_{m_{[S]}}\left(1 + \frac{[P]}{K_{m_{[P]}}}\right) + [S]} \tag{2.15}$$

Therefore, with the two types of mechanisms discussed above, one could easily derive the rate expression algebraically applying the rules of Briggs and Haldane. However, mechanisms of enzyme system do not always follow the simplified route as those shown in *Figure 2.2* and *2.3.*

A system could also have two enzyme-substrate complexes as shown below;

$$[E] + [S] \underset{k_{-1}}{\overset{k_1}{\rightleftharpoons}} [ES] \underset{k_{-2}}{\overset{k_2}{\rightleftharpoons}} [EP] \underset{k_{-3}}{\overset{k_3}{\rightleftharpoons}} [E] + [P]$$

Figure 2.5: Enzyme-catalysed reaction with 2 intermediate complexes.

With such system, the algebraic manipulation will become tedious and cumbersome especially when the number of species in the mechanism increase accordingly. A simple method devised by King and Altman, (King and Altman, 1956) is presented here which will be used throughout this work in order to derive the rate expression for the model system.

The mechanism of reaction shown in *Figure 2.5* is initially arranged in such a way that each enzyme species is connected in a circular form, this can be clearly seen when the free enzyme species [E] on the far right of the mechanism is dropped and then connected to [E] on the far left. This rearrangement is depicted in *Figure 2.6.* Such a form is important in the graphical derivation of rate expression according to King-Altman method which is described in detail in the subsequence paragraph.

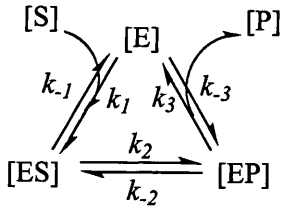

Figure 2.6: King-Altman arrangement of enzyme mechanism from *Figure 2.5.*

Before proceeding with the method of King and Altman, there is another way of representing an enzyme mechanism. The method was introduced by Cleland (1963*a*,*b*) among others, to describe inhibition in a particular reaction. The notation generally separates between the substrate and product involved in a reaction together with all the enzyme complexes. For the system given in *Figure 2.5*, the Cleland's notation can be represented as follows;

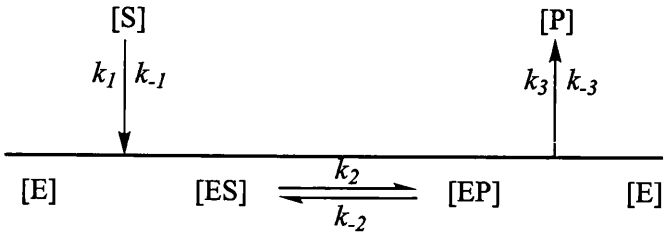

Figure 2.7: Cleland's notation for enzyme reaction with two enzyme complexes.

King-Altman Method of Deriving Rate Expressions

The method is entirely based on the steady-state kinetics of several enzyme containing species $[EX]_i$. The concentration of these species relative to the total concentration of enzyme, $[E]_T$ given by;

$$\frac{[EX]_i}{[E]_T}$$

is a quotient of two summation of terms. Each of these terms is the product of $(n-1)$ different rate constants and the appropriate concentrations. Similarly, each term in the numerator of the expression for;

$$\frac{[EX]_m}{[E]_T}$$

involves the rate constants as well as concentrations associated with reaction steps happen individually or in sequence that lead to the enzyme containing species $[EX]_m$.

In addition to that, the $(n-1)$ rate constants in each term are associated with $(n-1)$ reaction steps where each of the $(n-1)$ different enzyme containing species $[EX]_i$ is a reactant, given that $i \neq m$. All of the possible combinations of $(n-1)$ rate constants which follow this rule are present as numerator terms in the expression for $\frac{[EX]_m}{[E]_T}$ while the denominator terms for $\frac{[EX]_m}{[E]_T}$ is the sum of several different numerators. The total number of combinations of $(n-1)$ rate constants can be computed using elementary probability. If a reaction mechanism involves m reversible steps inter–converting the n different $[EX]_i$'s, the total number of combinations of

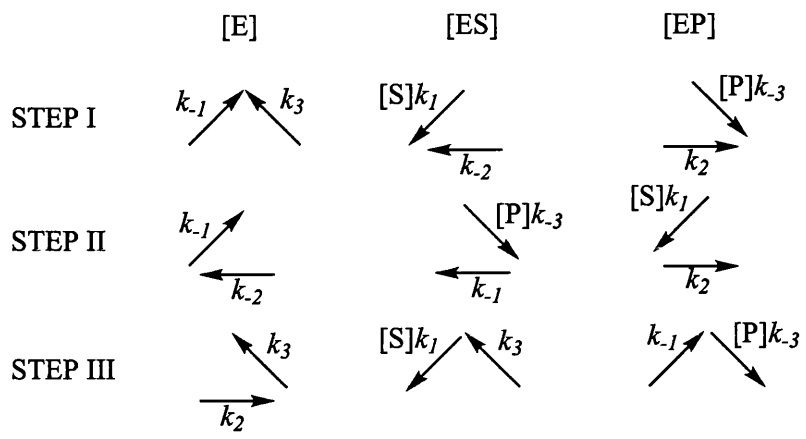

Figure 2.8: Schematic representation of the King-Altman method.

m steps taken $(n-1)$ at a time is given by;

$$ {}_mC_{(n-1)} = \frac{m!}{(n-1)!(m-n-1)!}. $$

From this total number of combinations, some may involve cycles of reaction steps. These combinations are not included since they do not conform with the stated requirements. Therefore, for every cycle consisting of r steps, where r is within $2 \leq r \leq (n-1)$, there should be

$$ {}_{(m-r)}C_{(n-1-r)} = \frac{(m-r)!}{(n-1-r)!(m-n+1)!} $$

combinations that must be deducted from the total. This can be applied schematically based on *Figure 2.6* and depicted in *Figure 2.8.*

The schematic representation of the relative concentration of each enzyme complex species is directly proportional to the summation of the three rate constant terms in each column shown in *Figure 2.8.* This can be combined into;

$$ \frac{[E]}{[E]_T} = (k_{-1}k_3 + k_{-1}k_{-2} + k_2k_3) \tag{2.16} $$

$$ \frac{[ES]}{[E]_T} = ([S]k_1k_{-2} + [P]k_{-1}k_{-3} + [S]k_1k_3) \tag{2.17} $$

$$\frac{[EP]}{[E]_T} = ([P]k_{-3}k_2 + [S]k_1k_2 + [P]k_{-1}k_{-3}) \tag{2.18}$$

and the total enzyme concentration, $[E]_T$ is given as

$$[E]_T = [E] + [ES] + [EP]. \tag{2.19}$$

Since the species balance of the product formation is given by,

$$\frac{d[P]}{dt} = \frac{([EP]k_3 - [E][P]k_{-3})[E_T]}{[E]_T} \tag{2.20}$$

Therefore, substituting equations (2.16) to (2.19) into (2.20) results in;

$$\frac{d[P]}{dt} = \frac{(k_1k_2k_3[S] - k_{-1}k_{-2}k_{-3}[P])[E]_T}{k_{-1}k_{-2} + k_{-1}k_3 + k_2k_3 + (k_1k_{-2} + k_1k_3 + k_1k_2)[S] + (k_{-2}k_{-3} + k_{-1}k_{-3} + k_2k_3)[P]} \tag{2.21}$$

Upon simplification of the rate constant terms into the kinetic constants as described previously, equation (2.21) should reduce into a similar form to that of equation (2.15).

Mathematical Description of the King-Altman Method

King-Altman method can be mathematically described using matrix operations of linear algebra. Cramer's rule which is mainly used in solving simultaneous equations can be applied here in order to determine the relative concentration of all enzyme intermediate complexes $[EX]_i$ in enzyme-catalysed systems. The theorem and proof of Cramer's rule are supplied in *Appendix D* for further reference. Now, consider the system of enzyme mechanism similar to that of *Figure 2.5* for n number of intermediates. Generally, let the number of enzyme complexes present in an enzyme reaction equal to $[EX]_i$. Thus, at the steady-state condition;

$$-\sum_{j=1}^{n} k_{ij}\frac{[EX]_i}{[E]_T} + \sum_{j=1}^{n} k_{ji}\frac{[EX]_j}{[E]_T} = 0, j \neq i \tag{2.22}$$

where k_{ij} represents the product of rate constants and the associated concentration factors. The relative concentrations of enzyme intermediate complexes can be summarised in the form of,

$$\sum_{i=1}^{n} \frac{[EX]_i}{[E]_T} = 1.$$

As an example, consider the m^{th} enzyme intermediate complex, $[EX]_m$ to set up n steady-state linear equations. Applying Cramer's rule in order to determine the relative concentration $[EX]_m$ leads to;

$$\frac{[EX]_m}{[E]_T} = \frac{\begin{vmatrix} -\Sigma k_{1j} & k_{21} & \cdots & k_{n1} \\ k_{12} & -\Sigma k_{2j} & \cdots & k_{n2} \\ \vdots & \vdots & \vdots & \vdots \\ 1 & 1 & 1 & 1 \\ . & . & . & . \\ k_{1n} & k_{2n} & \cdots & -\Sigma k_{nj} \end{vmatrix}}{\begin{vmatrix} -\Sigma k_{1j} & k_{21} & \cdots & k_{n1} \\ \vdots & \vdots & \vdots & \vdots \\ 1 & 1 & 1 & 1 \\ . & . & . & . \\ k_{1n} & k_{2n} & \cdots & -\Sigma k_{nj} \end{vmatrix}} \tag{2.23}$$

It is apparent that the denominator of the determinant equation (2.23) above has the same expression as that of every $\frac{[EX]_i}{[E]_T}$ summation of n numerators. Thus, consider the numerator of equation (2.23) and upon a reduction into $(n-1) \times (n-1)$ determinant, gives;

$$(-1)^{2m} \begin{vmatrix} -\Sigma k_{1j} & k_{21} & \cdots & k_{n1} \\ k_{12} & -\Sigma k_{2j} & \cdots & k_{n2} \\ k_{13} & k_{23} & -\Sigma k_{3j} & k_{n3} \\ . & . & . & . \\ k_{1n} & k_{2n} & \cdots & -\Sigma k_{nj} \end{vmatrix} \tag{2.24}$$

The diagonal elements of the above matrix obviously show the possible values from 1 to n for all index j, while the elements represented by index m give the enzyme intermediate complexes which only occur as a final index in a term of each of the expanded diagonal elements given by

$$\alpha_{ii} = \sum_{j=1}^{n} k_{ij}, i \neq m.$$

This concludes a detail description of the King-Altman method of deriving any enzyme-catalysed rate expressions. The method will be most useful especially in dealing with the first section of *Chapter 3* as well as in the kinetic studies of cyclohexanone monooxygenase enzyme-catalysed Baeyer-Villiger reaction system in the subsequent section of the same chapter.

2.1.2 Parameter Estimation for Simple Rate Expressions

An analysis of enzyme kinetics would not be complete if it does not quantitatively describe the kinetic parameters of the system. The values are important especially if one wants to compare the binding properties of two different enzyme-catalysed reactions. Consider a system described by a simple mechanism shown in *Figure 2.2* where a substrate, $[S]$ binds with an enzyme, $[E]$ forming an enzyme-substrate complex that dissociate irreversibly to form a product, $[P]$ and a free enzyme. The reaction rate of such system is expressed mathematically by equation (2.8) and it is governed by two kinetic parameters, V_{max} and K_m. For the mechanism described above, V_{max} is a measure of catalytic efficiency of an enzyme, while K_m described the affinity of enzyme binding property. K_m is initially defined by rate constant terms as;

$$K_m = \frac{(k_{-1} + k_2)}{k_1}$$

and if

$$k_{-1} \gg k_2$$

hence, the first definition of K_m reduces to

$$K_m = \frac{k_{-1}}{k_1}.$$

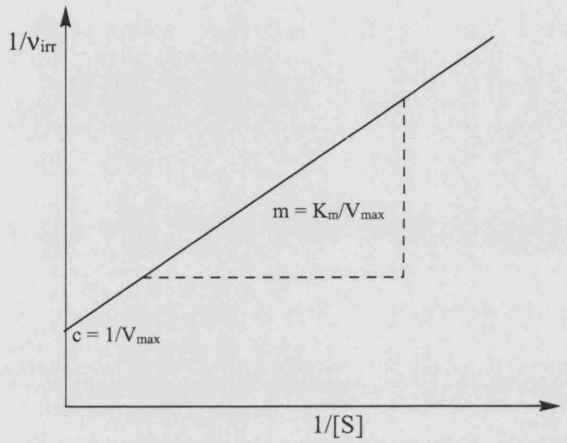

Figure 2.9: Graphical plot to determine V_{max} and K_m.

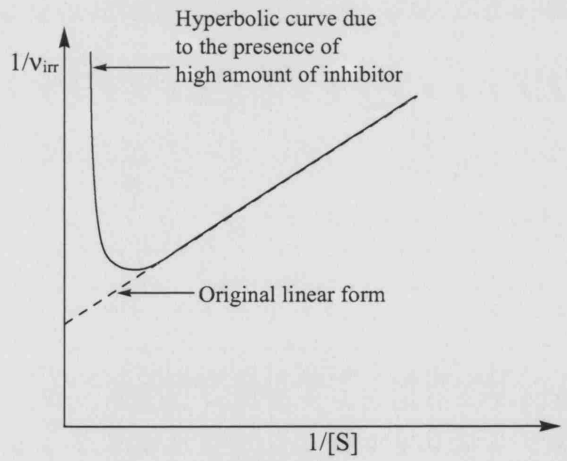

Figure 2.10: The effect of high concentration of inhibitor on the shape of the curve (e.g. substrate concentration, [S] in non-competitive substrate inhibition).

This form of K_m is called the true equilibrium dissociation constant of an enzyme-catalysed reaction or sometimes denoted as K_S to differentiate from that of the Michaelis constant.

A simple method of finding these parameters is by manipulating equation (2.8) into a linear form of $y = mx + c$. Inverting both left and righthand sides gives equation (2.8) of the form;

$$\frac{1}{v_{irr}} = \frac{K_m}{V_{max}}\left(\frac{1}{[S]}\right) + \frac{1}{V_{max}} \tag{2.25}$$

It transforms into a linear equation which can easily be plotted in order to obtained both V_{max} and K_m. Comparing that with the general linear form, the gradient, m is represented by $\frac{K_m}{V_{max}}$ and the y-intercept, c is defined by $\frac{1}{V_{max}}$. This method of determining the parameters is called the Lineweaver-Burk plot and it is shown graphically in *Figure 2.9.* The method can also be applied to systems with inhibitions either by the same substrate or by other external inhibitor, provided that the level of inhibition is low enough for the initial rate values. If the value of inhibitor is extremely high such that it exceeds the allowable range, a graph of the form given in *Figure 2.10* should be obtained. With such a plot, it is not possible to accurately determine both kinetic parameters and therefore, another alternative should be sought. A method known as progress curve analysis of enzyme-catalysed reaction that was initially introduced by Bates and Frieden (1973*a*,*b*) and successfully applied by Duggleby and Morrison (1977, 1978); Boeker (1984, 1987); Duggleby and Wood (1989); Frieden (1994); Goudar *et al.* (1999) and Straathof (2001) can be used to tackle this present problem. A complete description of the progress curve method of treating the rate expression as well as a suitable experimental work that follows the analysis will be discussed in the next chapter of this work.

2.2 Dynamic Analysis of Enzyme-Catalysed Systems

The analysis of the enzyme system, previously described revolves around the steady-state analysis based on the assumption proposed by Briggs and Haldane. It is mainly used to simplify the differential equations defining species balances within the system. The assumption is rather *crude* and sometimes it does not accurately define the dynamic of each species within an enzyme reaction. Attempts to study the molecular dynamics of enzyme system which described the mechanism for generation of dynamic behaviour in terms of molecular structure was initilised

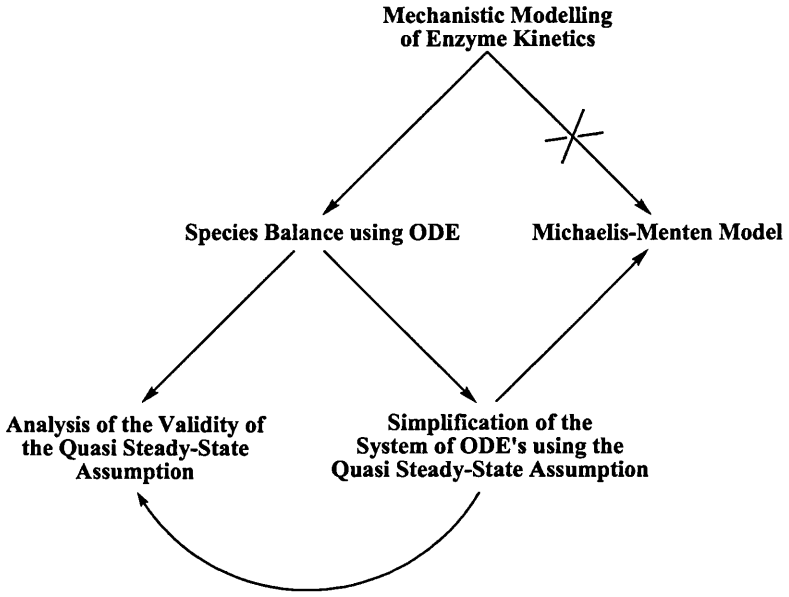

Figure 2.11: Relationship between a system of ordinary differential equations (ODE's) of enzyme intermediates and the application of the quasi steady-state assumption which leads to the Michaelis-Menten model.

by a few authors, namely, Heineken *et al.* (1967); Cha (1970); Lim (1973); Crooke *et al.* (1979); Palsson (1987) and most recently from Segel and Slemrod (1989); Schnell and Maini (2000) and Tzafriri (2003).

One of the most important studies of the kinetics of enzyme system is the assumption used to express the enzyme-substrate interactions in terms of the Michaelis-Menten model. This can only be achieved by looking at the mechanism of enzyme species described by the autonomous ordinary differential equations. A diagram showing the interconnection between these studies is given in *Figure 2.11.* The small cross that leads to the Michaelis-Menten model shows that the expression can only be formed by taking the route on the left hand side of the figure. Therefore it is obvious that the construction of the model is highly dependent on the simplification suggested by Briggs and Haldane and the validity of such an assumption should be fully understood. The first work of Heineken *et al.* (1967) marked the beginning of dynamic analysis of enzyme-catalysed reaction which the main objective was to prove the validity of the Briggs-Haldane

assumption. Such an analysis is important especially if a reaction occurs *in vivo*, where enzyme concentration is usually present at a higher or at least the same level to that of substrate. Such a condition will break the assumption and the use of the Michaelis-Menten model for any kinetic studies would only lead to erroneous parameter values.

The main objective of this work is to fully understand the dynamics behind the Michaelis-Menten model that could not be described by the steady-state approach. This will then lead to the understanding of the mechanisms by which biochemical networks generate and regulate any biological processes. Results from this analysis will provide a better understanding when modelling the system of enzyme-catalysed Baeyer-Villiger reaction in the following chapter. The literature referred during this present study have not shown any detailed modelling work of cyclohexanone monooxygenase enzyme (Zambianchi *et al.*, 2000, 2002). The kinetics of such an enzyme have not been properly studied, where the plot of the rate of reaction was analysed using the whole cell system, which values are not appropriate in describing the kinetics of the particular enzyme itself (Doig *et al.*, 2001, 2002). In a similar work, the rate plots also show that the whole cell is affected by both substrate and product concentrations during the course of reactions (Chen *et al.*, 2002). This phenomenon has been successfully modelled by Chen and Woodley (2002), however, the use of polynomial function based on the neural network modelling could not give the kinetic parameters which values are utmost important in the study of enzyme kinetics. In order to re-analyse the above results, the experiment was repeated in this work and the rates were plotted in *Figures H* and *H* for variable substrate and product concentrations respectively. These initial rate values are important in an attempt to obtain the kinetic parameters of the whole-cell reaction that exhibits both substrate and product inhibitions which will be discussed in *Chapter 2.* These values are not particularly useful in such an analysis, but they can be used for a purpose of comparing with the actual parameters based on a different technique in studying enzyme kinetics.

Attempts to obtain the kinetic parameters for the monooxygenase enzyme were also carried out by Zambianchi *et al.* (2000) using the natural substrate (cyclohexanone) at very low concentrations. Such work could only be described by applying the basic Michaelis-Menten model without inhibition, which results are not particularly important in an industrial scale

biotransformation with a high concentration of substrate.

In subsequent sections, theoretical analyses on the assumptions used to model the Michaelis-Menten kinetics were carried out. These were done using a simple mechanism of enzyme reaction shown in *Figure 2.2.* The use of the mechanism with one enzyme-substrate complex should simplify the analysis that follows. Since the assumption is based on the rate of disappearance of the enzyme-substrate complex with the presence of minute amount of enzyme, therefore, the initial analysis was carried out using every species in the given figure. The study of each species taking part in the mechanism will provide a general idea on how the quasi steady-state is imposed on the system and subsequently look at the effect of varying the amount of enzymes in a reaction. It is highly important to understand that the purpose of quasi steady-state assumption is basically to simplify the rate equation into a manageable form (following the route shown in *Figure 2.11*) so that the kinetic parameters from the expression can be estimated.

The stability of the system was also analysed based on the eigenvalues generated from its Jacobian matrix. This was carried out on the same system but with two different assumptions, standard and total quasi steady-state, which will be further explained in Section 2.2.1. Due to the *superstability* behaviour of the system, further analysis on the eigenspaces at equilibrium point was also carried out.

2.2.1 Effect of Enzyme to Substrate Ratio on the Dynamics of Enzyme System

Any systems described by differential equations either autonomous or non-autonomous type, exhibits somewhat interesting dynamic behaviours. Similar to that of enzyme-catalysed reaction, the degenerate typed system of ordinary differential equations gives a vast amount of information to be explored and numerically analysed. Here, the simplest mechanism of one substrate, [S] and one product, [P] with an intermediate complex, [ES] was fully explained.

Consider the system which was previously described in Section 2.1.1, by a set of autonomous differential equations (2.1) to (2.4). The equations are stated again for easy reference.

$$\frac{d[E]}{dt} = -k_1[E][S] + (k_{-1} + k_2)[ES]$$

Condition	$[E]_T$	$[S]_0$	k_1	k_{-1}	k_2	μ	σ	α
A	2.5	2.5	10	1	10	1.0	0.44	0.4
B	0.001	10	10	1	10	0.0001	0.11	0.1
C	10	0.001	10	1	10	10000	1100	1000

Table 2.2: Conditions used for the analysis of standard and total quasi steady-state assumptions. Values adapted from Schnell and Maini (2002).

$$\frac{d[S]}{dt} = -k_1[E][S] + k_{-1}[ES]$$

$$\frac{d[ES]}{dt} = k_1[E][S] - (k_{-1} + k_2)[ES]$$

$$\frac{d[P]}{dt} = k_2[ES]$$

Defining the total enzyme concentration, $[E]_T$ as the sum of the free enzymes, [E] and intermediate complex, [ES] and upon substitution into equations (2.2) and (2.3) leads to two simple equations describing the rate of substrate consumption, $\frac{d[S]}{dt}$ and the formation of enzyme-substrate complex, $\frac{d[ES]}{dt}$.

$$\frac{d[S]}{dt} = -k_1[E]_T[S] + (k_1[S] + k_{-1})[ES]$$

$$\frac{d[ES]}{dt} = k_1([E]_T - [ES])[S] - (k_{-1} + k_2)[ES]$$

The system is apparently not under the influence of the product, [P], therefore, the term $\frac{d[P]}{dt}$ can be decoupled from the above system. The analysis carried out in this section was based on the conditions described previously by Schnell and Maini (2002) and they are tabulated in *Table 2.2.*

The Dynamics of System with Standard Quasi Steady-State Assumption

In order to simplify the analysis, both equations (2.5) and (2.6) are rendered dimensionless with the initially defined parameters given in *Table 2.3.* Upon substitution of these parameters, the system reduces to;

$$\dot{x} = -x + (x + \sigma - \alpha)y \tag{2.26}$$

$$\mu\dot{y} = x - (x + \sigma)y \tag{2.27}$$

Dimensionless parameter	Defined variable	Dimensionless parameter	Defined variable
x	$\frac{[S]}{[S]_0}$	σ	$\frac{k_{-1}+k_2}{k_1[S]_0}$
y	$\frac{[ES]}{[E]_T}$	μ	$\frac{[E]_T}{[S]_0}$
τ	$k_1[E]_T t$	α	$\frac{k_2}{k_1[S]_0}$

Table 2.3: Parameters used to render coupled differential equations (2.5) and (2.6) into dimensionless form with $[S]_0$ as the total substrate concentration. The terms defined the values in *Table 2.2.*

where, $\dot{x}$ and $\dot{y}$ denote $\frac{dx}{dt}$ and $\frac{dy}{dt}$ respectively.

The method applied in the above derivation is based on the standard quasi steady-state assumption (sQSSA) initially proposed by Briggs and Haldane. The purpose of the system of equations is to estimate the range of parameter μ, defined as the ratio of total enzyme to the total substrate present in a reaction medium. In order to prove the similarity of the dimensionless form of equations to that given by (2.8), letting the left hand side of equation (2.27) equals to zero when $\mu \ll 1$ therefore $x - (x + \sigma)y \approx 0$ according to the QSSA and hence, with further simplification, it reduces into;

$$y = \frac{x}{(x + \sigma)} \tag{2.28}$$

and substitution of equation (2.28) into that of (2.26), a similar expression to that given by (2.8) should be obtained.

$$\dot{x} = -\frac{\alpha x}{(x + \sigma)} \tag{2.29}$$

For the purpose of this study, by preserving $\dot{y}$, the time trajectories of both x and y can be followed and compared as the ratio μ varies (i.e. $\mu \to 1$ and $\mu \gg 1$). The change of system's dynamics due to the variation of μ within the equations puts it in a category of degenerate case in singular perturbation (Heineken *et al.* (1967); Chang and Howes (1984); Schneider and Wilhelm (2000)). Further reading on the analysis of singular perturbation of enzyme-catalysed reaction can be referred to Segel (1988).

Simulation of the system with $\mu = 0.0001$ (Condition B, according to *Table 2.2*) is given in *Figure 2.12.* The corresponding phase-space plot in *Figure 2.13* clearly shows the two distinct

trajectories; fast and slow motions. These can be characterised in two different time scales; the time that characterises the duration of the initial transient during which it is assumed that the initial substrate concentration is unaltered but the enzyme-substrate intermediate proceeds through a rapid increase, and the time that describes the quasi steady-state period which the concentration of the enzyme-substrate intermediate is assumed to be at a steady-state with respect to the instantaneous substrate concentration, thus, the approximation of

$$\frac{d[ES]}{dt} = 0$$

applies. On the other hand, if Condition A is used for simulation, such characteristics are no longer apparent in the simulation given in *Figure 2.14*. Therefore, the assumption, (standard quasi steady-state) is immediately invalid. A similar behaviour is observed in *Figure 2.15* when μ is greatly increased with the value given in Condition C.

Eigenvalues analysis: Consider the system given by equations (2.26) and (2.27), upon linearisation, the Jacobian matrix, J_s for standard quasi steady-state assumption can be written as;

$$J_s = \begin{pmatrix} -1+y & x-\alpha+\sigma \\ \frac{1-y}{\mu} & -\left(\frac{x+\sigma}{\mu}\right) \end{pmatrix} \tag{2.30}$$

This leads to the eigenvalues of the system in terms of variables x and y;

$$\lambda_{s(1,2)} = \begin{pmatrix} -\frac{1}{2\mu}[(x+\sigma)+(1-y)\mu]\left(1+\sqrt{1-\frac{4\alpha\mu(1-y)}{[(x+\sigma)+(1-y)\mu]^2}}\right) \\ -\frac{1}{2\mu}[(x+\sigma)+(1-y)\mu]\left(1-\sqrt{1-\frac{4\alpha\mu(1-y)}{[(x+\sigma)+(1-y)\mu]^2}}\right) \end{pmatrix} \tag{2.31}$$

The trivial solutions of the system can be obtained by putting $\dot{x} = \dot{y} = 0$, thus

$$(x^*, y^*) = (0, 0).$$

This point can be clearly observed from *Figure 2.13* where the trajectory is attracted into one equilibrium point, i.e. the origin of the plot. Therefore, upon substitution of values of x^* and

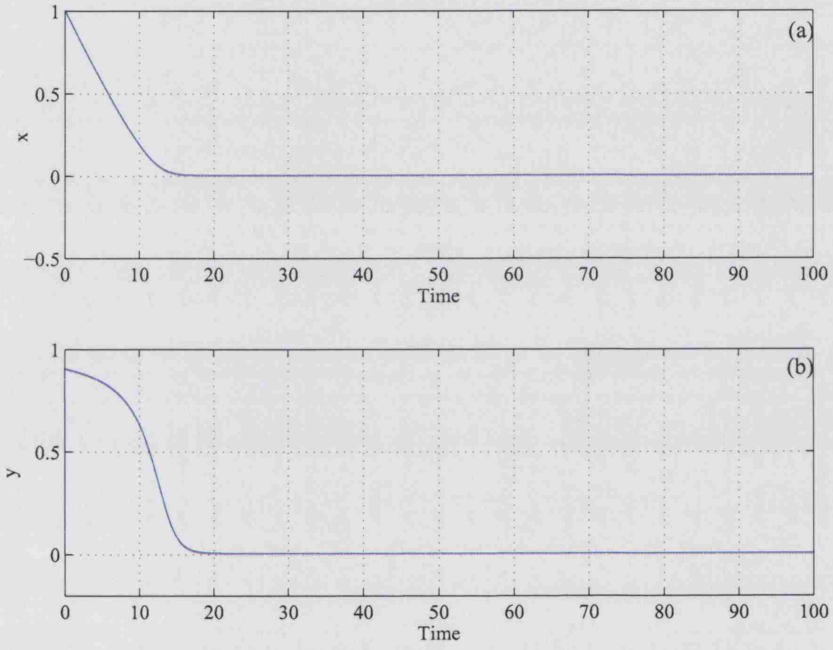

Figure 2.12: Time histories for both (a) x and (b) y at $\mu = 0.0001$, $\sigma = 0.11$ and $\alpha = 0.1$ (Following condition B from *Table 2.2*).

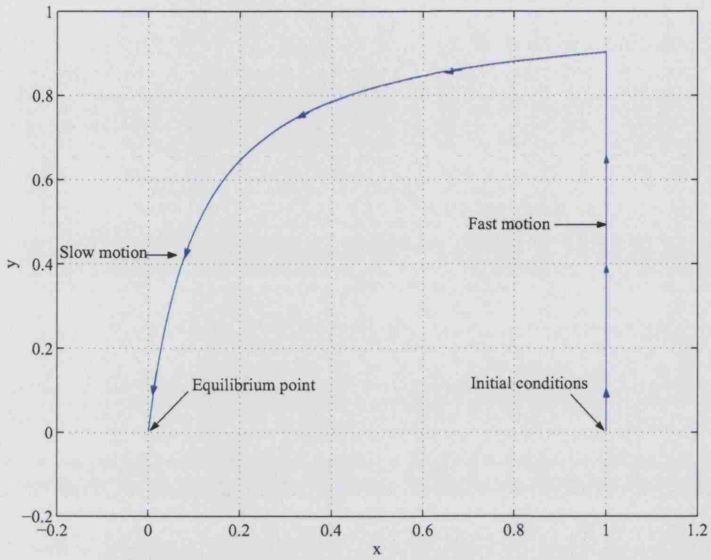

Figure 2.13: Corresponding phase-plane plot of *Figure 2.12.*

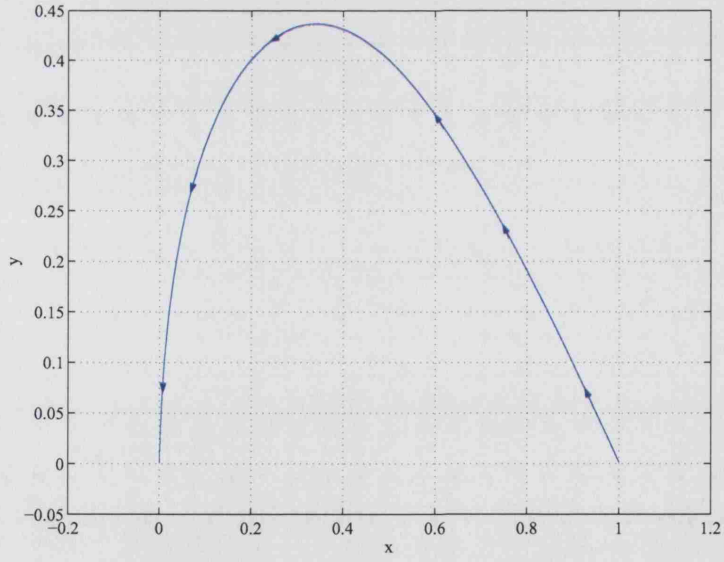

Figure 2.14: Phase-plane plot of system with $\mu = 1$ (Condition A), fast and slow trajectories are not apparent.

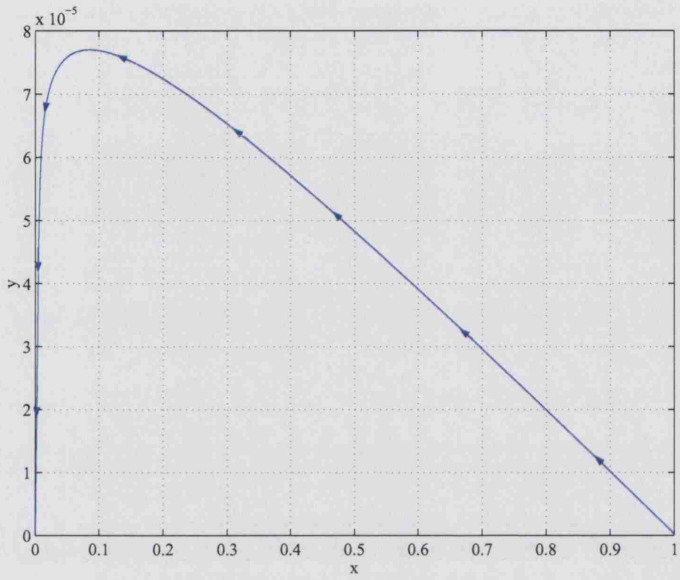

Figure 2.15: Phase-plane plot of system with $\mu = 10000$ (Condition C), a shift between fast and slow trajectories.

y^* into equation (2.31), results in the stability characteristic of this particular point, $\lambda^*_{s(1,2)}$;

$$\lambda^*_{s(1,2)} = \begin{pmatrix} -\frac{1}{2\mu}\left[(\sigma+\mu)\left(1+\sqrt{1-\frac{4\alpha\mu}{(\sigma+\mu)^2}}\right)\right] \\ -\frac{1}{2\mu}\left[(\sigma+\mu)\left(1-\sqrt{1-\frac{4\alpha\mu}{(\sigma+\mu)^2}}\right)\right] \end{pmatrix} \tag{2.32}$$

where the determinant, $\det(J^*)$ and trace, $\mathrm{tr}(J^*)$ of the Jacobian matrix are given by,

$$\det(J^*_s) = \frac{\alpha}{\mu} \tag{2.33}$$

and

$$\mathrm{tr}(J^*_s) = -\left(1+\frac{\sigma}{\mu}\right) \tag{2.34}$$

Since the necessary and sufficient conditions for the existence of local stability are given by; $\det(J^*) > 0$ and $\mathrm{tr}(J^*) < 0$, therefore, from equations (2.33) and (2.34), it can be deduced that the system preserved its stability for all values of μ, in other words, the existence of *superstability* for $\forall\mu \in \mathbb{R}^+$. At the given stability conditions, the range of y and μ at nontrivial steady-state

should follow;

$$y < 1 \tag{2.35}$$

and

$$\mu_s < \frac{x+\sigma}{y-1}. \tag{2.36}$$

These can be expressed in terms of the original form according to *Table 2.2* where;

$$[ES] < [E]_T,$$

$$[E]_T - [ES] > 0$$

thus,

$$[E] > 0 \tag{2.37}$$

and

$$K_m > [ES] - [E]_T - [S]$$

since,

$$[S]_0 = [S] + [ES]$$

hence,

$$[ES] < \frac{K_m + [S]_0 + [E]_T}{2} \tag{2.38}$$

at a particular time t. Inequality (2.37) shows that the free enzyme, [E] must be readily available for the reaction to proceed to completion such that the local stability is maintained throughout the course of reaction. While the next condition, (2.38) refers to the intermediate complex [ES], which should be less than half of the sum of K_m, $[E]_T$ and $[S]_0$. These conditions add to the previously given rules for quasi steady-state assumption, ($[E]_T \ll [S]_0$) and that given by Palsson (1987), ($[E]_T \ll K_m \ll [S]_0$) for the two time scales; $[E]_T \ll K_m$ for longer time scale that leads to quasi steady-state behaviour and obeys the zeroth order for the outer singular perturbation solution (Heineken *et al.*, 1967) and that for $K_m \ll [S]_0$ justifies the zeroth order of the inner singular perturbation solution at an invariant substrate concentration.

In addition to the above stability criteria, the trace, $\mathrm{tr}(J_s^*)$ is also closely related to the *divergence* of the system. This can be represented by a function, F integrated over a volume $V(t)$ with $\mathbf{V}$ represents the vector field which described the flow. This can be expressed as,

$$\frac{d}{dt}\int_V F dv = \int_V \left(\frac{dF}{dt} + F\nabla.\mathbf{V}\right) dv$$

and applying to the system of sQSSA gives

$$\frac{\partial \dot{X}}{\partial x} + \frac{\partial \dot{Y}}{\partial y} = -\left(1 + \frac{\sigma}{\mu}\right),$$

where $\dot{X}$ and $\dot{Y}$ represent $\dot{x}$ and $\dot{y}$ respectively. Since the *divergence* of the system is negative in the regions of phase space, therefore the system is dissipative. For a system described by sQSSA, σ and μ are positive, thus, the *divergence* should be negative everywhere in the phase space. This is clearly depicted in *Figures 2.13* to *2.15.*

Apart from looking at the particular determinant, (det) and trace, (tr) of the system, the discriminant, D from the characteristic equation of the form

$$\lambda^2 + b\lambda + c = 0$$

can also be used to determine the different type of trajectories (Thompson and Stewart (2002)). From the Jacobian matrix given by equation (2.30), the discriminant, D is given by,

$$D = \left(\frac{\mu + \sigma}{\mu}\right)^2 - \frac{4\alpha}{\mu} \tag{2.39}$$

and for the existence of two distinct roots, D should be positive such that;

$$D > 0$$

this can only be achieved when

$$\left(1 + \frac{\sigma}{\mu}\right)^2 - 4\left(\frac{\alpha}{\mu}\right) > 0$$

$$\sigma > 2\sqrt{\alpha\mu} - \mu \tag{2.40}$$

which can be expressed in its normal form,

$$K_m > 2\sqrt{K[E]_T} - [E]_T \tag{2.41}$$

where K is defined as the Van-Slyke-Cullen constant (Van Slyke and Cullen, 1914, 1917).

The variation of eigenvalues $\lambda^*_{s(1,2)}$ corresponds to the change of μ is plotted in *Figures 2.16(a)* and *2.16(b)* respectively. Both plots clearly show that as the parameter μ changes, both eigenvalues tend to be *more* negative, this statement confirmed the previous deduction regarding the existence of *superstability* in the system of one intermediate complex of an enzyme-catalysed reaction.

The Dynamics of System with Total Quasi Steady-State Assumption

From the dynamic analysis of the system described by the standard quasi steady-state assumption, one main conclusion could be drawn, the system is very stable such that any changes of μ does not change the stability of the system, but rather the dynamic behaviour of the trajectory. The change of trajectory of the system actually rules out the standard quasi steady-state assumption, therefore, in order to preserve its validity, Borghans *et al.* (1996) had devised a new system that extends to higher values of μ. This was termed as the total quasi steady-state assumption (tQSSA).

The derivation of the system following the total quasi steady-state assumption was again based on equations (2.5) and (2.6) and by introducing $[S]_0$ as the total substrate concentration, together with $[E]_T$,

$$[S]_0 = [ES] + [S]$$

and upon substitution into these equations and changing $[S]_0$ with $[S]$ results in a system given by,

$$\frac{d[S]}{dt} = -k_2[ES] \tag{2.42}$$

$$\frac{d[ES]}{dt} = k_1([E]_T - [ES])([S] - [ES]) - (k_{-1} + k_2)[ES] \tag{2.43}$$

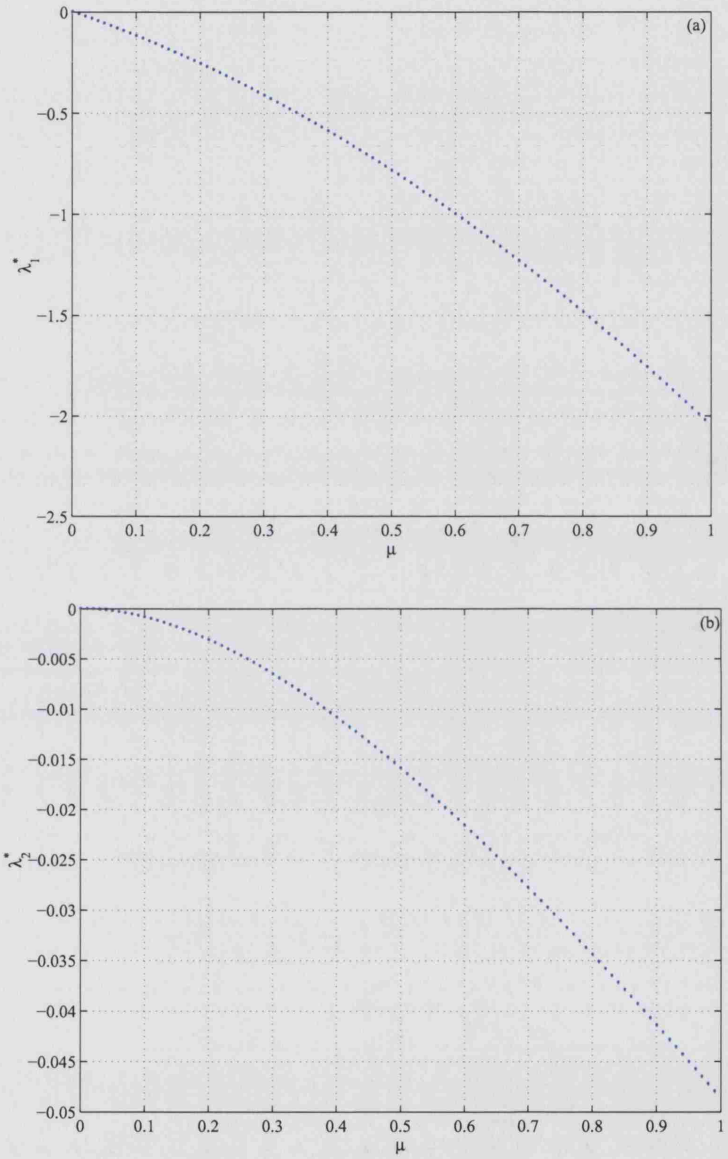

Figure 2.16: Change of eigenvalues (a) $\lambda^*_{s(1)}$ and (b) $\lambda^*_{s(2)}$ corresponds to the change of μ for sQSSA and tQSSA.

Using a similar form of dimensionless parameters defined previously in *Table 2.2* except for

$$u = \frac{[S]}{[S]_0}$$

and

$$v = \frac{[ES]}{[E]_T}$$

gives

$$\dot{u} = -\alpha v \tag{2.44}$$

$$\mu\dot{v} = (u - v\mu)(1 - v) - \sigma v \tag{2.45}$$

where $\dot{u}$ and $\dot{v}$ denote the usual differential form of $\frac{du}{dt}$ and $\frac{dv}{dt}$ respectively. Numerical simulations of the system according to *Table 2.2* at different conditions are presented below as a comparison to that of the standard form given previously. The shape of *Figure 2.18* resembles that of *2.13*, this explains that at a very low ratio of enzyme to substrate concentration, both assumptions are applicable for the derivation of Michaelis-Menten model. The trajectories of the consecutive figures, (*Figures 2.19* and *2.20*) are preserved even when μ is significantly increased. This observation shows that tQSSA is valid either at a very low or high enzyme concentration.

In order to prove the numerical solution observed from the above simulations, a similar analysis based on the eigenvalues as well the criteria resulted from the necessary and sufficient conditions for local stability was carried out. These were then compared with the analysis of the sQSSA.

Eigenvalues analysis: Linearising equations (2.44) and (2.45) results in the Jacobian matrix;

$$J_t = \begin{pmatrix} 0 & -\alpha \\ \frac{1-v}{\mu} & -\left(\frac{u+(1-v)\mu-v\mu+\sigma}{\mu}\right) \end{pmatrix} \tag{2.46}$$

with a general eigenvalue terms,

$$\lambda_{t(1,2)} = \begin{pmatrix} -\frac{1}{2\mu}[(u+\sigma)+(1-2v)\mu]\left(1+\sqrt{1-\frac{4\alpha\mu(1-v)}{[(u+\sigma)+(1-2v)\mu]^2}}\right) \\ -\frac{1}{2\mu}[(u+\sigma)+(1-2v)\mu]\left(1-\sqrt{1-\frac{4\alpha\mu(1-y)}{[(u+\sigma)+(1-2v)\mu]^2}}\right) \end{pmatrix} \tag{2.47}$$

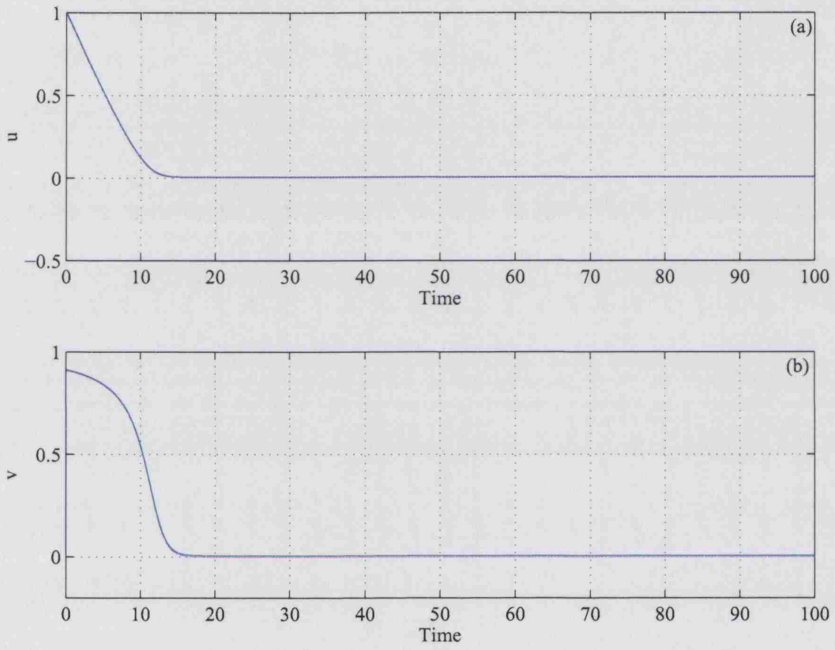

Figure 2.17: Time histories for both (a) u and (b) v at $\mu = 0.0001$, $\sigma = 0.11$ and $\alpha = 0.1$ (Following condition B from *Table 2.2*).

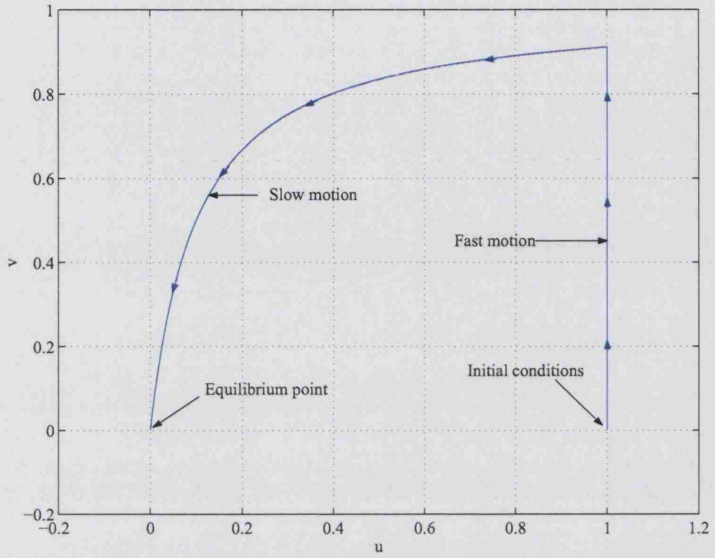

Figure 2.18: Corresponding phase-plane plot of *Figure 2.17*.

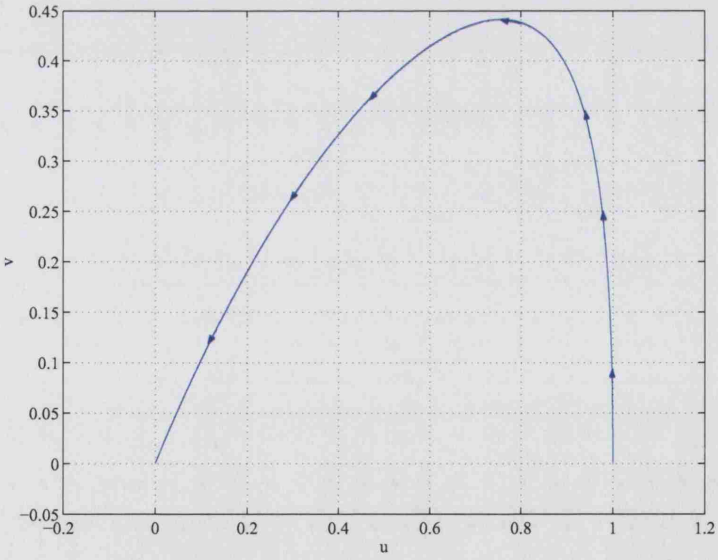

Figure 2.19: Phase-plane plot of system with $\mu = 1$ (Condition A), fast and slow trajectories are preserved for tQSSA.

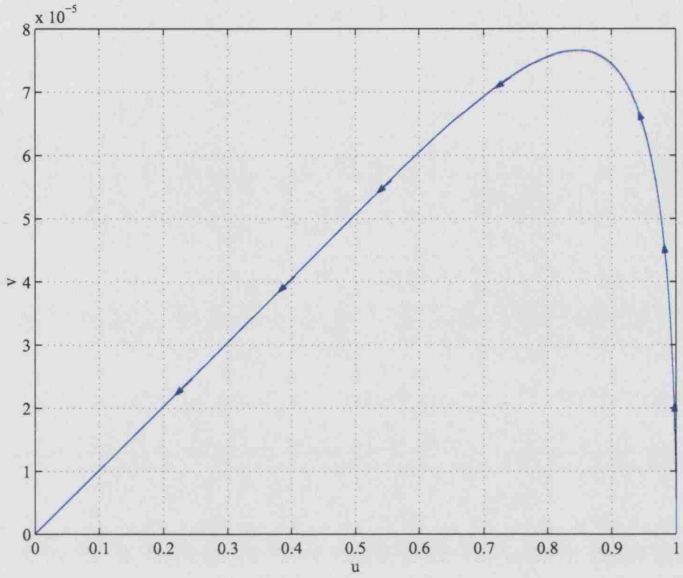

Figure 2.20: Phase-plane plot of system with $\mu = 10000$ (Condition C), a similar trajectory as that for $\mu = 1$.

and these values at the trivial solution,

$$(u^*, v^*) = (0, 0)$$

are given by,

$$\lambda^*_{t(1,2)} = \begin{pmatrix} -\frac{1}{2\mu}\left[(\sigma+\mu)\left(1+\sqrt{1-\frac{4\alpha\mu}{(\sigma+\mu)^2}}\right)\right] \\ -\frac{1}{2\mu}\left[(\sigma+\mu)\left(1-\sqrt{1-\frac{4\alpha\mu}{(\sigma+\mu)^2}}\right)\right] \end{pmatrix} \tag{2.48}$$

By comparing equation (2.48) to that of (2.32), it can be deduced that both systems share the same eigenvalues, which means that *superstability* exists for the system following the tQSSA. Therefore, the analysis of tr and det of this system at equilibrium point gives the same terms as that for the sQSSA.

$$\det(J^*_t) = \frac{\alpha}{\mu} \tag{2.49}$$

and

$$\mathrm{tr}(J^*_t) = -\left(1+\frac{\sigma}{\mu}\right) \tag{2.50}$$

However, at the nontrivial solution, conditions differ from that of the sQSSA were obtained;

$$v < 1 \tag{2.51}$$

and

$$\mu_t > \frac{(u+\sigma)}{(2v-1)} \tag{2.52}$$

By changing the dimensionless terms into the normal forms gives;

$$[E] > 0 \tag{2.53}$$

$$[ES] > \frac{K_m + [S]_0 + [E]_T}{3} \tag{2.54}$$

The first condition is common for the existence of *superstability*, however, the condition given by (2.54) suggests that at any time t, the concentration of [ES] should be more than one third of the total K_m, $[S]_0$ and $[E]_T$.

Analysis on the *divergence* and discriminant of the above system were also carried out. Since the system shared the same eigenvalues as that of the sQSSA, therefore, it also resulted in similar terms for both *divergence* and discriminant. As pointed out previously, the *divergence* is represented by $\left[-\left(1+\frac{\sigma}{\mu}\right)\right]$ and when μ was chosen as the bifurcation parameter, increasing μ would result in the function to be more negative, thus local stability was preserved.

Eigenspaces Analysis of Equilibrium Points for sQSSA and tQSSA

The analysis of eigenvalues presented previously does not differentiate the behaviour of the trajectories described by the numerical solutions. Therefore further analysis of the eigenspaces of systems described by both assumptions is required.

In this section, the special eigenspaces that could describe an equilibrium point of any dynamical systems were initially defined. Let $\mathbb{R}^n$ represents the direct sum of the three subspaces denoted by E^s, E^u and E^c which are defined as follows;

Stable eigenspace, E^s: The space spanned by the eigenvectors whose corresponding eigenvalues have negative real parts.

$$E^s = span\{e_1, \ldots, e_s\}$$

Unstable eigenspace, E^u: The space spanned by the eigenvectors whose corresponding eigenvalues have positive real parts.

$$E^u = span\{e_{s+1}, \ldots, e_{s+u}\}$$

Centre eigenspace, E^c: The space spanned by the eigenvectors whose corresponding eigenvalues have a real part of zero.

$$E^c = span\{e_{s+u+1}, \ldots, e_{s+u+c}\}$$

and $s+u+c=n$. If a system is described by $\dot{y} = Df(\bar{x})y$, $y \in \mathbb{R}^n$ with $Df(\bar{x})$ is a constant $n \times n$ matrix has solutions with initial conditions entirely contained in either E^s, E^u or E^c, they must forever remain in that particular subspace for all time. For instance, if solutions starting in E^s, it will approach $y=0$ asymptotically as $t \to +\infty$ and for solutions starting in E^u, it will approach $y=0$ asymptotically as $t \to -\infty$. This behaviour is termed as invariant subspaces or "manifolds". The introduction of invariant manifolds will be further mentioned in Section 2.3.2 for system affected by substrate and product inhibitions which resulted in a mixed-type inhibition during the course of reaction.

Eigenvectors Analysis for System Described by sQSSA: Using equations (2.26) and (2.27), the eigenvectors of Jacobian matrix described by sQSSA, at equilibrium point is given by;

$$J_s^* \mathbf{e}_i = \lambda_i^* \mathbf{e}_i$$

or;

$$(\lambda_i^* \mathbf{I} - J_s^*)\mathbf{e}_i = 0 \tag{2.55}$$

where $\mathbf{e}_i$ denotes the eigenvectors of the system. Thus with $\lambda_{s,1}^*$,

$$\begin{pmatrix} -1-\lambda_{s,1}^* & -\alpha+\sigma \\ \frac{1}{\mu} & -\frac{\sigma}{\mu}-\lambda_{s,1}^* \end{pmatrix} \begin{pmatrix} e_{1,1}^s \\ e_{1,2}^s \end{pmatrix} = 0 \tag{2.56}$$

this gives eigenvectors of the form;

$$\mathbf{e}_1^s = \begin{pmatrix} -\frac{1}{2}\left(\mu - \sigma + \sqrt{(\mu+\sigma)^2 - 4\alpha\mu}\right) \\ 1 \end{pmatrix} \tag{2.57}$$

similarly, with $\lambda^*_{s,2}$;

$$\mathbf{e}_2^s = \begin{pmatrix} -\frac{1}{2}\left(\mu - \sigma - \sqrt{(\mu+\sigma)^2 - 4\alpha\mu}\right) \\ 1 \end{pmatrix} \tag{2.58}$$

Therefore, the eigenvectors corresponding to the eigenvalues $\lambda^*_{s,(1,2)}$ can be simplified as;

$$\mathbf{e}^s_{(1,2)} = \begin{pmatrix} -\frac{1}{2}\left(\mu - \sigma \pm \sqrt{(\mu+\sigma)^2 - 4\alpha\mu}\right) \\ 1 \end{pmatrix} \tag{2.59}$$

Eigenvectors Analysis for System Described by tQSSA: A similar analysis was used to obtain the eigenvectors for system described by tQSSA. Using Jacobian matrix of equations (2.44) and (2.45) at (u^*, v^*)=(0,0) and $\lambda^*_{t,1}$ gives;

$$\begin{pmatrix} 0 - \lambda^*_{t,1} & -\alpha \\ \frac{1}{\mu} & -\left(\frac{\mu+\sigma}{\mu}\right) - \lambda^*_{t,1} \end{pmatrix} \begin{pmatrix} e^t_{1,1} \\ e^t_{1,2} \end{pmatrix} = 0 \tag{2.60}$$

Using the same method with $\lambda^*_{t,2}$, the eigenvectors of this system are in the form of;

$$\mathbf{e}^t_{(1,2)} = \begin{pmatrix} \frac{1}{2}\left(\mu + \sigma \mp \sqrt{(\mu+\sigma)^2 - 4\alpha\mu}\right) \\ 1 \end{pmatrix} \tag{2.61}$$

	$\mu = 0.0001$	$\mu = 1.0$	$\mu = 10000$
$\lambda^*_{s,1}$	-1100.09	-1.06409	-1.01110
$\begin{pmatrix} e^s_{(1,1)} \\ e^s_{(2,1)} \end{pmatrix}$	$\begin{pmatrix} -9.09843 \times 10^{-6} \\ 1.0 \end{pmatrix}$	$\begin{pmatrix} -0.529446 \\ 0.848344 \end{pmatrix}$	$\begin{pmatrix} -9010.98 \\ 1.0 \end{pmatrix}$
$\lambda^*_{s,2}$	-0.909016	-0.375907	-0.0989024
$\begin{pmatrix} e^s_{(1,2)} \\ e^s_{(2,2)} \end{pmatrix}$	$\begin{pmatrix} 0.109251 \\ 0.994014 \end{pmatrix}$	$\begin{pmatrix} -0.0639618 \\ -0.997952 \end{pmatrix}$	$\begin{pmatrix} 110.9758 \\ 1.0 \end{pmatrix}$

Table 2.4: Eigenvalues and corresponding eigenvectors for system defined by sQSSA.

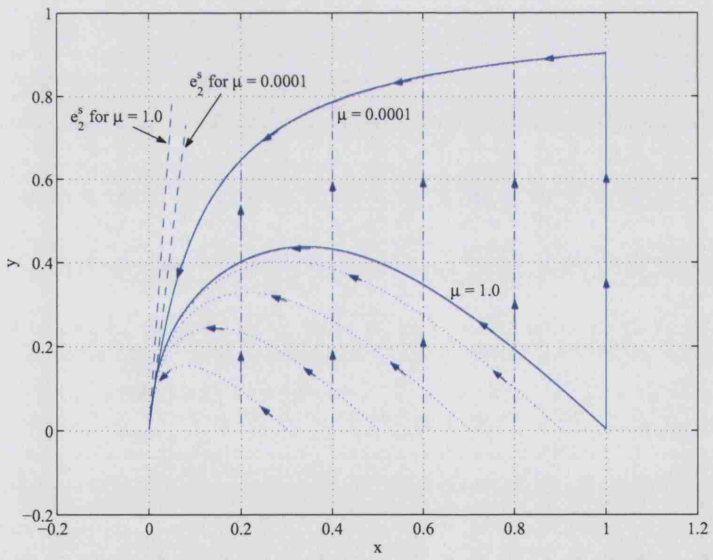

Figure 2.21: Numerical simulation of system defined by sQSSA for $\mu = 0.0001$ and $\mu = 1.0$ at different initial conditions with the corresponding eigenvectors.

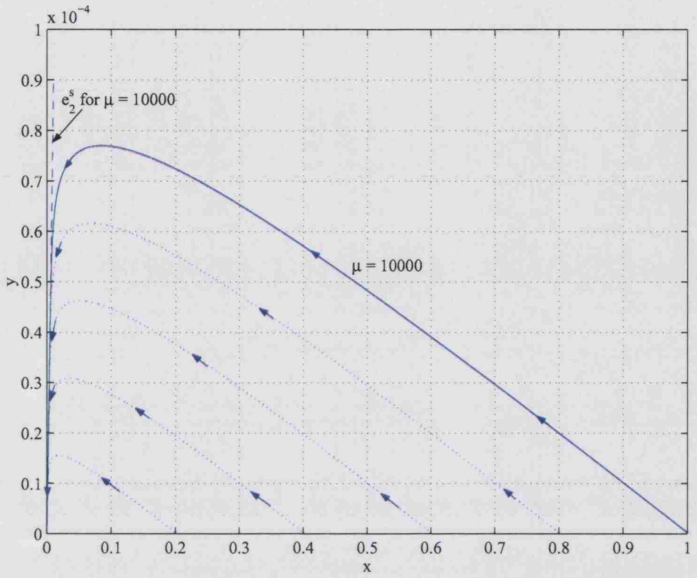

Figure 2.22: Numerical simulation of system defined by sQSSA for significantly large μ, ($\mu = 10000$) at different initial conditions.

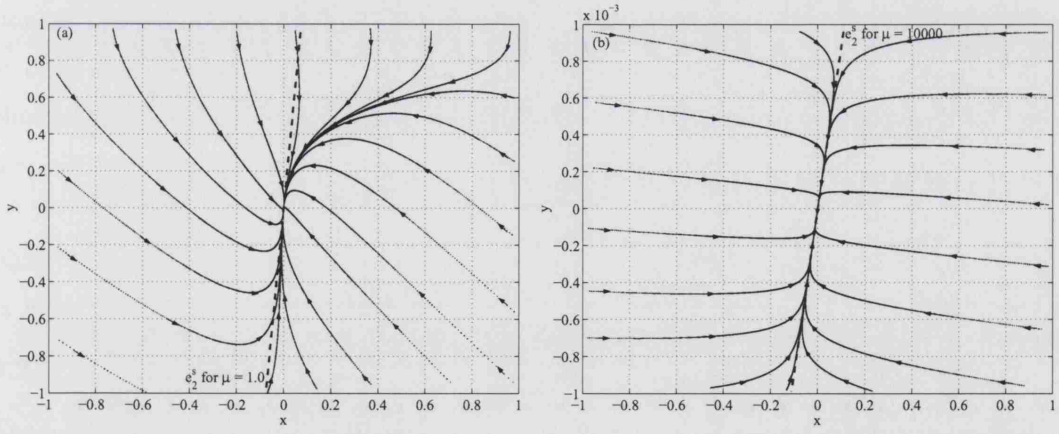

Figure 2.23: Phase-plane ($x \times y$) of sQSSA at different initial conditions (a) Condition A and (b) Condition C.

Since the eigenvectors $\mathbf{e}^s_{(1,2)}$ and $\mathbf{e}^t_{(1,2)}$ corresponded to the eigenvalues of standard and total QSSA respectively, which resulted in *superstability* criteria, they consequently represent the stable subspaces, E^s for both systems in $\mathbb{R}^2$ i.e. $E^s_s = span\{e^s_1, e^s_2\}$ and $E^s_t = span\{e^t_1, e^t_2\}$. All eigenvalues and eigenvectors corresponding to conditions described in *Table 2.2* are given in *Table 2.4* for system with sQSSA and that in *Table 2.5* for system with tQSSA. These vectors could be shown as lines on $(x \times y)$ or $(u \times v)$ phase-plane at which the trajectories are attracted as they converged into the equilibrium point, i.e. the origin. *Figure 2.21* clearly shows the eigenspaces of system defined by sQSSA at different initial conditions for $\mu = 0.0001$ and $\mu = 1.0$, (since the numerical solution for $\mu = 10000$ lies in the range of 10^{-5}, therefore, the plot was omitted from *Figure 2.21* and separately plotted in *Figure 2.22*). Apparently, the trajectories for $\mu = 0.0001$ are attracted into an invariant line such that the change of initial conditions do not seem to change its path. This behaviour is not apparent for system of the same magnitude of enzyme to substrate concentration, $\mu = 1.0$ or even at higher value of μ. The phase-plane of these particular conditions in a 4-quadrant plot is shown in *Figure 2.23* for a clear picture of the vector e^s_2. The trajectories at various initial conditions were characterised as a *stable sink* towards the equilibrium point on $\mathbb{R}^2$.

A similar condition also occurred for the system described by tQSSA for a very low μ. However, at an equal magnitude of total enzyme and substrate concentrations, the trajectories at different initial conditions slowed down as they converged towards the equilibrium point. Similar plots were devised for the system defined by tQSSA and shown in *Figure 2.24* for both $\mu = 0.0001$ and $\mu = 1.0$ and *Figure 2.25* for $\mu = 10000$.

In order to compare the dynamics exhibit by the phase-plane of the system described by sQSSA to that of tQSSA, similar plots of $(u \times v)$ for Condition A and Condition C are shown in *Figure 2.26.*

2.2.2 Comparison between the Transient and Steady-State Kinetics

The analysis carried out in the previous section apparently shows the behaviour that could not be described with the normal steady-state method. One of the most successful analyses undertaken using the transient method is the proof of the quasi steady-state assumption. By proving this, makes the use of the steady-state kinetics to describe enzyme catalysis more convincing especially

	$\mu = 0.0001$	$\mu = 1.0$	$\mu = 10000$
$\lambda^*_{t,1}$	-1100.09	-1.06409	-1.01110
$\begin{pmatrix} e^t_{(1,1)} \\ e^t_{(2,1)} \end{pmatrix}$	$\begin{pmatrix} -9.09016 \times 10^{-5} \\ 1.0 \end{pmatrix}$	$\begin{pmatrix} 0.351868 \\ 0.93605 \end{pmatrix}$	$\begin{pmatrix} 989.024 \\ 1.0 \end{pmatrix}$
$\lambda^*_{t,2}$	-0.909016	-0.375907	-0.0989024
$\begin{pmatrix} e^t_{(1,2)} \\ e^t_{(2,2)} \end{pmatrix}$	$\begin{pmatrix} 0.109349 \\ 0.994003 \end{pmatrix}$	$\begin{pmatrix} 0.728712 \\ 0.68482 \end{pmatrix}$	$\begin{pmatrix} 10110.98 \\ 1.0 \end{pmatrix}$

Table 2.5: Eigenvalues and corresponding eigenvectors for system defined by tQSSA.

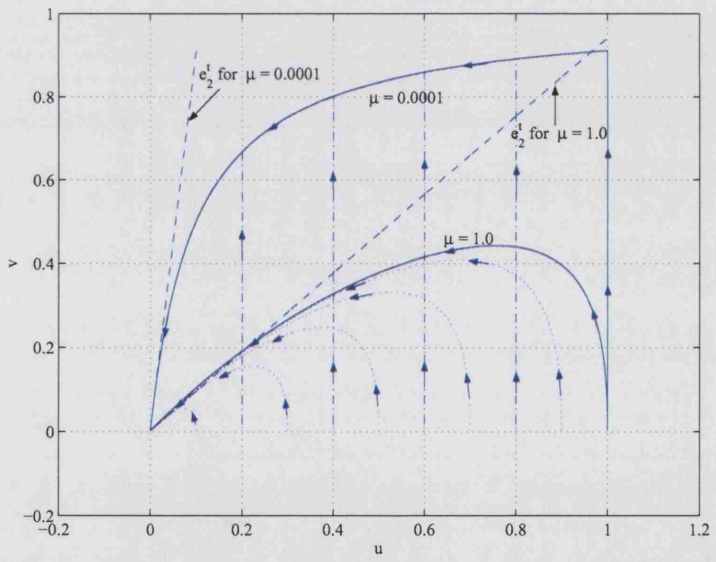

Figure 2.24: Numerical simulation of system defined by tQSSA for $\mu = 0.0001$ and $\mu = 1.0$ at different initial conditions with the corresponding eigenvectors.

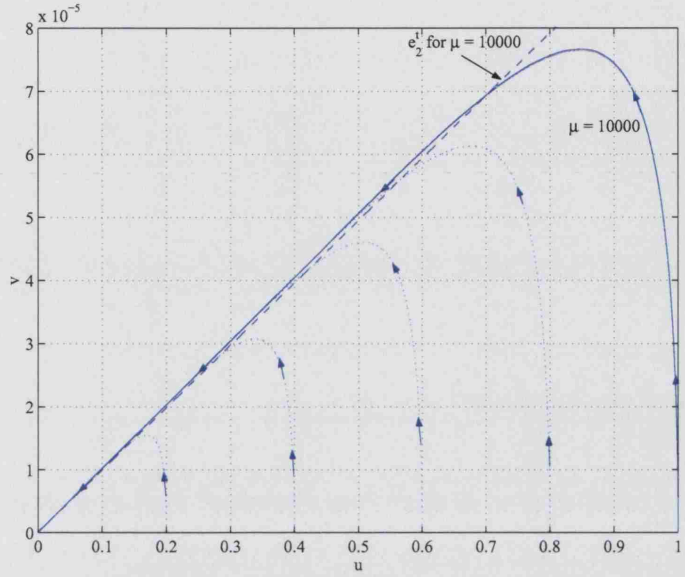

Figure 2.25: Numerical simulation of system defined by tQSSA for $\mu = 10000$ at different initial conditions with the corresponding eigenvectors.

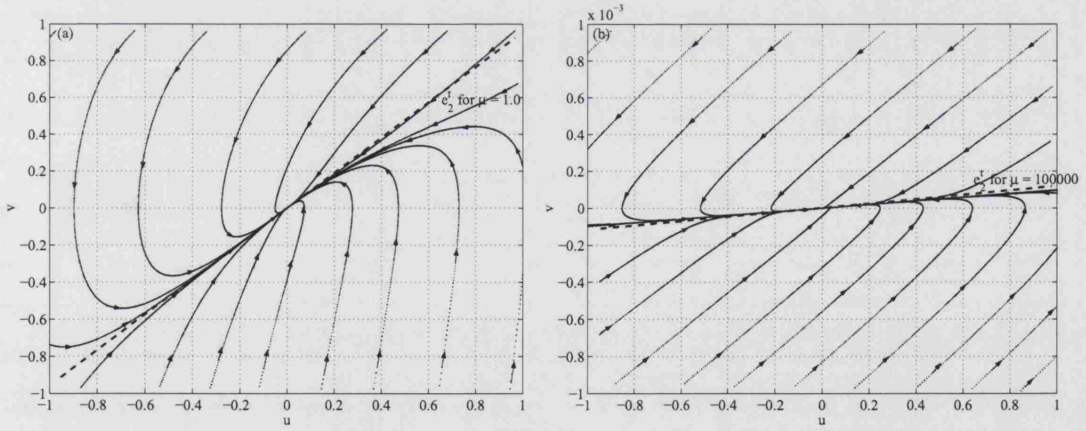

Figure 2.26: Phase-plane ($u \times v$) of tQSSA at different initial conditions (a) Condition A and (b) Condition C.

for the data fitting technique.

In the current work, the dynamics of the system described by sQSSA and tQSSA were analysed. This has led to the proposal of the new conditions for both systems to maintain their stabilities during the reaction. The steady-state kinetics obtained by applying the assumption only resulted in a single form of differential equation, and the solution of the equation described only the product formation or substrate depletion depending on the differential operator used on the left hand side of the equation. Therefore, applying the steady-state kinetics alone does not give much information especially on the formation of intermediate complexes which could finally relates to the binding properties of enzymes' active sites.

The transient analysis is also capable to characterise the eigenspaces of the vector fields described by the trajectories of both systems. The fast and slow motions exhibited during the course of reaction are apparent with the phase-plane plots and the eigenvectors that governed the flows. Both systems are found to follow the given assumption at a very low ratio of total enzyme to substrate concentration. At a particular value, the trajectories are attracted into a line at which the change of initial conditions of the systems do not alter the flow towards the equilibrium point. This result clearly described the degenerate form of differential equations as an outcome of the unique mechanism of enzyme-catalysed reactions.

2.3 Dynamics of Enzyme-Catalysed Reactions with Inhibitions

Most of the enzymes-catalysed reactions are exposed to other external chemicals such as substrates, side products, cofactor, co-substrate, etc. during the course of reaction. The presence of any of these chemicals will reduce the rate of product formation due to the incorrect binding of the substrate or blocking of the enzyme's active site. This however can be controlled by lowering the concentration of any of these components, for instance, by using a small amount of substrate to start a reaction or continuously removing the product during a reaction, such that the accumulation will not affect the reaction rate. Such chemicals are termed as inhibitors. In the perspective of living cells, the presence of the so called inhibitor actually regulates the cell activity and metabolism for cell growth as well as for the immune system. A complete understanding of the effect of inhibition towards enzyme reaction is important in order to explain the

specificity of an enzyme, the physical and chemical *architecture* of the active site and the kinetic mechanism of the reaction. Such information could only be shown using the dynamic analysis of the enzyme mechanism with a particular inhibition.

In this work, the dynamic behaviour of an enzyme-catalysed reaction with the presence of multiple inhibitors were analysed. This would later explain a similar type of inhibition occurred in the model system which will be discussed in Section 2.4. Prior to the dynamic analysis of an enzyme-catalysed reaction with inhibition, each species taken part in the reaction was described by an ordinary differential equation. With the system of equations, the transient behaviour of each species could be observed. Roussel and Fraser (1993) have stated that with such method, a geometrical picture of the system's time evolution should be apparent compared to the steady-state analysis and a rich variety of behaviour could be obtained. The analysis based on the simple Michaelis-Menten mechanism was comprehensively described using this geometrical technique by Nguyen and Fraser (1989).

This section is divided into two main parts; the analysis of behaviour of the system due to the change of parameters i.e. bifurcation analysis and some preliminary work on the existence of an invariant manifold in the inhibited enzyme-catalysed systems. New findings based on the substrate and product inhibitions will be discussed with an aid of simulations of the true dynamic steady–state of the equilibrium point.

Enzyme Inhibition with One Intermediate Complex, [ES]

Consider an enzyme-catalysed reaction with substrate and product inhibitions following the mechanism shown in *Figure 2.27* with one intermediate complex, [ES]. The substrate, [S] binds with the free enzyme, [E] producing the competitive type inhibition and that for product, [P] exhibits the uncompetitive type inhibition when it binds with the enzyme-substrate complex, [ES], and both inhibitions result in a mixed-type inhibition (Segel, 1993).

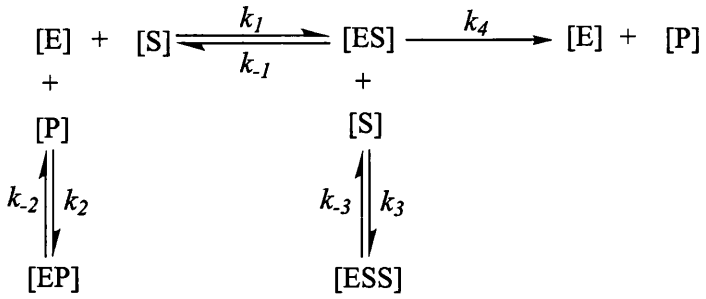

Figure 2.27: Mechanism of enzyme-catalysed reaction with substrate and product inhibitions (mixed-type inhibition).

Each species within the system could be described by ordinary differential equations in the form of;

$$\frac{d[S]}{dt} = -k_1[S][E] + k_{-1}[ES] - k_3[ES][S] + k_{-3}[ESS] \tag{2.62}$$

$$\frac{d[ES]}{dt} = k_1[S][E] - k_{-1}[ES] - k_3[ES][S] + k_{-3}[ESS] - k_4[ES] \tag{2.63}$$

$$\frac{d[EP]}{dt} = k_2[E][P] - k_{-2}[EP] \tag{2.64}$$

$$\frac{d[ESS]}{dt} = k_3[ES][S] - k_{-3}[ESS] \tag{2.65}$$

$$\frac{d[P]}{dt} = k_4[ES] - k_2[E][P] + k_{-2}[EP] \tag{2.66}$$

and the total enzyme concentration, $[E]_T$ is given by;

$$[E]_T = [E] + [ES] + [EP] + [ESS] \tag{2.67}$$

In order to simplify the system of equations, (2.67) is substituted for [E] into equations (2.62) to (2.66) and upon rendering into dimensionless form, they are reduced into;

$$\frac{ds}{d\tau} = -(1 - u - v - w)s + (\beta - \alpha s)u + \gamma w \tag{2.68}$$

$$\mu\frac{du}{d\tau} = (1 - u - v - w)s - (\beta + \rho + \alpha s)u + \gamma w \tag{2.69}$$

$$\mu\frac{dv}{d\tau} = (1-u-v-w)\eta p - \varepsilon v \tag{2.70}$$

$$\mu\frac{dw}{d\tau} = \alpha us - \gamma w \tag{2.71}$$

$$\frac{dp}{d\tau} = \rho u - (1-u-v-w)\eta p + \varepsilon v \tag{2.72}$$

where the dimensionless parameters are defined as $s = \frac{[S]}{[S]_0}$, $u = \frac{[ES]}{[E]_T}$, $v = \frac{[EP]}{[E]_T}$, $w = \frac{[ESS]}{[E]_T}$, $p = \frac{[P]}{[S]_0}$, $\alpha = \frac{k_3}{k_1}$, $\beta = \frac{k_{-1}}{k_1[S]_0}$, $\varepsilon = \frac{k_{-2}}{k_1[S]_0}$, $\eta = \frac{k_2}{k_1}$, $\mu = \frac{[E]_T}{[S]_0}$, $\rho = \frac{k_4}{k_1[S]_0}$ and $\gamma = \frac{k_{-3}}{k_1[S]_0}$. All variables within the system are dependent upon one another, therefore equations (2.68) to (2.72) are useful for the analysis that follows.

Non-existence of Steady-State Solutions

If one applies the steady–state analysis, the system of equations could be reduced following the sQSSA discussed previously, with $\mu \ll 1$, $\frac{du}{d\tau} = 0$, $\frac{dv}{d\tau} = 0$ and $\frac{dw}{d\tau} = 0$, thus

$$\frac{dp}{d\tau} = \frac{s\gamma\varepsilon\rho}{\varepsilon\gamma(\beta+\rho) + s\varepsilon(\gamma+s\alpha) + p\gamma\eta(\beta+\rho)} \tag{2.73}$$

dividing both nominator and denominator by $(\gamma\epsilon\rho)$ gives,

$$\frac{dp}{d\tau} = \frac{s}{\left(\frac{\beta}{\rho}+1\right)\left(1+\frac{p\eta}{\epsilon}\right) + \frac{s}{\rho}\left(1+\frac{s\alpha}{\gamma}\right)} \tag{2.74}$$

and upon substitution with the normal forms of these parameters results in the usual terms of rate expression with substrate and product inhibitions given below,

$$\frac{d[P]}{dt} = \frac{V_{max}[S]}{K_m\left(1+\frac{[P]}{K_{i_{[P]}}}\right) + [S]\left(1+\frac{[S]}{K_{i_{[S]}}}\right)} \tag{2.75}$$

where $K_{i_{[S]}}$ and $K_{i_{[P]}}$ define the substrate and product inhibition constants respectively.

Initial analysis of the existence of trivial solution of the enzyme-catalysed system with substrate and product inhibitions described by five autonomous differential equations was carried

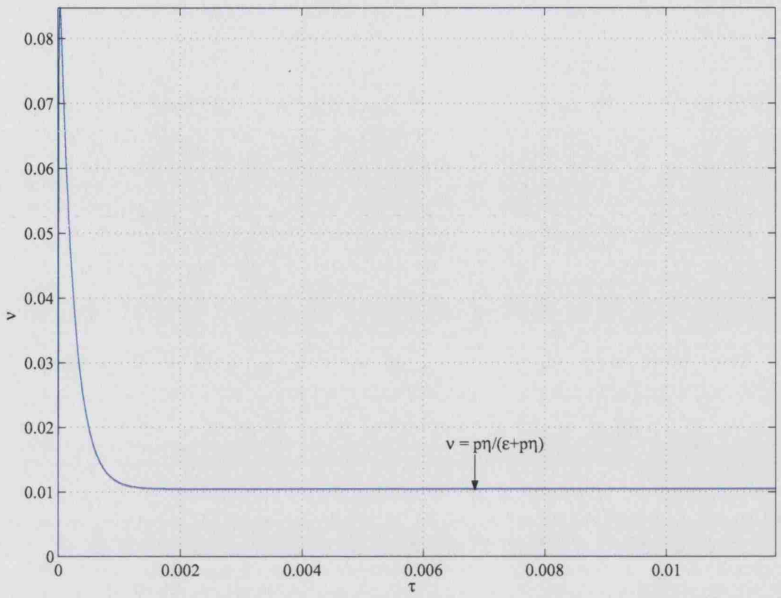

Figure 2.28: Formation of enzyme-product complex, v with respect to the dimensionless time, τ.

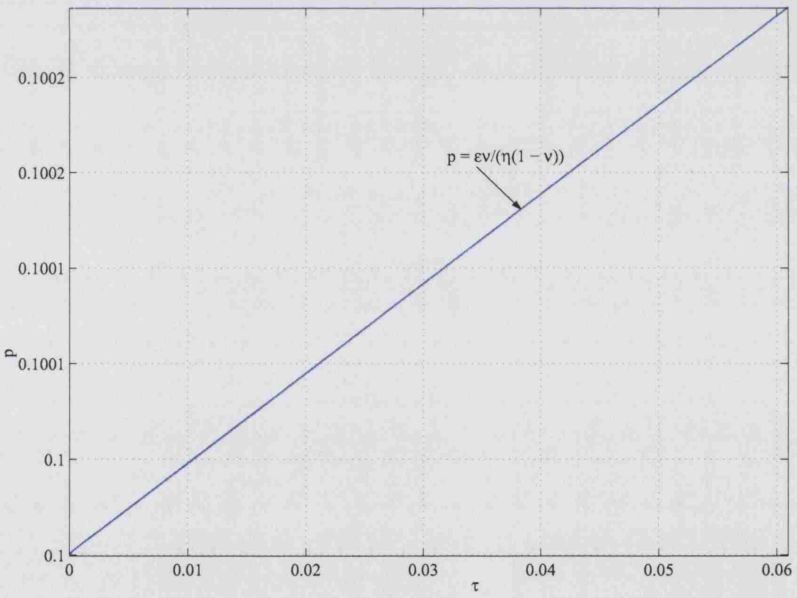

Figure 2.29: Continuous formation of product, p with respect to the dimensionless time, τ. Simulation shows no steady-state solution as $\tau \to \infty$.

out. Linearising the system of equations into Jacobian matrix, J_{inh} leads to,

$$J_{\text{inh}} = \begin{pmatrix} -1+u+v+w-u\alpha & s(1-\alpha)+\beta & s & s+\gamma & 0 \\ \frac{1-u-v-w-u\alpha}{\mu} & \frac{-s(1+\alpha)-\beta-\rho}{\mu} & -\frac{s}{\mu} & \frac{\gamma-s}{\mu} & 0 \\ 0 & -\frac{p\eta}{\mu} & -\frac{(\varepsilon+p\eta)}{\mu} & -\frac{p\eta}{\mu} & \frac{(1-u-v-w)\eta}{\mu} \\ \frac{u\alpha}{\mu} & \frac{s\alpha}{\mu} & 0 & -\frac{\gamma}{\mu} & 0 \\ 0 & p\eta+\rho & \varepsilon+p\eta & p\eta & -(1-u-v-w)\eta \end{pmatrix} \tag{2.76}$$

upon calculating the determinant, $\det(J_{\text{inh}})$ and trace, $\text{tr}(J_{\text{inh}})$ result in

$$\det(J_{\text{inh}}) = 0$$

and

$$\text{tr}(J_{\text{inh}}) = \frac{1}{\mu}\left((1+\alpha)s + p\eta + \mu\left[1-(1+\eta)(u+v+w)+u\alpha+\eta\right] + (\beta+\gamma+\varepsilon+\rho)\right).$$

The zero determinant shows that the degenerate system of autonomous differential equations is singular, this is always true for system with feedback product inhibition (results for other types of product inhibitions are not shown), thus, a complete trivial solution is not possible. Attempt to solve such a system only leads to four coordinate values with one value being dependent to another;

$$(s^*, u^*, v^*, w^*, p^*) = (0, 0, \frac{p\eta}{\varepsilon+p\eta}, 0, \frac{\varepsilon v}{\eta(1-v)})$$

Such a problem can be explained using the method of singular perturbation of a singular-type system of differential equations. A comprehensive work on the singular, singularly perturbed chemical reaction system can be referred to Gu *et al.* (1989) for further understanding. The non-existence steady-state point suggests that the system can infinitely proceed as $\tau \rightarrow \infty$, as long as there is enough product dissociates from the enzyme-product complex, [EP] continuously forming [E] and [P]. The product formed irreversibly from the enzyme-substrate complex will immediately bind with the free enzyme and inhibit the substrate from attacking the enzyme's active site. This will reduce the amount of active sites for substrate binding hence reduces the

rate of formation of product.

The formation of enzyme-product complex, [EP] represented by dimensionless variable v is shown in *Figure 2.28*, while the infinitely formed product, p is shown in the subsequence figure. For both simulations, parameters used are as follows; $\alpha = 1.0$, $\beta = 0.01$, $\gamma = 0.05$, $\varepsilon = 0.05$, $\eta = 1.0$, $\rho = 0.1$ and $\mu = 0.00001$.

Global Analysis

Due to the nature of the system described above, further analysis on its trivial solution and that the stability related to the solution could not be carried out. Another method was used in order to resolve the presence problem. By introducing the total amount of substrate, $[S]_0$ and that the total product, $[P]_0$, the system can be further reduced into a simple 3–dimensional form. Let,

$$[S]_0 = [S] + [ES] + [ESS] + [P]$$

and

$$[P]_0 = [P] + [EP]$$

the system is now dependent upon both constants, $[S]_0$ and $[P]_0$. Substituting these into equations (2.62) to (2.66) together with the total enzyme concentration, $[E]_T$ given by (2.67) results in,

$$\begin{aligned}\frac{d[S]}{dt} &= -([E]_T - [P]_0 - [S]_0)[S] + \left[K_{Eq} - \kappa_1([S] + K_{i_{[S]}})\right][ES] - ([S]^2 + 2[S][P]) \\ &- \kappa_2([S] + [P] - [S]_0) \end{aligned} \tag{2.77}$$

$$\begin{aligned}\frac{d[ES]}{dt} &= ([E]_T - [P]_0 - [S]_0)[S] - \left[K_m + \kappa_1([S] + K_{i_{[S]}})\right][ES] + ([S]^2 + 2[S][P]) \\ &- \kappa_2([S] + [P] - [S]_0) \end{aligned} \tag{2.78}$$

$$\begin{aligned}\frac{d[P]}{dt} &= \kappa_3[ES] - ([E]_T - [P]_0 - [S]_0)[P] - (2[P]^2 + [P][S]) \\ &+ K_{i_{[P]}}([P_0 - [P]) \end{aligned} \tag{2.79}$$

where the parameters are not defined in terms of dimensionless form, instead, the normal kinetic constants are used with $K_{Eq} = \frac{k_{-1}}{k_1}$, $K_m = \frac{(k_{-1}+k_4)}{k_1}$, $K_{i_{[S]}} = \frac{k_{-3}}{k_3}$, $K_{i_{[P]}} = \frac{k_{-2}}{k_2}$, $\kappa_1 = \frac{k_3}{k_1}$, $\kappa_2 = \frac{k_{-3}}{k_1}$ and $\kappa_3 = \frac{k_4}{k_2}$. The system described above allows one to vary the amount of initial substrate and product that caused inhibition and reduced the rate of reaction. Variation of these properties can be explained using the method of bifurcation theory that probes the variation of dynamic behaviour of the system (Crawford, 1991; Chow and Hale, 1996). The next section presents a detail analysis on the effect of mixed-type inhibition towards the dynamics of the system and the type of bifurcation that it exhibits.

Multiplicity of the Steady-State Solutions

The solution of the above system is entirely depend on the level of nonlinearity of the given ordinary differential equations. Although the explicit steady-state solutions were found, the results could not be stated here due to their long algebraic forms. The parameter values given in *Table 2.6* are chosen in order to simplify the solution into a numerical form. These parameters, especially the inhibition constants for the substrate and product, were selected such that the effect of inhibition by both species is at the same level and kept at lower magnitudes, (0.5mM, typical values; 0.5–200mM according to the binding of inhibitors to the active-site of a particular enzyme). The values of the Michaelis constant and that of the equilibrium constant were taken in a range between 1–10mM for a typical enzyme-catalysed reaction. The three additional constants; κ_1, κ_2 and κ_3 resulting from the simplification method are arbitrary values.

The equilibrium points are obtained by putting $\frac{d[S]}{dt} = \frac{d[ES]}{dt} = \frac{d[P]}{dt} = 0$. Initially, with the absence of the total initial substrate and product concentrations, ($[S]_0 = [P]_0 = 0$), a steady-state solution is found where $([S]^*, [ES]^*, [P]^*) = (0, 0, 0)$. Obviously, the absence of the substrate at the start of the reaction will result in no product formation and an increase of this value to 1.0mM resulted in $([S]^*, [ES]^*, [P]^*) = (0.31, 0.20, 0.17)$ as the equilibrium solution. However, the system starts to produce multiple steady-state solutions when a particular initial amount of product, $[P]_0$ was used. A value of $[P]_0 = 2.50$mM with the same value of $[S]_0$, resulted in three steady-state equilibrium solutions; $([S]_1^*, [ES]_1^*, [P]_1^*) = (-0.50, -0.11, 1.61)$, $([S]_2^*, [ES]_2^*, [P]_2^*) = (-0.45, 2.03, -0.81)$ and $([S]_3^*, [ES]_3^*, [P]_3^*) = (-0.50, 2.36, -0.86)$.

The above results indicate that at certain values of $[P]_0$, the system behaves in such a way

that the solution bifurcates from having one equilibrium point into three different solutions. We divided the studies of the system into 2 parts; the effect of increasing the total initial substrate concentration and the total initial product concentration. The results were than compared to the experimental results with similar initial substrate and product conditions.

Stability Analysis

Preliminary analysis of the eigenvalues of the system was carried out. This is essential in order to determine the stability of the reaction mechanism. Linearisation of equations (2.77) to (2.79) leads to,

$$J_{sp}=\begin{pmatrix} -\Delta-2([P]+[S])-[ES]\kappa_1-\kappa_2 & K_{Eq}-\kappa_1([S]+K_{i_{[S]}}) & -(2[S]+\kappa_2) \\ \Delta+2([P]+[S])-[ES]\kappa_1-\kappa_2 & -(K_m+\kappa_1([S]+K_{i_{[S]}})) & 2[S]-\kappa_2 \\ -[P] & \kappa_3 & -(\Delta+4[P]+[S]+K_{i_{[P]}}) \end{pmatrix} \tag{2.80}$$

where Δ represents $([E]_T - [P]_0 - [S]_0)$ and the eigenvalues obtained from the characteristic polynomial of equation (2.80) are given by,

$$\lambda_i^{sp} = \begin{pmatrix} \lambda_1 \\ \lambda_2 \\ \lambda_3 \end{pmatrix}.$$

Although the roots of the polynomial of J_{sp} can be expressed analytically, the solution could not be simply interpreted due to its long algebraic form. The only method of interpreting these eigenvalues is to locally describe the steady-state solution. The solutions at the steady-state points is found where;

$$([S]^*, [ES]^*, [P]^*) = (0, 0, 0)$$

using the parameters given in *Table 2.6.* Having the above equilibrium point, the eigenvalues of the system at this particular point are able to be determined, hence, taking into account only the real part of λ_i^{sp},

$$\lambda_1^{sp} < \lambda_2^{sp} = \lambda_3^{sp}.$$

Parameters	Parameter values
K_{Eq}	0.5mM
$K_{i_{[S]}}$	0.5mM
$K_{i_{[P]}}$	0.5mM
K_m	1.5mM
κ_1	1.0(–)
κ_2	0.5(–)
κ_3	1.0(–)

Table 2.6: Parameters for system with substrate and product inhibitions.

This result shows that without the presence of the initial substrate and product concentrations, the system remains locally asymptotically stable throughout the reaction. Further analysis on the change of $[S]_0$ and $[P]_0$ is discussed in the following section.

2.3.1 Bifurcation Analysis

The study of bifurcation of the system governed by the substrate and product inhibitions was the first attempt carried out in this work and it has not been attempted elsewhere. The behaviour of the feedback product inhibition that resulted in the singular form of equations made it an unattractive system to carry out the analysis. However, with the appropriate simplification described previously, the singular system of equations was reduced into a lower dimensional form. With the new form of autonomous ordinary differential equations, bifurcation analysis based on varying the amount of inhibitors i.e. the initial concentrations of substrate and product was carried out.

In order to monitor the bifurcation behaviour for the system described by the 3 autonomous differential equations, the parameters $[S]_0$ and $[P]_0$ were varied during the simulation. The system was initially operated in the absence of the product and the plots of the parameter against the state space with variable total initial substrate concentrations are shown in *Figures 2.30* to *2.32*. The simulations carried out with the forward and backward continuations with a step size of 0.01 using the continuation software supplied by Dhooge *et al.* (2003) on MATLAB® environment. The initial conditions were kept constant in each continuation run in the given figures.

Apparently, there is no sign of any branching of solutions as the total initial substrate

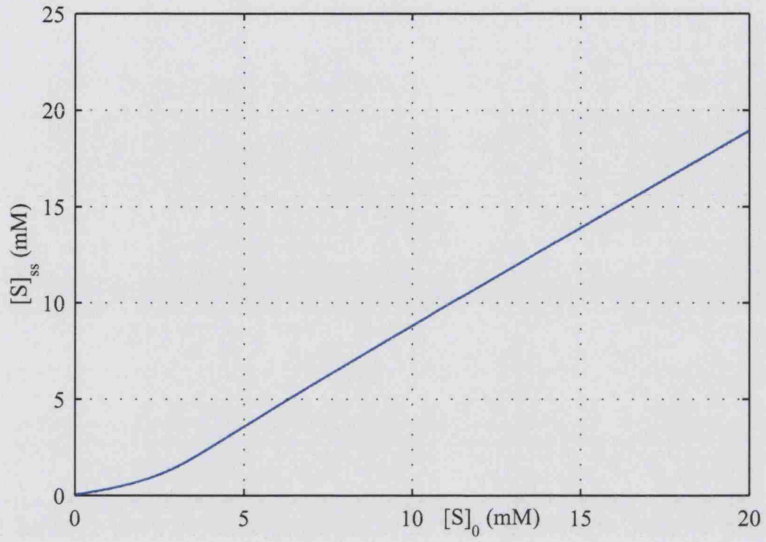

Figure 2.30: Diagram showing the effect of varying the total initial substrate on the remaining substrate present at steady-state in the reaction medium, ($[P]_0 = 0$ and the other parameters are shown in *Table 2.6*).

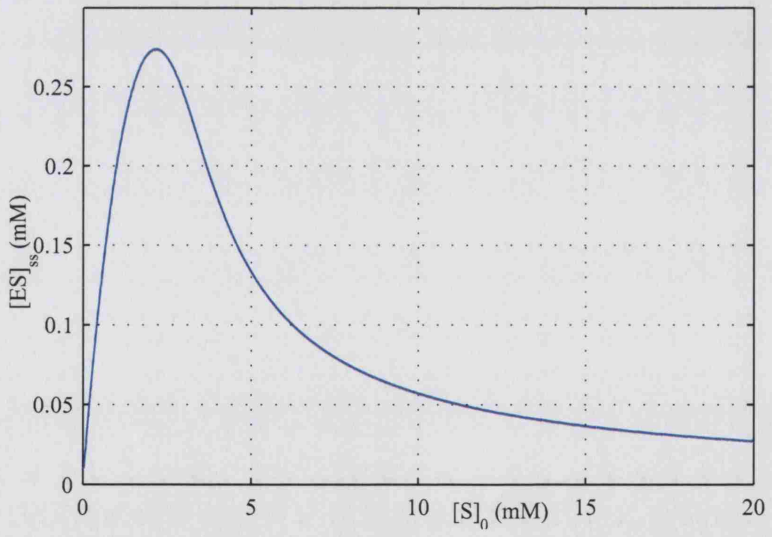

Figure 2.31: Diagram showing the effect of varying the total initial substrate on the formation of intermediate complex at steady-state $[ES]_{ss}$, ($[P]_0 = 0$ and the other parameters are shown in *Table 2.6*).

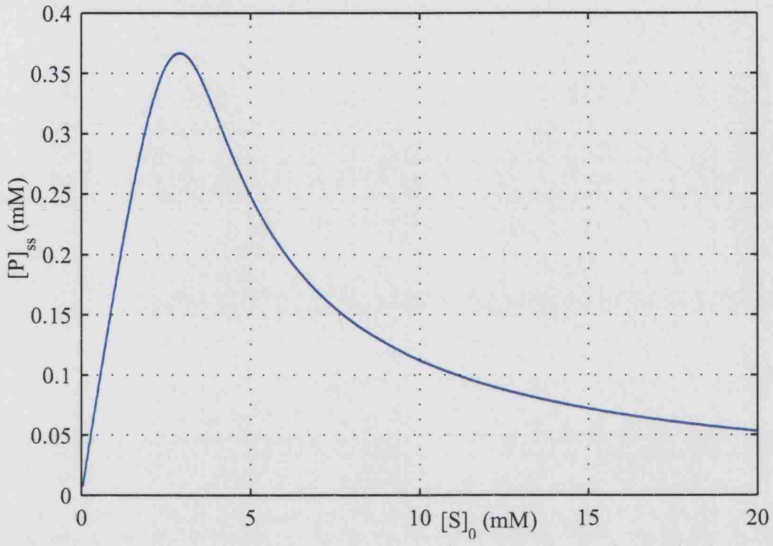

Figure 2.32: Diagram showing the effect of varying the total initial substrate on the formation of product at steady-state $[P]_{ss}$, ($[P]_0 = 0$ and the other parameters are shown in *Table 2.6*).

concentration was varied. The curves for the 3 species shown in the given figures could be explained using the eigenvalue plot in *Figure 2.33*. The 3 sets of eigenvalues are concentrated in the fourth quadrant of the plot, which give them the negative signs throughout. Therefore, local stability exists no matter how high the total concentration of substrate, $[S]_0$ changes throughout the system. As depicted in *Figure 2.30*, the amount of available substrate gradually increased as its total initial concentration was increased. This is due to the effect of substrate inhibition, as the active-sites of the enzyme were inhibited by the excess amount of substrate, the free substrate then started to accumulate in the reaction medium and therefore, resulted in a high amount unconverted substrate. On the other hand, the concentration of the intermediate complex at steady-state, $[ES]_{ss}$ and the product, $[P]_{ss}$ started to decrease after the initial concentration of substrate reached a value of approximately, 2.5mM. Such a behaviour is also due to the effect of inhibition to the particular enzyme. The amount of intermediate complex as well as the product formed reached a maximum at the same concentration of the total initial substrate, and the values began to decrease. The blocking of the specific enzyme's active-sites by the substrate led to the decrease of the formation of the specific intermediate complex which could also lead to

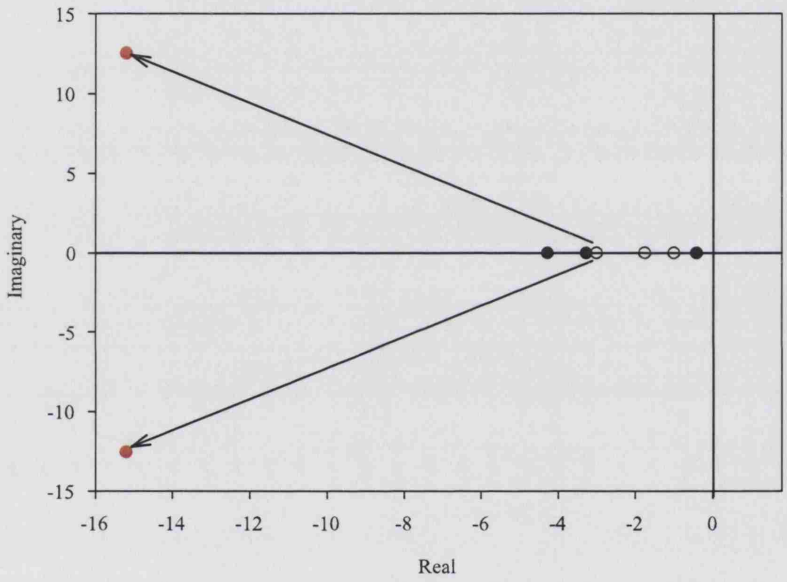

Figure 2.33: Eigenvalues plot representing the solutions obtained in *Figures 2.30* to *2.32* for $[S]_0 = 1.5$mM, '•', $[S]_0 = 3.5$mM, '○' and $[S]_0 = 15$mM, '•' at $[P]_0 = 0$mM.

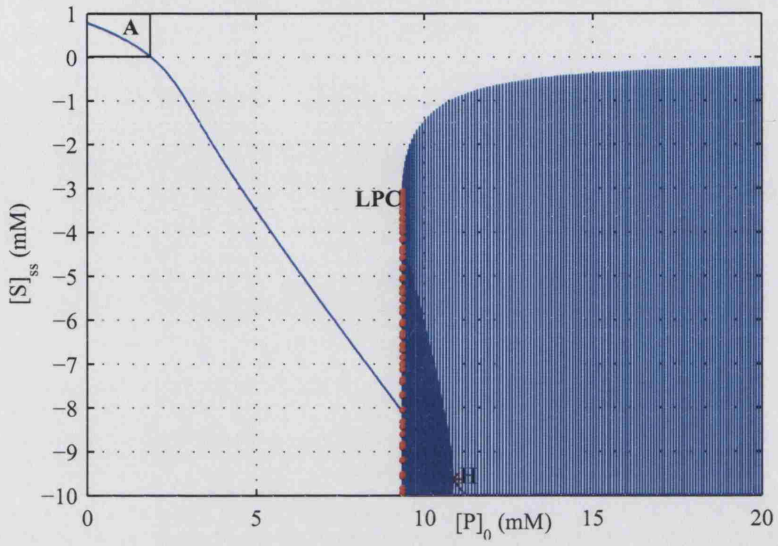

Figure 2.34: Bifurcation diagram showing the effect of varying the total initial product concentration towards the consumption of substrate, $[S]_{ss}$ at steady-state ($[S]_0 = 1.5$mM and the other parameters are shown in *Table 2.6*. Region A is in the positive quadrant and within the limit of experimental observation).

the decrease of the formation of the particular product, [P].

A similar analysis with the presence of a small amount of the total initial product concentration, $[P]_0$ was also undertaken. The results obtained were similar to that described previously. Therefore, it can be concluded that the uncompetitive substrate inhibition does not give rise to bifurcation phenomena. According to the mechanism of enzyme-catalysed reaction shown previously, the product formed during the reaction is bound to the free enzyme via feedback inhibition. The characteristics of feedback typed inhibition has been discussed previously by Higgins (1967) which was found to exhibit a number of bifurcation phenomena. The results of varying the initial amount of product concentration are shown in *Figures 2.34* to *2.36*.

The abbreviation H in the diagrams locates the onset of Hopf bifurcation at $[P]_{0,H} = 11.374848$mM that leads to the formation of limit cycle from a stable equilibrium point. The first or local Lyapunov exponent[1] at this Hopf point was calculated as 1.432749×10^{-1}, which

[1]Lyapunov characteristic exponents of a trajectory measure the average long-term exponential rate of divergence of all adjacent trajectories based on the limit as time goes to infinity.

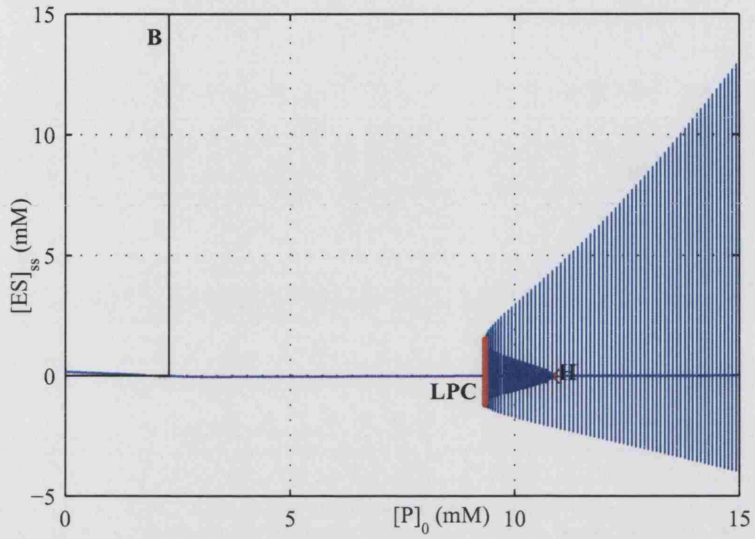

Figure 2.35: Bifurcation diagram showing the effect of varying the total initial product concentration during the formation of intermediate complex $[ES]_{ss}$ at steady-state, ($[S]_0 = 1.5$mM and the other parameters are shown in *Table 2.6*. Region B is in the positive quadrant and within the limit of experimental observation).

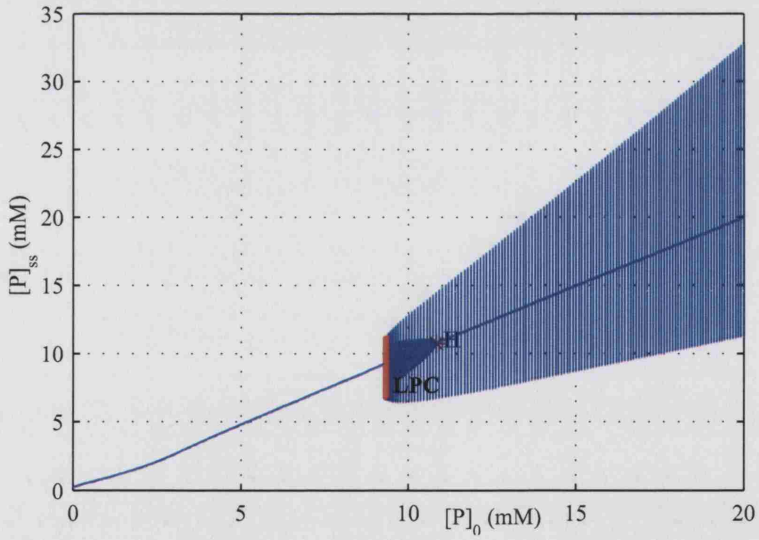

Figure 2.36: Bifurcation diagram showing the effect of varying the total initial product concentration during the formation of product $[P]_{ss}$ at steady-state, ($[S]_0 = 1.5$mM and the other parameters are shown in *Table 2.6*).

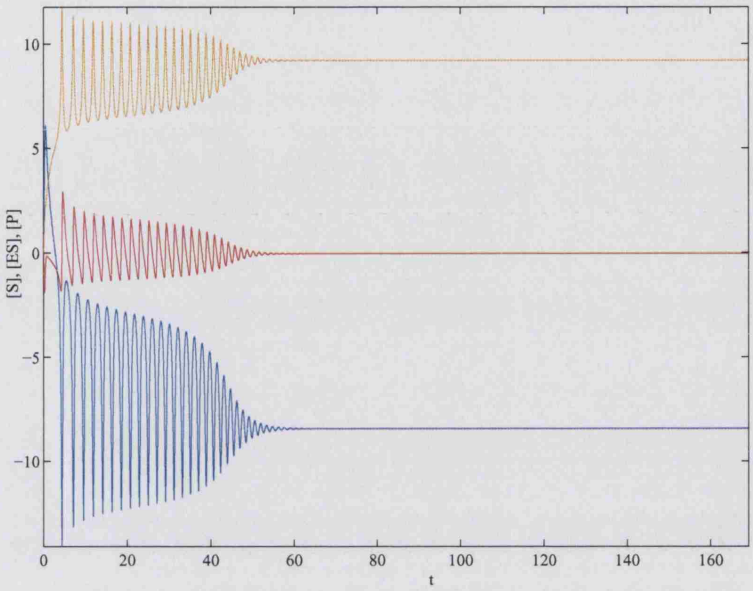

Figure 2.37: The time trajectories of the available amount of substrate, [S] (blue line), the amount of intermediate complex, [ES] (red line) and the amount of product formed, [P], (orange line) forming a stable focus at $[P]_0 = 9.4\text{mM}$.

explained that the point exhibited a subcritical Hopf bifurcation. The beginning of the limit cycle is marked by the abbreviation, LPC (limit point cycle) at $[P]_{0,\text{LPC}} = 9.470245\text{mM}$ in the bifurcation diagrams. The time trajectories of each species are shown in *Figures 2.37* and *2.38*.

The change of the total initial product concentration obviously produced an interesting dynamical phenomena compared to that of the previous study on the change of the total initial substrate concentration. The shift of the stability criteria from the stable node to the stable focus and consequently to sustained oscillations due to the onset of Hopf bifurcation is clearly described by the individual bifurcation diagrams of [S], [ES] and [P] respectively. A simplified version of *Figure 2.36* is given in *Figure 2.40*. The lines indicate the paths of the respective solutions as the bifurcation parameter $[P]_0$ evolves. However, during an experimental analysis, it is unlikely that we could only see an increase of the total initial product concentration such that the bifurcation diagram behaves in a way shown in *Figure 2.41*. Under these conditions, the system can produce a self-exited oscillation following a Hopf bifurcation. However, this

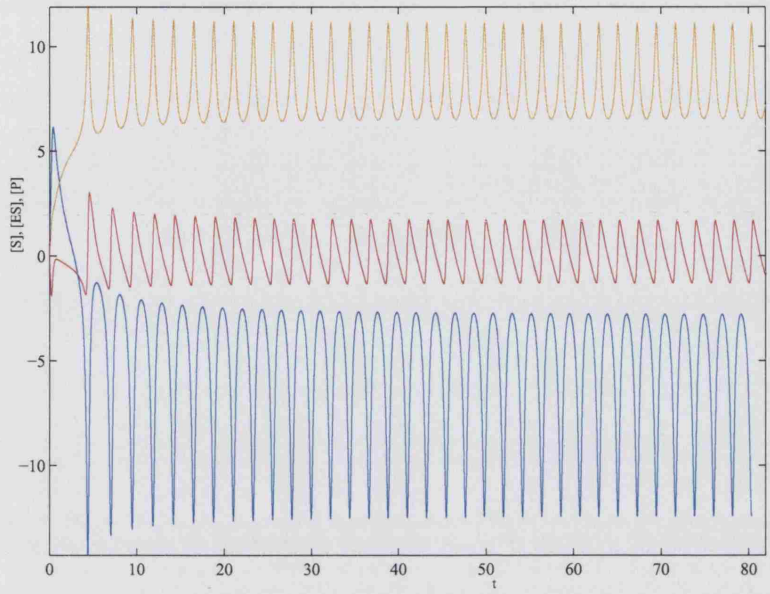

Figure 2.38: The time trajectories of the available amount of substrate, [S] (blue line), the amount of intermediate complex, [ES] (red line) and the amount of product formed, [P], (orange line) during the period of sustained oscillations at $[P]_0 = 9.6\text{mM}$.

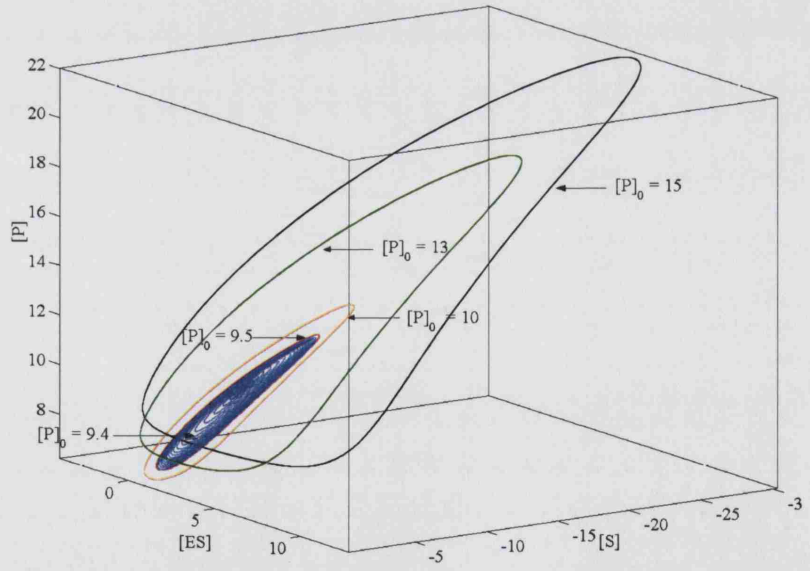

Figure 2.39: The transition of stable focus to the formation of limit cycles in the 3–dimensional phase-space diagram.

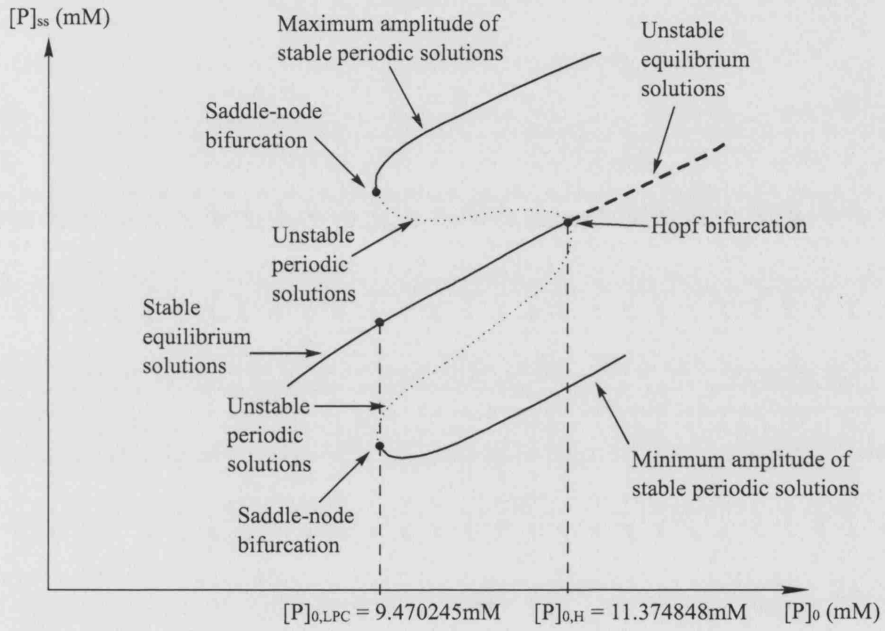

Figure 2.40: A schematic bifurcation diagram from *Figure 2.36* for an exact behaviour, showing the solution paths of Hopf and saddle node bifurcations that give the transition from stable node to self-sustained oscillation.

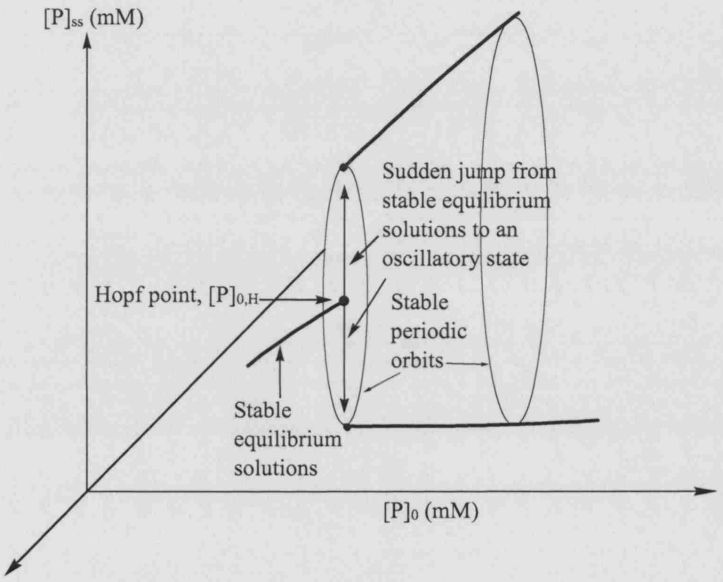

Figure 2.41: Bifurcation diagram of an increase of the total initial product concentration, $[P]_0$ in a real experimental procedure, showing a sudden jump of solutions from a stable equilibrium to an oscillatory state with a Hopf point, $[P]_{0,H}$.

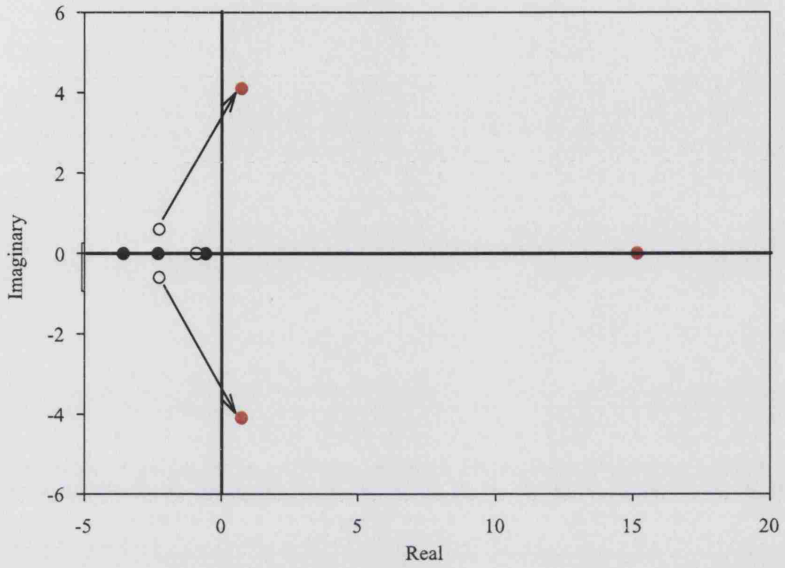

Figure 2.42: The movement of eigenvalues describing the transition form a stable node to Hopf bifurcation. $[P]_0 = 2mM$, '•', $[P]_0 = 4mM$, '○' and crossing the y–axis at $[P]_0 = 9.5mM$, '•'.

bifurcation is of subcritical type and for an evolving parameter, the system jumps to large amplitude oscillations from the stable equilibrium solution. Even when the static equilibrium solution is stable, a full global dynamic analysis shows that its basin of attraction reduces as the Hopf bifurcation is approached so that even small perturbations from the stable solution can lead to dynamic evolution onto the periodic solution. Therefore, a local, analytic stability analysis is no longer sufficient to guarantee robustness of the equilibrium steady-state. It is also believed that the results presented here could never be seen experimentally. The regions A and B marked in *Figures 2.34* and *2.35* respectively are the only limits where experimental data can be observed.

Such a transition is due to the movement of the eigenvalues from the negative real values on the x–axis in the second quadrant to the imaginary values on the y–axis and finally crossing the y–axis giving rise to the Hopf bifurcation. This movement can be shown using a simple plot given in *Figure 2.42*. *Figure 2.39* also shows the transition from the stable focus to the

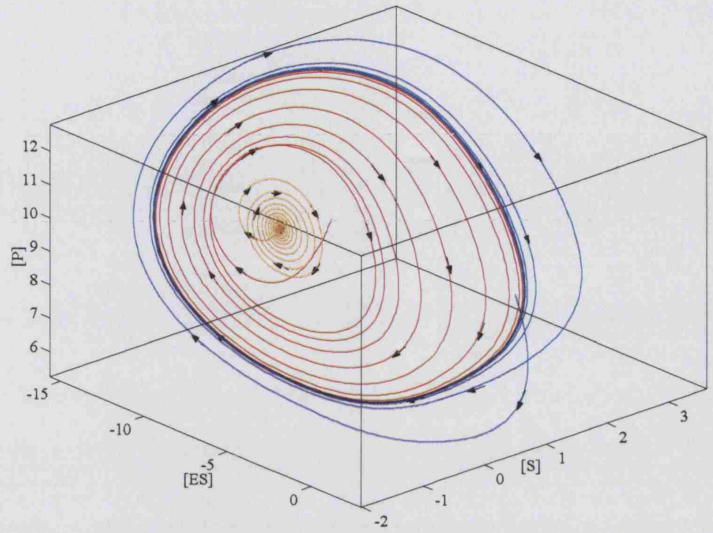

Figure 2.43: The different flows exhibited at $[P]_0 = 10mM$ (below the Hopf point). The stable fixed point before the onset of Hopf bifurcation leads to a stable focus when the initial condition starts near this fixed point. The other two trajectories (blue and red lines) are attracted to a limit cycle at different initial conditions away from the basin of attraction of the stable focus.

formation of periodic orbits at different values of $[P]_0$. In addition, in order to show the different flows observed before the Hopf point and that after the Hopf point, 3–dimensional phase-space diagrams were plotted at different initial conditions where different basin of attractions were detected. These are clearly shown in *Figures 2.43* and *2.44*.

The study of bifurcation on the system affected by substrate and product inhibitions has given an interesting dynamical phenomena. However, the results based on such an analysis could not be explained especially when the solutions bifurcate in the forth quadrant of the plot i.e. on the negative y–axis. The results obtained in this work also inconsistent to that established by Roussel and Fraser (1993) on the global analysis of the simple enzyme-catalysed mechanism. It is believed that the simplification used by the group only applies to the system that is governed only by one type of inhibition, either by the substrate or product species. The existence of the two types of inhibitions in a single enzyme-catalysed reaction only leads to the results described previously.

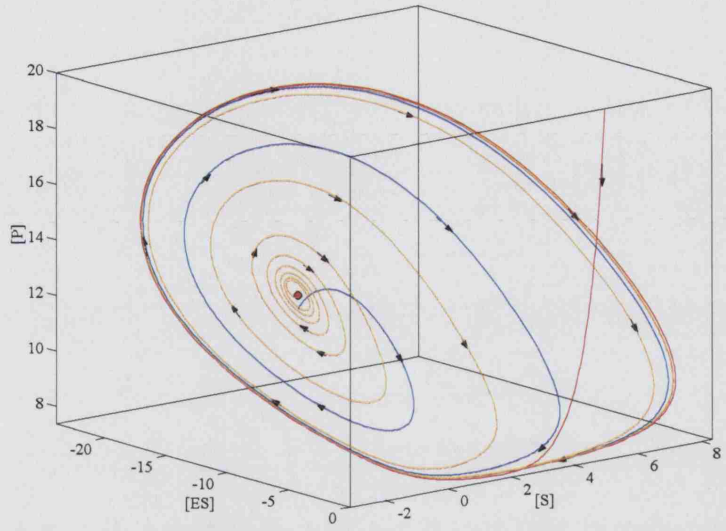

Figure 2.44: The different flows exhibited at $[P]_0 = 13mM$ (above the Hopf point). The unstable point represented by the red dot repelled the two trajectories which started near the point. Both trajectories are attracted to the limit cycle (blue and orange lines). A similar behaviour is observed for the initial point started away from this unstable fixed point.

2.3.2 Invariant Manifold of the Rate Expression Describing Enzyme Catalysis

In order to obtain the trajectory governed by the substrate, product and the intermediate complexes, the closed form of autonomous ordinary differential equations were further reduced following the *chain rule* of calculus. The form of equation omits the time scale from the trajectory, therefore, produces the only required variables for the invariant manifold. A similar form of expression can be obtained for the product formation. However, using the method of global analysis introduced by Fraser (1988); Roussel and Fraser (1990, 1991) and Roussel and Fraser (1993), which is only applicable to one type of inhibition, the result from such an analysis using the same system could lead to a similar behaviour to that obtained in the bifurcation study. Further reading on the method of global analysis can be referred to the publications cited above.

2.4 Summary and Conclusion

The transient dynamics as well as the steady-state analysis of an enzyme-catalysed system have been found to give completely different results, and both are important in the study of enzyme-catalysed reactions. Such results were obtained based on a simple mechanism of a reaction between an enzyme and a single substrate.

Initially, the dynamics of the system were analysed based on the two assumptions; the sQSSA assumption proposed by Briggs and Haldane and the tQSSA assumption proposed by Borghans *et al.* (1996). A comparison between these assumptions was undertaken and new conditions for the stability of the nontrivial steady-state were proposed. It was also found that the two systems of equations shared the same eigenvalues with a different set of eigenvectors. This was studied based on the trajectories of the systems and they were found to exhibit a degenerate case in singular perturbation at low ratios of total enzyme to total substrate concentrations which later proved the validity of the two assumptions. However, an increase of such a ratio left the sQSSA to be invalid due to the shift of the trajectories, which made the assumption of $\frac{d[ES]}{dt} \approx 0$ became unacceptable. Such an increase only gave a slight shift of the trajectories for the tQSSA and therefore, preserved the validity of the assumption.

The complexity of an enzyme-catalysed reaction was increased by introducing the effect of inhibitions within the system. An enzyme reaction inhibited by the substrate and product concentrations was studied and the effect of increasing the total initial amount of inhibitors were analysed. The dynamics of the system was studied based on the bifurcation theory. The theory was used as a tool to track the branching of the steady-state solutions of the system. It was found that an increase of the total initial substrate concentration gave no branching phenomena which also concluded that the system was asymptotically stable. On the other hand, an increase of the total initial product concentration led to sustained oscillations from a stable sink which resulted from the Hopf bifurcation. However such an analysis could not be related to the actual enzyme catalysis due the negative values of the solutions. This analysis has led to a conclusion that in order to study an enzyme-catalysed system, one should initially attempt to understand the mechanism of a particular reaction before pursuing with the steady-state analysis and the only technique which can be used to carry out such work is to describe the system in terms of

differential forms. With a complete set of differential equations, the trajectory of each species involved in a reaction could be monitored and individually analysed.

Chapter 3

Kinetic Studies of an Isolated Cyclohexanone Monooxygenase Enzyme System with a Progress Curve Analysis

3.1 Introduction

3.1.1 Kinetic Study of Enzyme-Catalysed Systems

The study of the kinetics of enzyme-catalysed reaction is often based on the Michaelis-Menten model. The usual kinetic parameters from the model include V_{max} and K_m. These values could easily be used to find the ratio of the second order rate constant, $\frac{k_{cat}}{K_m}$, which explains the catalytic efficiency of an enzyme in a specific reaction. The methods of determining these parameters should be considered as one of the important tasks since these values are crucial in characterising enzymes, especially their binding properties and their efficiencies.

The most common techniques used to estimate the values of V_{max} and K_m are, the direct fitting of the experimental data to the model equation by the nonlinear regression technique, and the method of transforming the data according to the linear form of the model equation and hand-plot the points. The latter technique has been summarised in *Chapter 2.* A similar technique to that of the linear transformation known as the direct linear plot has also been developed by Eisenthal and Cornish-Bowden (1974) and statistically analysed by the same group (Cornish-Bowden and Eisenthal, 1974). The method is however applicable only to the standard

Michaelis-Menten model with a single inhibition term. Between these two methods, the nonlinear regression has been found not only giving a better estimate of the parameter values but it also gives less estimation errors. Other advantages would be the *standard error* of the accuracy of the parameters that it provides during the analysis and the inherent subjectivity that one could avoid with the graphical method (line drawn by eye in a double-reciprocal plot).

Another popular method of estimating the kinetic parameters utilising the nonlinear regression is the progress curve analysis (Duggleby and Morrison, 1977, 1978) which in some other publications it is termed as the method of integrated rate expression (Fernley, 1974; Nimmo and Atkins, 1974; Boeker, 1987). The technique is similar to that of the direct data fitting to the model equation, but it avoids the experimental data to be differentiated i.e. the initial rate of reaction is unnecessary. Such a method rarely determines the rate directly and the process of differentiating the data is necessarily inexact. In addition, the percentage error would probably be very high if the assay method is discontinuous and the change in concentration is not linear with time (Duggleby, 1995, 2001). This would give unreliable values of the rate of a particular reaction and limits the amount of quantitative and mechanistic information that can be deduced about the enzyme.

This chapter mainly discusses the method of progress curve analysis applied to cyclohexanone monooxygenase enzyme system. The study is based on the rate expression derived using the King-Altman technique which will be carefully described in detail in Section 3.2. A general introduction about the enzyme and its catalytic property is discussed in the following section. A recent finding of a similar enzyme (phenylacetone monooxygenase) which has the same property as that of cyclohexanone mooxygenase is also explained. The binding sites of such an enzyme provides a general picture of the enzyme under investigation. Attempts to determine all the kinetic constants from the rate expression were made and the values were carefully tabulated at the end of this chapter.

3.1.2 Cyclohexanone Monooxygenase Enzyme: A Model System

The reaction catalysed by monooxygenase enzyme has been previously described in *Chapter 1.* The enzyme catalyses the insertion of molecular oxygen into the carbon–carbon bond of linear or cyclic ketones forming the corresponding esters or lactones in Baeyer-Villiger reaction. Prior

to the kinetic modelling, the reaction mechanism of enzyme-catalysed Baeyer-Villiger reaction should be fully understood for further kinetic studies. This section discusses in particular, the summary of method of determining the reaction mechanism of enzyme-catalysed Baeyer-Villiger reaction. This follows the derivation of the rate expression for the conversion of bicyclic-ketone forming chiral lactones.

The Mechanism of Monooxygenase Enzyme-Catalysed Baeyer-Villiger Reaction

The first mechanism of Baeyer-Villiger reaction was proposed by Criegee in 1948 describing the reversible addition of the peracid terminal oxygen to the carbonyl which yields the key tetrahedral intermediate that later undergoes concerted fragmentation to products (Stewart, 1998). For similar type of systems, the irreversible rearrangement of the tetrahedral intermediate is rate limiting and subjected to the acid catalysis. This was then explained by Schwab (1981) whom investigated in particular, oxygenase enzyme-catalysed Baeyer-Villiger reaction using deuterium NMR where the intermediary of flavin C–4a hydroperoxide (FlCOOH) was found in the flavin monooxygenase action.

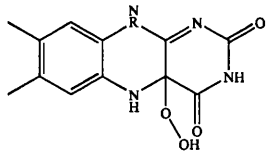

Figure 3.1: Hydroperoxide intermediate scheme.

Many proposals on the mechanistic analysis of the system suggested that the mechanism followed a nucleophilic attack of $FlOO^-$ on the substrate ketone or a nucleophilic attack by enolized ketone on the distal oxygen of FlCOOH, a carbonyl oxide derivative of flavin. The use of hydrogen isotope at C–2 attached at the chiral centre is required in order to enzymatically produce chiral C–6 caprolactone. Such a method has been found inconclusive about the way Baeyer-Villiger reaction mechanism should be arranged. This was mainly due to the less evident of the label exchange on the NMR analysis. Ryerson *et al.* (1982) later proposed a mechanism involving both the 4a–peroxyflavin and the 4a–hydroxyflavin intermediates with the presence of cofactor as electrons donor. This was then improved by Sheng *et al.* (2001) incorporating

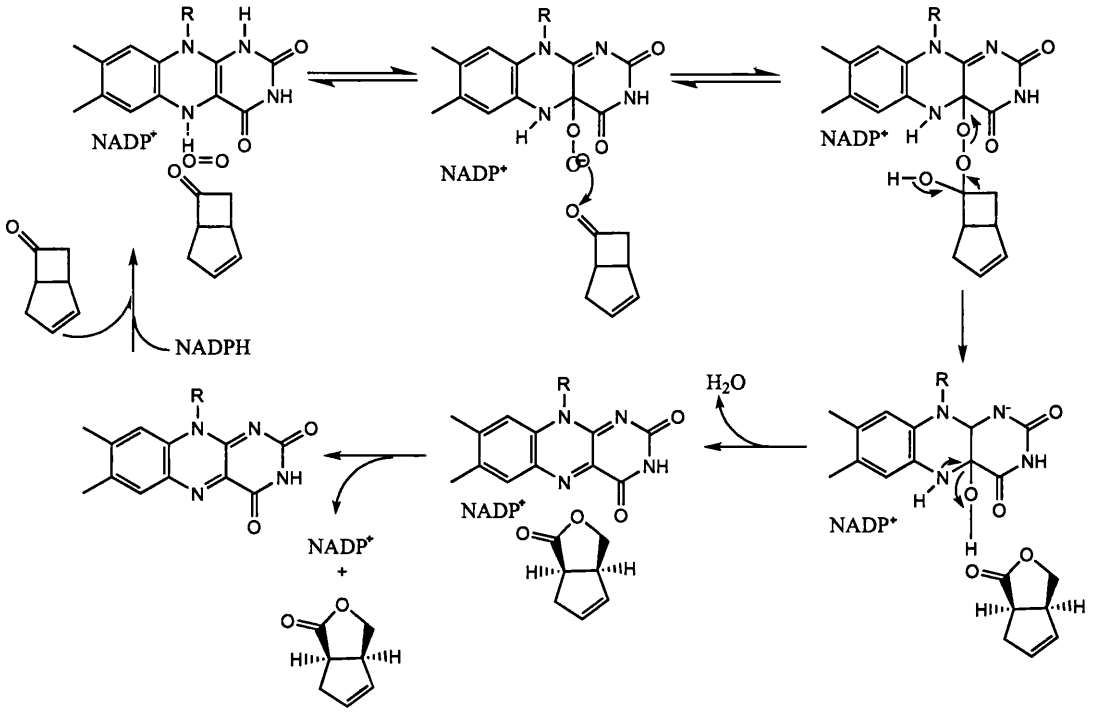

Figure 3.2: Mechanism of monooxygenase enzyme-catalysed conversion of bicyclo[3.2.0]hept-2-en-6-one to (-)1(S)5(R)2-oxabicyclo-[3.3.0]oct-6-en-3-one.

cofactor, molecular oxygen and substrate. A complete schematic diagram of the mechanism based on the natural substrate (cyclohexanone) proposed by Ryerson *et al.* (1982) and Sheng *et al.* (2001) is given in *Figure 3.2.*

Only recently, the work of Malito *et al.* (2004) towards crystalizing Baeyer-Villiger monooxygenase enzyme has successfully proven the earlier proposed mechanism. The result which was based on phenylacetone monooxygenase, (PAMO) enzyme-catalysed conversion of phenylacetone to phenylacetate has been shown that it followed a similar mechanism of the nonenzymatic reaction. Based on an X–ray diffraction analysis, the enzyme expressed from *Thermobifida fusca* is monomeric with molecular mass of 62kDa and catalyses reaction in the presence of FAD and NADPH (52kDa monomeric cyclohexanone monooxygenase obtained from *Acinetobacter cal-*

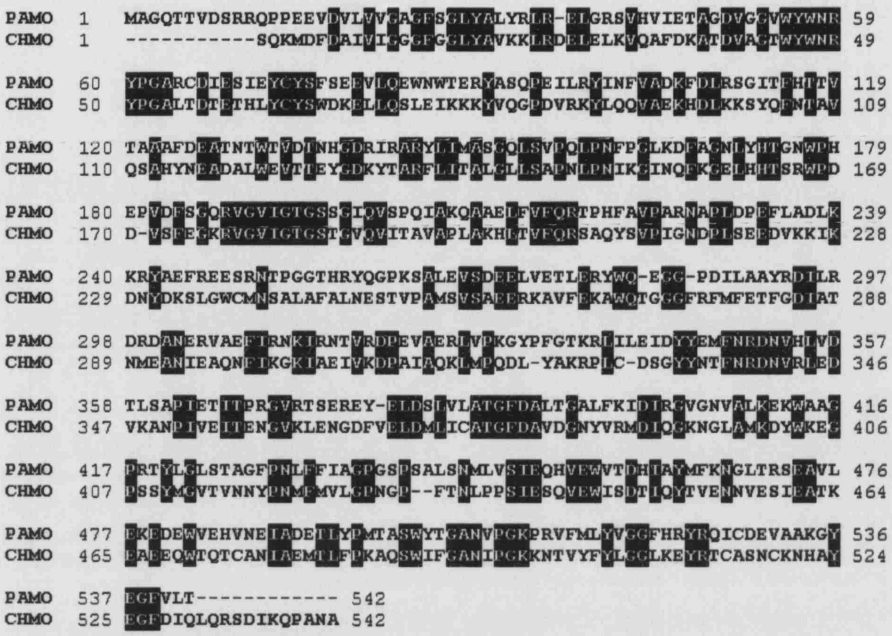

Figure 3.3: Sequence alignment of the two types of of monooxygenases.

coaceticus with similar requirements to undergo catalytic reaction (Willetts, 1997)). Since the crystal structure of CHMO is still unavailable, a comparison between both proteins can only be carried out by looking at their sequence alignments. The alignment of PAMO enzyme from *Thermobifida fusca* and CHMO enzyme from *Acinetobacter calcoaceticus* is given in *Figure 3.3.* Although there are two different substrates used to carry out these reactions, the active sites of monooxygenase enzymes should preserve its positions, therefore, the properties of active sites of CHMO enzyme could be studied from the available PAMO enzyme structure. The structure consists of two domains; the FAD-binding domain and the NADPH-binding domain. The FAD-binding domain consists of 3 C–terminal α–helices that are not available in the corresponding domain of disulphide oxidoreductases, while the NADPH-binding domain shown as a long protruding loop that occupies the adenine site (*Figure 3.4(b)*), exhibits a large insertion of 120 amino acids after the $\beta\alpha\beta$ unit that forms at the centre of the NADPH-binding site (*Figure 3.4*). Such an insertion of residues forms an α–helical subdomain which interacts with the FAD-binding domain forming part of the active site. Residues from the given subdomain were found to

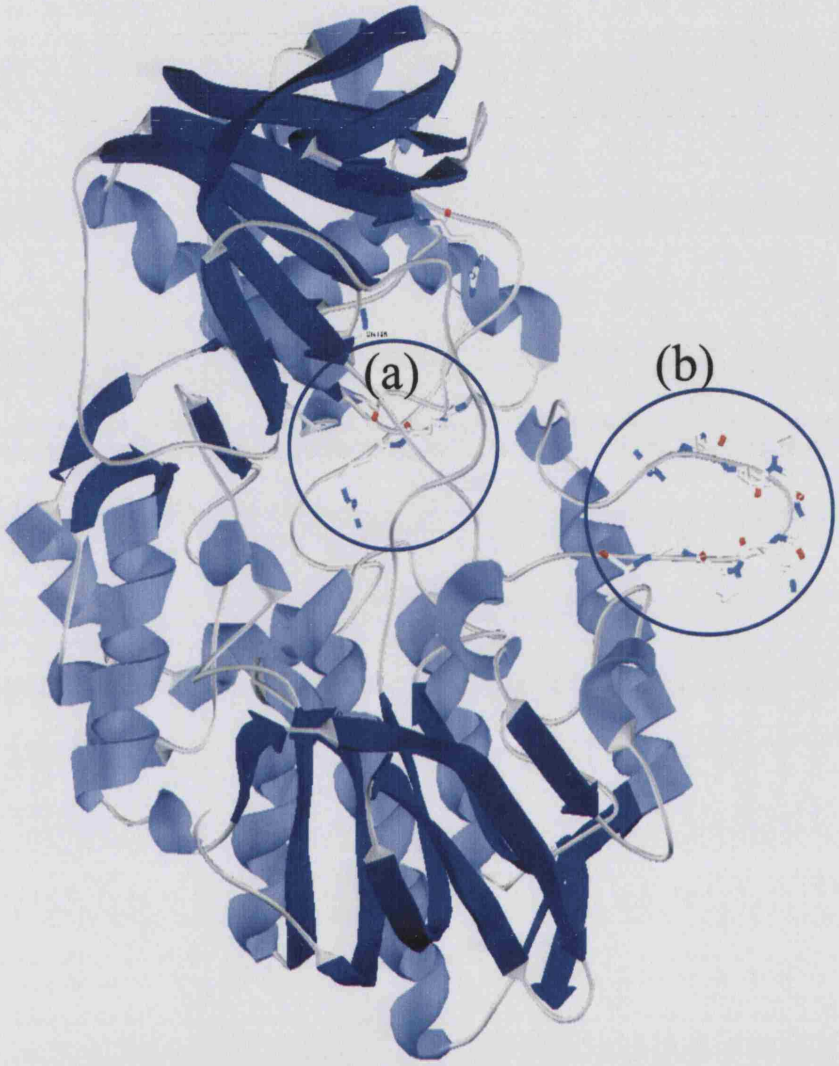

Figure 3.4: The monomer of phenylacetone monooxygenase, (PAMO) showing the active site and binding domains of (a) FAD and (b) $NADP^+$. The structure was rendered from the sequence provided by Malito *et al.* (2004).

display poor conservation and this has provided a peculiar characteristic of the 3–dimensional topological structure of Baeyer-Villiger type of enzyme. Such finding has also supported the proposed mechanisms by Alphand and Furstoss (1992); Kelly (1996) and Ottolina *et al.* (1996).

3.2 Derivation of the Rate Expression of Cyclohexanone Monooxygenase Enzyme-Catalysed Baeyer-Villiger Reaction

In order to obtain the rate expression of enzyme-catalysed Baeyer-Villiger reaction, the method of King-Altman was applied in this work. However, for the purpose of checking the work, the method of Briggs-Haldane was also applied and solved using Mathematica® and it can be referred to in *Appendix A*. The King-Altman method of mapping the enzyme species was used and from the given mechanism of bicyclo[3.2.0]hept-2-en-6-one reaction, a simple representation according to the method can be formed (*Figure 3.6*). The notations used to represent the enzyme species are defined in *Figure 3.5.*

Apparently, in *Figure 3.6* there are two intermediate complexes involved; [$E_{CHMO}Co^{+}HOOS$] and [$E_{CHMO}Co^{+}(H_2O)P$] and they were formed due to the isomerisation of central complexes. Since both species represented separate entities with the corresponding rate constants for their conversion, these complexes could be combined such that the interconversion acted as a single intermediate enzyme complex. However, the final form of the rate expression should be the same to that of the form without such a simplification. This method is useful if the mechanism describing an enzyme-catalysed reaction is as complex as the one treated in this work. When these central complexes were combined, they were usually considered together as a single corner of interconversion pattern. The number of patterns of every species involved in the reaction could be determined using the combinatorial expression given by

$$ {}_mC_{(n-1)} = \frac{m!}{(n-1)!(m-n-1)!}. $$

As apparently observed from *Figure 3.6* there are 6 number of lines corresponding to 6 number of enzyme species, thus, 6 number of patterns should be obtained from the mapping of each species. *Figure 3.6* can be mapped into individual enzyme species and they are shown in *Figure*

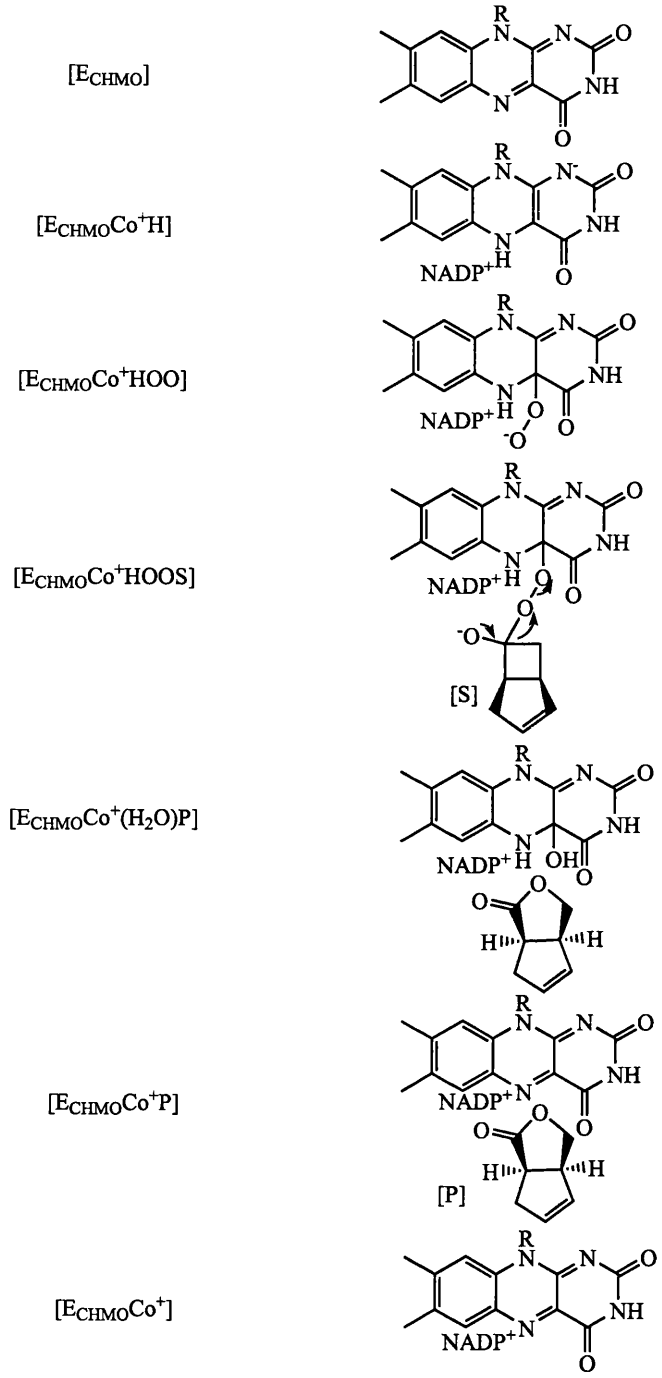

Figure 3.5: Simplified notations representing enzyme intermediate complexes.

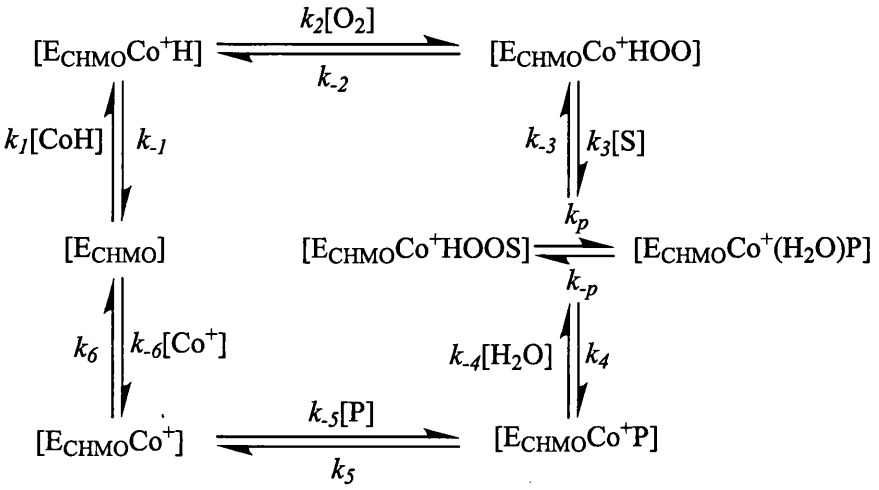

Figure 3.6: King-Altman representation of cyclohexanone monooxygenase enzyme-catalysed conversion of bicyclo[3.2.0]hept-2-en-6-one.

3.7. These enzyme intermediate complexes were expressed in terms of $\frac{[E_{CHMO}]}{[E_T]}$, $\frac{[E_{CHMO}Co^+H]}{[E_T]}$, $\frac{[E_{CHMO}Co^+HOO]}{[E_T]}$, $\frac{[E_{CHMO}Co^+HOOS] \rightleftharpoons [E_{CHMO}Co^+(H_2O)P]}{[E_T]}$, $\frac{[E_{CHMO}Co^+P]}{[E_T]}$ and $\frac{[E_{CHMO}Co^+]}{[E_T]}$ with $[E]_T$ defined as

$$\begin{aligned}[E]_T &= [E_{CHMO}] + [E_{CHMO}Co^+H] + [E_{CHMO}Co^+HOO] \\ &+ ([E_{CHMO}Co^+HOOS] \rightleftharpoons [E_{CHMO}Co^+(H_2O)P]) \\ &+ [E_{CHMO}Co^+P] + [E_{CHMO}Co^+] \end{aligned} \quad (3.1)$$

All expressions are given in terms of rate constants, k_i. The concentration of water molecules formed during the reaction was considered to be at one molar, therefore, the terms $k_{-4}[H_2O]$ can be reduced into k_{-4}. The other terms such as, [S], [P], [CoH], $[O_2]$ and $[Co^+]$ represent substrate, product, reduced cofactor, molecular oxygen and oxidised cofactor concentrations respectively.

$$\begin{aligned}\frac{[E_{CHMO}]}{[E_T]} &= \frac{1}{[E_T]}(k_2k_3k_4k_5k_6[O_2][S]+k_{-1}k_{-2}k_{-3}k_{-4}k_{-5}[P]+k_{-1}k_3k_4k_5k_6[S] \\ &+ k_{-1}k_{-2}k_{-3}k_{-4}k_6+k_{-1}k_{-2}k_{-3}k_5k_6+k_{-1}k_{-2}k_4k_5k_6) \end{aligned} \quad (3.2)$$

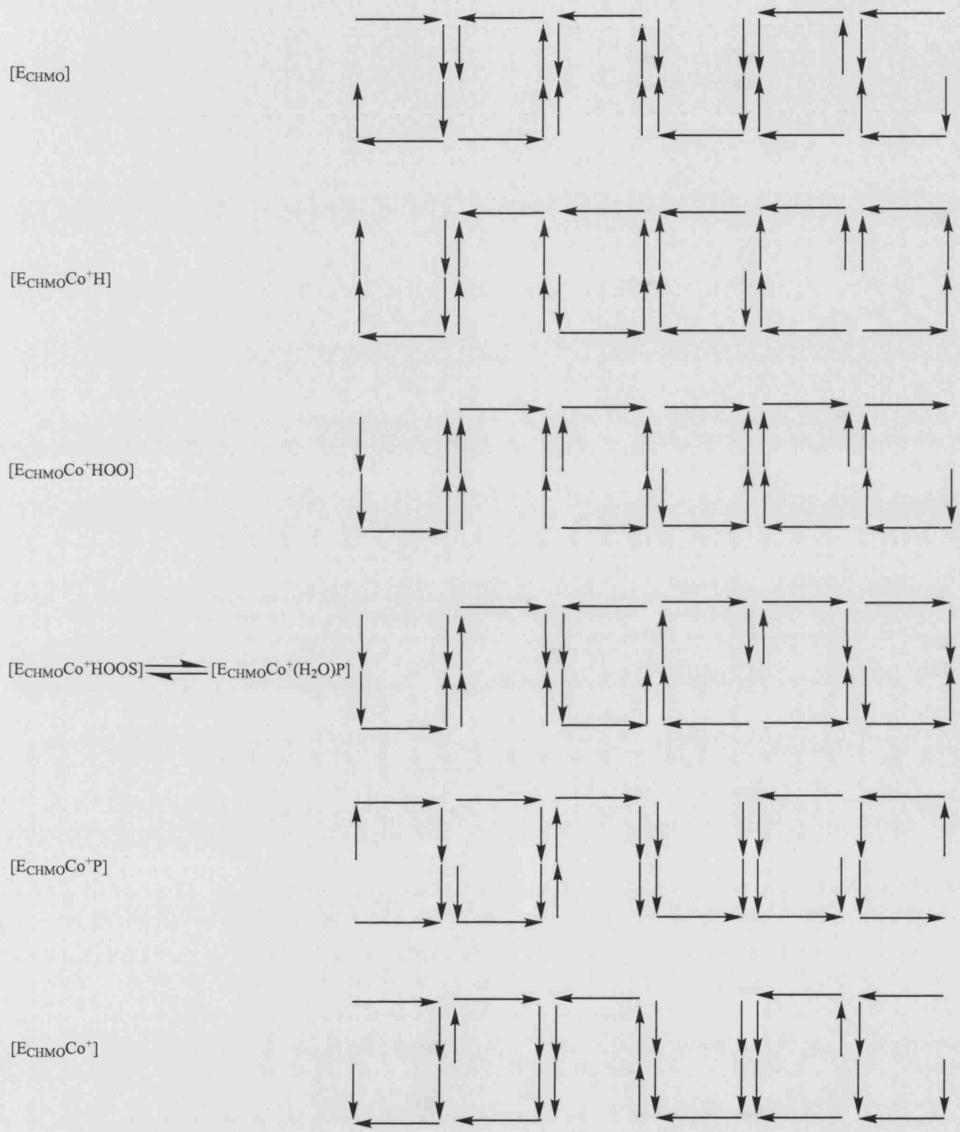

Figure 3.7: Patterns obtained from mapping of reaction routes from *Figure 3.6.*

$$\begin{aligned}\frac{[E_{CHMO}{}^{Co^+H}]}{[E_T]} &= \frac{1}{[E_T]}(k_1k_3k_4k_5k_6[CoH][S]+k_{-2}k_{-3}k_{-4}k_{-5}k_{-6}[P][Co^+] \\ &+ k_{-2}k_1k_4k_5k_6[CoH]+k_{-2}k_{-3}k_1k_5k_6[CoH] \\ &+ k_1k_{-2}k_{-3}k_{-4}k_{-5}[CoH][P] \\ &+ k_{-2}k_{-3}k_{-4}k_1k_6[CoH]) \end{aligned} \tag{3.3}$$

$$\begin{aligned}\frac{[E_{CHMO}{}^{Co^+HOO}]}{[E_T]} &= \frac{1}{[E_T]}(k_{-1}k_{-3}k_{-4}k_{-5}k_{-6}[P][Co^+] \\ &+ k_{-3}k_{-4}k_1k_2k_6[CoH][O_2] \\ &+ k_{-3}k_{-4}k_{-5}k_1k_2[CoH][O_2][P] \\ &+ k_{-3}k_{-4}k_{-5}k_{-6}k_2[O_2][P][Co^+] \\ &+ k_{-3}k_1k_2k_5k_6[CoH][O_2] \\ &+ k_1k_2k_4k_5k_6[CoH][O_2]) \end{aligned} \tag{3.4}$$

$$\begin{aligned}\frac{[E_{CHMO}{}^{Co^+HOOS}]\rightleftharpoons[E_{CHMO}{}^{Co^+(H_2O)P}]}{[E_T]} &= \frac{1}{[E_T]}(k_{-1}k_{-4}k_{-5}k_{-6}k_3[Co_+][S][P] \\ &+ k_{-4}k_1k_2k_3k_6[CoH][O_2][S] \\ &+ k_{-1}k_{-2}k_{-4}k_{-5}k_{-6}[P][Co_+] \\ &+ k_1k_2k_3k_5k_6[CoH][O_2][S] \\ &+ k_{-4}k_{-5}k_1k_2k_3[O_2][CoH][S][P] \\ &+ k_{-4}k_{-5}k_{-6}k_2k_3[O_2][S][P][Co^+]) \end{aligned} \tag{3.5}$$

$$\begin{aligned}\frac{[E_{CHMO}{}^{Co^+P}]}{[E_T]} &= \frac{1}{[E_T]}(k_{-5}k_1k_2k_3k_4[CoH][O_2][S][P] \\ &+ k_{-5}k_{-6}k_2k_3k_4[O_2][S][Co^+][P] \\ &+ k_1k_2k_3k_4k_6[CoH][O_2][S] \\ &+ k_{-1}k_{-5}k_{-6}k_3k_4[S][P][Co^+] \\ &+ k_{-1}k_{-2}k_{-5}k_{-6}k_4[P][Co^+] \\ &+ k_{-1}k_{-2}k_{-3}k_{-5}k_{-6}[P][Co^+]) \end{aligned} \tag{3.6}$$

$$\begin{aligned}\frac{[E_{CHMO}{}^{Co^+}]}{[E_T]} &= \frac{1}{[E_T]}(k_{-1}k_{-6}k_3k_4k_5[O^+][S] \\ &+ k_{-1}k_{-2}k_{-3}k_{-4}k_{-6}[Co^+] \\ &+ k_{-6}k_2k_3k_4k_5[O_2][S][Co^+] \\ &+ k_1k_2k_3k_4k_5[CoH][O_2][S] \\ &+ k_{-1}k_{-2}k_{-6}k_4k_5[Co^+] \\ &+ k_{-1}k_{-2}k_{-3}k_{-6}k_5[Co^+]) \end{aligned} \tag{3.7}$$

Since $\frac{d[P]}{dt}$ is given by;

$$\frac{d[P]}{dt} = k_5[E_{CHMO}Co^+P] - k_{-5}[E_{CHMO}Co^+][P]$$

therefore the rate of product formation is obtained by substituting equations (3.6) and (3.7) into the above expression and hence,

$$\frac{d[P]}{dt} = \frac{(k_1k_2k_3k_4k_5k_6[CoH][O_2][S] - k_{-1}k_{-2}k_{-3}k_{-4}k_{-5}k_{-6}[P][Co^+])[E]_T}{[E]_T} \tag{3.8}$$

Since $[E]_T$ is defined by equation (3.1) and upon substitution of the enzyme intermediate complexes given by equations (3.2) to (3.7), one would obtain the rate expression of cyclohexanone monooxygenase enzyme-catalysed Baeyer-Villiger reaction.

$$\begin{aligned}
\frac{d[P]}{dt} &= (k_1k_2k_3k_4k_5k_6[CoH][O_2][S] \\
&- k_{-1}k_{-2}k_{-3}k_{-4}k_{-5}k_{-6}[P][Co^+])[E]_T\{(k_{-2}k_{-1}k_4k_5k_6+k_{-3}k_{-2}k_{-1}k_5k_6 \\
&+ k_{-4}k_{-3}k_{-2}k_{-1}k_6)+(k_{-4}k_{-3}k_{-2}k_1k_6+k_{-3}k_{-2}k_1k_5k_6+k_{-2}k_1k_4k_5k_6)[CoH] \\
&+ k_{-1}k_3k_4k_5k_6[S]+(k_1k_2k_4k_5k_6+k_{-3}k_1k_2k_5k_6+k_{-4}k_{-3}k_1k_2k_6)[CoH][O_2] \\
&+ k_1k_4k_5^2k_6[CoH][S]+k_2k_3k_4k_5k_6[O_2][S] \\
&+ (k_1k_2k_3k_5k_6+k_1k_2k_3k_4k_6+k_{-4}k_1k_2k_3k_6+k_1k_2k_3k_4k_5)[CoH][O_2][S] \\
&+ k_{-6}k_{-1}k_3k_4k_5[S][Co^+]+k_{-5}k_{-4}k_{-3}k_{-2}k_1[CoH][P]+k_{-6}k_2k_3k_4k_5[Co^+][O_2][S] \\
&+ k_{-5}k_{-4}k_{-3}k_{-2}k_{-1}[P]+(k_{-6}k_{-2}k_{-1}k_4k_5+k_{-6}k_{-2}k_{-3}k_{-1}k_5+k_{-6}k_{-4}k_{-3}k_{-2}k_{-1})[Co^+] \\
&+ (k_{-6}k_{-5}k_{-2}k_{-1}k_4+k_{-6}k_{-5}k_{-3}k_{-2}k_{-1}+k_{-6}k_{-5}k_{-4}k_{-2}k_{-1}+k_{-6}k_{-5}k_{-4}k_{-3}k_{-1} \\
&+ k_{-6}k_{-5}k_{-4}k_{-3}k_{-2})[P][Co^+]+(k_{-6}k_{-5}k_{-1}k_3k_4+k_{-6}k_{-5}k_{-4}k_{-1}k_3)[S][P][Co^+] \\
&+ k_{-5}k_{-4}k_{-3}k_1k_2[CoH][O_2][P]+k_{-6}k_{-5}k_{-4}k_{-3}k_2[O_2][P][Co^+] \\
&+ (k_{-5}k_1k_2k_3k_4+k_{-5}k_{-4}k_1k_2k_3)[CoH][O_2][S][P] \\
&+ (k_{-6}k_{-5}k_2k_3k_4+k_{-6}k_{-5}k_{-4}k_2k_3)[O_2][S][P][Co^+]\}^{-1}
\end{aligned} \tag{3.9}$$

This is then further simplified by introducing the kinetic constant terms which reduced all the rate constant terms in the above equation. Hence, the final form of $\frac{d[P]}{dt}$ can be written as;

$$\begin{aligned}
\frac{d[P]}{dt} &= (V_{max_f}V_{max_r}[CoH][O_2][S] \\
&- \left(\frac{V_{max_f}V_{max_r}}{K_{eq}}\right)[P][Co^+])(V_{max_r}K_{m_{[S]}}K_{i_{[CoH]}}K_{i_{[O_2]}}+V_{max_r}K_{m_{[S]}}K_{i_{O_2}}[CoH] \\
&+ V_{max_r}K_{m_{[O_2]}}K_{i_{[CoH]}}[S]+V_{max_r}K_{m_{[S]}}[CoH][O_2]+V_{max_r}K_{m_{[O_2]}}[CoH][S] \\
&+ V_{max_r}K_{m_{[CoH]}}[O_2][S]+V_{max_r}[CoH][O_2][S]+\left(\frac{V_{max_r}K_{m_{[O_2]}}K_{i_{[CoH]}}}{K_{i_{[Co^+]}}}\right)[S][Co^+] \\
&+ \left(\frac{V_{max_r}K_{m_{[CoH]}}}{K_{i_{[Co^+]}}}\right)[O_2][S][Co^+]+\left(\frac{V_{max_f}K_{m_{[Co^+]}}}{K_{eq}}\right)[P]+\left(\frac{V_{max_f}}{K_{eq}}\right)[P][Co^+] \\
&+ \left(\frac{V_{max_r}K_{m_{[O_2]}}K_{i_{[CoH]}}}{K_{i_{[P]}}K_{i_{[Co^+]}}}\right)[S][P][Co^+]+\left(\frac{V_{max_f}K_{m_{[Co^+]}}}{K_{i_{[CoH]}}K_{i_{[O_2]}}K_{eq}}\right)[CoH][O_2][P] \\
&+ \left(\frac{V_{max_r}K_{m_{[CoH]}}K_{i_{[S]}}}{K_{i_{[Co^+]}}K_{i_{[P]}}}\right)[O_2][P][Co^+]+\left(\frac{V_{max_f}K_{m_{[Co^+]}}}{K_{i_{[S]}}K_{i_{[CoH]}}K_{i_{[O_2]}}K_{eq}}\right)[CoH][O_2][S][P] \\
&+ \left(\frac{V_{max_r}K_{m_{[CoH]}}}{K_{i_{[P]}}K_{i_{[Co^+]}}}\right)[O_2][S][P][Co^+]+\left(\frac{V_{max_f}K_{m_{[Co^+]}}}{K_{i_{[CoH]}}K_{eq}}\right)[CoH][P] \\
&+ \left(\frac{V_{max_f}K_{m_{[P]}}}{K_{eq}}\right)[Co^+])^{-1} \qquad (3.10)
\end{aligned}$$

This expression consists of one Haldane relationship which can be represented by;

$$K_{eq} = \left(\frac{V_{max_f}}{V_{max_r}}\right)\frac{K_{m_{[P]}}K_{i_{[Co^+]}}}{K_{m_{[S]}}K_{i_{[CoH]}}K_{i_{[O_2]}}}$$

During the catalytic process, it was assumed that inhibition only caused by the product (lactone), $[P]$ in the forward reaction, thus dropping the term, $[Co^+]$ reduces equation(3.10) into;

$$\begin{aligned}
\frac{d[P]}{dt} &= (V_{max_f}[CoH][O_2][S])(K_{m_{[S]}}K_{i_{[CoH]}}K_{i_{[O_2]}}+K_{m_{[S]}}K_{i_{[O_2]}}[CoH]+K_{m_{[O_2]}}K_{i_{[CoH]}}[S] \\
&+ K_{m_{[S]}}[CoH][O_2]+K_{m_{[O_2]}}[CoH][S]+K_{m_{[CoH]}}[O_2][S]+[CoH][O_2][S])^{-1} \qquad (3.11)
\end{aligned}$$

For a reaction at variable substrate concentrations, the rate expression simplifies into a manageable form shown below;

$$\frac{d[P]}{dt} = \frac{V_{max}[S]}{K_{m_{[S]}}\left[[S]+\frac{K_{i_{[O_2]}}}{[O_2]}\left(1+\frac{K_{i_{[CoH]}}}{[CoH]}\right)\right]+[S]\left[\frac{K_{m_{[O_2]}}}{[O_2]}\left(1+\frac{K_{i_{[CoH]}}}{[CoH]}\right)+\left(1+\frac{K_{m_{[CoH]}}}{[CoH]}\right)\right]} \qquad (3.12)$$

The final equation above therefore describes the *velocity* of the Baeyer-Villiger oxidation reaction. However, the model equation only represents the reaction with substrate concentration. As

the substrate concentration increases, the rate follows the standard Michaelis-Menten curve shown previously. Apparently, the product term that causes product inhibition is absent in the denominator of the expression (3.12). In an actual process reaction, the *velocity* plot does not show a similar curve as that of the Michaelis-Menten model. In fact, the system is affected by substrate and product concentrations during the course of reaction (Chen *et al.*, 2002). A preliminary analysis of the effect of substrate and product inhibitions towards the enzyme-catalysed reaction is discussed in the subsequence chapter. In order to follow the actual reaction mathematically, an appropriate model incorporating the dead-end inhibition that described such conditions should be used.

A Model System with Dead-End Inhibition

The complete rate expression given by equation (3.12) only gives the standard Michaelis-Menten model. With such a model, the effect of increasing the substrate or product does not change the *velocity* of the reaction. Therefore, the dead-end inhibition by substrate and product have been introduced in the model.

Definition: Dead-end inhibition is a type of inhibition caused by compounds that react with one or more enzyme forms giving out a complex which cannot participate in the reaction.

In order to describe an enzyme-catalysed Baeyer-Villiger reaction, a simplification on the mechanism was made. Assuming that the reaction is only affected by substrate and product and that the supplied molecular oxygen as well as the cofactor, NADPH is not limited during the reaction, therefore, the simplified form of the mechanism can be written in the form suggested by Cleland (*Figure 3.8*). Following the same method of deriving the rate expression, the final *velocity* equation of the given mechanism can be written as;

$$\begin{aligned}\frac{d[P_{OxaBicyclo}]}{dt} &= V_{max_f} V_{max_r} \left([S_{Bicyclo}] + \frac{[P_{OxaBicyclo}]}{K_{eq}}\right) \\ &\quad (V_{max_r} K_{m_{[Bicyclo]}} + V_{max_r}[S_{Bicyclo}] + \frac{1}{K_{i_{[Bicyclo]}}} V_{max_r}[S_{Bicyclo}]^2 \\ &+ \frac{1}{K_{i_{[OxaBicyclo]}}} V_{max_r}[S_{Bicyclo}][P_{OxaBicyclo}] + \frac{V_{max_f}}{K_{eq}}[P_{OxaBicyclo}])^{-1} \end{aligned} \quad (3.13)$$

considering only the irreversible reaction by dropping the term $\frac{[P_{OxaBicyclo}]}{K_{eq}}$ and dividing equation

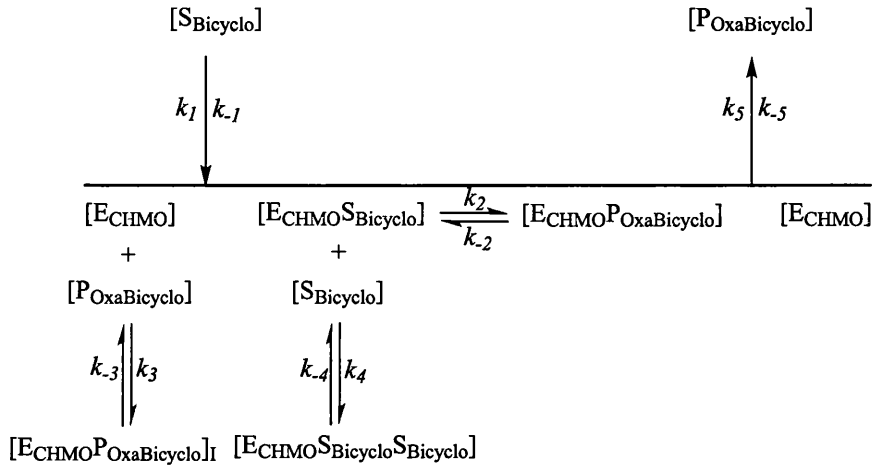

Figure 3.8: Cleland's notation (Cleland, 1963*a*,*b*) of mixed-type dead-end inhibition of enzyme-catalysed Baeyer-Villiger bioconversion.

(3.13) by V_{max_r} resulted in one Haldane relationship;

$$K_{eq} = \left(\frac{V_{max_f}}{V_{max_r}}\right)\left(\frac{K_{m_{[OxaBicyclo]}}}{K_{m_{[Bicyclo]}}}\right)$$

hence,

$$v = \frac{d[P_{OxaBicyclo}]}{dt} = \frac{V_{max}[S_{Bicyclo}]}{K_{m_{[Bicyclo]}}\left(1+\frac{[P_{OxaBicyclo}]}{K_{m_{[OxaBicyclo]}}}\right)+[S_{Bicyclo}]\left(1+\frac{[S_{Bicyclo}]}{K_{i_{[Bicyclo]}}}+\frac{[P_{OxaBicyclo}]}{K_{i_{[OxaBicyclo]}}}\right)} \tag{3.14}$$

Further rearrangement of the above equation leads to;

$$v = \frac{V^{app}_{max}[S_{Bicyclo}]}{K^{app}_{m_{[Bicyclo]}} + [S_{Bicyclo}]} \tag{3.15}$$

where;

$$V^{app}_{max} = \frac{V_{max}}{1+(\frac{[S_{Bicyclo}]}{K_{i_{[Bicyclo]}}}+\frac{[P_{OxaBicyclo}]}{K_{i[OxaBicyclo]}})}$$

and

$$K^{app}_{m_{[Bicyclo]}} = \frac{K_{m_{[Bicyclo]}}\left(1+\frac{[P_{OxaBicyclo}]}{K_{m_{[OxaBicyclo]}}}\right)}{1+(\frac{[S_{Bicyclo]}}{K_{i_{[Bicyclo]}}}+\frac{[P_{OxaBicyclo]}}{K_{i_{OxaBicyclo}}})}$$

By comparing equation (3.14) to that of (3.12), it can be clearly observed that the terms $K_{i_{[Bicyclo]}}$ and $K_{i_{[OxaBicyclo]}}$ describing the inhibition constants for substrate and product respectively, exist as denominators for substrate and product concentration terms; $[S_{Bicyclo}]$ and $[P_{OxaBicyclo}]$. Therefore, increasing the concentration values, will decrease the *velocity* expression of the reaction. On the other hand, for a *velocity* describes by equation (3.12), whereby increasing the concentration terms will not affect the rate expression of the whole system. With these results it can be concluded that by incorporating the dead-end typed inhibition, the model theoretically follows the actual course of the enzyme-catalysed Baeyer-Villiger reaction.

3.3 Method of Progress Curve Analysis in an Enzyme-Catalysed Reaction

Among other methods used to follow the enzyme-catalysed reaction, progress curve analysis has been found to be the most suitable and less complicated. Even though the treatment of the rate expression is mathematically cumbersome, but the end result would be more accurate compared to the graphical method of hand-drawn Lineweaver-Burk or perhaps the fitting of the rate expression to the experimental rate data which was found to be inappropriate in dealing with multivariable systems. This is due to a direct estimation of parameters using the integrated rate expression with enough data from the progress curve experiments. On the other hand, the former procedures require a number of points (individual rate) to be determined individually from each substrate or product concentration used during the initial rate experiment. These values are then fitted or hand-drawn according to the given rate expression. Furthermore, the method of obtaining these rates is very much exposed to rounding error and plotting inaccuracy and could lead to the incorrect estimation of the enzyme kinetic parameters. Bates and Frieden (1973*a*), have been using the integrated rate expression approach in describing the curve of a number of enzyme reactions. The interest of utilising the method gradually increases and many complex analysis of enzymatic pathways have been discovered and mathematically modelled.

3.3.1 Materials and Method

Chemicals and Enzyme

The purified substrate, (bicyclo[3.2.0]hept-2-en-6-one) and products, ((-)1(S)5(R)2-oxabicyclo-[3.3.0]oct-6-en-3-one and (-)1(R)5(S)3-oxabicyclo[3.3.0]-oct-6-en-2-one) were a kind gift from Fluka (Buchs, Switzerland). All other chemicals were obtained from Sigma Chemical Co. (Poole, Dorset, UK), while the fermentation media were ordered from Fluka (Buchs, Switzerland). The enzyme was kindly donated by Dr. John Ward from the Department of Biochemistry and Molecular Biology, University College London, where it was cloned from *Acinetobacter calcoaceticus* and transferred into *Escherichia coli* TOP10[pQR239] for large scale fermentations in the Department of Biochemical Engineering, University College London.

Biocatalyst Fermentation

Escherichia coli fermentations for the biocatalyst production were performed in a 7-litre fermenter with 5-litre working volume (LH 210 fermenter, Bioprocess Engineering Services, Charing, Kent, UK) fitted with three equally spaced top driven six bladed turbine impellers and four diametrically opposed baffles. The dissolved oxygen tension (DOT) was measured by a polarographic oxygen electrode (Ingold, Messtechnik, Urdorf, Switzerland). The pH of the fermentation medium was controlled using a sterilised Ingold pH probe (Ingold, Messtechnik, Urdorf, Switzerland) at pH 7 ($\pm$0.05) by metered addition of 3M KOH and 3M H_3PO_4. The inlet air required during the fermentation was filtered using the 0.2μm filters (Gelman Sciences, Ann Arbor, MI, USA) and the exhaust gas from the fermenter was determined by mass spectrometry (Prima 600, VG Gas Analysis, Winsford, Cheshire, UK). All data logging and the exhaust gas measurements were recorded using the RT-DAS program (Acquisition System, Guildford, Surrey, UK).

Prior to each fermentation, the fermenter was steam sterilised at 121°C for 20min at 1.0bar with all media components and 0.5ml·l^{-1} polypropylene glycol 2000 to prevent foaming. After cooling to 37°C, the pH was adjusted to 7 and ampicillin was added prior to inoculation. The fermenter was inoculated with 500ml (10% of the total volume) broth grown overnight. During the growing phase, the agitation rate was maintained at 1000r.p.m and varied between 250r.p.m

to 1500r.p.m. During the fermentation process, the vessel was aerated with filtered air, sparged at $1l \cdot min^{-1}$ (0.67vvm). The fermentation profile of *Escherichia coli* TOP10[pQR239] has also been described in detail elsewhere (Doig *et al.*, 2001).

The growth of *Escherichia coli* was closely monitored based on the optical density of the fermentation broth. This monitoring is highly important for the induction period at approximately 3 hours after the start of the fermentation. $2.4g \cdot l^{-1}$ of arabinose was used to induce the cell during the second stage of the fermentation and this was done when the optical density reached 7–8OD_{670} reading. The process was then carried out for another 3 hours after the induction period until the cell reached approximately 20OD_{670} reading.

A calibration curve of the growth of the biocatalyst was plotted by sampling the fermenter every 30 minutes during the fermentation process. About 5ml of sample was drawn from the fermenter and checked for its optical density (BioMate 3 spectrophotometer, ThermoSpectronic, Rochester, NY, USA). 1ml of the same sample was centrifuged (Biofuge 13, Heraeus Sepatech, Brentwood, UK) in an oven-dried 1ml microfuge tube for 2 minutes at 13000r.p.m. and left to dry in the oven set at 100°C for 24 hours.

During the fermentation process, the dry cell weight concentrations ($g_{dcw}l^{-1}$) were also determined. This was based on the known amount of dry cell weight against the optical density of the cell obtained previously (*Appendix G*). The fermentation profile as well as the cell growth can be shown in a combined plot given in *Figure 3.9*. The growth of biomass can be apparently seen from the plot. After the period of 6 hours of fermentation, the growth appeared to have stopped and reached a steady-state at approximately $15g_{dcw}l^{-1}$. This is due to the depletion of glycerol in the broth which makes the metabolism of the cell decreases and the continued growth would not be possible. It is also apparent from *Figure 3.9* that the level of oxygen in the fermentation vessel is approximately 0%. This shows that the molecular oxygen has been completely consumed during the aerobic growth of *E. coli*. During the same fermentation, the source of oxygen from the filtered air was kept at a constant flow such that it would not affect the formation of enzyme after the induction towards the end of the fermentation period. This was achieved by controlling the impeller speed instead of increasing the flowrate of air into the vessel.

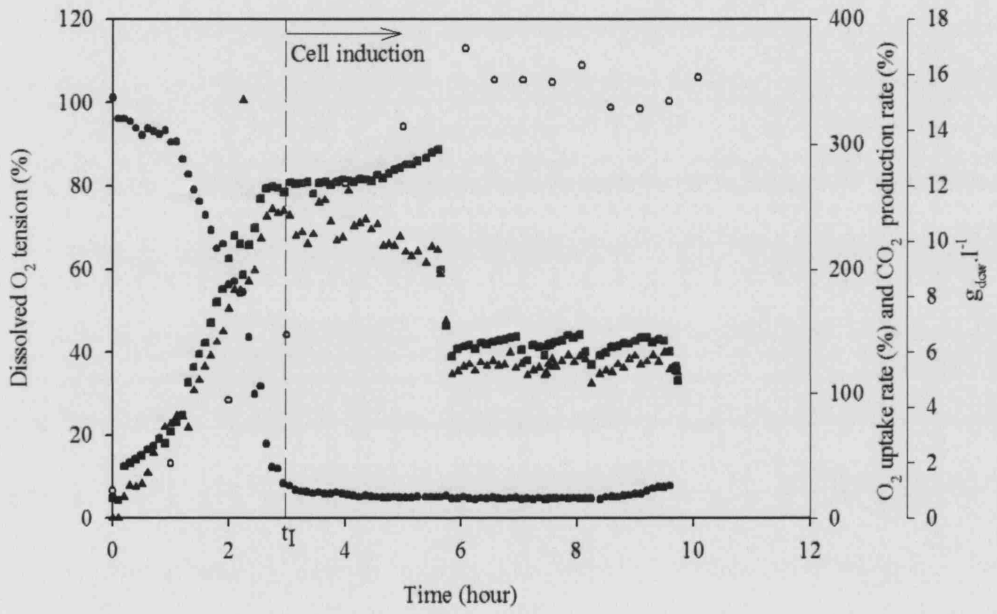

Figure 3.9: Fermentation profile of *E. coli* TOP10[pQR239] with '•', Dissolved O_2 tension (%), '■', O_2 uptake rate (%), '▲', CO_2 production rate (%) and '○', Dry cell weight ($g_{dcw}l^{-1}$). t_I represents the time at which the cell was induced with arabinose.

Analytical Assay

During bioconversions, samples were removed and extracted 1:1 with $1mg{\cdot}ml^{-1}$ naphthalene in ethyl acetate. Naphthalene served as an internal standard for quantification of the bicyclic-ketone and the corresponding lactones. For the chromatography assay, 1µl samples were injected into an XL–2 gas chromatograph (Perkin-Elmer, Norwalk, CT) fitted with an AT–1701 column (30m×0.54mm)(Alltech, Carnforth, Lancaster, UK) and the concentration determined from an external calibration curve. The GC temperature program was set at 100°C and held for 5min and then increased at a rate of $10°C{\cdot}min^{-1}$ up to 240°C. The coefficient of variance for this assay was ± 3% quoted at 95% confidence interval which was based on 6 independently prepared standard solutions (concentration range $25–2000mg{\cdot}l^{-1}$ and $R^2 > 98\%$). The standard calibration graphs are supplied in *Appendix G.*

Experimental Method for Progress Curve Analysis

The rate of enzyme reaction can be obtained via enzymatic assay by monitoring the reduction of substrate, product formation or co-factor reduction, provided that any of the above components give an obvious peak on the spectrophotometer. In this work, both substrate and product did not give any obvious peak with the spectrophotometer scan, therefore, the only source of detection is the cofactor (NADPH) oxidation (wavelength measured at 340nm). The assay was carried out using (Kontron, (Watford, Herts, UK), Uvikon 922 variable wavelength spectrophotometer) and 1.5ml quartz cuvette as a reaction vessel.

1ml whole-cell obtained from the fermentation was centrifuged and the cell was added with 50mM Tris-HCL reaction buffer(50mM Tris-HCL pH 9.0 and $7.14g{\cdot}l^{-1}$ bovine serum albumin) and thoroughly mixed. The well-mixed components was then sonicated using Soniprep 150 MSE, Sanyo, Crawley, Sussex, UK, for 10 seconds on and 10 seconds off for 5 cycles at 8µm and centrifuged for another 1 minute to separate the cell debris. Lysed cell should be kept below 5°C to maintain the enzyme activity throughout the experiment. The reaction buffer was initially bubbled with 80% oxygen to air composition in order to keep the dissolved oxygen at a maximum level and it was kept at a constant reaction temperature of 37°C. 700µl of the same buffer was prepared in the cuvette and let to equilibrate to the controlled temperature

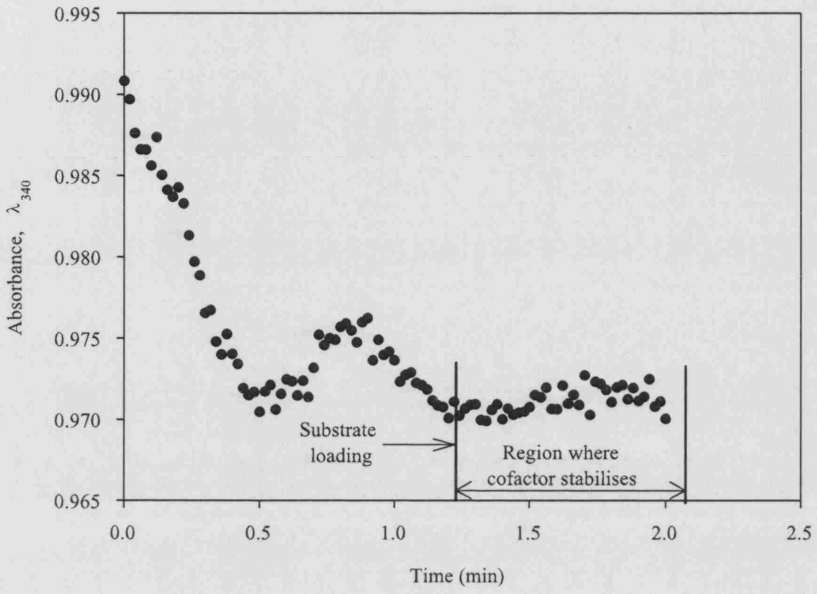

Figure 3.10: Region where cofactor, (NADPH) stabilises before reaction can be carried out.

of the spectrophotometer (37°C). 100µl of the supernatant from the lysed and centrifuged cell was added to the reaction medium and they were measured as blank. Spectrophotometer was set to zero and 100µl of NADPH (0.161mM or stated otherwise) was added. The reading was let to stabilise for approximately 1 to 2 minutes before 100µl of substrate was added to begin the reaction. The molar ratio of cofactor to substrate was kept constant between 50 to 60 to 1 ratio. This will make sure that the substrate is completely converted without any cofactor limitation. Region of cofactor stability is plotted in *Figure 3.10.* This figure shows the suitable time at which the substrate should be loaded into the reaction medium. Inappropriate loading of substrate will only lead to the measurement of cofactor instability rather than the reduction of cofactor due to bioconversion.

The progress of substrate conversion over time is assumed to be proportional to the rate of NADPH depletion due to the binding of cofactor to the enzyme structure. This can be

mathematically described as:

$$\frac{d[\text{NADPH}]}{dt} = \frac{d[S_{Bicyclo}]}{dt} \tag{3.16}$$

The enzymatic reaction was measured for 4 minutes until most of the substrate was fully converted. This is prior to the analysis of the progress curve with the modelled kinetic expression which is discussed in the next section. The raw data obtained from the spectrophotometric analysis should be converted into concentration units (mM). This is particularly important since the initial data read by the spectrophotometer are in the form of absorbance (Abs). Following the Beer's Law;

$$Abs_{340} = \varepsilon C l$$

where Abs_{340} represents the absorbance at wavelength, λ = 340nm, ε gives the extinction coefficient (ε = 6.22ml·μmol^{-1}·cm^{-1}), C, represents the concentration of the measured data in (mM) and l represents the length of the light path (l = 1cm). Rearranging the above equation gives,

$$C = \frac{Abs_{340}}{\varepsilon l}(mM)$$

This value agrees with the concentration of NADPH used during the reaction since 0.161mM converts to approximately 1.00142 Abs_{340} which is the maximum value detected by the spectrophotometer. All data captured from the spectrophotometric analysis were converted using the above law for further analysis.

3.3.2 Mathematical Treatment of the Rate Expression of Cyclohexanone Monooxygenase Enzyme-Catalysed Reaction

The method of progress curve analysis depends entirely on the kinetic expression derived from the reaction mechanism. The experimental data in the form of progressing reaction is left untouched, thus errors are not introduced within the raw data. The expression given by equation (3.14) describing the enzyme-catalysed Baeyer-Villiger reaction is used to mimic the reaction in

progress,

$$v = \frac{d[P_{OxaBicyclo}]}{dt} = \frac{V_{max}[S_{Bicyclo}]}{K_{m_{[Bicyclo]}}\left(1 + \frac{[P_{OxaBicyclo}]}{K_{m_{[OxaBicyclo]}}}\right) + [S_{Bicyclo}]\left(1 + \frac{[S_{Bicyclo}]}{K_{i_{[Bicyclo]}}} + \frac{[P_{OxaBicyclo}]}{K_{i_{[OxaBicyclo]}}}\right)}$$

Before it is possible to describe such reaction, the above rate expression needs to be integrated and the procedure is clearly discussed in the next section.

Integrated Rate Expression

For the purpose of obtaining the progress curve, equation (3.14) was divided by $[S_{Bicyclo}]$ on both nominator and denominator and changing the term $\frac{d[P_{OxaBicyclo}]}{dt}$ into $\frac{d[S_{Bicyclo}]}{dt}$ with a minus sign on the right hand side and rearranging gives;

$$\int \left[\frac{K_{m_{[Bicyclo]}}}{[S_{Bicyclo}]}\left(1 + \frac{[P_{OxaBicyclo}]}{K_{m_{[OxaBicyclo]}}}\right) + \left(1 + \frac{[S_{Bicyclo}]}{K_{i_{[Bicyclo]}}} + \frac{[P_{OxaBicyclo}]}{K_{i_{[OxaBicyclo]}}}\right)\right] d[S_{Bicyclo}] = -V_{max}\int dt \tag{3.17}$$

since the variables consist of $[P_{OxaBicyclo}]$ and $[S_{Bicyclo}]$ thus a dependent term, z represents the amount of substrate formed at any given time, was introduced in order to avoid multivariables integration. This is given by;

$$z = [S_{Bicyclo}]_0 - [P_{OxaBicyclo}] \tag{3.18}$$

with $z = [S_{Bicyclo}]$. Substituting these into equation (3.17) and integrating from $[S_{Bicyclo}]_0$ to z gives;

$$\begin{aligned} -V_{max}\int_0^t dt &= \int_{[S_{Bicyclo}]_0}^{z}\left[\frac{K_{m_{[Bicyclo]}}}{z}\left(1 + \frac{[S_{Bicyclo}]_0 - z}{K_{m_{[OxaBicyclo]}}}\right)\right] dz \\ &+ \int_{[S_{Bicyclo}]_0}^{z}\left(1 + \frac{z}{K_{i_{[Bicyclo]}}} + \frac{[S_{Bicyclo}]_0 - z}{K_{i_{[OxaBicyclo]}}}\right) dz \end{aligned} \tag{3.19}$$

hence,

$$\begin{aligned} \ln(z)\left[K_{m_{[Bicyclo]}}+\frac{K_{m_{[Bicyclo]}}[S_{Bicyclo}]_0}{K_{m_{[OxaBicyclo]}}}\right] &+ z\left[1-\frac{K_{m_{[Bicyclo]}}}{K_{m_{[OxaBicyclo]}}}+\frac{[S_{Bicyclo}]_0}{K_{i_{[OxaBicyclo]}}}\right] \\ &+ z^2\left[\frac{1}{2K_{i_{[Bicyclo]}}}-\frac{1}{2K_{i_{[OxaBicyclo]}}}\right] \\ &= -V_{max}t \end{aligned} \tag{3.20}$$

The integrated rate equation is now in the form of singular variable. Further simplification by substituting the kinetic parameters with new parameters α, β and γ corresponding to the square brackets in the above equation leads to;

$$F(z,t) = e^{-\frac{1}{\alpha}(V_{max}t+\beta z+\gamma z^2)} - z \tag{3.21}$$

New parameters	Kinetic parameter terms
α	$\left[K_{m_{[Bicyclo]}}+\frac{K_{m_{[Bicyclo]}}[S_{Bicyclo}]_0}{K_{m_{[OxaBicyclo]}}}\right]$
β	$\left[1-\frac{K_{m_{[Bicyclo]}}}{K_{m_{[OxaBicyclo]}}}+\frac{[S_{Bicyclo}]_0}{K_{i_{[OxaBicyclo]}}}\right]$
γ	$\left[\frac{1}{2K_{i_{[Bicyclo]}}}-\frac{1}{2K_{i_{[OxaBicyclo]}}}\right]$

Table 3.1: New parameters defining the kinetic parameter terms in the box brackets in equation (3.20).

Simulation of the above function with the given arbitrary parameter values is shown in *Figure 3.11.* Since the estimation of these parameters is based on the nonlinear regression, i.e. with the basic Gauss-Newton method thus, the differential form of equation (3.20) with respect to the appropriate parameters are required. Method of obtaining these terms can be referred to *Appendix B.* The modified Gauss-Newton method described by Marquardt (1963) normally quoted as the Levenberg-Marquardt algorithm, which formed one of MATLAB®'s Optimization Toolbox® (MathWorks, 1993–2001) was also applied to the experimental progress curve data. *Figure 3.11* clearly shows the depletion of substrate represented by variable z, thus the function is ready to be fitted using the nonlinear regression technique together with the progress curve

data.

Kinetic Parameter Estimation

The nonlinear regression based on the modified Gauss-Newton algorithm was used in all fitting procedures. The progress curve data were obtained using the experimental method described in the previous section and they were done in 20 repeats for the purpose of getting the best accuracy.

The objective function used for the estimation of the kinetic parameters was rearranged such that the independent variable is positioned on the left hand side of the equation. Modifying equation (3.21) gives;

$$t = -\frac{\alpha}{V_{max}}z - z^2\frac{\beta}{V_{max}} - \frac{\gamma}{V_{max}}\ln(z) \tag{3.22}$$

The equation obviously could not be put in terms of variable z. It is a transcendental type of equation and the solution of which is in a closed form (Fritsch *et al.*, 1973; Schnell and Mendoza, 1997). Solution via method suggested by Goudar *et al.* (1999) utilising Lambert's ω–function of the form $\omega(x)e^{\omega(x)} = x$ for closed form function is not possible since the system consists of a squared variable z which upon simplification differed to that of the standard function.

Normal fitting was used with the progress curve data and one of the the best fitting curves from the 20 repeat experiments is shown in *Figure 3.12.* The parity plot of the similar fitting is given in the subsequence figure. Values of all kinetic constants estimated from the fitting procedure are tabulated in *Table 3.2.* The rate expression used in the above analysis can be simplified in the form of apparent values of K_m and V_{max} which represented by K_m^{app} and V_{max}^{app} respectively. Values found in this analysis were compared with the current available literature.

3.4 Discussion

A detail kinetic analysis of cyclohexanone monooxygenase enzyme-catalysed Baeyer-Villiger reaction has been completely established in this work. The rate expression describing the particular reaction has been carefully derived based on the *true* mechanism of its reaction. Therefore, the kinetic constants estimated here specifically described the Michaelis constants as well as the inhibition constants for the respective substrate and product affecting the rate of enzyme-catalysed

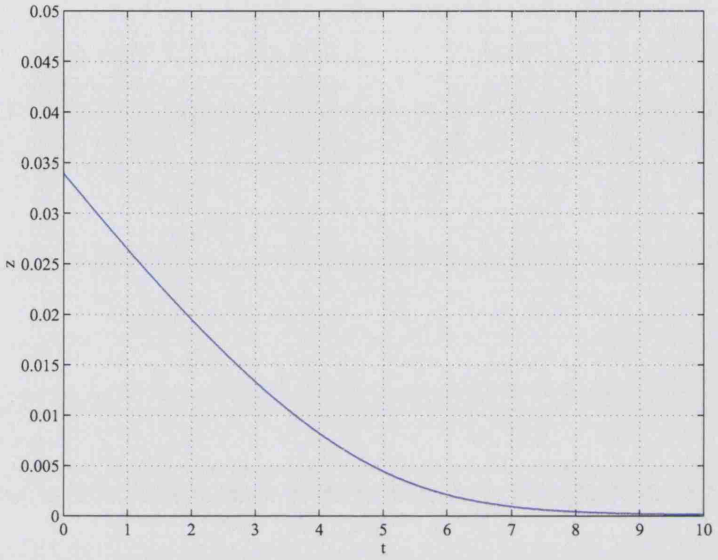

Figure 3.11: Simulation of the simplified rate expression given by equation (3.21) with α=0.1, β=10, γ=0.01 and V_{max}=0.1.

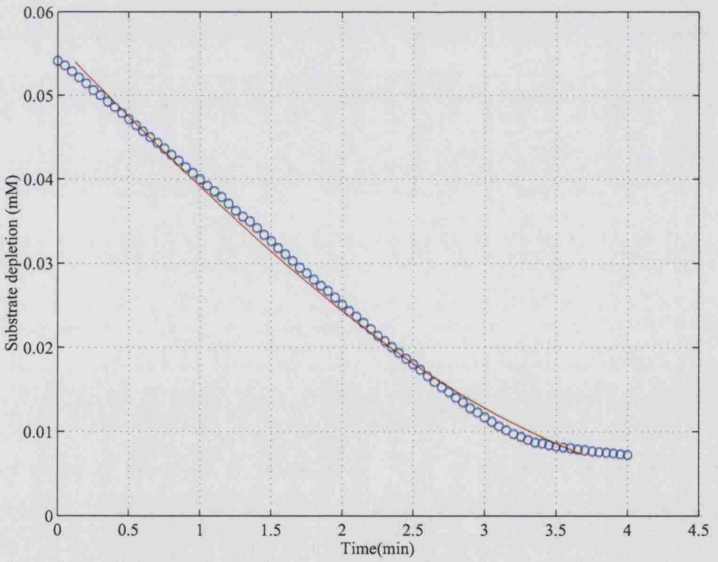

Figure 3.12: Fitting of experimental progress curve data with integrated rate expression (3.22);('o' experimental data, '–' fitted curve, $[S_{Bicyclo}]_0 = 0.000904$mM, [NADPH] = 0.06mM.)

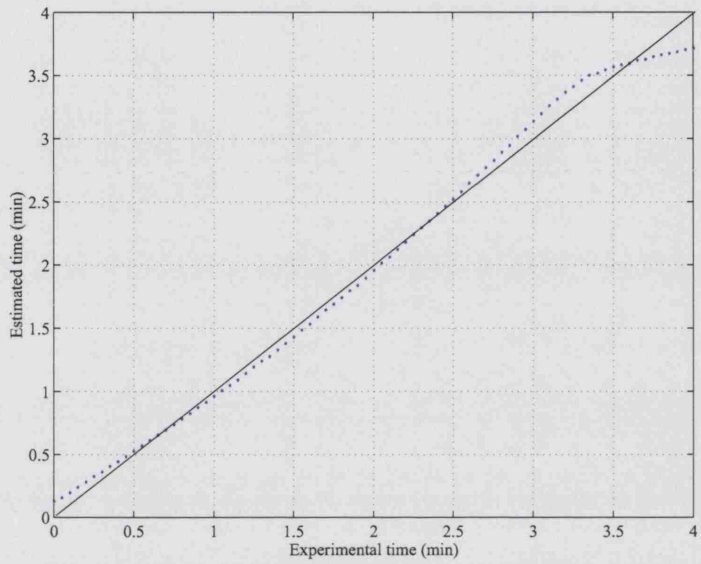

Figure 3.13: Comparison between the actual time data and the estimated time using the nonlinear regression technique.

Kinetic constants	Estimated values	Literature values
$V_{max}(\mu M.min^{-1}.g^{-1})$	21.6 ± 0.05	N.G
$K_{m_{[Bicyclo]}}(mM)$	0.016 ± 0.154	$0.05 - 0.09$
$K_{m_{[OxaBicyclo]}}(mM)$	5.940 ± 0.946	N.D
$K_{i_{[Bicyclo]}}(mM)$	640.791 ± 1.765	0.12
$K_{i_{[OxaBicyclo]}}(mM)$	799.795 ± 0.934	N.D

Table 3.2: Values of kinetic constants from progress curve analysis and simplified initial rate study obtained by Zambianchi *et al.* (2000, 2002) of cyclohexanone monooxygenase enzyme-catalysed Baeyer-Villiger reaction (N.G: not given, N.D: not determined).

Apparent kinetic constants	Estimated values (1)	Estimated values (2)
V_{max}^{app}	0.022	0.015
K_m^{app}	0.016	0.297

Table 3.3: Apparent kinetic constants obtained from (1) rearranged rate expression given by equation (3.15) with previously defined kinetic constants and (2) parameters estimated using Lambert's ω–function.

Baeyer-Villiger reaction.

The main obstacle encountered during the analysis was fitting the kinetic data to the derived rate expression. Previous kinetic analysis of the similar reaction undertook by Zambianchi *et al.* (2000) did not clearly describe the rate expression governing the reaction. It was assumed that a basic uncompetitive substrate inhibition has been used by the author to describe the reaction. Such an assumption was inappropriate since the product formed during the reaction is also affecting the rate of the entire reaction. This behaviour can be apparently seen in the plot supplied in *Appendix H* as a supplement for the initial rate experiment. In order to incorporate the substrate and product terms into the rate expression, a mechanism with dead-end inhibition was introduced and it was termed as the mixed-typed UNI–UNI sequential mechanism. The normal type mechanism (mechanism given in *Figure 3.6*) derived without these terms would only give the basic Michaelis-Menten curve.

As was mentioned earlier, the problem arose when the experimental data; either the initial rate or the progress curve were to be fitted to the particular rate expression. The main reason; the product function that appears on the right hand side of the equation. A number of techniques have been used in order to resolve this present problem and the most efficient above all is the fitting of integrated rate expression. Although the method is suitable to the available rate expression, the arrangement of the objective function is rather awkward since the fitting determines the time variable instead of the substrate consumed. This is mainly because the function that described the integrated rate could not be arranged in such a way that the substrate is a function of time, or in other words, it is of a transcendental type function.

An attempt to solve the 'closed form' equation was undertaken based on a function known as the Lambert's ω–function. This technique was used basically to rearrange the transcendental type equation such that it could be reduced into a time function. Such method failed due to the appearance of a squared variable in the objective function. Therefore, the only method left is to estimate the time, based on the substrate consumption data. Even though time was the estimated values, the parameters resulted from the fitting procedure were relatively similar compared to that of the previous analyses. The method of treatment of the integrated rate expression using Lambert's ω–function is summarised in *Appendix C*, utilising a simple

Michaelis-Menten expression. An attempt was also made to fit the progress curve data to the given equation since the Michaelis-Menten function of a simple kinetic mechanism is similar to that of the apparent kinetic equation given by rate expression (3.15). Values of K_m^{app} and V_{max}^{app} are given in *Table 3.3.* Since the apparent rate expression was in the form of simple Michaelis-Menten model, therefore the fitting of the progress curve data to the ω–function failed to give a similar values to that of the simplified function.

There is not much work being published especially on the kinetics of enzyme-catalysed Baeyer-Villiger reaction. The complexity of its mechanism as well as the method of determining the kinetic constants has led many to assume that the reaction follows a simple rate expression. Zambianchi *et al.* (2000) has tried to describe a similar reaction kinetically but the rate expression used to obtain the kinetic data was not clearly mentioned. This has made the parameters estimated in this work unable to be compared to any literature values. *Table 3.2* shows the current kinetic values and the values quoted from Zambianchi *et al.* (2000) and Zambianchi *et al.* (2002). Apparently, the Michaelis constant, $K_{m_{[Bicyclo]}}$ for the substrate is about the same magnitude as that determined by Zambianchi *et al.* (2000). However, the substrate inhibition constant differed significantly to the value given in the same publication. This probably due to the unsuitable function used to describe the kinetics of Baeyer-Villiger reaction in their work. For a reaction inhibited by either substrate or product, or perhaps by both species, the inhibition constants always being the denominator of a particular inhibitor. This type of arrangement forces the rate curve to bent towards the x–axis, i.e. lowering the rate of that reaction. Such a behaviour could only be observed with a very high value of inhibition constant within the magnitude of 10 or perhaps 100mM. The results are shown in *Table 3.2.*

3.5 Summary and Conclusion

It can be seen in this work that the method of determining the kinetic constants of an enzyme-catalysed reaction varies depending on the rate expression of that particular reaction. The complexity of this expression is however governed by its reaction mechanism. In order to obtain the *true* kinetics of an enzyme-catalysed reaction, the derivation of the rate expression should be based on an established mechanism. This will lead to the full description of the particular

enzyme-catalysed system.

This work also proved that the progress curve analysis could successfully determine the kinetic constants accurately provided that it is supplied with enough experimental data. It was also shown previously that the progress data of either substrate depletion or product formation could be easily captured via appropriate experimental techniques of observing the reaction. Unlike the progress curve, the initial rate method requires a high experimental effort however, the determination of the kinetic constants is rather simple and depends upon the complexity of a particular rate expression. The analysis carried out in this work also found that the non-continuous initial rate method failed to determined the rate expression that is governed by two variables; substrate and product. Attempts to estimate the kinetic parameters using such a method could only lead to erroneous values.

One might argue that the theoretical analysis would not give a true description of an actual experimental result obtained using the available experimental technique in view of the fact that the intermediate complexes formed during an enzyme-catalysed reaction is not possible to capture. Their rate of formation and conversion from and to another species respectively are relatively high, therefore, such work rarely gives interest for further investigation. Recently, several methods of looking at the formation of intermediate complexes have been devised and one method which has been widely used is the stopped-flow spectrophotometric techniques. Sheng *et al.* (2001) and Rodriguez-Lopez *et al.* (2000) have successfully applied a similar method to analyse the mechanism of cyclohexanone monooxygenase enzyme-catalysed reaction and the activity of diphenolase enzyme respectively which had led them to carefully define mechanisms of both reactions. From this argument, it can be concluded that in order to design new experiments to investigate a system of enzyme catalysis, the understanding of a postulated mechanism is highly required.

Generally, it can be concluded that the kinetic analysis of an enzyme-catalysed reaction can only be understood by looking at the mechanism of a particular reaction. A reaction might not be described by a simple mechanism that produces a straightforward rate expression and in this case a new mechanism with higher complexity should be sought. It should also be emphasised that the fit of a mechanism to the experimental data does not always prove the right mechanism.

This should be clear when the fitting errors for a given mechanism are significantly high compared to the estimated parameters themselves. This would strongly suggest that such a mechanism is incorrect.

Chapter 4

Process Modelling of Biocatalytic Reactions

4.1 Introduction

Process modelling that involves biological organisms for the production of fine chemicals has been considered as one of the important fields in biochemical and bioprocess engineering. The terms 'process model' can be defined as a set of equations that includes the necessary input data to solve the model system and allows one to predict the behaviour of a certain process system.

Millions of dollars have been invested by major drugs related industries especially in research and development for the production of these new chemicals (Thayer and McCoy, 2001). This is due to the fact that almost all biological based experiments require environment that is highly sterile and have to undergo a number of repeat experiments to confirm a particular result. With such delicate and highly expensive procedures, process simulation of a similar system based only on a few laboratory results is an alternative that could reduce such high expenses.

Apart from the cost reducing strategy, process modelling could also provide a measure of order to our experience and observations as well as to make specific predictions about certain aspects that one has experienced (Bailey, 1998). Therefore, in order to fulfill such requirements, a model system should be finely defined and the problem that it is intended to solve should be carefully addressed.

This chapter combines the results from the kinetic analysis of cyclohexanone monooxygenase enzyme–catalysed Baeyer–Villiger reaction with modelling of the whole biocatalytic process

system. Reactions carried out in batch and fed–batch conditions were modelled and comparison as well as predictions were made based on the results from the experimental observations.

Previously, there has been an attempt to model the same reaction. The method was based on the artificial neural network, (ANN) (Chen *et al.*, 2002; Chen and Woodley, 2002) which on one hand produced a fast analysis but on the other, it failed to describe the kinetics of the reaction. The same technique is normally used to model a control system which the raw data can be easily collected from an online measurement. Not only that, data obtained form such a measurement should be more than enough to *train* a polynomial function within the neural network procedure. Numerous works have been successfully carried out using ANN especially in the area of biotechnology where control of a process was the main objective (Kurtanjek, 1994; Montague and Morris, 1994). From all biological processes treated via ANN, fermentation has been a popular system frequently investigated. ANN model of baker's yeast production has been carried out by Kurtanjek (1994) which the training was based on the data provided from an industrial plant, while Shene *et al.* (1999) has managed to predict the effect of medium composition and temperature during the fermentation of *Zymomonas mobilis.* A new technique of hybrid modelling has also been introduced where the results from the neural network analysis were combined with that of the normal mathematical process model. With such a combination, they have also been able to predict the kinetic parameters from the mathematical model, i.e. specific growth rate, μ_M, Monod constant, K_M and total product yield coefficient, $Y_{X/S}$ in a cellular growth described by Monod model.

Modelling of biological system can be divided into two main categories; an unstructured type and a structured type models. Both carry different level of complexity which sometimes ended up with a similar solution. Summary of these type of models are given in the two subsequent sections.

4.1.1 Unstructured Models

The simplest method of describing fermentation of any biological cells is based on the unstructured type modelling. In this case, the cell involved in the process is regarded as a *black box*, where every substrate entering the cell only results in product going out, this is clearly depicted in *Figure 4.1(a).* Any minute chemical interactions within the cell is assumed to be negligible.

Using this simple idea, a system can just be described using a single rate expression for a batch or with additional inlet and outlet terms for a chemostat (CSTR) type process. For instance, in a fermentation of any bacterial cells, the growth rate is described using an expression normally known as the Monod model given by $\mu_x = r_x = \frac{\mu_{max} S}{K_M + S}$, where μ_x is the specific growth rate depends only on the variable S. μ_{max} is the maximum growth when the nutrient, S are present in sufficient amounts and K_M is the Monod constant describing the amount of substrate, S at the half of the maximum growth rate. Such variation of μ_x with substrate, S makes it behaves in the same fashion as does the enzymatic rate described by the Michaelis-Menten kinetics.

Simplified Reactor Modelling

The simplification provided by the unstructured type modelling makes the construction of a model system, a straight forward method. The system only describes the change of amount of variable surrounding the cell rather than taking into account the reaction taking place within the cell (Nielsen and Villadsen, 1992). Therefore, the final expression only consists of a few variables which will give enough information regarding the reaction rate of a system.

However, there is a drawback of using this type of simplification. Consider a reaction that depends on an additional component, for example, a second substrate that lies within the cell compartment, and without such component, the reaction will not proceed and the product will not be formed. Apparently, the unstructured model fails to address this situation and a complete model construction based on the structured method has to be sought.

4.1.2 Structured Models

Structured model of a cellular system is a model with detail description of cellular activity of an individual cell together with the reaction under investigation. By considering these into a model system, one could obtain a *true* representation of various activities occurring in a single cell. Structured models are based on a compartmental description of the cell mass which is given in *Figure 4.1(b)*. Generally, it is experimentally difficult to accurately determine the rate of reaction of each compartment within the cellular system (r_1 and r_2). In order to obtain a realistic structured model, one has to devise a mechanism or pathways of the reaction that

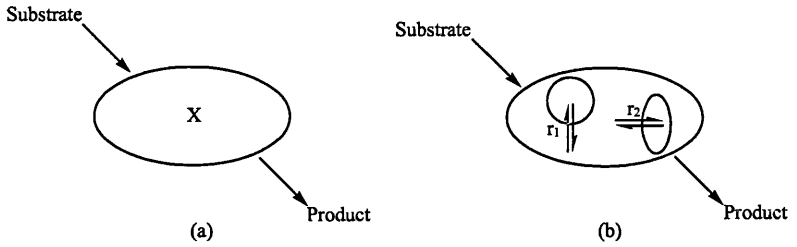

Figure 4.1: (a) Unstructured and (b) structured type models with r_1 and r_2 represent the compartments within the cell with individual rate of reaction.

finally results in the terms r_1 and r_2. Despite the difficulties and complex analysis, Ataai and Shuler (1985*a*) and Steinmeyer and Shuler (1989) have successfully constructed the structured models for the growth of *Escherichia coli* and *Saccharomyces cerevisiae* respectively.

4.1.3 Dynamic Behaviours of Process Modelling

Modelling of the dynamic behaviour of biochemical processes has played an important part in bioprocess design and operations. The simulation that results from a completely modelled system could lead to the study of the operability and controllability of continuous processes operating at nominal steady–state when the system is under a relatively small external perturbation. One could also develop procedures for start–up and shut–down of these processes. Changes on the operating procedures such as batch to continuous operation or perhaps the design of the whole process could easily be carried out using the process model. A basic procedure for model building is schematically explained in the following figure.

A simple transient state model has been used throughout this work to follow the bioconversion of ketone, forming a racemic mixture of chiral lactones. It uses material balances of the participating components, i.e. substrate consumption and product formation. This also incorporates the rate expression which the kinetic constants previously estimated in *Chapter 3.* Since the reaction has been assumed to be isothermal, therefore, there should be no transfer of energy between the reactor and the participating reaction species, hence, energy equation should be excluded from the model system. The conservation laws based on the fundamental physical laws were applied as a method to integrate variables as well as parameters involved in a process system into a complete set of mathematical relations. Such equations have been widely applied

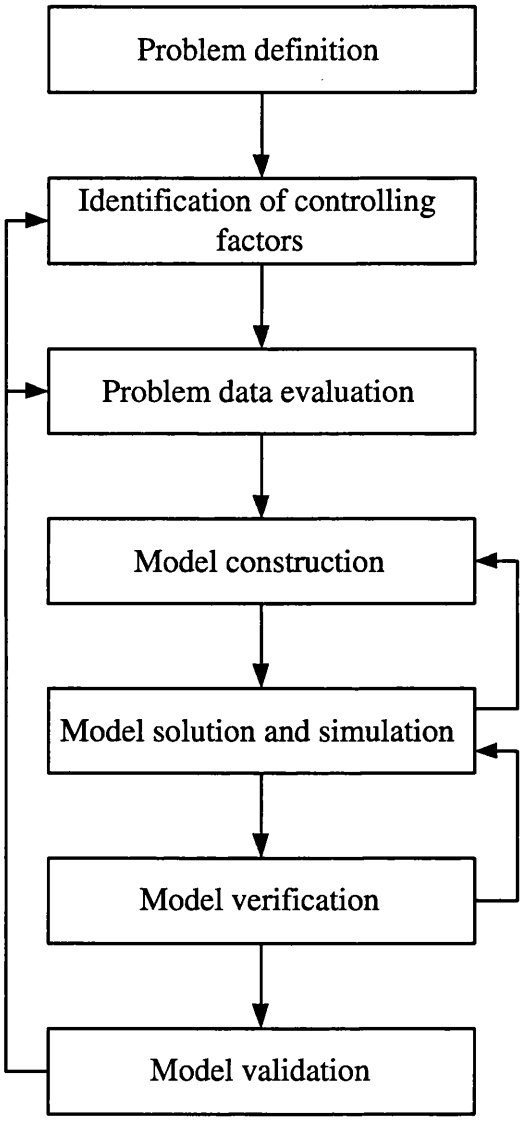

Figure 4.2: Schematic representation of dynamic modelling procedure.

in the construction of models describing batch and fed-batch bioreactors. When the variables and parameters are in place, a bioreactor that consists of a mixture of substrate and product is assumed to be *perfectly mixed* such that to reduce the computational complexity of the model. Imperfect mixing could only lead to solution of 3–dimensional fluid dynamics with turbulence behaviour characterised by complex equations. This assumption is particularly important for models describing continuous stirred tank reactors, (CSTRs).

4.2 Modelling and Simulation of the Whole-Cell Biotransformation System

4.2.1 Batch System

Model Construction

The conversion of bicyclo[3.2.0]hept-2-en-6-one, $[S_{Bicyclo}]$ to chiral lactones ((-)1(S)5(R)2-oxabicyclo[3.3.0]oct-6-en-3-one and (-)1(R)5(S)3-oxabicyclo[3.3.0]-oct-6-en-2-one), $[P_{OxaBicyclo}]$ could be mathematically described following the conservation laws that give a system with 2 simple ordinary differential equations. Since there are no inflow and outflow into and out of the system (*Figure 4.3(a)*), the laws reduce into a simple generation terms on the right hand side. Let the rate of reaction describing the conversion of the above components represented as, $r_{s,p}$, at a certain working volume, V_r, therefore, a system of 2 coupled differential equations can be simply written as,

$$\begin{aligned} \frac{d(V_r[S_{Bicyclo}])}{dt} &= -V_r r_{s,p} \\ \frac{d(V_r[P_{OxaBicyclo}])}{dt} &= V_r r_{s,p} \end{aligned} \tag{4.1}$$

The amount of components in the units of (mmol) from the above system could be changed into the concentration units of (mM) by expanding the terms on the left hand side of system (4.1)

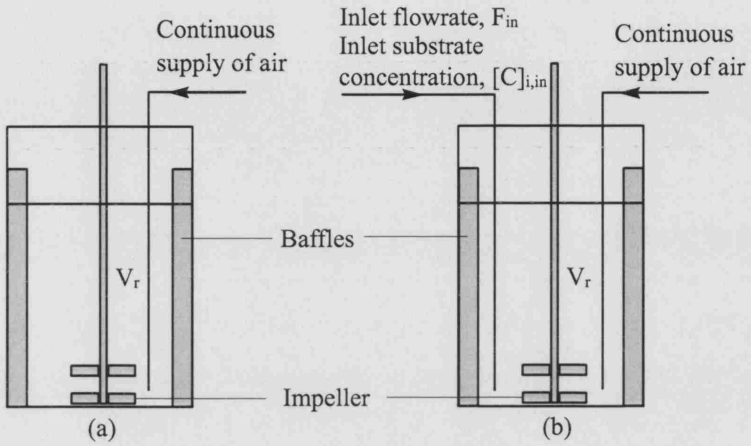

Figure 4.3: (a) Batch and (b) fed-batch configurations of bioreactor for biotransformation. F_{in} represents the inlet flowrate into the bioreactor with the initial concentration of inlet component i, given by $[C]_i$.

and dividing by the total volume of reaction medium in the reactor which leads to;

$$\begin{aligned} \frac{d[S_{Bicyclo}]}{dt} &= -r_{s,p} \\ \frac{d[P_{OxaBicyclo}]}{dt} &= r_{s,p} \end{aligned} \tag{4.2}$$

where $r_{s,p}$ is the terms given by;

$$r_{s,p} = \frac{V_{max}[S_{Bicyclo}]}{K_{m_{[Bicyclo]}}\left(1+\frac{[P_{OxaBicyclo}]}{K_{m_{[OxaBicyclo]}}}\right)+[S_{Bicyclo}]\left(1+\frac{[S_{Bicyclo}]}{K_{i_{[Bicyclo]}}}+\frac{[P_{OxaBicyclo}]}{K_{i_{[OxaBicyclo]}}}\right)}$$

This completes the model for bioconversion of bicyclo[3.2.0]hept-2-en-6-one to chiral lactones in a batch configuration.

Model Simulation and Mathematical Analysis

Initially, the system described above was simulated using arbitrary values of time and concentration. However, the values kinetic parameters in the rate expression, were from the estimated values found in *Chapter 3.* Such a simulation was undertaken in order to observe the similarity

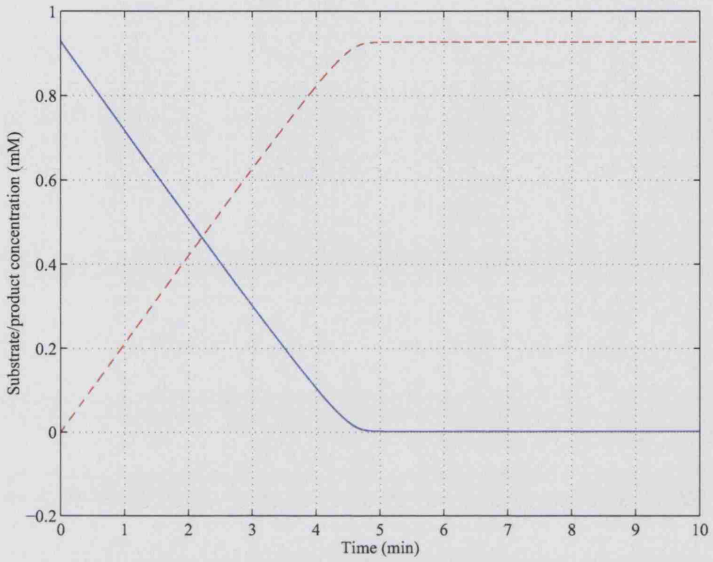

Figure 4.4: Simulation of the reaction carried out in a batch reactor at the initial concentrations of substrate and product at $t = 0$; $[S_{Bicyclo}](0) = 0.9259\text{mM}$ and $[P_{OxaBicyclo}](0) = 0\text{mM}$ respectively. All kinetic parameters are referred to *Table 3.2* using the enzyme obtained from $10\text{g}_{dcw}\text{l}^{-1}$ cell density. Substrate consumption, '–' and product formation, '– –'.

of the curve to the real experimental observation. Consider the system simulated at an initial substrate concentration of $1.0\text{g}\cdot\text{l}^{-1}$, the curve obtained is given in *Figure 4.4*. Reaction in a batch reactor configuration obviously goes to completion after about 5 minutes according to the given model. It is clear that at a given initial value of substrate concentration, an initial rate of product formation could be determined and with an aid of simulations using a range of substrate concentrations, an obvious picture of the effect of inhibition could be observed. Subsequent figure gives a simulation of a batch reaction with a range of substrate between $0.01\text{g}\cdot\text{l}^{-1}$ to $5.0\text{g}\cdot\text{l}^{-1}$ (0.081–40.32mM).

As the initial concentration of substrate, $[S_{Bicyclo}](0)$ was increased, the rate of bioconversion of substrate to product gradually decreased. This is shown in the enlarged area of box (a) of *Figure 4.5*. At a very low concentration of substrate, for instance $0.01\text{g}\cdot\text{l}^{-1}$, the reaction progressed slowly. When the concentration was increased, the conversion started to speed up, up to a point where it gradually decreased again. This signifies that inhibitions have taken place

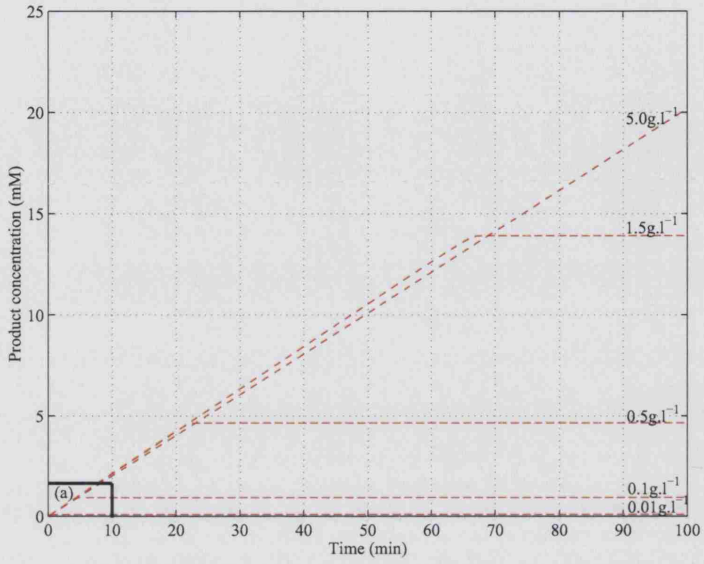

Figure 4.5: Simulation of system (4.2) at different initial substrate concentrations and the enlarged box is given in the next figure.

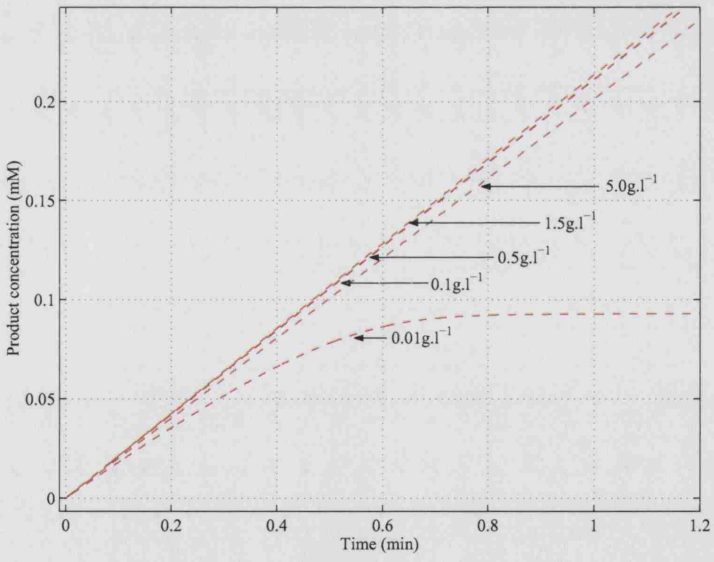

Figure 4.6: The enlarged area (a) showing a slight deviation of the rate observed as the initial substrate concentration is increased to 5.0g·l^{-1}.

in the reaction. The rate however does not vary significantly, this is due to the kinetic parameters governing the rate expression, $r_{s,p}$ as well as the amount of product formed, $[P_{OxaBicyclo}]$ which the term also relates to the particular rate expression.

It is apparent that the results from the above simulations gave a large deviation from the whole-cell plot of the initial rate given in *Appendix G*. The rate plotted for the increase of the initial substrate concentration started to decrease after about $1.5 g \cdot l^{-1}$ of substrate concentration, while the rate from the simulations only started to give an effect at the amount of $5.0 g \cdot l^{-1}$ of substrate. From these observations, it can be concluded that the use of the whole cell to carry out the biotransformation of bicyclo[3.2.0]hept-2-en-6-one depends on two main factors; the effect of the substrate towards the cell and the inhibition of the substrate towards the enzyme within the cell. It should be noted that the model describing the biotransformation of the given substrate did not include the effect of either substrate or product towards the *E. coli* cell. Such work could only be investigated using the flow cytometric analysis where the viability of the cell could be continuously monitored at different substrate concentrations. The investigation of the same system based on the flow cytometric analysis can be referred to the work of OShitu (2005) or for a more general investigation from the work of Marx *et al.* (2003); Lewis *et al.* (2004); Hewitt and Petit (2004); Wallberg *et al.* (2005) and da Silva *et al.* (2005).

Analysis of the system given by differential equations (4.2) was used to clearly prove the above simulation. The steady–state of the system could not be determined since both equations have similar terms on the right hand side. Therefore, the calculation of steady-state by putting equations (4.2) in the form of;

$$-r_{s,p} = 0$$

$$r_{s,p} = 0$$

only led to no solution. This result shows that the system strongly depends on the initial conditions in order to start the process. The system should follow the valid initial conditions where solutions of the given differential equations will describe the actual bioconversion reaction, these are given by, $[S_{Bicyclo}](0) > 0$ and $[P_{OxaBicyclo}](0) \geq 0$.

4.2.2 Fed-Batch System

Model Construction

For the fed-batch system, the conservation laws around the boundary of the diagram given in *Figure 4.3(b)* can be written as;

$$\frac{d(V_r[S_{Bicyclo}])}{dt} = F_{[S_{Bicyclo}],in}[S_{Bicyclo}]_{in} - V_r r_{s,p} \tag{4.3}$$

for substrate consumption and

$$\frac{d(V_r[P_{OxaBicyclo}])}{dt} = V_r r_{s,p} \tag{4.4}$$

for product formation. Since there is a continuous amount of substrate being fed into the reactor, therefore, the reactor volume should vary with time and this could be simply described below;

$$\begin{aligned} \frac{dV_r}{dt} &= F_{[S_{Bicyclo}],in} \\ \int_{V_0}^{V_r} dV_r &= F_{[S_{Bicyclo}],in} \int_{t_0}^{t} dt \\ V_r &= F_{[S_{Bicyclo}],in}(t - t_0) + V_0 \end{aligned} \tag{4.5}$$

where V_0 is the initial volume at $t = 0$, (t_0). With further rearrangement, the differential equations (4.3) and (4.4) could be expanded into the form given below;

$$\begin{aligned} V_r \frac{d[S_{Bicyclo}]}{dt} &= F_{[S_{Bicyclo}],in}[S_{Bicyclo}]_{in} - \frac{dV_r}{dt}[S_{Bicyclo}] - V_r r_{s,p} \\ V_r \frac{d[P_{OxaBicyclo}]}{dt} &= V_r r_{s,p} - F_{[S_{Bicyclo}],in}[P_{OxaBicyclo}] \end{aligned} \tag{4.6}$$

Since the flowrate of the inlet substrate is given by $\frac{dV_r}{dt} = F_{[S_{Bicyclo}],in}$ and by substituting this into system (4.6) and dividing by V_r, it simplifies into the form given below;

$$\begin{aligned} \frac{d[S_{Bicyclo}]}{dt} &= \frac{F_{[S_{Bicyclo}],in}}{V_r}([S_{Bicyclo}]_{in} - [S_{Bicyclo}]) - r_{s,p} \\ \frac{d[P_{OxaBicyclo}]}{dt} &= r_{s,p} - \frac{F_{[S_{Bicyclo}],in}}{V_r}[P_{OxaBicyclo}] \end{aligned} \tag{4.7}$$

The term $\frac{F_{[S_{Bicyclo}],in}}{V_r}$ in the above equations is normally known as the *dilution rate* of a (bio)reactor and it is denoted as D (Bailey and Ollis, 1986). It is used to characterise the holding time or processing rate in a CSTR. Simplifying the dimension of D gives the reciprocal of the mean residence time of components in a bioreactor. Incorporating the term D in system of differential equations (4.7) gives,

$$\begin{aligned} \frac{d[S_{Bicyclo}]}{dt} &= D\left([S_{Bicyclo}]_{in} - [S_{Bicyclo}]\right) - r_{s,p} \\ \frac{d[P_{OxaBicyclo}]}{dt} &= r_{s,p} - D[P_{OxaBicyclo}] \end{aligned} \tag{4.8}$$

The system consists of 4 different parameters which could be varied during the simulation and they include, the dilution rate, D, the initial concentrations of substrate and product, $[S_{Bicyclo}]$ and $[P_{OxaBicyclo}]$ respectively and finally, the initial concentration of substrate being fed into the reactor, $[S_{Bicyclo}]_{in}$. The next section discusses the effect of varying these parameters and results are given in the form of simulated graphs as well as mathematical analysis.

Model Simulation and Mathematical Analysis

One of the advantages of fed-batch reactor configuration is the ability to control the amount of substrate feeding for bioconversion. When a correct amount of substrate is fed into the reactor, the reaction rate of bioconversion can be controlled such that the effect of substrate inhibition could be avoided, hence, maintaining the rate of product formation.

Consider the system given by the coupled differential equations (4.8). If it is given that a bioconversion occurs in a 2l bioreactor with 1l working volume, at the feeding rate of $0.01\text{l}\cdot\text{min}^{-1}$, with initial substrate concentration of 1mM and in the absence of substrate and product components in the bioreactor at time, $t = 0$, the simulation results in a plot given in *Figure 4.7*. The simulation clearly shows that at a low feeding rate, only a small amount of substrate accumulated within the bioreactor. Almost all substrate is converted into product which is depicted by the line parallel to the x-axis in the given figure. As the reaction proceeds, the product starts to accumulate in the reactor until it reaches a steady-state value, this is not shown in the simulated graph, however, it can be mathematically shown using the steady-state analysis. Apart from the increase of product formation, the volume of the medium in the bioreactor should also increase

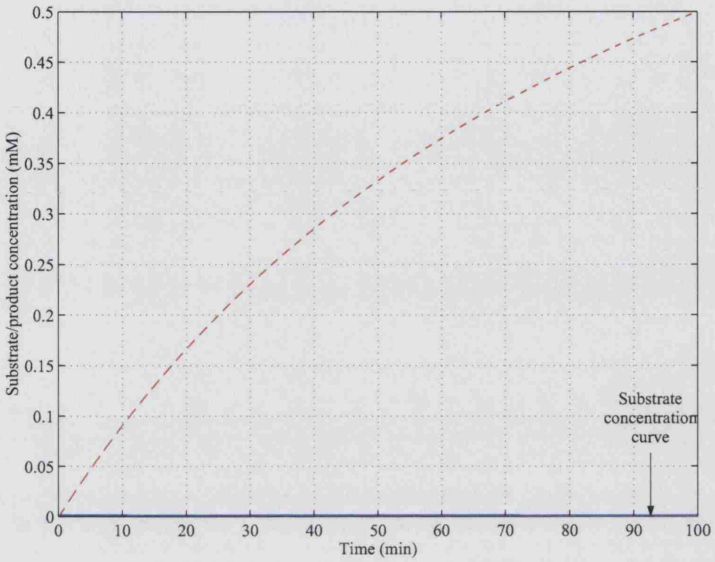

Figure 4.7: Simulation of the fed–batch bioconversion with conditions of $F_{in} = 0.01\text{l}\cdot\text{min}^{-1}$, $[S_{Bicyclo}]_{in} = 1\text{mM}$, $[S_{Bicyclo}](0) = 0$ and $[P_{OxaBicyclo}](0) = 0$. '–' substrate consumption, '– –' product formation.

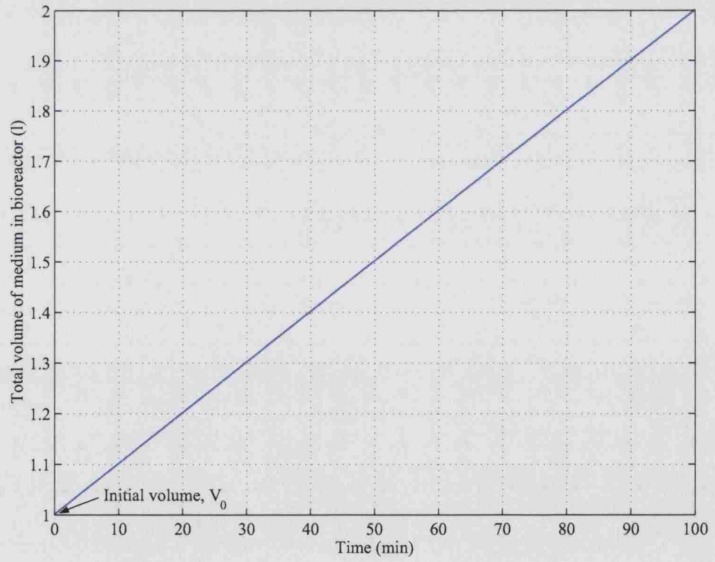

Figure 4.8: Increase of volume of reaction medium during continuously feeding of substrate.

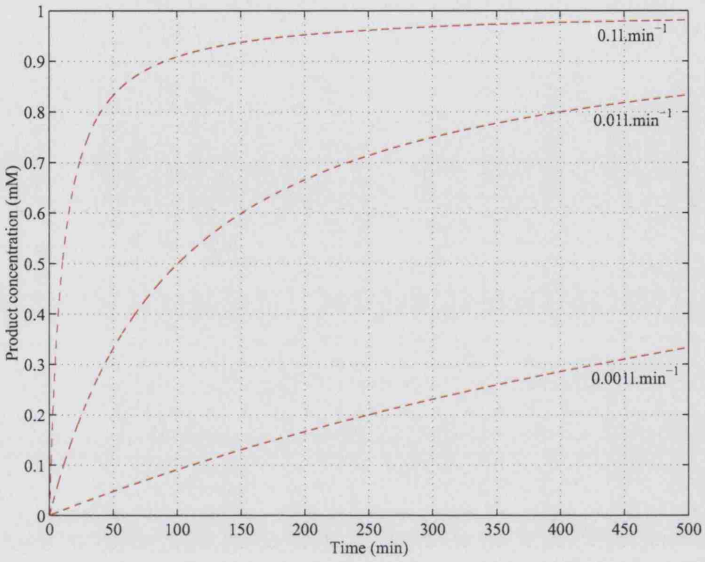

Figure 4.9: Effect of different feeding rates towards product formation.

as the substrate is being fed. This is clearly depicted in *Figure 4.8*.

The effect of feeding rate of substrate to the rate of product formation can be observed by varying the value of the inlet flowrate, F_{in}. This is important especially in controlling the amount of substrate in the reaction medium such that it would not inhibit the reaction and lower the rate of product formation. The effect of variable flowrates towards the rate of product formation is given in *Figure 4.9*. The simulation also shows that at different feeding rates, the maximum product formed also changes i.e. the steady-state increases as the flowrate of ketone increases. The rate of product formation as it approaches this constant value also varies with respect to the feeding rate. It should be noticed from the rate expression of cyclohexanone monooxygenase enzyme-catalysed Baeyer-Villiger reaction, such accumulation of product within the reactor could also lead to the increase of product inhibition which consequently lowering the rate of its formation. Therefore, it is suggested that for a reaction carried out in a fed-batch bioreactor, a process should be frequently shut-down when the level of product is relatively high. The reaction medium that consists of traces of substrate, biomass and a large amount of product should undergo a suitable downstream processes to separate the mixture into their individual

components.

Simulation of the fed-batch process model described in the previous paragraph was mathematically analysed. Such an analysis can be used to check the stability of the model system. Consider the system of equations that consists of equation (4.5) and that a coupled equations (4.7);

$$\frac{dV_r}{dt} = F_{[S_{Bicyclo}],in}$$

$$\frac{d[S_{Bicyclo}]}{dt} = \frac{F_{[S_{Bicyclo}],in}}{V_r}([S_{Bicyclo}]_{in} - [S_{Bicyclo}]) - r_{s,p}$$

$$\frac{d[P_{OxaBicyclo}]}{dt} = r_{s,p} - \frac{F_{[S_{Bicyclo}],in}}{V_r}[P_{OxaBicyclo}]$$

When the left hand side of the above equations are let to be equal to zero, such that, $\frac{dV_r}{dt} = 0$, $\frac{d[S_{Bicyclo}]}{dt} = 0$, and $\frac{d[P_{OxaBicyclo}]}{dt} = 0$, they should be reduced into the form given below;

$$F_{[S_{Bicyclo}],in} = 0 \tag{4.9}$$

$$\frac{F_{[S_{Bicyclo}],in}}{V_r}([S_{Bicyclo}]_{in} - [S_{Bicyclo}]) - r_{s,p} = 0 \tag{4.10}$$

$$r_{s,p} - \frac{F_{[S_{Bicyclo}],in}}{V_r}[P_{OxaBicyclo}] = 0 \tag{4.11}$$

At zero feeding rate of substrate, equations (4.10) and (4.11) are further reduced into the similar form as that in the batch configuration, and attempt to solve such system could only lead to error. The only method to analyse the system is to decouple equation (4.9) from the above set of equations and to accomplish this, the 3 equations above need to be rendered into a dimensionless set of equations. It should be noticed that there is no standard form of non-dimensionalising a system of differential equations, there may be other ways of setting the parameters and one of them is given in *Table 4.1.* The fed-batch model defined in the form of dimensionless terms

Dimensionless form	Terms defining the dimensionless form
$\bar{F}$	$\frac{F_{[S_{Bicyclo}],in}}{V_0 \bar{t}}$
$\bar{V}$	$\frac{V_r}{V_0}$
$\bar{t}$	$\frac{F_{[S_{Bicyclo}],in}}{V_r}$
τ	$t\bar{t}$
x_s	$\frac{[S_{Bicyclo}]}{[S_{Bicyclo}]_{in}}$
x_p	$\frac{[P_{OxaBicyclo}]}{[S_{Bicyclo}]_{in}}$
κ_{m_s}	$\frac{K_{m_{[Bicyclo]}}}{[S_{Bicyclo}]_{in}}$
κ_{m_p}	$\frac{K_{m_{[OxaBicyclo]}}}{[S_{Bicyclo}]_{in}}$
κ_{i_s}	$\frac{K_{i_{[Bicyclo]}}}{[S_{Bicyclo}]_{in}}$
κ_{i_p}	$\frac{K_{i_{[OxaBicyclo]}}}{[S_{Bicyclo}]_{in}}$
Da	$\frac{V_{max}}{\bar{t}[S_{Bicyclo}]_{in}} = \frac{k_5[E]_T}{\bar{t}[S_{Bicyclo}]_{in}}$

Table 4.1: Dimensionless parameters defining the dimensionless form of the fed-batch model.

could be written as follows;

$$\begin{aligned} \frac{d\bar{V}}{d\tau} &= \bar{F} \\ \frac{dx_s}{d\tau} &= 1 - x_s - DaR(x_s, x_p) \\ \frac{dx_p}{d\tau} &= -x_p + DaR(x_s, x_p) \end{aligned} \tag{4.12}$$

where $R(x_s, x_p)$ is defined as the dimensionless rate expression given by;

$$R(x_s, x_p) = \frac{x_s}{\kappa_{m_s}\left(1 + \frac{x_p}{\kappa_{m_p}}\right) + x_s\left(1 + \frac{x_s}{\kappa_{i_s}} + \frac{x_p}{\kappa_{i_p}}\right)}$$

Apparently, the first differential equation from system (4.12) contains no variables which can be related to the last two differential equations, thus, it can now be omitted from the analysis. The term Da is commonly known as the Damköhler number which characterises the reaction rate constant k_5 and in some way also related to the amount of available biocatalyst used in a particular reaction (Uppal *et al.*, 1974; Agrawal *et al.*, 1982; Aris, 1993). Defining the new

system as;

$$\begin{aligned} \frac{dx_s}{d\tau} &= 1 - x_s - DaR(x_s, x_p) \\ \frac{dx_p}{d\tau} &= -x_p + DaR(x_s, x_p) \end{aligned} \tag{4.13}$$

where the vector notation is in the form of

$$\frac{d\mathbf{x}}{d\tau} = f(\mathbf{x}, Da) \tag{4.14}$$

and examining the steady-state condition by putting

$$f(\mathbf{x}, Da) = 0$$

leads to

$$Da = \frac{1 - x_s^{ss}}{R(x_s^{ss}, x_p^{ss})} \tag{4.15}$$

where x_s^{ss} and x_p^{ss} refer to the concentrations of substrate and product at the steady-state condition respectively. This gives effect to the rate of product formation since;

$$x_p^{ss} = -\frac{A \pm \sqrt{\kappa_{i_p}\kappa_{m_p}\left(4Dax_s^{ss}\kappa_{i_s}^2 B + A^2\right)}}{2\kappa_{i_s} B} \tag{4.16}$$

with

$$A = \left\{(x_s^{ss})^2 + (x_s^{ss} + \kappa_{m_s})\kappa_{i_s}\right\}\kappa_{i_p}\kappa_{m_p}$$

and

$$B = x_s^{ss}\kappa_{m_p} + \kappa_{i_p}\kappa_{m_s}$$

which only valid with the negative square root of (4.16). This function also suggests that the system could never end up with the steady-state at the origin which proves the characteristic of the fed-batch bioreactor configuration. The stability of this steady-state can be found by

putting system (4.13) into a linear matrix form given by;

$$J_{s,p} = \begin{pmatrix} -1 + \frac{Da}{R(x_s,x_p)} \left[\frac{x_s\left(1+\frac{x_p}{\kappa_{i_p}}+\frac{2x_s}{\kappa_{i_s}}\right)}{R(x_s,x_p)} - 1 \right] & \frac{Dax_s\left(\frac{x_s}{\kappa_{i_p}}+\frac{\kappa_{m_s}}{\kappa_{m_p}}\right)}{R(x_s,x_p)^2} \\ -\frac{Da}{R(x_s,x_p)} \left[\frac{x_s\left(1+\frac{x_p}{\kappa_{i_p}}+\frac{2x_s}{\kappa_{i_s}}\right)}{R(x_s,x_p)} - 1 \right] & -1 - \frac{Dax_s\left(\frac{x_s}{\kappa_{i_p}}+\frac{\kappa_{m_s}}{\kappa_{m_p}}\right)}{R(x_s,x_p)^2} \end{pmatrix} \tag{4.17}$$

which is then used to find the determinant of the form,

$$\det(J_{s,p}) = 1 - \frac{Da}{R(x_s,x_p)^2}\left(x_s + \frac{x_s x_p}{\kappa_{i_p}} - \frac{x_s^2}{\kappa_{i_p}} + \frac{2x_s^2}{\kappa_{i_s}} - \frac{\kappa_{m_s} x_s}{\kappa_{m_p}} - 1\right) \tag{4.18}$$

with the corresponding trace,

$$\mathrm{tr}(J_{s,p}) = -2 + \frac{Da}{R(x_s,x_p)^2}\left\{x_s\left(1+\frac{x_p}{\kappa_{i_p}}+2\frac{x_s}{\kappa_{i_s}}\right) - x_s\left(\frac{x_s}{\kappa_{i_p}}+\frac{\kappa_{m_s}}{\kappa_{m_p}}\right) - R(x_s,x_p)\right\} \tag{4.19}$$

The determinant and trace from equations (4.18) and (4.19) clearly give the necessary and sufficient conditions for the existence of local stability of the isothermal fed-batch system. Combination of these equations or from the matrix given by (4.17), a characteristic equation which leads to eigenvalues of the given system could be determined. From the given matrix, a function in term of variable λ can be written as;

$$\begin{aligned} \lambda^2 &+ \lambda\left[2 - \frac{Da}{R(x_s,x_p)^2}\left(x_s + \frac{x_s x_p}{\kappa_{i_p}} - \frac{x_s^2}{\kappa_{i_p}} + 2\frac{x_s^s}{\kappa_{i_s}} - \frac{\kappa_{m_s} x_s}{\kappa_{m_p}} - R(x_s,x_p)\right)\right] \\ &+ 1 - \frac{Da}{R(x_s,x_p)^2}\left(x_s + \frac{x_s x_p}{\kappa_{i_p}} - \frac{x_s^2}{\kappa_{i_p}} + 2\frac{x_s^2}{\kappa_{i_s}} - \frac{\kappa_{m_s} x_s}{\kappa_{m_p}} + R(x_s,x_p)\right) \\ &= 0 \end{aligned} \tag{4.20}$$

which then solved for eigenvalues, $\mathbf{\Lambda}$;

$$\mathbf{\Lambda} = \begin{pmatrix} \lambda_1 & \lambda_2 \end{pmatrix}^\top \tag{4.21}$$

where,

$$0 < \lambda_1 < \lambda_2$$

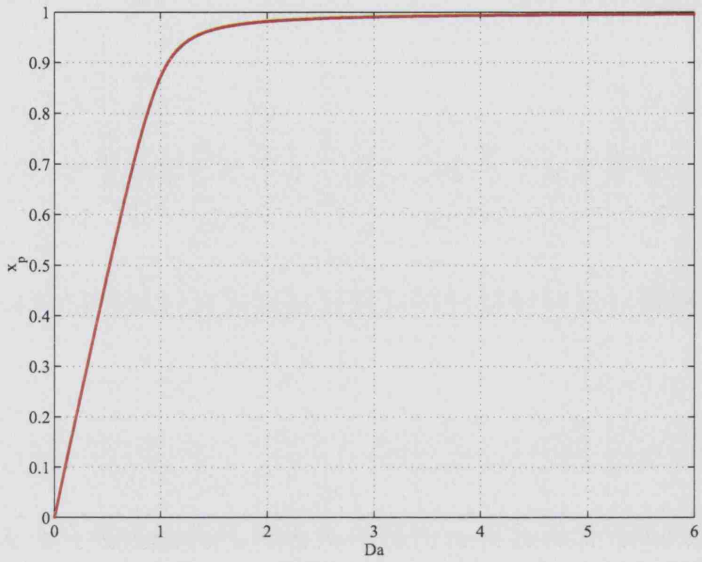

Figure 4.10: Effect of changing Da on the steady-state points.

which confirmed the previous determinant and trace analyses for local stability. This result could be visualised on a graphical plot for a range of values of Da. A stable point is observed after a period of gradual increase of product formation which again proves the system of equations with steady-state points being locally asymptotically stable.

4.3 Experimental Validation

Prior to process modelling of Baeyer-Villiger reaction, experimental data was collected based on the two different reactor configurations; batch and fed-batch reactors. Both reactions were undertaken at different reactor working volumes, therefore, experimental comparison between these data is rather inappropriate, although they were carried out using the same biocatalyst (CHMO-expressed *E. coli*). The main objective of the experiment is to compare the collected data with the simulation of the process model, so that the model can be said to actually describe the physical phenomena. For batch type reactor configuration, mini-reactors with 60ml working volume was used at different substrate concentrations. The fabrication of this reactor has been clearly explained in *Chapter 2.* Whereas, for fed-batch configuration, the reaction was carried out in a 7l bioreactor at 5l working volume.

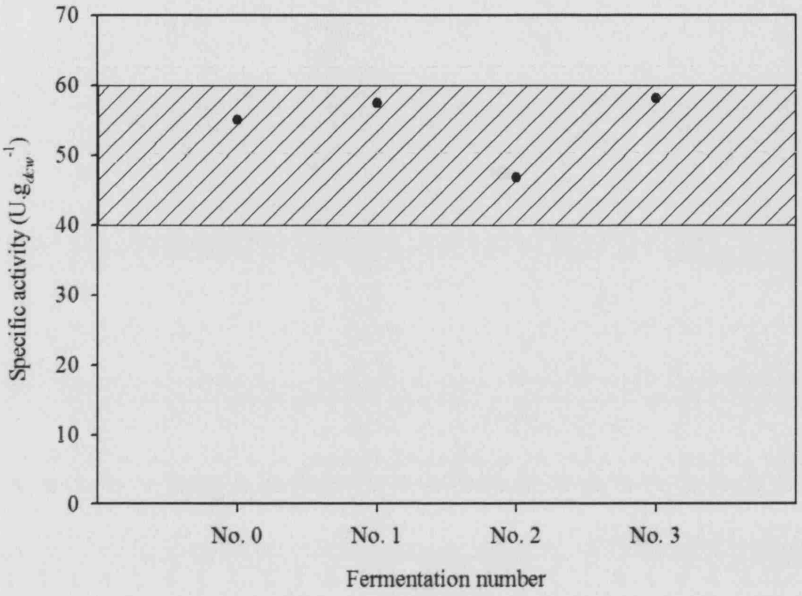

Figure 4.11: The plot of specific activity of biocatalyst from 3 fermentations. The specific activity for fermentation No. 0 is obtained from Doig *et al.* (2002) for comparison. The shaded area shows the limit of biocatalyst activity where biotransformation is carried out. Biocatalyst that gives activity below this lower limit would not be used for biotransformation.

This section is divided into 2 main parts; experimental procedures and comparison of data with the model simulations.

4.3.1 Materials and Method

Batch Reactor

Biocatalyst for biotransformation was obtained from the fermentation of CHMO-expressed *E.coli* TOP10[pQR239]. Fermentation procedure has been explained in detail in *Chapter 3*, Section 3.2.1. During this work, a number biocatalyst fermentations were carried out and the specific activity of each of them was determined before starting a biotransformation reaction, so that approximately the same amount of enzyme is used in a reaction. This is important in order to get a consistent results in all biotransformation processes. A plot of the specific activity from a few biocatalyst fermentations is given in *Figure 4.11* above. The purified substrate,

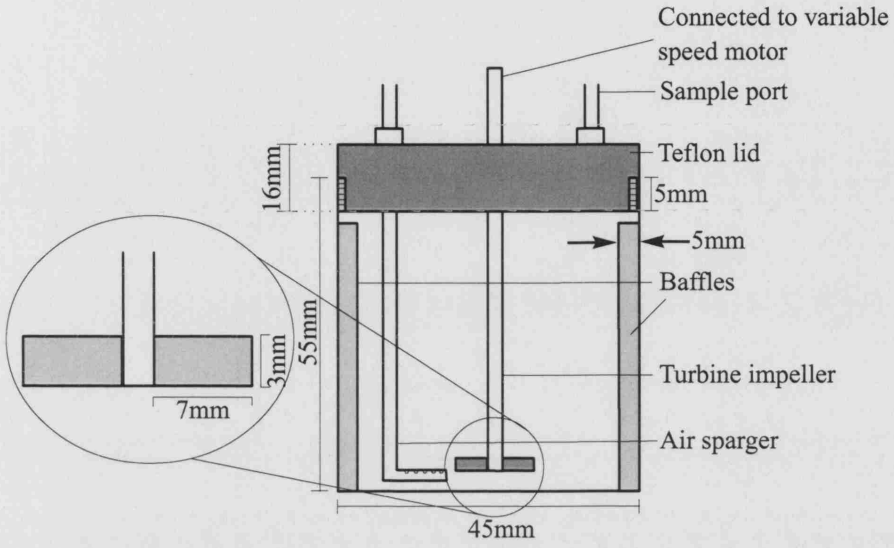

Figure 4.12: Mini reactor configuration for bioconversion.

(bicyclo[3.2.0]hept-2-en-6-one) and products, ((-)1(S)5(R)2-oxabicyclo[3.3.0]oct-6-en-3-one and (-)1(R)5(S)3-oxabicyclo[3.3.0]oct-6-en-2-one) were a kind gift from Fluka (Buchs, Switzerland). All other chemicals were obtained from Sigma Chemical Co. (Poole, Dorset, UK), while the fermentation media were ordered from Fluka (Buchs, Switzerland).

Mini Reactor Fabrication

Mini reactors were used to carry out the whole cell biotransformation. They were made of 80ml beakers. The removed edge gave a round flat edge for the insertion of the teflon lid. The lid was made such that it fitted to the beaker and prevented any leakage of the reaction broth. Five separate holes were made on top of the lid, mainly to fit the agitator, the air sparger and a sampling port. Two remaining ports were closed with the metal bolts. Miniature baffles which were fitted inside each beaker were made of stainless steel joined together with metal wire to prevent movement during agitation.

Figure 4.12 clearly shows the size and configuration of the mini reactor. Four similar designs were made so that reaction could be carried out simultaneously with 4 different parameters. All four reactors were immersed in a water bath. The warm liquid in the water bath was

levelled with the reaction medium in the reactors. The temperature was set at 37°C during biotransformation and the agitators were connected with rubber connectors to a variable speed motor so that the reaction mixtures were mixed at the same agitation (600–800r.p.m). Air was supplied into the reactor via an air pump connected to the four different rotameters.

The method is similar to the initial rate data, however, in order to obtain the curves that describe the complete reaction, data was continuously taken for 150min of reaction. 3 different concentrations ($0.6g{\cdot}l^{-1}$, $0.95g{\cdot}l^{-1}$ and $1.3g{\cdot}l^{-1}$) of substrate were added into the reactor in order to start the reaction.

Fed-Batch Reactor

E.coli TOP10[pQR239] was obtained and grown in a similar way described previously and all chemicals were used at their highest purity.

The fed-batch bioreactor for ketone bioconversion was set-up using the 7l fermenter initially used for the fermentation of biocatalyst. 5l biomass was measured and set as the initial reactor volume, V_r. An external peristaltic pump (101 U/R, Watson-Marlow Limited, Falmouth, Cornwall, UK) was connected to the fermenter to deliver continuous amount of substrate required for a particular bioconversion. Reactor temperature was set at 37°C and maintained at pH 7.0. The pH of the biomass was controlled using 3M of phosphoric acid (H_3PO_4) and 3M of potassium hydroxide (KOH) and they were connected to the separately controlled peristaltic pumps mounted together with the fermenter. $10g{\cdot}l^{-1}$ of glycerol was added as a carbon source for the biomass (the amount of glycerol initially available in the complex media components was assumed to deplete during the course of fermentation).

Bioconversion of bicyclo[3.2.0]hept-2-en-6-one was started when the chemical was pumped into the bioreactor. Samples were taken every 30min for 240min of reaction. Part of the sample collected was used to check the growth of biomass during the reaction and the remaining sample was extracted with ethyl acetate to separate the remaining substrate and product (organic phase) from the biomass (aqueous phase). All sample were analysed using gas chromatography and a similar assay described in Section 3.3.1 was used.

4.3.2 Model Simulations and Experimental Comparison

Biotransformation in the Batch Bioreactor

Three different concentrations of substrate were used to start the batch biotransformation of bicyclo[3.2.0]hept-2-en-6-one. Similar substrate concentrations were also used to simulate the batch model of the particular reaction.

The first reaction was started with concentration below that in the inhibition range. $0.6g{\cdot}l^{-1}$ (5.56mM) of substrate results in the plot given in *Figure 4.13*. The concentration was then increased to $0.95g{\cdot}l^{-1}$, a value where inhibition just started to give effect to the rate of reaction (*Figure 4.14*). Finally substrate concentration of $1.3g{\cdot}l^{-1}$, a value where substrate inhibition started to lower the rate of product formation which can be clearly seen in *Figure 4.15*.

From the three figures showing the comparisons of the model curve and the experimental plot, it is obvious that the lines and the points are separated far apart from each other. The shifts are all presented by arrows pointing from the lines towards the data points. The inhibition due to the increase of substrate concentration is apparent from the reduction of the rate of reaction given by both the data points and the model simulations. The shift of data points from the simulated lines is greater for reaction with relatively high substrate concentration ($1.30g{\cdot}l^{-1}$). This behaviour could be explained with not just the effect of inhibition, but also the diffusional rate of substrate into the cell and with both effects combine, results in even lower rate of product formation. Another observation could also be pointed out from the same figure which concerned with the crossing point between the substrate consumption and product formation. It is clear that the amount of substrate consumed is far higher than the amount of product being formed. This suggests that the product formed within the cell compartment takes longer time to diffuse out due to its larger molecular weight and structure compared to that of the substrate.

The shift of the experimental points away from the simulation path is basically due to two reasons mentioned previously; the effect of substrate and product towards the cell and the enzyme and the diffusional effect from the cell membrane. It should be iterated here that the model was constructed based on the unstructured type, therefore, the effect of diffusion caused by the cell membrane was assumed to be negligible. However, the data collected from the batch

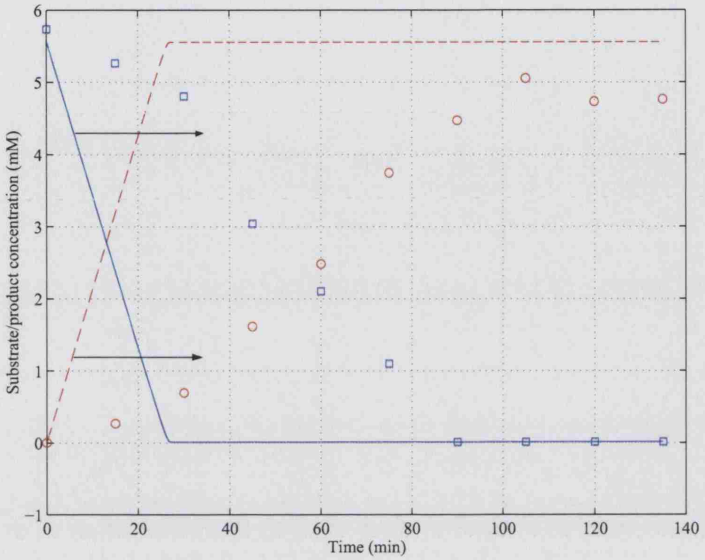

Figure 4.13: Batch biotransformation of substrate at $[S_{Bicyclo}](0) = 0.6\text{g}\cdot\text{l}^{-1}$. '–' substrate and '– –' product concentrations (simulation curves), '□' substrate and '○' product concentrations (experimental data).

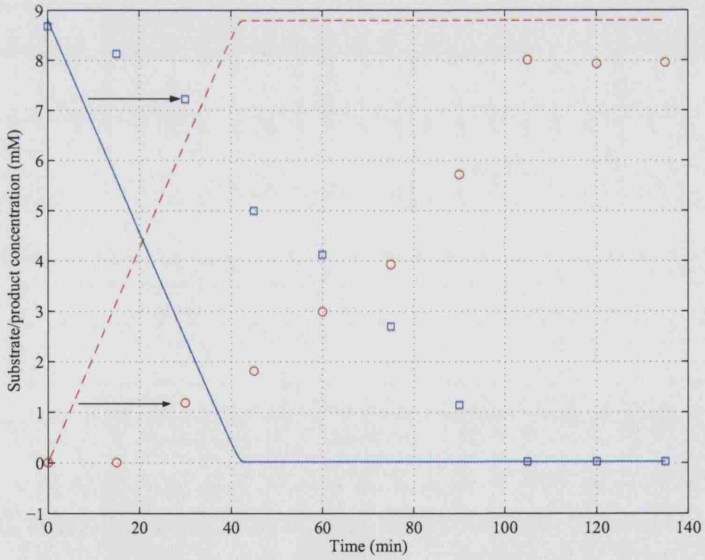

Figure 4.14: Batch biotransformation of substrate at $[S_{Bicyclo}](0) = 0.95\text{g}\cdot\text{l}^{-1}$. '–' substrate and '– –' product concentrations (simulation curves), '□' substrate and '○' product concentrations (experimental data).

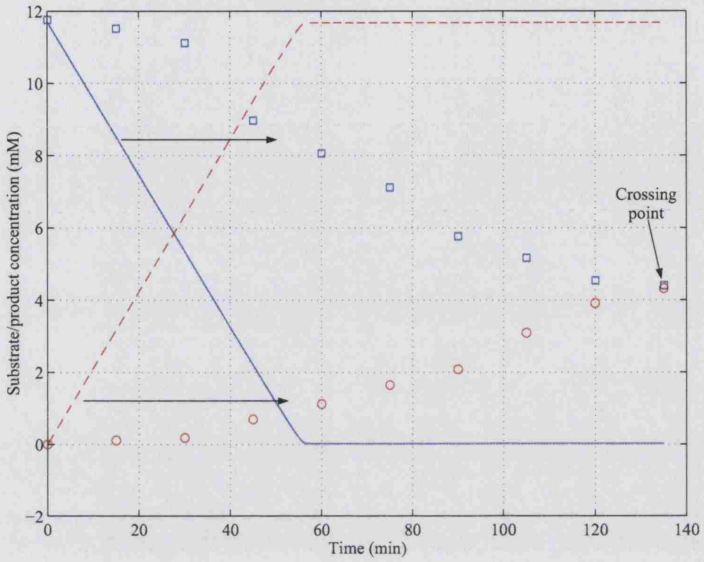

Figure 4.15: Batch biotransformation of substrate at $[S_{Bicyclo}](0) = 1.30\text{g}\cdot\text{l}^{-1}$. '—' substrate and '– –' product concentrations (simulation curves), '□' substrate and '○' product concentrations (experimental data).

reactor configuration was based on the reactions with membrane encapsulated enzyme or whole cell biocatalyst, and it has given a huge different from the model without the diffusional terms. It should now be apparent that diffusion does play an important part in substrate delivery into the cell before it binds with the particular enzyme and converted to product and travels out of the cell. Further analysis on the diffusion of substrate and product into and out of the individual cell was investigated and the results will be discussed at length in *Chapter 5.*

Biotransformation in the Fed-Batch Bioreactor

It has been shown that the inhibition caused by substrate and product in the Baeyer-Villiger reaction substantially affects the rate of its reaction. Batch type reactor is not the best solution since it does not provide any control of either substrate or product within the system. Fed-batch bioreactor configuration shown in *Figure 4.3(b)* could be the solution to the above problem. However, the system is still under the effect of product due to its accumulation after a certain period of reaction time. This problem could be solved by incorporating the system with a continuous removal of product or normally termed as the "*in situ* product removal" (ISPR) (Lye

and Woodley, 1999; Ahmed *et al.*, 2001). This specific type of process is still under investigation and therefore the work was not considered as part of this study.

The purpose of the continuous feeding of substrate is to avoid the reaction from being affected by the excess amount of substrate, therefore maintaining the formation of product in the bioreactor. Since an excessive accumulation of product could also lead to inhibition, thus, a regular process shut-down has to be practised for this particular process system by using the technique mentioned in the previous paragraph.

Simulations were carried out based on the same flowrates applied to the experimental procedure. Three different flowrates were chosen for this comparison and they include; 3.33×10^{-5} $l\cdot min^{-1}$, $4.17\times10^{-4}l\cdot min^{-1}$ and $8.33\times10^{-4}l\cdot min^{-1}$ with the first value gives the rate of substrate consumption lower than that of the inhibition range and the last two with values outside this range. *Figure 4.16* compares the experimental data with the simulated curve of process reaction at a very low substrate feeding rate. The model seems to give a comparable result with the data points collected from the experiment. At this particular flowrate, there was no accumulation of substrate in the reactor, therefore, the effect of substrate inhibition was completely avoided. The simulated line for substrate concentration at almost 0mM suggests that every amount of substrate fed into the reactor was completely converted into product.

However, the curves started to shift when the substrate is fed at a higher rate. In the higher feeding rate experiments, the reactor was batched with a small amount of substrate then the pump was started to deliver the amount required. According to the complete model system, an increase of substrate feeding rate, increases its concentration in the reactor which is higher than the rate of its conversion, thus, inhibition starts to affect the process. This can be seen from the low concentration of product formed during the conversion and a fast accumulation of substrate within the reactor. Although the behaviour is well defined using the model system, the experimental plot of the reaction gave a completely different result with the same conditions. A similar result was observed when the flowrate increases to $8.33\times10^{-4}l\cdot min^{-1}$. *Figure 4.18* clearly shows the contrast between the simulated curves and the experimental plot.

Figures 4.17 and *4.18* also show a peculiar experimental result compared to that of the simulated curves. Apart from the deviation, the experimental points for product formation

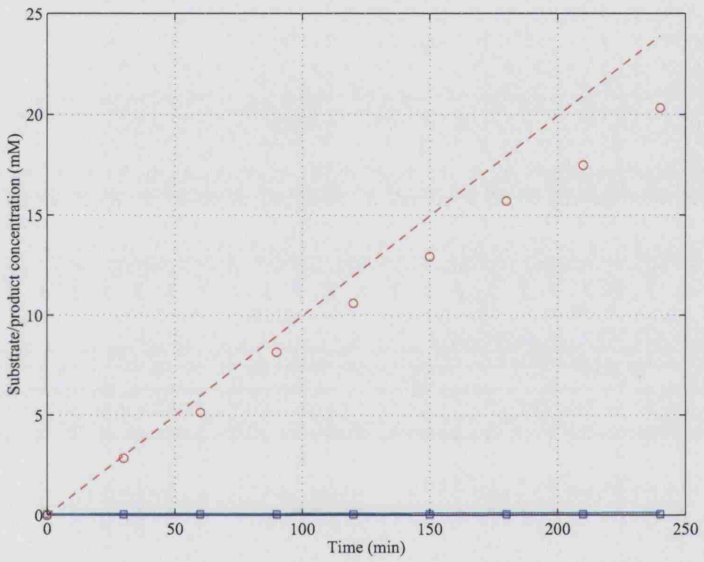

Figure 4.16: Fed-batch biotransformation of ketone at $0 g \cdot l^{-1}$ initial concentrations of substrate and product in the reactor and the feeding rate of $3.33 \times 10^{-5} l \cdot min^{-1}$. '–' substrate and '– –' product concentrations (simulation curves), '□' substrate and '○' product concentrations (experimental data).

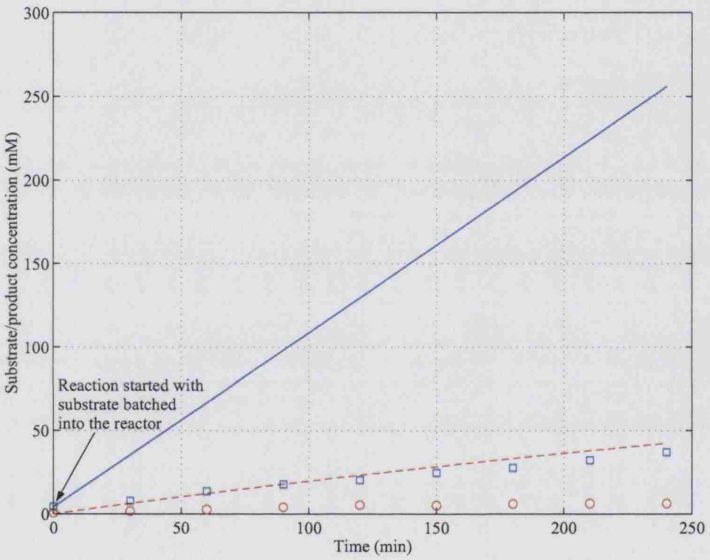

Figure 4.17: Fed-batch biotransformation of ketone at $0.4 g \cdot l^{-1}$ initial concentrations of substrate and product in the reactor and the feeding rate of $4.17 \times 10^{-4} l \cdot min^{-1}$. '–' substrate and '– –' product concentrations (simulation curves), '□' substrate and 'o' product concentrations (experimental data).

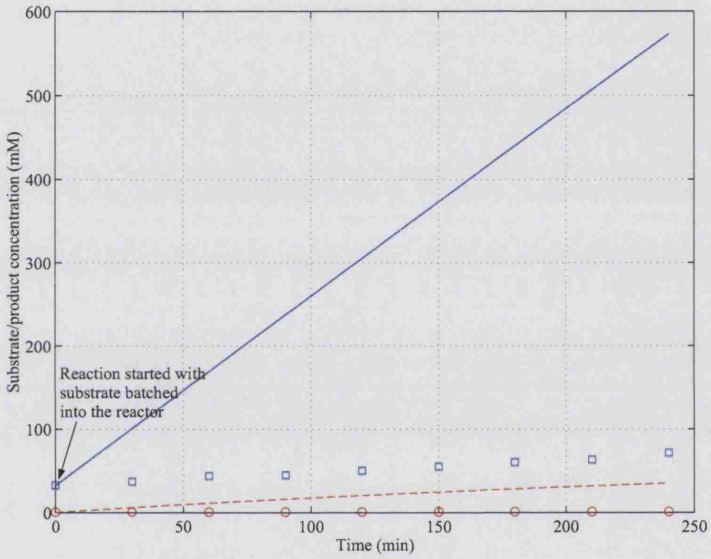

Figure 4.18: Fed-batch biotransformation of ketone at $3.5 g \cdot l^{-1}$ initial concentrations of substrate and product in the reactor and the feeding rate of $8.33 \times 10^{-4} l \cdot min^{-1}$. '–' substrate and '– –' product concentrations (simulation curves), '□' substrate and '○' product concentrations (experimental data).

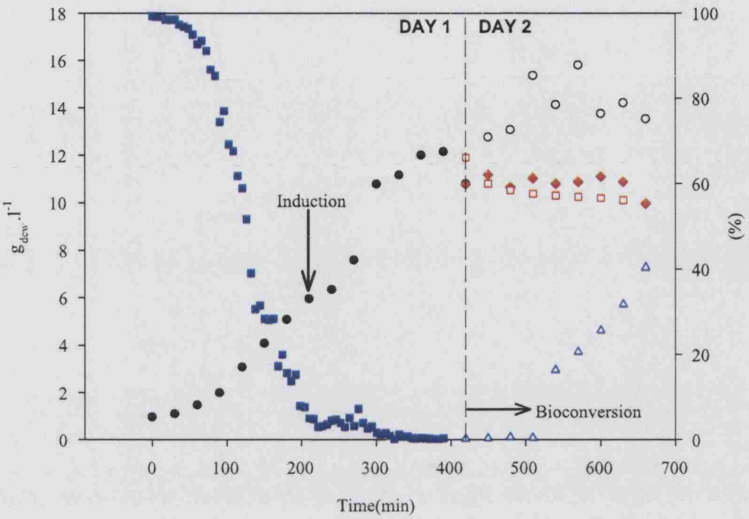

Figure 4.19: Plot of cell viability after fermentation (Day 1) to Day 2 for bioconversion. Dissolved oxygen tension (DOT) is also plotted for comparison. '●' cell growth during fermentation, '■' DOT during fermentation, '○' cell growth during bioconversion (4.17×10^{-4}l·min^{-1}), '♦' cell growth during bioconversion (8.33×10^{-4}l·min^{-1}), '△' DOT during bioconversion (4.17×10^{-4}l·min^{-1}), and '□' DOT during bioconversion (8.33×10^{-4}l·min^{-1}).

seems to reach the steady-state period after about 120min of reaction. This is most obvious with a higher flowrate of substrate. The maximum product formed is only in a range between 0.3–0.6mM with an increasing amount of substrate. Such a result is not only due to the substrate inhibition but it could also be suggested that the excess amount of substrate in the reaction medium could give a toxic environment to the biocatalyst which consequently resulted in a cell death (inactive biocatalyst). During this period, bioconversion is still believed to proceed with the presence of enough amount of enzyme in the cell. However, since the reaction requires cofactor (NADPH) binding with the enzyme before the substrate could take part in the reaction, the absence of the cofactor within the cell would terminate the reaction and lead to a constant rate of product formation. This statement can be shown using the cell growth plot during the bioconversion process at 2 different feeding rates of substrate.

Figures 4.19 divides the plot into two parts, the fermentation process and the bioconversion reaction. The growth of biocatalyst during the fermentation, reached a maximum at approx-

imately $12 g_{dcw} l^{-1}$. Fermentation was then stopped when the cell density started to level off. Further fermentation would only lead to the cell starvation due to the lack of carbon source (glycerol) which would then change the cell metabolism. Metabolic changes would increase the pH of the media and resulted in the cell to break open. In order to maintain the activity of the cell, it was kept in the temperature of -4°C for further use.

This amount of biocatalyst was then used on day 2 to carry out the biotransformation reaction. The cell seems to stay at the same density as on day 1. The amount of cell present during the bioconversion reaction was continuously checked. During the reaction at $4.17 \times 10^{-4} l \cdot min^{-1}$ of flowrate of substrate, the cell density increased until about $14.2 g_{dcw} l^{-1}$ and it started to decrease towards the end of the bioconversion. The amount of oxygen available in the media was maintained at 0% DOT, however, after 90min of reaction, the DOT started to increase which means that the cells have not utilised the dissolved oxygen for metabolism. The effect was more apparent with the higher flowrate of substrate. There was no obvious pattern that the cells were growing, in fact, the points stayed at the same level for 3 hours and started to decrease. The level of DOT was maintained between 55–65% until the reaction was terminated.

4.4 Summary and Conclusion

The study of biotransformation of enzyme-catalysed Baeyer-Villiger reaction via mathematical modelling has led to the understanding of the bioreactor system. Substrate and product diffusions into and out of the cells have been clearly found to give a tremendous effect to the whole-cell reaction. This problem can be solved by constructing a model of rate expression that includes both the effect of inhibition and diffusion (Garcia *et al.*, 1996). A successful estimate of kinetic parameters should be obtained using the whole-cell system, however they do not describe the actual kinetics of the enzyme that has taken part in the bioconversion, in fact, due to the incorporation of diffusion by immobilising of either the enzyme or the whole-cell, these parameters provide no information regarding the specificity and efficiency of the enzyme which will be more useful in enzyme characterisation. The effect of substrate inhibition towards the biotransformation of bicyclo[3.2.0]hept-2-en-6-one also results in the reduction of the reaction rate.

However, inhibition is not the only reason that caused the loss of enzyme activity during the bioconversion. Cell death which resulted the disconnection of the link between enzyme and cofactor regeneration is also affected by the excess amount of substrate in the reaction medium. This does not only lead to the low rate of product formation, but also the termination of the whole biotransformation reaction. In order to address the present situation, a new expression that relates both the substrate and product and the naturally produced cofactor within the cell should be constructed. However, the experimental procedure which can be used to analyse this relationship is not a straight forward technique, for example, the stop-flow assay should be used for the kinetic analysis that requires sophisticated equipment together with a number of data fittings with a large expression. Therefore, such an investigation is only looked into in the form of mathematical model and analysis. A comprehensive investigation regarding the cofactor dependent reaction which could lead to the termination of biotransformation reaction is discussed in *Chapter 6* of this work.

In a mathematical modelling point of view, in order to follow the exact behaviour of the experimental data, the rate of diffusion terms that causes the shift of the simulated lines should be incorporated within the model system. Such work requires more rigorous mathematical techniques as well as new algorithm for model simulation. The technique as well as the theoretical method of obtaining diffusion coefficient, ($\mathscr{D}$) is discussed in detail in *Chapter 5*. The effect of cell death towards biotransformation reaction is another major obstacle in describing the reaction mathematically. A new set of experimental technique should also be used to study such a behaviour, for instance, the flow cytometric method of classifying the viability of cells during a reaction. Since the technique has not been considered in this work, thus, this effect will only be mentioned in brief in *Chapter 6*.

Chapter 5

Theoretical Investigation of Reaction-Diffusion Phenomena in a Cellular System

5.1 Introduction

The phenomena of reaction and diffusion have become important in catalytic engineering whenever a large deviation is observed between the experimental data and the simulated model described by the original rate equation of the heterogeneous type reaction. In reaction engineering, a complete characterisation of different type of diffusions caused by different catalysts and reactor configurations has already been established (Whitaker, 1986). These systems which are mainly described by partial differential equations have been numerically solved, and the solutions have been graphically mapped for different geometrical shapes of catalysts and reactor parameters (Cohen and Alexander, 1986; Halling *et al.*, 2003). For a basic theoretical reaction-diffusion study, it is most desirable that the model takes the simplest form of equations with an appropriate justification. This could later show the relationship that they bear to more complex forms. This concept has been reiterated by Aris (1975) in his two-volume manual of chemical reactions affected by diffusion phenomena.

A similar method has also been used to describe the diffusional phenomena in biological reaction system (Ochoa *et al.*, 1986, 1987). In fact, there have been many successful work carried out in this area, especially in understanding the system of immobilised enzyme (Santoyo *et al.*, 1993; Schroën *et al.*, 2002; Chen *et al.*, 2003; Esterl *et al.*, 2003). A summary of the model

system describing the effect of diffusion in immobilised enzyme is given in Section 5.2.1.

However, little have been investigated on the diffusion occurring through the cellular membrane. Diffusion of chemical components into the cellular system is mainly due to the membrane permeabilisation (Lee *et al.*, 1999). The cell membrane is known to be permeable to certain chemicals especially the nutrients for the growing purposes. However, there are some chemical compounds that can only be transported with a given amount of energy to the cell membrane. The opening on the surface of the lipid bilayer, is controlled by the amount of energy supplied by the ATP or the ADP. This type of diffusion is termed as the active transport. Such a diffusion is mainly referred to the movement of charged components, such as the metal ions through the membrane (Aris and Keller, 1972). Another type of diffusion which is only depend on the concentration gradient is known as the passive transport. This type of diffusion normally deals with the organic substances where the molecules are free from any charges, these include the natural substrate of a particular bacterial cell such as glucose and glycerol. Therefore, it can be assumed that the transfer of most of the organic substrates into the cell structure is mainly due to the passive transport. The substrate permeates through millions of pore-like cavities, known as porins which are randomly spread across the entire surface of the cell membrane (Nikaido and Rosenberg, 1981; Martinez *et al.*, 1992).

Consider the structure of *E. coli* with the surface of the membrane consists of the porin structure that allows external components to travel into and out of the cell (*Figure 5.1*). *Figure 5.1(b)* shows the actual layers of the cell wall that made up the permeable membrane of *E. coli*. The simplified form of the structure is given in *Figure 5.1(a)*. A detail modelling technique using the given structure is further discussed in Section 5.2.2.

5.2 Diffusional Effect of Biocatalytic Reactions

Immobilisation of enzyme or whole-cell has been commonly used as a technique in biocatalyst recycling. It was found that the technique can actually reduce the cost of biocatalyst production and the number of times for which it is produced. The method also reduces the number of unit operations in product purification during a downstream processing. These statements clearly show that the technique has been well investigated in biochemical and pharmaceutical research

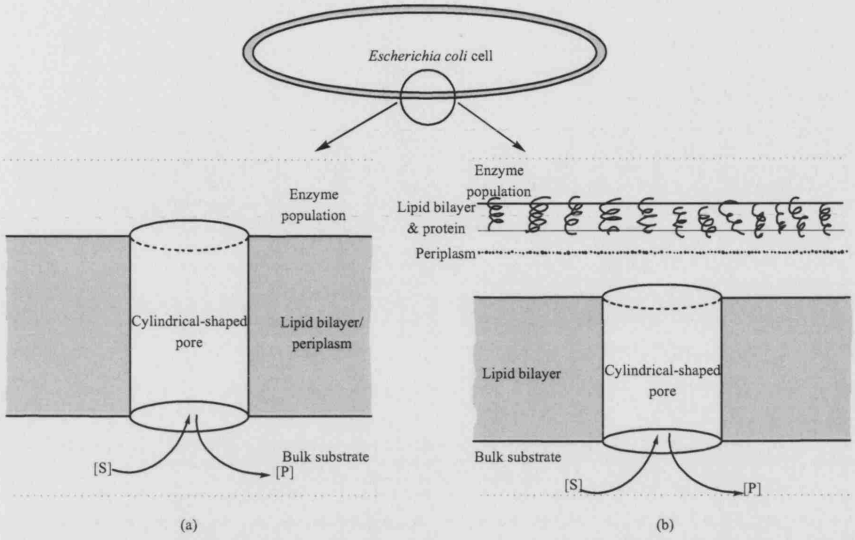

Figure 5.1: (a) Simplified version of membrane cell structure of *E. coli* and (b) the actual structure of the same membrane with a single porin/pore for nutrients transport.

for the production of large amount of chemicals.

A similar situation applies to the mathematical modelling of the immobilisation systems. As a process gradually develops, prediction of its efficiency and productivity are required before a large-scale production can be taken up. In the dynamic modelling of immobilisation systems, the law of diffusion describing the different of outlet and inlet concentrations is usually applied. Fick's Law of diffusion which describes this phenomena can be written as,

$$J_y = -\mathscr{D}_i \frac{\partial C_i}{\partial y}$$

and a simple diffusion equation utilising the above term with a constant diffusivity is given by;

$$\frac{\partial C_i}{\partial t} = \mathscr{D}_i \frac{\partial}{\partial y}\left(\frac{\partial C_i}{\partial y}\right) \tag{5.1}$$

where C_i represents the concentration of a component i diffusing through the membrane, y describes the distance of a component travelling through the membrane and these make up the concentration gradient given by, $\frac{\partial C_i}{\partial y}$ and finally, the diffusion constant $\mathscr{D}_i$, that defines the

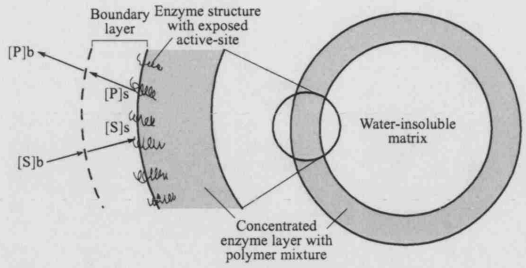

Figure 5.2: Transfer of substrate from the bulk phase to the surface of an immobilised bead via external diffusion.

amount of component diffuses through an area on the surface of the cell membrane. Further simplification of the diffusive flux, J is given in a vector form utilising the *grad* operator,

$$\mathbf{j} = -\mathscr{D}\nabla\mathbf{c} \tag{5.2}$$

The basic notation of Fick's Law will be used throughout this work in order to explain the anomaly previously observed in *Chapter 4*.

5.2.1 Diffusion Due to Enzyme Immobilisation

Enzyme immobilisation has become commonplace in biotransformation reaction. The diffusional behaviour of substrate on the surface of the immobilised bead has been comprehensively studied. The usual external mass transfer diagram showing the movement of bulk substrate onto the surface of the bead is given in *Figure 5.2*. The figure only shows the simplest method of enzyme immobilisation, however, there are other techniques which could be used such as the covalently bonded enzyme to the silica-alumina matrix (Ladero *et al.*, 2001) or the carrier made up of copolymer of ethylene glycol dimethylacrylate with acrylic acid, hydroxyethyl methacrylate and acrylamide (Bulmus *et al.*, 1998). These techniques were based on the external substrate diffusion on the surface of the individual bead. Concentrated amount of enzyme present on the smooth surface of the bead would be the cause of the surface reaction resulted from the external diffusion of the substrate component.

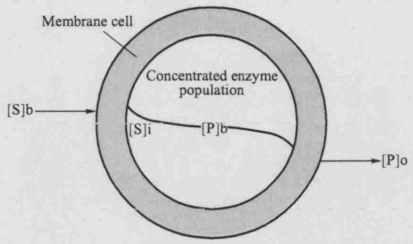

Figure 5.3: Internal diffusion of substrate and product due to passive transport. *E. coli* cell is assumed to be spherical shape for modelling simplicity.

5.2.2 Diffusion Due to Cell Membrane Permeability

Among the immobilisation techniques mentioned previously, the whole-cell catalysis can be categorised as a naturally formed immobilised enzyme. In this investigation, *E. coli*; a Gram-negative type bacteria was considered, which membrane consists of periplasm structure that leads to diffusion-limited enzyme reaction. This differs from the diffusion occurs in the immobilised enzyme. Substrate normally needs to diffuse into the cell through the porous membrane and reacts with the appropriate enzyme within the cell. The transfer of this organic substrate is governed by the passive type transport due to the effect of concentration gradient between the external and the internal structure of the cell. The same goes to the product formed inside the cell boundary, since the amount of product is more concentrated in the internal structure of the cell, thus, it tends to diffuse out into the environment of less product concentration. In this case, the transfer of substrate and product is described by the internal mass transfer and it is schematically shown in *Figure 5.3*.

The transport of the substrate and product is based on the two other criteria; molecular sizes of the given components and the radius of the porin structure on the surface of the membrane. *In vivo* enzyme reaction actually triggers different kinetic behaviour to that of the normal isolated enzyme reaction. For the isolated enzyme system, it is always assumed that the enzyme population is such that lower than the given substrate concentration which the kinetics obeys the Michaelis-Menten model. On the other hand, in an *in vivo* reaction, the assumption fails to address this matter since the population of enzyme bound within the membrane is highly concentrated compared to the slowly diffused substrate. Such cases have been theoretically

discussed in *Chapter 2.*

The analysis of the diffusion of the substrate and product through a minute porin structure should begin with the determination of the molecular size of the particular substrate (bicyclo[3.2.0]hept-2-en-6-one) and product ((-)1(S)5(R)2-oxabicyclo[3.3.0]oct-6-en-3-one and (-)1(R)5(S)3-oxabicyclo[3.3.0]oct-6-en-2-one). The algorithm implemented within the Chem3D Ultra®, Version 8.0, parts of ChemOffice2004® was used to determine the size of these molecules according to their minimum bond energies. The 3–dimensional structure of the three molecules are given in *Figures 5.4* and *5.5* for substrate and products respectively. The resulted values from the bond energy minimisation are given in *Table 5.1.*

Chemical compound	Radius (Å)
bicyclo[3.2.0]hept-2-en-6-one	2.850
(-)1(S)5(R)2-oxabicyclo[3.3.0]oct-6-en-3-one	3.030
(-)1(R)5(S)3-oxabicyclo[3.3.0]oct-6-en-2-one	2.525

Table 5.1: Radius of chemical structure for substrate and products.

The properties of porin structure are tabulated below;

Properties	Dimension
Radius	0.6nm
Number of pores	1×10^5
Membrane thickness	0.3nm[†], 11nm[‡]
	7–9nm[§], 7.5–10nm[¶]
	3nm[*], $\ll$200nm[♣], 4–5nm[♠]
Porin cross sectional area	1.13×10^5nm^2[,†], 4.15×10^6nm^2[,‡]
Average surface area per cell	3×10^6nm^2[,†]

[†](Nikaido and Rosenberg, 1981), [‡](Hölzel, 1999),[¶](Robert, 1999),

[♣](Baker, 1966),[♠](Kuchel and Gregory, 1988),

[*](Chen and Vincent, 2000),[§](Curtis and Barnes, 1989)

Table 5.2: Properties of porin and membrane structures of *E. coli.*

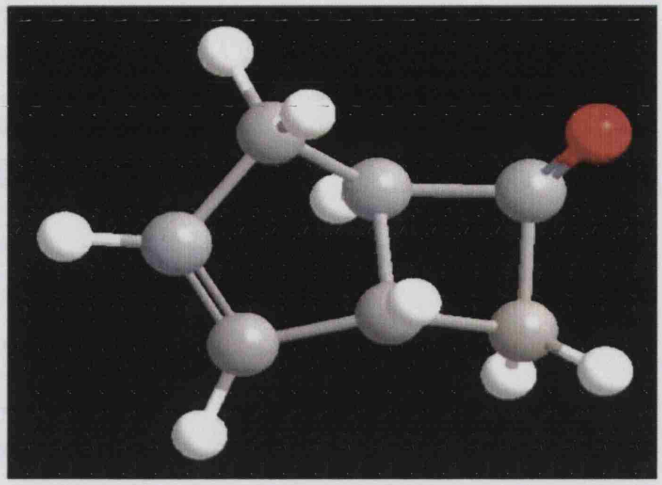

Figure 5.4: Molecular structure of bicyclo[3.2.0]hept-2-en-6-one with diameter, d_K=5.70Å.

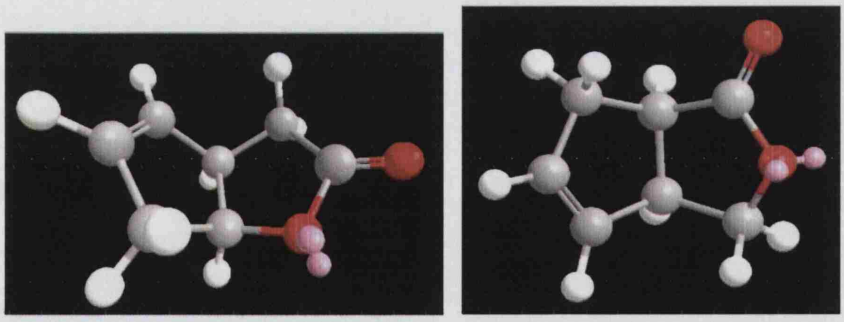

Figure 5.5: Molecular structures of (-)1(S)5(R)2-oxabicyclo[3.3.0]oct-6-en-3-one (left) and (-)1(R)5(S)3-oxabicyclo[3.3.0]oct-6-en-2-one (right) with diameters $d_{L,1}$=6.06Å and $d_{L,2}$=5.05Å respectively.

From the given values, it can be seen that the radii of the substrate and one of the chiral products are approximately equal and the size of these components are relatively smaller than that of the porin size. These values are much smaller compared to the other organic components determined by Schultz and Solomon (1961) for L–arabinose, D–glucose and lactose. This gives an initial intuition about the diffusional behaviour of these components through the porin's opening structure. However, these values are still bound to the experimental errors and correction values that relate the porin size and the size of the substrate.

Renkin (1954) had successfully come up with a correlation that incorporated the dimensions of porin and the size of the liquid solute, and it is given by;

$$\frac{a}{a_0} = \left(1 - \frac{r_{sol}}{R_p}\right)^2 \left[1 - 2.104\left(\frac{r_{sol}}{R_p}\right) + 2.09\left(\frac{r_{sol}}{R_p}\right)^3 - 0.95\left(\frac{r_{sol}}{R_p}\right)^5\right] \tag{5.3}$$

where it was then used to determine the theoretical values of the permeability constants of the corresponding solutes; i.e. substrate and products. Equation (5.3) has also taken into account the effect of steric hindrance at the entrance of the porin structure as well as the frictional resistance within its wall. The theoretical permeability constant, P_{theory} is given by;

$$P_{theory} = \left(\frac{\mathscr{D}}{l}\right)\left(\frac{a_0}{A}\right)\left(\frac{a}{a_0}\right) \tag{5.4}$$

in which a, a_0, r_{sol}, R_p, $\mathscr{D}$, l and A are the effective area of the porin, its total cross-sectional area of all the porins present, radius of the solute, radius of the porin, the free diffusion coefficient, the thickness of the cell membrane and the total area of the membrane respectively. However, there are other factors that were not considered in the above correlations; the hydrophobicity of substrates and the effect of different charges between substrates and the surface of the cell. These factors could also contribute to the different results observed in the previous chapter.

5.3 Modelling of Reaction-Diffusion Phenomena in The Whole-Cell Biotransformation System

This section incorporates the results obtained from the process model established in *Chapter 4* with the diffusional terms caused by the membrane cell structure. Determination of the

diffusion coefficients for the substrate and product are based on the Stoke-Einstein correlation of component i, and the relationship is given by;

$$\mathscr{D}_i = \frac{k_B T}{f} \tag{5.5}$$

where f is the friction factor correlation that relates the solute's viscosity and its radius, and for this particular work, the term f is given by;

$$f = 6\pi\mu_0 r_{sol}$$

or otherwise the Wilke-Chang correlation for small solute diffusivity (Perry and Chilton, 1993);

$$\mathscr{D}_i = 7.4 \times 10^{-8} \frac{T(\chi M)^{\frac{1}{2}}}{V_m^{0.6}\mu_0} \tag{5.6}$$

where k_B, T, μ_0 and r_{sol} represent, the Boltzmann's constant, the absolute temperature, the solute's viscosity and the solute's radius respectively for the Stoke-Einstein correlation while, χ, M, V_m represent the interaction parameter between solute and solvent (normally water) with the value of 2.26, the molecular weight of solute and the volumetric mass respectively for the Wilke-Chang correlation. All other terms are similar to equation (5.5).

In the next 3 subsections, values of the diffusion constants for bicyclic ketone and lactone are presented which lead to the approximation of the theoretical values of permeability constant for both components. Subsequent section then gives a complete model of biotransformation reaction incorporating the diffusion-reaction terms using the approximated diffusion constants, $\mathscr{D}_i$ and their effective diffusivities, $\mathscr{D}_{e,i}$ for the substrate and product. The introduction of the Thiele modulus, Φ as a benchmark to characterise the effect of diffusion would be the main objective of the study of the reaction-diffusion phenomena in biological organisms. Finally, the method of solving the system of partial differential equations via Crank-Nicolson discretisation technique is explained in Section 5.3.3.

5.3.1 Determination of Diffusion Constants, $\mathscr{D}_{\mathcal{K}}$ and $\mathscr{D}_{\mathcal{L}}$

The diffusion coefficients for substrate and products were determined using the correlation given by equation (5.5). The values were then used to obtain the permeability coefficients of these components with the use of Renkin relationship given by equation (5.3). All values obtained from this calculation are listed in *Table 5.3.* Since the reaction produces a racemic mixture of chiral oxabicyclic-lactones, an average value of the radii was used to determine the properties listed in the particular table.

Properties	**Solute components**	
	Bicyclic-ketone	**Oxabicyclic-lactone**
Diffusion coefficient, $\mathscr{D}_{\mathcal{K},\mathcal{L}}(\mathrm{m^2s^{-1}})$	8.924×10^{-10}	9.368×10^{-10}
$\left(\frac{a}{a_0}\right)(-)$	0.0853	0.0997
Permeability constant, $P_{theory}(\mathrm{ms^{-1}})$	9.570×10^{-3}	0.0117

Table 5.3: Diffusion and permeability constants for ketone and lactone at reaction temperature, 37°C (310.16K). Calculation based on properties of cell given by Nikaido and Rosenberg (1981).

The use of diffusivity values in modelling of the effect of diffusion in the whole-cell system via partial differential equation directly omits the boundary conditions that differentiate the membrane and the inner structure of the cell i.e. the thickness of a membrane. According to Hogben (1960), the assumption stated by *Fickian* diffusion makes it difficult to stipulate the boundary which permits the use of the differential equations. Such a model is clearly shown in *Figure 5.6.* More importantly, the inclusion of the diffusion coefficient, $\mathscr{D}_i$ predisposes to treating it as a constant rather than a complex function of the other variables of the equation (Crank, 1975). Therefore, the use of *Fickian* diffusion in a reaction-diffusion model does imply some *a priori* assumptions regarding the nature of the membrane.

5.3.2 Reaction-Diffusion Model of Whole-Cell Biotransformation System

The mathematical modelling of the reaction-diffusion system based on the internal mass transfer through the porous medium of the living cell is a complicated procedure due to the shape of the *E. coli.* In order to reduce such a complexity, 4 main assumptions were initially put together;

1. the shape of the cell is assumed to be spherical (*Figure 5.3*) rather than its normal oval shape, this would simplify the model of the different transfer fluxes at different radii of the oval configuration
2. the reaction system is operated at an isothermal condition, therefore, there would be no transfer of heat from the bulk liquid to the internal structure of the cell
3. the diffusion of substrate and product is only due to the internal mass transfer, external diffusion is assumed to be negligible due to the perfect mixing of the reaction medium
4. the diffusion of substrate and product obeyed Fick's law and the value of diffusivity, $\mathscr{D}$ is constant throughout the the membrane cell.

With the four main assumptions presented above, a model consists of mass balances of substrate and product into and out of the cell ensemble was constructed. This was again based on the conservation laws of mass mentioned previously in *Chapter 4*.

Analogy of Porin Structure to Micro-pores on Porous Solid Particle

With regard to assumption (4), the diffusion of the particular substrate and product through the cell membrane does not always occur in a straight forward manner. The structure of porin on the surface of the membrane is not always arranged in such a way that its cylindrical shape is perpendicular to the surface of the membrane, therefore a correction factor is required to take into account this effect which leads to the new diffusivity value;

$$\mathscr{D}_{e,i} = \mathscr{D}_i \frac{\varepsilon_p}{\tau_p} \tag{5.7}$$

where $\mathscr{D}_{e,i}$ is the effective diffusion constant of components i, with ε_p represents the fractional free space (porosity) and τ_p represents the tortuosity factor of the porin structure.

The term ε_p can be estimated by calculating

$$\begin{aligned} \varepsilon_p &= \frac{pore\ volume\ of\ particle}{total\ volume\ of\ particle} \\ &= \frac{V_g \rho_c}{V_g \rho_c + 1} \\ &= \rho_p V_g \end{aligned} \tag{5.8}$$

where V_g refers to the void volume per gram of cells, ρ_c represents the density of the cell and ρ_p gives the density of the porous cells. However, the use of the relationship given by equation (5.7) to predict the effective diffusion constant is somewhat limited because of the uncertainty of the value approximated by τ_p, therefore, Wakao and Smith (1964) had come up with an expression for $\mathscr{D}_{e,i}$ without taking into account the tortuosity factor, and it is given by;

$$\mathscr{D}_{e,i} = \bar{D}_{i,M}\varepsilon_{p,M}^2 + \frac{\varepsilon_{p,\mu}^2(1+3\varepsilon_{p,M})}{1-\varepsilon_{p,M}}\bar{D}_{i,\mu} \tag{5.9}$$

and the terms $\bar{D}_{i,M}$ and $\bar{D}_{i,\mu}$ are obtained by applying

$$\frac{1}{\bar{D}_{i,M}} = \frac{1}{\mathscr{D}_i} + \frac{1}{(\mathscr{D}_K)_{i,M}}$$

and

$$\frac{1}{\bar{D}_{i,\mu}} = \frac{1}{\mathscr{D}_i} + \frac{1}{(\mathscr{D}_K)_{i,\mu}}$$

where $(\mathscr{D}_K)_{i,M}$ and $(\mathscr{D}_K)_{i,\mu}$ are the Knudsen diffusivity terms, for macro- and micro-pores respectively. $\mathscr{D}_K$ is initially defined in terms of the average molecular velocity, $\bar{v}$ given by;

$$\mathscr{D}_K = \frac{2}{3}\bar{v}R_p$$

which froms a simple kinetic theory and it can be written as,

$$\mathscr{D}_{mean} = \frac{1}{3}\bar{v}\lambda_p$$

For a cell ensemble with minute porin structure, only micro-pore effect is considered ($\varepsilon_M = 0$), thus equation (5.9) reduces into the simplest form given by,

$$\mathscr{D}_{e,i} = \bar{D}_{i,\mu}\varepsilon_{p,\mu}^2 \tag{5.10}$$

Besides using the Knudsen-type diffusion to determine the effective diffusivity, the value can also be determined using the correlation of ε_p andτ_p proposed by Steward and Johnson (Aris,

1975);

$$\varepsilon_p = \iint \pi R_p^2 \Delta L \sec(\theta) n(R_p, \theta) dR_p d\theta$$

where ΔL is the change of total length per unit volume, and,

$$\frac{1}{\tau_p} = \iint \frac{2R_p}{2R_p + \lambda_p} \cos^2(\theta) \varepsilon_p(R_p, \theta) dR_p d\theta$$

where λ_p represents the molecular mean free path based on collection of straight cylindrical tubes of various lengths and diameters (with cylindrical pores of radius, R_p) and making an angle θ with the z–direction.

From the above discussion, it is apparent that the diffusion describes by Knudsen is closely related to the mean free path of the molecules which at low pressure, the value could be very much larger than the diameter of the cylindrical tube. On the other hand, in the liquid-based diffusion, this value is very small, such that the Knudsen diffusion is not significant, thus, the diffusion rate is unaffected by the pore diameter and pressure. In this case, the effective diffusivity is determined by the molecular diffusivity and the pore structure of the catalyst particle. Since the molecules in liquids are close together, the diffusion of one component is strongly affected by the force fields of the nearby molecules and the pore wall. As a result, diffusivities are concentration dependent and difficult to predict and as an approximation, the diffusion flux of a liquid component in a single pore may be expressed as that given by equation (5.1).

In view of the fact that the Knudsen diffusion failed to describe the diffusion of liquid molecules and that the estimation of the effective diffusion using equation (5.9) could only lead to error, an approximation of the value was calculated by taking one-third of the actual substrate and product diffusivities as proposed by Siggia and co-workers (Siggia *et al.*, 2000);

$$\mathscr{D}_{e,i} = \frac{1}{3}\mathscr{D}_i$$

where in order to average the angle of tubes, it was assumed that they are isotropically distributed in 3–dimensional configurations.

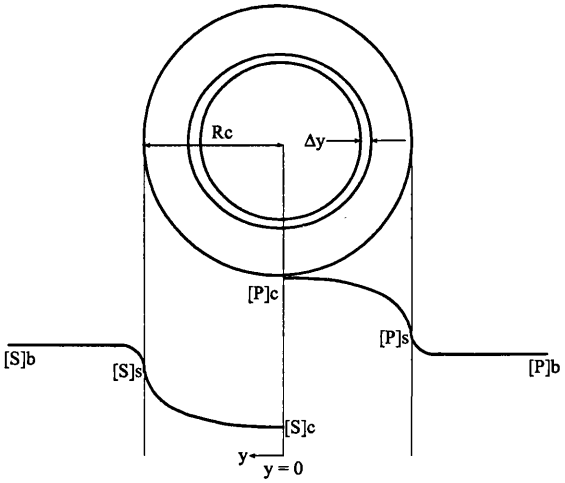

Figure 5.6: Movement of substrate into and product out of the spherical cell against the position for the biocatalytic reaction.

Mathematical Model of the Reaction and Diffusion in the Whole-Cell Biocatalytic System

The model system was constructed based on the the conservation laws mentioned previously in *Chapter 4*. The cell ensemble in the reaction broth is the heterogeneous medium in which the porin structure are distributed and it is the inner part of this structure where biocatalyst is highly concentrated. The substrate, i.e. the bicyclic-ketone (bicyclo[3.2.0]hept-2-en-6-one) diffuses into the cell structure, reacts with the active biocatalyst and converts into products, lactones ((-)1(S)5(R)2-oxabicyclo[3.3.0]oct-6-en-3-one and (-)1(R)5(S)3-oxabicyclo[3.3.0]oct-6-en-2-one), which diffuse out of the cell ensemble due to the concentration gradient between the inner cell and the bulk liquid. Balances of components i according to conservation laws could be written in the transient state in terms of x, y and z–space as;

$$V_c\frac{\partial C_i}{\partial t} = (A_x J_x)|_x - (A_x J_x)|_{x+\delta x} + (A_\psi J_\psi)|_\psi - (A_\psi J_\psi)|_{\psi+\delta\psi} + (A_\theta J_\theta)|_\theta - (A_\theta J_\theta)|_{\theta+\delta\theta} - V_c r_{s,p} \tag{5.11}$$

where A_x, A_ψ and A_θ represent the microscopic area of the spherical shape given by $(y\Delta y\Delta\theta)$, $(y^2\Delta\psi\Delta\theta\sin\theta)$ and $(y\Delta y\Delta\psi\sin\theta)$ respectively where y is the radius of the sphere defined in

Figure 5.6. Upon substitution with the *Fickian* diffusion terms given by $J_x = -\mathscr{D}_{e,i}\frac{\partial C_i}{\partial y}$, $J_\psi = -\frac{\mathscr{D}_{e,i}}{y\sin\theta}\frac{\partial C_i}{\partial \psi}$ and $J_\theta = -\frac{\mathscr{D}_{e,i}}{y}\frac{\partial C_i}{\partial \theta}$ for the x, y and z components respectively and with further simplification and rearrangement, equation (5.11) can be expanded into a 3–dimensional space-time system given by;

$$\frac{\partial C_i}{\partial t} = \frac{1}{y^2}\frac{\partial}{\partial y}\left(y^2\mathscr{D}_{e,i}\frac{\partial C_i}{\partial y}\right) + \frac{1}{y^2}\frac{1}{\sin^2\theta}\frac{\partial}{\partial \psi}\left(\mathscr{D}_{e,i}\frac{\partial C_i}{\partial \psi}\right) + \frac{1}{y^2}\frac{1}{\sin\theta}\frac{\partial}{\partial \theta}\left(\mathscr{D}_{e,i}\sin\theta\frac{\partial C_i}{\partial \theta}\right) - r_{s,p} \tag{5.12}$$

Considering only the radial diffusion, the model system in terms of the coupled partial differential equations for the substrate consumption and product formation reduces into a simple form given by;

$$\begin{aligned}\frac{\partial[S_{Bicyclo}]}{\partial t} &= \frac{1}{y^2}\frac{\partial}{\partial y}\left(y^2\mathscr{D}_{e,[S_{Bicyclo}]}\frac{\partial[S_{Bicyclo}]}{\partial y}\right) - r_{s,p}\\ \frac{\partial[P_{OxaBicyclo}]}{\partial t} &= \frac{1}{y^2}\frac{\partial}{\partial y}\left(y^2\mathscr{D}_{e,[P_{OxaBicyclo}]}\frac{\partial[P_{OxaBicyclo}]}{\partial y}\right) + r_{s,p}\end{aligned} \tag{5.13}$$

With the initial conditions;

$$[S_{Bicyclo}](0) = [S_{Bicyclo}]_b,\ [P_{OxaBicyclo}](0) = 0$$

and the boundary conditions with symmetry about the central of the sphere;

$$\frac{\partial[S_{Bicyclo}]}{\partial y} = 0,\ y = R_c$$

$$\frac{\partial[P_{OxaBicyclo}]}{\partial y} = 0,\ y = 0$$

and

$$\mathscr{D}_{e,[S_{Bicyclo}]}\frac{\partial[S_{Bicyclo}]}{\partial y} = k_{c,s}([S_{Bicyclo}]_b - [S_{Bicyclo}]),\ y = R_c$$

$$-\mathscr{D}_{e,[P_{OxaBicyclo}]}\frac{\partial[P_{OxaBicyclo}]}{\partial y} = k_{c,p}([P_{OxaBicyclo}]_b - [P_{OxaBicyclo}]),\ y = 0$$

where $k_{c,s}$ and $k_{c,p}$ refer to the mass transfer coefficient of the respective substrate and product in the external film of the cell membrane at radius, R_c. However, the boundary conditions due to the external mass transfer can be avoided by assuming a perfect mixing condition within the stirred tank, hence, the boundary conditions can be simplified into;

$$[S_{Bicyclo}] = [S_{Bicyclo}]_b, \; y = R_c$$

and

$$[P_{OxaBicyclo}] = [P_{OxaBicyclo}]_b, \; y = 0$$

For brevity, the system can be expanded and written in terms of the *Laplacian* operator, which form will be used throughout this work;

$$\begin{aligned} \frac{\partial[S_{Bicyclo}]}{\partial t} &= \mathscr{D}_{e,[S_{Bicyclo}]}\left(\frac{2}{y}\nabla[S_{Bicyclo}] + \nabla^2[S_{Bicyclo}]\right) - r_{s,p} \\ \frac{\partial[P_{OxaBicyclo}]}{\partial t} &= \mathscr{D}_{e,[P_{OxaBicyclo}]}\left(\frac{2}{y}\nabla[P_{OxaBicyclo}] + \nabla^2[P_{OxaBicyclo}]\right) + r_{s,p} \end{aligned} \quad (5.14)$$

where $r_{s,p}$ represents the rate expression of the enzyme-catalysed Baeyer-Villiger reaction, given by;

$$r_{s,p} = \frac{V_{max}[S_{Bicyclo}]}{K_{m_{[Bicyclo]}}\left(1+\frac{[P_{OxaBicyclo}]}{K_{m_{[OxaBicyclo]}}}\right)+[S_{Bicyclo}]\left(1+\frac{[S_{Bicyclo}]}{K_{i_{[Bicyclo]}}}+\frac{[P_{OxaBicyclo}]}{K_{i_{[OxaBicyclo]}}}\right)}$$

Rendering the system into a dimensionless form reduces (5.13) into;

$$\begin{aligned} \frac{1}{(y^*)^2}\nabla\left[(y^*)^2\nabla[S_{Bicyclo}]^*\right] &= \phi_s\left(\frac{\partial[S_{Bicyclo}]^*}{\partial t^*} + r^*_{s,p}\right) \\ \frac{1}{(y^*)^2}\nabla\left[(y^*)^2\nabla[P_{OxaBicyclo}]^*\right] &= \phi_p\left(\frac{\partial[P_{OxaBicyclo}]^*}{\partial t^*} - r^*_{s,p}\right) \end{aligned} \quad (5.15)$$

which leads to the definition of ϕ_s and ϕ_p for the substrate and product respectively, and they are given by;

$$\phi_s = \frac{R_c^2 V_{max}}{\mathscr{D}_{e,[S_{Bicyclo}]}K^*_{m_{[Bicyclo]}}}$$

$$\phi_p = \frac{R_c^2 V_{max}}{\mathscr{D}_{e,[P_{OxaBicyclo}]}K^*_{m_{[Bicyclo]}}}$$

with the new initial conditions;

$$[S_{Bicyclo}]^*(0) = [S_{Bicyclo}]_b^*,\ [P_{OxaBicyclo}]^*(0) = 0$$

and the corresponding boundary conditions;

$$\frac{\partial [S_{Bicyclo}]^*}{\partial y^*} = 0,\ y^* = 1$$

$$\frac{\partial [S_{Bicyclo}]^*}{\partial y^*} = v(1 - [S_{Bicyclo}]^*),\ y^* = 1$$

which reduces into

$$[S_{Bicyclo}]^* = [S_{Bicyclo}]_b^*,\ y^* = 1$$

for negligible external film mass transfer and that for product, the boundary conditions are given by;

$$\frac{\partial [P_{OxaBicyclo}]^*}{\partial y^*} = 0,\ y^* = 0$$

$$-\frac{\partial [P_{OxaBicyclo}]^*}{\partial y^*} = v(1 - [P_{OxaBicyclo}]^*),\ y^* = 0$$

or

$$[P_{OxaBicyclo}]^* = [P_{OxaBicyclo}]_b^*,\ y^* = 0$$

where v represents the Sherwood number (Sh) which is made up of $\frac{k_{c,i}d}{\mathscr{D}_{e,i}}$ for components i.

In order to analyse the characteristic of the given Thiele modulus, system (5.15) was set at the steady-state condition, which reduced the system of partial differential equations into a simple system of ordinary differential equations given below;

$$\begin{aligned} \frac{1}{(y^*)^2}\nabla\left[(y^*)^2\nabla[S_{Bicyclo}]^*\right] &= \Phi_s^2 r_{s,p}^* \\ \frac{1}{(y^*)^2}\nabla\left[(y^*)^2\nabla[P_{OxaBicyclo}]^*\right] &= -\Phi_p^2 r_{s,p}^* \end{aligned} \tag{5.16}$$

which upon integration, the constants defined by ϕ_s and ϕ_p changed into;

$$\Phi_s = \frac{R_c}{3}\sqrt{\frac{V_{max}}{\mathscr{D}_{e,[S_{Bicyclo}]}K_{m_{[Bicyclo]}}}}$$

$$\Phi_p = \frac{R_c}{3}\sqrt{\frac{V_{max}}{\mathscr{D}_{e,[P_{OxaBicyclo}]}K_{m_{[Bicyclo]}}}}$$

with the corresponding boundary conditions;

$$\frac{d[S_{Bicyclo}]^*}{dy^*} = 0,\ y^* = 1$$

$$[S_{Bicyclo}]_b^* = 1,\ y^* = 1$$

and

$$\frac{d[P_{OxaBicyclo}]^*}{dy^*} = 0,\ y^* = 0$$

$$[P_{OxaBicyclo}]^* = 0,\ y^* = 1$$

With the expansion and the change of notation of system (5.16), it is then reduced into a simple system of integrable ordinary differential equations;

$$\begin{aligned}\frac{1}{(y^*)^2}\frac{d}{dy^*}\left((y^*)^2\frac{d[S_{Bicyclo}]^*}{dy^*}\right) &= \Phi_s^2 r_{s,p}^* \\ \frac{1}{(y^*)^2}\frac{d}{dy^*}\left((y^*)^2\frac{d[P_{OxaBicyclo}]^*}{dy^*}\right) &= -\Phi_p^2 r_{s,p}^*\end{aligned} \tag{5.17}$$

The nonhomogeneous nonlinear system of higher order differential equations could be analytically solved with the given dimensionless rate expression, $r_{s,p}^*$;

$$r_{s,p}^* = \frac{[S_{Bicyclo}]^*}{\left(1+\frac{[P_{OxaBicyclo}]^*}{K_{m[OxaBicyclo]}^*}\right) + [S_{Bicyclo}]^*\left(1+\frac{[S_{Bicyclo}]^*}{K_{i[Bicyclo]}^*}+\frac{[P_{OxaBicyclo}]^*}{K_{i[OxaBicyclo]}^*}\right)}$$

The application of Laplace Transform to analytically solve the system apparently led to failure, this is due to the large denominator terms similar to that of Langmuir-Hinshelwood kinetic expressions previously treated by Chu and Hougen (1962) and Roberts and Satterfield (1965)

for gaseous reaction given by;

$$r = \frac{kp_A}{1 + K_A p_A + \ldots + K_i p_i + \ldots}$$

where p_i represents the partial pressure of the reacting components, i and K_i is the respective constants of each component. Instead a direct integration with the defined Dirichlet boundary conditions was applied. Consider the depletion of the substrate in the system of ordinary differential equations (5.17) with the corresponding reaction rate terms;

$$\frac{1}{(y^*)^2}\frac{d}{dy^*}\left((y^*)^2\frac{d[S_{Bicyclo}]^*}{dy^*}\right) = \Phi_s^2 r_s^* \tag{5.18}$$

Simplifying the rate expression into a manageable form and at a constant value of $[P_{OxaBicyclo}]^*$ gives;

$$r_s^* = \frac{[S_{Bicyclo}]^*}{A + \frac{([S_{Bicyclo}]^*)^2}{B} + (1+C)[S_{Bicyclo}]^*}$$

where $A = \left(1 + \frac{[P_{OxaBicyclo}]^*}{K^*_{m_{[OxaBicyclo]}}}\right)$, $B = K^*_{i_{[Bicyclo]}}$ and $C = \frac{[P_{OxaBicyclo}]^*}{K^*_{i_{[OxaBicyclo]}}}$ which form closely resembles that of the nonlinear Langmuir-Hinshelwood type kinetics. Using a direct integration of the above equations together with the given boundary conditions which upon completion of the first part of the boundary condition gives;

$$\left.\frac{dC_s^*}{dy^*}\right|_{y^*=1} = \Phi_s^2 r_s^*\left(y^* - \frac{R^3}{(y^*)^2}\right) \tag{5.19}$$

and with the new variables defining $[S_{Bicyclo}]^*$ and $[S_{Bicyclo}]_b^*$ as C_s^* and $C_{s,b}^*$ respectively. Such an equation can only be solved numerically and the differential form of the component with respect to the cell radius, y^* for $y^* = 1$, leads to;

$$\Phi_s^2 = \frac{1}{r_s^*}\left(\frac{(y^*)^2}{(y^*)^3 - R^3}\right)\left.\frac{dC_s^*}{dy^*}\right|_{y^*=1} \tag{5.20}$$

where the term becomes invalid when $y^* = R$. The above Thiele modulus is often used to characterise the diffusional effect of a chemical reaction and an enzyme-catalysed reaction via immobilisation technique. The next section discusses the similar characteristic, focusing on the

whole bacterial cell system.

Simulations of both transient and steady-state conditions of the system were also carried out by applying the appropriate numerical method which the technique and detail results are discussed in Section 5.3.3.

Characterisation of the Effectiveness Factor for the Whole-Cell Biocatalysis

One of the most important criteria which could be made use of the Thiele modulus is the effectiveness factor represented by η. The effectiveness factor of an enzyme-catalysed whole-cell reaction can be generally defined as;

$$\eta = \frac{actual\ rate\ with\ porin\ diffusion}{rate\ evaluated\ in\ the\ absence\ of\ porin\ diffusion}$$

where for small Φ, the porin diffusion seems to give no effect to the rate of substrate conversion. On the other hand, a large Φ which results in $\eta \ll 1.0$ gives a rapid decrease in substrate concentration during the transport into the porin structure, hence, the rate of biotransformation reaction is strongly influenced by the chemical reaction instead of the diffusion caused by the porins. Such characterisation is particularly important in dealing with cells of different types, either Gram-positive or Gram-negative, which the membrane structures of both types differ, or perhaps cells with different shapes and sizes.

If the rate of biotransformation of a substrate in the whole-cell system is given by $\mathbf{r_c}$, where the radius of a single cell is represented by R, therefore;

$$\mathbf{r_c} = \frac{1}{m_c} A_c \mathscr{D}_{e,s} \left(\frac{dC_s}{dy}\right)\Bigg|_{y=R} \tag{5.21}$$

with m_c is the mass of a particular cell given by, $m_c = \frac{4}{3}\pi y^3 \rho_c$ and A_c is its cross sectional area, thus equation (5.21) reduces into;

$$\mathbf{r_c} = \frac{3}{y\rho_c} \mathscr{D}_{e,s} \left(\frac{dC_s}{dy}\right)\Bigg|_{y=R} \tag{5.22}$$

which leads to the general form of effectiveness factor for a spherical geometry;

$$\eta = \frac{3\mathscr{D}_{e,s}}{y\rho_c r_s}\left(\frac{dC_s}{dy}\right)\Big|_{y=R} \tag{5.23}$$

Equation (5.23) clearly shows that, η is highly dependent on the steady-state form of equation (5.17) given by $\left(\frac{dC_s}{dy}\right)_{y=R}$. In order to observe the characteristic of Thiele modulus, a trivial first-order rate equation in a spherical particle was first considered, this term has been completely derived and its analytical dimensionless form is given by;

$$\frac{dC_s^*}{dy^*}\Big|_{y^*=R} = \frac{3\Phi}{R\ \tanh(3\Phi)} - \frac{1}{R}$$

and upon substitution into equation (5.23), leads to;

$$\eta = \frac{1}{\Phi}\left(\frac{1}{\tanh(3\Phi)} - \frac{1}{3\Phi}\right) \tag{5.24}$$

This effect can be pictured graphically by plotting equation (5.24) on the logarithmic axes given in *Figure 5.8.*

Clearly, the red line plotted in *Figure 5.8* depicts the initially explained characteristics of Thiele modulus (for small values of Φ, $\eta \rightarrow 1.0$). Such a value gives no effect on the rate due to the intraparticle mass transport, which means that the reaction is entirely controlled by the chemical reaction rate. The small values of Thiele modulus can be obtained by having a small particle, which is a good criterion for the cell ensembles. The values of diffusion constants of a substrate component through the membrane cell is also important in obtaining a small value of Φ. Finally, the rate of the bioconversion itself should be slow i.e. low enzyme activity which will result in low Thiele modulus and hence, negligible diffusion effect. As being marked by a straight line in *Figure 5.8*, for $\Phi \gg 5, (\Phi \gg \log 5)$, a good approximation of the effectiveness factor can be simplified into;

$$\eta \sim \frac{1}{\Phi} \tag{5.25}$$

as $\Phi \rightarrow \infty$, $\tanh(\Phi) \rightarrow 1$ and $\frac{1}{\Phi} \rightarrow 0$.

For an enzyme-catalysed reaction, having the rate expression of the form given by $r^*_{s,p}$, the

mathematical treatment is rather tedious due to the presence of the nonlinear denominator terms similar to that of the Langmuir-Hinshelwood expression. The steady-state form of the model has been derived in the previous section and therefore can be incorporated into the effectiveness factor relationship η, given by equation (5.24). The method which was initially applied in the area of chemical catalysis by Chu and Hougen (1962) and later by Roberts and Satterfield (1965) with further generalisation for reversible, isothermal reaction by Schneider and Mitschka (1966) based on the numerical integration technique, was used in the present study of the cellular diffusion and reaction.

The evaluation of the effectiveness factor for the nonlinear reaction rate expression $r(C_s)$ can be generally written as;

$$\eta = \frac{\int r(C_s)dV}{\int r(C_{s,b})dV} \tag{5.26}$$

which has been defined previously for spherical geometry by equation (5.23) and the dimensionless form of this equation is given by;

$$\eta = \frac{1}{\Phi_s^2}\left(\frac{dC_s^*}{dy^*}\right)_{y^*=1}$$

For the numerical treatment at steady-state condition at which the substrate concentration gradient at the surface of the cell, equation (5.18) is expanded into the form given below;

$$\frac{d^2C_s^*}{dy^{*2}} + \frac{2}{y^*}\frac{dC_s^*}{dy^*} = \Phi_s^2\left(\frac{C_s^*}{A + \frac{(C_s^*)^2}{B} + (1+C)C_s^*}\right) \tag{5.27}$$

In order to maintain the symmetry of this problem, substitution of $u = y^{*2}$ was made and equation (5.27) becomes

$$4u\frac{d^2C_s^*}{du^2} + 6\frac{dC_s^*}{du} = \Phi_s^2\left(\frac{C_s^*}{A + \frac{(C_s^*)^2}{B} + (1+C)C_s^*}\right) \tag{5.28}$$

together with the appropriate Dirichlet boundary conditions;

$$C_s^* = C_{s,b}^* \text{ and } u = 1$$

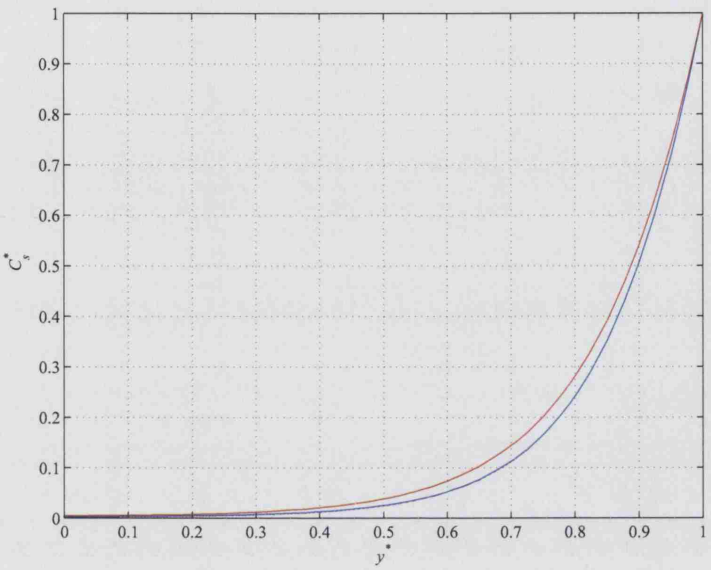

Figure 5.7: Plot of variation of substrate concentrations with respect to the radius from the centre of cell. Two different curves representing the effect of product inhibition towards the concentration gradient (red line with concentration ten times higher than that of the blue line).

The method of orthogonal collocation was used to estimate the function $\left(\frac{dC_s^*}{dy^*}\right)_{y^*=1}$ by evaluating $C_s^*(y^*)$. Further discretisation of equation (5.28) is explained in *Appendix F*. The method was then implemented in MATLAB® for visualisation of the corresponding concentration at various positions of radius, y^*.

The plot of the dimensionless substrate, C_s^* against the radius of the cell, y^*, at the given boundary conditions is given in *Figure 5.7*. The effectiveness factor at the given Thiele modulus is clearly marked in the subsequent figure. An apparent shift of the curve due to the presence of product concentration can be clearly observed. This result proved that the formation of product within the cellular system has changed the rate of bioconversion reaction as the substrate moved towards the centre of the cell. *Figure 5.8* however, gives a contradictory result of that shown from the comparison of the isolated enzyme model and the whole cell reaction. The effectiveness factor of diffusion limited reaction should lie on the curve where $\Phi \rightarrow 1.0$, since the region beyond this value results in a high diffusional effect. It is also obvious from the plot that the curve for CHMO reaction reaches a limiting values of η represented by a thick-dotted horizontal line in *Figure*

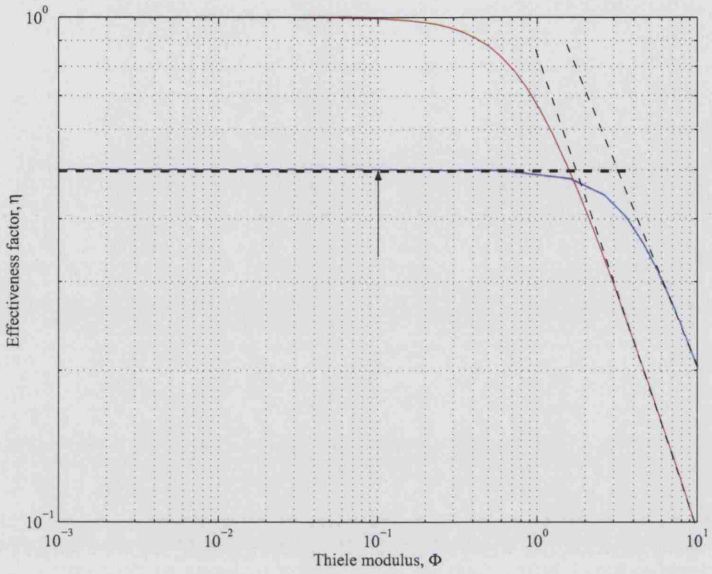

Figure 5.8: Effectiveness factor of the whole cell biocatalysis at different Thiele modulus. Blue line with the arrow shows the CHMO reaction with the rate expression of the form obtained in *Chapter 3*. The red line refers to the first-order rate equation.

5.8, which result was similar to the systems observed by Roberts and Satterfield (1966) and Halling *et al.* (2003). The results obtained from the study of the reaction-diffusion phenomena is not coherent with the statement mentioned above. It is suspected that the size of the cell measured in (μm) compensates the small value of the substrate diffusivity and therefore, leads to the Thiele modulus of less than the value which can affect the diffusion of the substrate into the cell. Further analysis of such an effect either experimentally or refinement of the available model equations should be taken into consideration in order to obtain a consistent result. The work undertaken here only provided a preliminary analysis of such a system where theoretical diffusivity correlations were used to obtain mainly all the mathematical constants.

5.3.3 Dynamic Model Simulation

Appropriate with the theme of this research, the system of partial differential equations is not only analysed at the steady-state conditions, the dynamics of the system has also been given the highest attention. Prior to the analysis of the effect of diffusion, the steady-state condition

was imposed to the system so that the diffusion characteristics of the whole-cell could be closely monitored via Thiele modulus. Such an analysis only provides the analytical results for which comparison and hypothesis could be made, however, graphical simulations are also required in the study of biocatalytic reaction-diffusion system. These could be used to prove the previous analytical work.

For the purpose of comparing the analytical results with the graphical simulation, system (5.15) was used to perform the discretisation, based on the finite difference method (*Appendix E*) with the correction given by the implicit Crank-Nicolson technique (Villadsen and Sorensen, 1969). The system consists of 2 coupled nonhomogeneous nonlinear second order partial differential equations of the parabolic form. These type of equations are not defined in a closed domain, but they propagate in an open domain. It is classified as having the characteristic form of $(B^2 - 4AC = 0)$ from the general function given by;

$$A(x,y)\frac{\partial^2 z}{\partial x^2} + B(x,y)\frac{\partial^2 z}{\partial x \partial y} + C(x,y)\frac{\partial^2 z}{\partial y^2} + f\left(x, y, z, \frac{\partial z}{\partial x}, \frac{\partial z}{\partial y}\right) = 0$$

The one dimensional parabolic system was transformed into a single array, i which later reduced into a system of ordinary differential equations. The coupled system is given in terms of the new variables, u_i for substrate consumption and v_i for product formation;

$$\begin{aligned}
\frac{\partial u_i}{\partial t^*} &= \frac{1}{\Phi_s^2}\left[\frac{1}{y_i^*(\Delta y^*)}\left(-u_{i-1} + u_{i+1}\right) + \frac{1}{(\Delta y^*)^2}\left(u_{i-1} - 2u_i + u_{i+1}\right)\right] - r^*_{u_i,v_i} \\
\frac{\partial v_i}{\partial t^*} &= \frac{1}{\Phi_p^2}\left[\frac{1}{y_i^*(\Delta y^*)}\left(-v_{i-1} + v_{i+1}\right) + \frac{1}{(\Delta y^*)^2}\left(v_{i-1} - 2v_i + v_{i+1}\right)\right] + r^*_{u_i,v_i}
\end{aligned} \tag{5.29}$$

with $r^*_{u_i,v_i}$ is given by;

$$r^*_{u_i,v_i} = \frac{u_i}{\left(1 + \frac{v_i}{K^*_{m_{[OxaBicyclo]}}}\right) + u_i\left(1 + \frac{u_i}{K^*_{i_{[Bicyclo]}}} + \frac{v_i}{K^*_{i_{[OxaBicyclo]}}}\right)}$$

The surface simulations of the discretised system in 1–dimensional space-time are given in 3 sets of figures for substrate and product at different values of Φ_s's and Φ_p's. The first set of

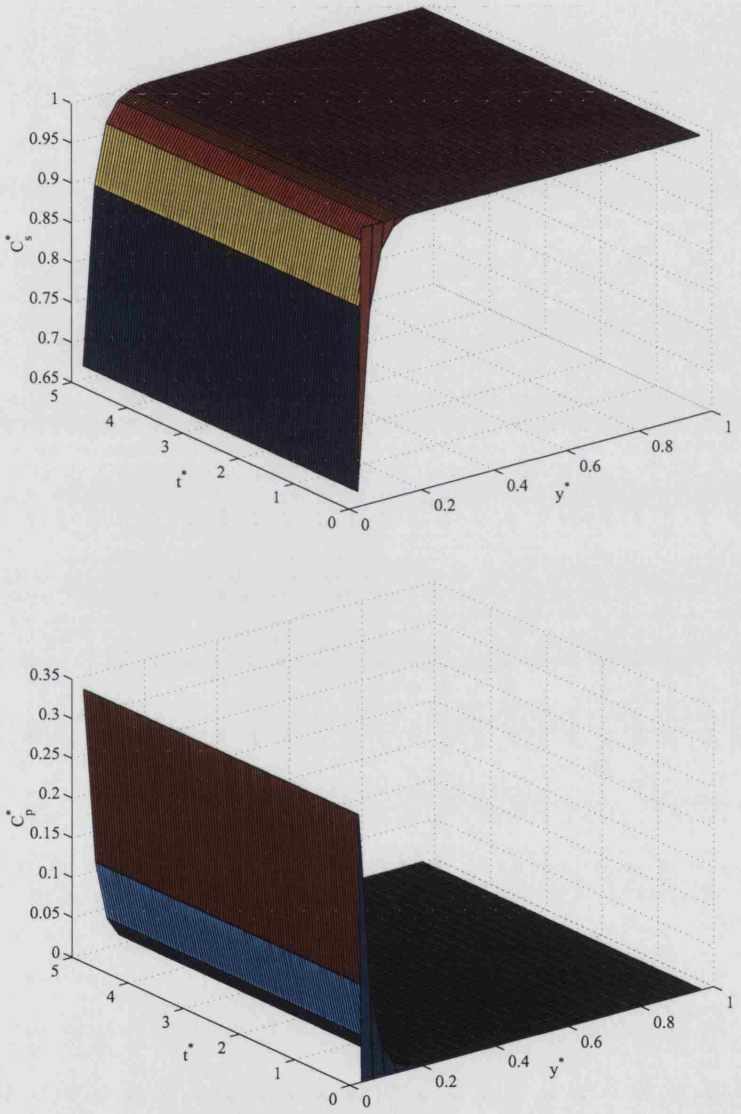

Figure 5.9: The effect of reaction-diffusion of substrate (above) and product (below) in 3 dimensional space-time plot at $\Phi_s = 1.89 \times 10^{-3}$ and $\Phi_p = 1.84 \times 10^{-3}$.

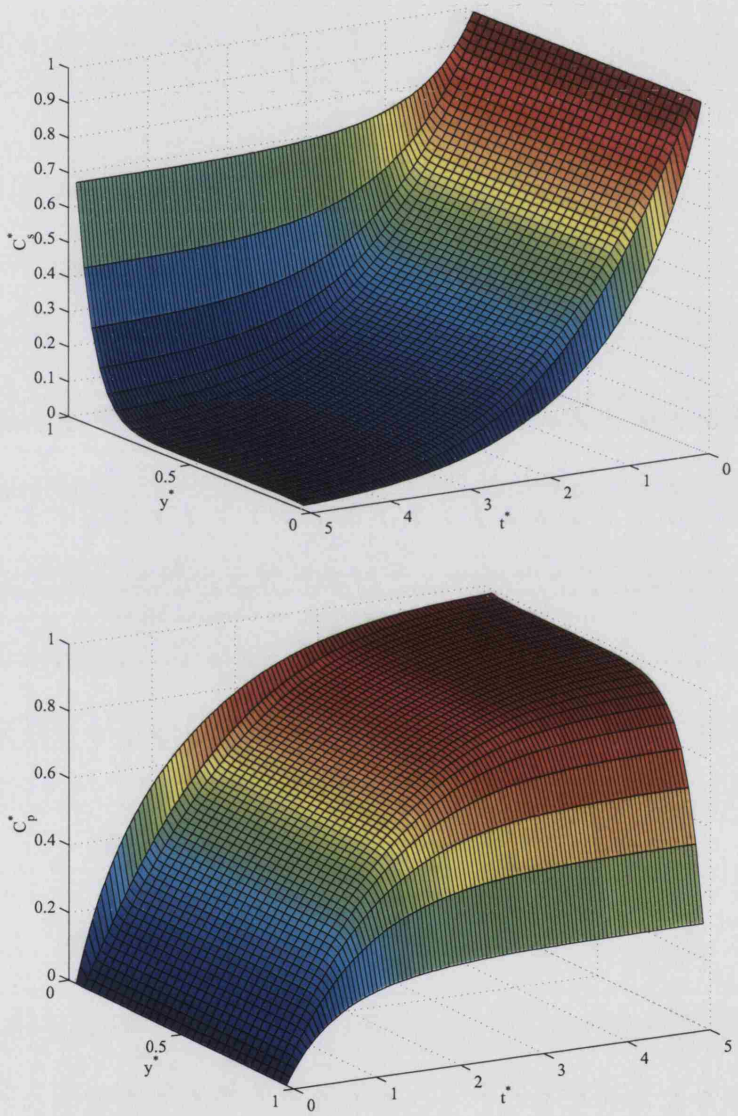

Figure 5.10: The effect of reaction-diffusion as Φ's increased from the original values if the whole-cell reaction possesses a lower rate of reaction ($\Phi_s = 1.89$ and $\Phi_p = 1.84$).

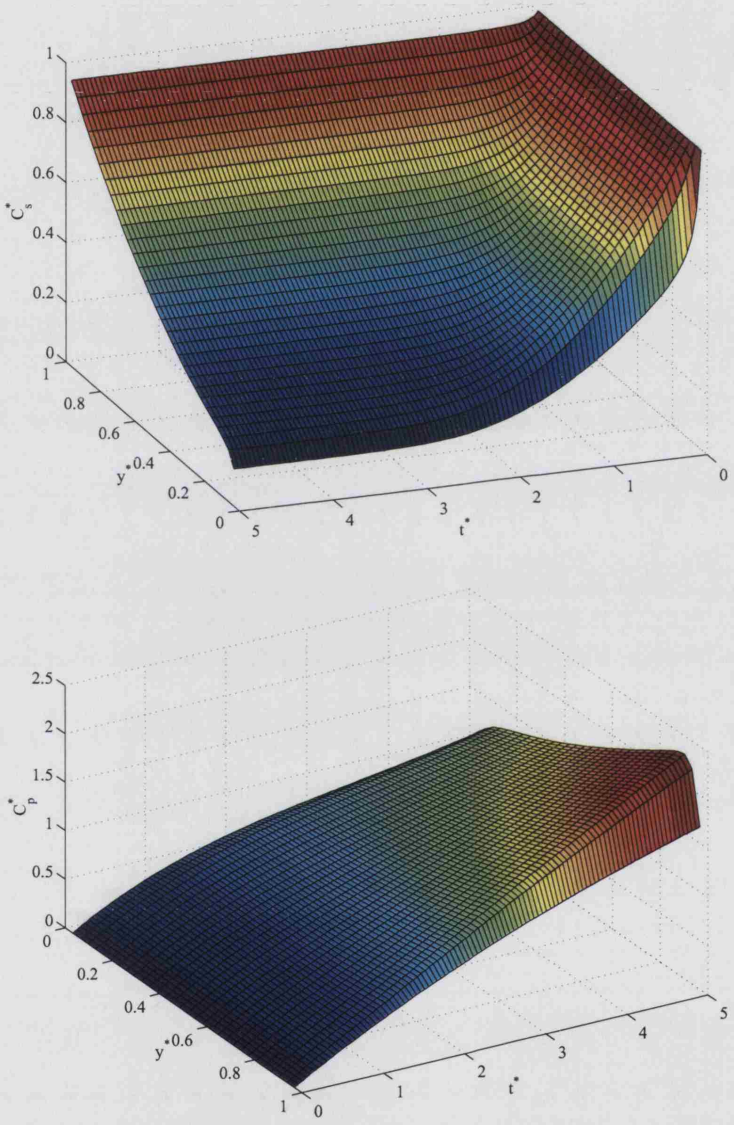

Figure 5.11: Same value of rate with different substrate diffusivity gives $\Phi_s = 5.97 \times 10^{-1}$ and $\Phi_p = 5.83$.

figures given in *Figure 5.9* shows the movement of the substrate along the radius of the cell and at the same time it reacts with the enzyme at the particular radius position. It is apparent from the two plots that the movement of substrate has no effect on diffusion and therefore, a nearly vertical rate is observed before the entire substrate is converted into the product and travels out of the cell.

The next set of figures depicts the space-time plots of a reaction-diffusion system influenced by the diffusion phenomena by a thousand fold of the given values of Φ's from the first set (*Figure 5.10*). The slow diffusion of substrate from the surface of the cell towards the centre can be clearly seen and it is simultaneously disappeared forming product as time progresses. This is shown by a flat surface at $t^* = 5$, at the centre of the cell where $y^* = 0$. A similar phenomena occurs for product component where the red surface shows the highest concentration of product at the centre of the cellular ensemble and it starts to fade as it travels towards the cell surface.

To further investigate the effect of the cellular reaction-diffusion phenomena, the value of Φ_s and Φ_p were varied such that one of the values was lowered by a factor of 10 (*Figure 5.11*). Such a change gave apparent effects on both substrate and product movement into and out of the cell respectively. The concentration gradient of the substrate as it moved towards the centre of the cell could be clearly observed compared to that of the substrate curve from the previous figure. A lower value of Φ_s, which could be due to the high diffusion constant, $\mathscr{D}_{e,s}$ of the given substrate and thus, high rate of diffusion, the substrate conversion was relatively slow at the start of the reaction and turns faster as the reaction proceeded. The 3–dimensional surface also shows that the rate of reaction was faster compared to the rate of diffusion of the substrate into the cell. However, the surface plot of product concentration was observed otherwise. The modulus of the product used for this simulation was 10 times lower compared to that of the substrate which means that the product diffusivity is comparatively lower than the substrate. However, since the rate of product formation is still slower than its rate of diffusion, most of the product formed are accumulated near the membrane cell as shown by the red mark in the second plot of *Figure 5.11.*

5.4 Summary and Conclusion

This chapter has given a clear description of the whole-cell reaction by introducing the effect of membrane diffusion. Such an analysis was based on the previous results in *Chapter 4* whereby the computer simulations of the mathematical model differed from that of the experimental data. It should be reiterated here that there was a delay between the data point and the simulated lines and it was assumed that such results were mainly caused by the diffusion limited reaction. The conclusion is however invalid when the diffusion terms were introduced into the model system. The effect is too small or almost negligible from the results obtained in this study. Therefore, the shift of the experimental points from the model simulations could not just be explained only by the effect of membrane diffusion, there are other factors that contributed to such results for instance, the un-permeated product within the cell membrane which consequently lowering the rate of the product formation and the hydrophobicity between the substrate and the cell due to the presence of different molecular charges.

The cyclohexanone monooxygenase enzyme is also known to depend on the cofactor binding before the oxidation reaction could take place, and cofactor formation is highly dependent on the availability of the carbon source i.e. glycerol, therefore, the amount of glycerol fed into the reaction mixture could be the other factor that contributed to the discrepancy between the model simulation and the experimental points. This argument will be further analysed in the subsequent chapter.

The study of the reaction-diffusion phenomena also suggests that the rate of substrate conversion is relatively low compared to that of the rate its being diffused into the cell. This is perhaps related to the initial investigation of the kinetics of the enzyme in *Chapter 3* where the isolated enzyme was used to carry out the experiment. From the work of Baldwin and co-workers (Baldwin and Woodley, 2005), it was found that the CHMO enzyme is highly sensitive to the amount of oxygen present in the reaction medium. The use of an excess amount of oxygen concentration in the previous analysis could result in the loss of enzyme's activity which consequently led to the low rate of reaction during the bioconversion. The result was particularly apparent when the reaction of the CHMO-enzyme catalysed bicyclic-ketone only gave the specific activity between 40 and 60U$\cdot g_{dcw}^{-1}$ as plotted in *Figure 4.11* in *Chapter 4* (value

of $55U{\cdot}g_{dcw}^{-1}$ was measured by Doig and co-workers, (Doig *et al.*, 2002)).

Further characterisation was also made with different molecular sizes of substrate and product which led to the different diffusional effects through the membrane cell as well as the effect of enzyme's activity that gave different values of V_{max}. These were incorporated within the model via Thiele modulus given by;

$$\Phi_{s,p} = \frac{R_c}{3}\sqrt{\frac{V_{max}}{\mathscr{D}_{e,(s,p)}K_{m_{[Bicyclo]}}}}$$

a dimensionless constant consists of the cellular radius, R_c, maximum rate of reaction, V_{max}, Michaelis constant, K_m and the components' diffusivity, $\mathscr{D}_{e,(s,p)}$. Based on the CHMO enzyme-catalysed Baeyer-Villiger reaction which the reaction rate is governed by the UNI–UNI non-competitive type inhibition, the value of Φ is considerably small such that the effectiveness factor lies in the region of the diffusion-free reaction. Therefore, the shift observed from the experimental data could be due to other factors mentioned previously.

Nevertheless, if a reaction follows the model constructed in this work whereby the effectiveness factor lies in the region of strong diffusional effects, the activity of the enzyme should be enhanced to a value that could shift the Thiele modulus to the diffusion-free region on the left hand side of the curve given in *Figure 5.8.* The activity of the particular enzyme could only be enhanced by increasing its concentration, which would increase the value of V_{max}, where the term is given by, $k_5[\mathrm{E}]_\mathrm{T}$. Such characterisations are believed to be the first approach carried out on the cellular system and it is applicable not only to the whole-cell reaction of similar microorganism, (*Escherichia coli*) but also to different type of organisms such as yeasts and fungi which could give different values of moduli from their different shapes and sizes.

Chapter 6

Cofactor Regeneration in an Enzyme-Catalysed Baeyer-Villiger Reaction

6.1 Introduction

The introduction of enzyme as a source of catalyst in chemical conversion has proven to be a successful attempt. Enzyme-catalysed chemical conversion is important especially in the production of chiral compounds such as esters and amino acids. However, most of the biocatalysts in current use are limited to cofactor-independent enzymes which perform some relatively simple chemical reactions. Comparatively, cofactor-dependent enzymes such as oxygenases and transferases are able to undertake much more complex conversions and catalysing a large number of synthetically useful reactions.

Cofactors are compounds with low molecular weight which exist naturally within the living organisms as a result of cellular metabolism. The presence of cofactor in a reaction mixture, sometimes provides the suitable active sites for a substrate to bind with the enzyme in order to form the required product. The synthesis of cofactors especially nicotinamide adenine dinucleotide (NADH) and nicotinamide adenine dinucleotide phosphate (NADPH) into their pure forms is a highly expensive procedure and the use of such compounds in a large amount to carry out other reactions will definitely increase the cost of these processes. Such a high demand of these compounds has turned the attention of some researchers into the use of natural form of cofactors. These are naturally occurring cofactors found in living cells where *in situ* regeneration

of the compound is taken place in a single cell during its growth period. The use of cofactors not only reduces the cost of the chemical synthesis but also prevent the accumulation of the inhibitory cofactor by-products in some chemical reactions (Zhao and van der Donk, 2003).

Cofactor regeneration can be achieved in two ways; the whole-cell biocatalysis (Cabral *et al.*, 1997) or a coupled reaction in an isolated enzyme system (Hogan and Woodley, 2000; Eckstein *et al.*, 2004). The former being the most popular to carry out biotransformation. This is due to the fact that the only control of the system is the carbon source that maintains the growth of the cell such that the cofactor for a particular reaction is readily available. In comparison, for the isolated enzyme system, an accurate amount of each component, especially the initial cofactor concentration needs to be supplied such that it is enough to drive the reaction to completion. Failure in providing a sufficient amount of cofactor will give an imbalance coupled reaction that can lead to the termination of the reaction.

Due to this reason, the study of cofactor availability in a particular reaction is the foremost important. The result could lead to the understanding of the rate of its consumption by the main reaction and at the same time the rate of its formation. Enzyme-catalysed Baeyer-Villiger reaction which could only proceed in the presence of cofactor has been used to study such a behaviour. One of the main challenges in the Baeyer-Villiger reaction system is to maintain the amount of cofactor being formed within the cell. This could be done by varying the amount of glycerol in the reaction mixture. The work will be mainly explained using mathematical modelling and later validated with the appropriate experimental work.

6.2 Modelling of the Bienzymatic System

The system of coupled enzyme-catalysed reaction can be depicted in *Figure 6.1.* The main Baeyer-Villiger reaction is given by the top reaction proceeding to the right with the presence of cofactor formed from the bottom reaction proceeding to the left together with the supplied molecular oxygen. In the next two following sections, the above reaction was transformed into a set of mathematical rate expressions consisted of the main components (1) to (4) given in the figure as well as the central component that connected the two reactions, i.e. the reduced nicotinamide adenine dinucleotide phosphate (NADPH) which later oxidised into $NADP^+$.

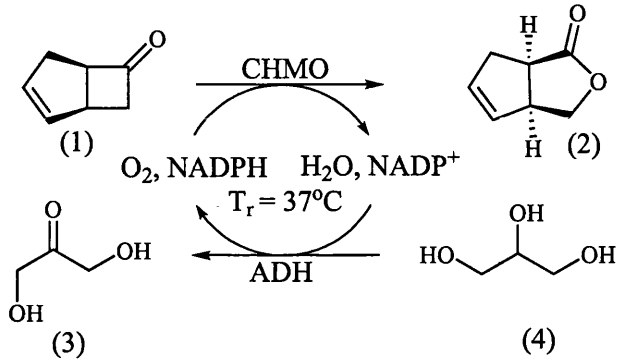

Figure 6.1: Bienzymatic (CHMO)-catalysed Baeyer-Villiger reaction and (ADH)-catalysed cofactor regeneration. (1) bicyclo[3.2.0]hept-2-en-6-one, (2) (-)1(S)5(R)2-oxabicyclo[3.3.0]oct-6-en-3-one, (3) dihydroxyacetone and (4) glycerol. T_r represents the reaction temperature.

6.2.1 BI–BI Mechanism of CHMO Enzyme-Catalysed Reaction

The simplified rate expression of Baeyer-Villiger reaction was previously derived in *Chapter 2*. The expression however did not take into account the presence of cofactor, therefore, resulted in the UNI–UNI reaction mechanism. Such a simplification is important especially when the experimental investigation is limited and required a special equipment to carry out the study of the kinetics of any enzyme–catalysed reaction. In this work the kinetics are only analysed theoretically, therefore, exact values of the kinetic constants are not particularly important. The only main objective of this analysis is to observe the mutual cooperation between the two coupled reactions and the stability of the system when small perturbation is imposed on one of the reactions.

Consider the NADPH as one of the reacting substrates, the rate expression of BI–BI mechanism was derived according to the King-Altman method as;

$$r_{(CHMO)} = \frac{{}^1V_{max}C_{co}C_s}{K_{m_{co}}K_{m_s}A' + C_{co}C_sB'} \tag{6.1}$$

where A' and B' are given by;

$$A' = \frac{K_{i_{co}}}{K_{m_{co}}}\left(1 + \frac{K_{m_{co+}}}{K_{i_{co+}}}\frac{C_p}{K_{m_p}}\left[1 + \frac{C_{co}}{K_{i_{co}}} + \frac{K_{m_{co}}}{K_{m_{co+}}}\frac{C_p}{K_{m_p}}\right]\right) + \frac{C_{co}}{K_{m_{co}}} + \frac{C_s}{K_{m_s}}\left(1 + \frac{C_p}{K_{i_p}} + \frac{C_{co+}}{K_{i_{co+}}}\right)$$

$$B' = 1 + \frac{C_s}{K_{m_s}}\left(1 + \frac{C_p}{K_{i_p}} + \frac{C_{co^+}}{K_{i_{co^+}}}\right) + \frac{C_p}{K_{i_p}}$$

where C_{co}, C_s and C_p are the concentrations of NADPH, substrate and product respectively and that for $K_{m_{co}}$, K_{m_s}, K_{m_p} and $K_{m_{co^+}}$ are the Michaelis constants for NADPH, substrate, product and oxidised cofactor respectively while $K_{i_{co}}$, $K_{i_{co^+}}$ and K_{i_p} are the inhibition constants for cofactor, oxidised cofactor and product respectively. Equation (6.1) describes a reaction with two substrates and two products which is normally termed as the ordered BI–BI kinetic mechanism.

6.2.2 Theorell-Chance Mechanism of Cofactor Regeneration

The mechanism was initially proposed by Theorell and Chance specifically used to describe the alcohol dehydrogenase enzyme-catalysed reaction (Segel, 1993). The main characteristic of Theorell-Chance mechanism that differs from the other Michaelis type expression, is the absence of the ternary central complex. Consider a reaction involving two substrates, [A] and [B] forming the products, [P] and [Q], the mechanism can be summarised using the Cleland's notation and it is given in *Figure 6.2(a)*. Such a mechanism is also known as the *hit and run* type mechanism which is clearly described by the two arrows in the middle of the route. According to the notation, substrate [A] binds with the enzyme, [E] to form a complex [EA], which then reacts with the second substrate [B] in a bimolecular process to form the products [P] and [Q] which therefore corresponds to the ordered BI–BI mechanism without forming the three-body complex intermediate.

This is similar to the reaction occurred in the cellular system as part of the metabolic route. The availability of glycerol provides a continuous production of cofactor and thus maintains the main Baeyer-Villiger bioconversion. A similar mechanism of the cofactor formation is given in *Figure 6.2(b)* and the rate expression can be obtained from the given notation applying the King-Altman method of kinetic derivation,

$$r_{ADH} = \frac{{}^2V_{max}C_{co}C_{gly}}{K'_{m_{co}}K_{m_{gly}}C' + C_{co}C_{gly}D'} \tag{6.2}$$

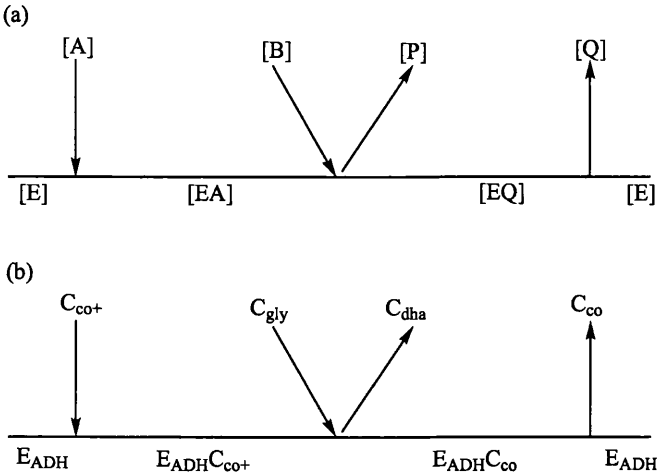

Figure 6.2: (a) General Theorell-Chance type mechanism of enzyme-catalysed reaction. (b) Mechanism describing the ADH enzyme-catalysed reaction (E_{ADH}), for cofactor recycling (adapted and corrected from the work of Pereira *et al.* (1994)).

where C' and D' are defined by;

$$C' = \frac{K'_{i_{co+}}}{K'_{m_{co+}}}\left(1 + \frac{C_{co+}}{K'_{i_{co+}}} + \frac{C_{co}}{K'_{i_{co}}}\right) + \frac{C_{gly}}{K_{m_{gly}}}\left(1 + \frac{C_{dha}}{K_{i_{dha}}}\frac{K_{i_{gly}}}{C_{gly}}\right)$$

$$D' = 1 + \frac{K_{m_{gly}}}{C_{gly}}\frac{C_{dha}}{K_{i_{dha}}} + \frac{K'_{m_{co+}}}{C_{co+}}\frac{C_{co}}{K'_{i_{co}}}\frac{C_{dha}}{C_{gly}}$$

where C_{co}, C_{co+}, C_{gly} and C_{dha} represent the concentrations of cofactor, oxidised cofactor, glycerol and dihydroxyacetone respectively, while $K_{m_{gly}}$ represents the Michaelis constant for glycerol component. The inhibition constants for glycerol and dihydroxyacetone are given by $K_{i_{gly}}$ and $K_{i_{dha}}$ respectively. All other constants give the same meaning as those defined previously for the CHMO reaction, however they are marked with ($'$) for the ADH system.

This completes the derivation of the rate expression described by the Theorell-Chance BI–BI mechanism. Equations (6.1) and (6.2) will be used in the following section to mathematically explain the effect of coupled bienzymatic system as well as the significance of the cofactor regeneration in an enzyme-catalysed system.

6.2.3 Modelling of Coupled Enzyme-Catalysed Reactions in a Stirred-Tank Bioreactor

The method of modelling the two coupled system is similar to that used to describe the unstructured type model of the fed-batch reaction discussed in *Chapter 4*. The conservation of mass around the bioreactor system was used for the substrate and glycerol components. A complete model system is given below;

For the rate of substrate feeding;

$$\frac{dV_{s,r}}{dt} = F_{s,in} \tag{6.3}$$

and that for glycerol feeding;

$$\frac{dV_{gly,r}}{dt} = F_{gly,in} \tag{6.4}$$

hence, the total component fed into the reactor results in;

$$\begin{aligned} \frac{d}{dt}(V_{s,r} + V_{gly,r}) &= F_{s,in} + F_{gly,in} \\ \frac{dV_T}{dt} &= F_{s,in} + F_{gly,in} \end{aligned} \tag{6.5}$$

The mass balance of the substrate within the reactor is given by;

$$\frac{dC_s}{dt} = \frac{F_{s,in}}{V_T}(C_{s,in} - C_s) - r_{CHMO} \tag{6.6}$$

and for the product balance;

$$\frac{dC_p}{dt} = r_{CHMO} - \frac{F_{s,in}}{V_T}C_p \tag{6.7}$$

Since the cofactor and its oxidised form connect the two enzyme systems, therefore, their balances should consist of both rate expressions. The final balances of both components can be written as;

$$\frac{dC_{co}}{dt} = r_{ADH} - r_{CHMO} - C_{co}\frac{(F_{s,in} + F_{gly,in})}{V_T} \tag{6.8}$$

and

$$\frac{dC_{co^+}}{dt} = r_{CHMO} - r_{ADH} - C_{co^+}\frac{(F_{s,in} + F_{gly,in})}{V_T} \tag{6.9}$$

The remaining balances are for the ADH enzyme-catalysed system comprises of glycerol and its product, dihydroxyacetone. Their conservation of mass are given by;

$$\frac{dC_{gly}}{dt} = \frac{F_{gly,in}}{V_T}(C_{gly,in} - C_{gly}) - r_{ADH} \tag{6.10}$$

for glycerol, and that for its product;

$$\frac{dC_{dha}}{dt} = r_{ADH} - \frac{F_{gly,in}}{V_T}C_{gly} \tag{6.11}$$

The rate expressions used in equations (6.6) to (6.11) are those given by equations (6.1) and (6.2). Since the system is to be theoretically analysed, it would be simpler to put the equations into the non-dimensional form. Upon rendering equations (6.6) to (6.11) dimensionless, the system reduces into the form given by;

$$\begin{aligned}
\dot{x_1} &= -x_1 + \frac{Da_1(1-x_1)x_3}{\mathscr{A}} \\
\dot{x_2} &= -x_2 + \frac{Da_1(1-x_1)x_3}{\mathscr{A}} \\
\dot{x_3} &= -\frac{Da_1(1-x_1)x_3}{\mathscr{A}} + \frac{Da_2(\Gamma - x_5)Tx_4}{\mathscr{B}} - x_3(1+T) \\
\dot{x_4} &= \frac{Da_1(1-x_1)x_3}{\mathscr{A}} - \frac{Da_2(\Gamma - x_5)Tx_4}{\mathscr{B}} - x_4(1+T) \\
\dot{x_5} &= -Tx_5 + \frac{Da_2(\Gamma - x_5)Tx_4}{\mathscr{B}} \\
\dot{x_6} &= -Tx_6 + \frac{Da_2(\Gamma - x_5)Tx_4}{\mathscr{B}}
\end{aligned} \tag{6.12}$$

where $\dot{x}$ represents the differential form, $\frac{d}{dt}$, with $\mathscr{A}$ and $\mathscr{B}$ are the denominators of equations (6.1) and (6.2) in dimensionless form. Da_1 and Da_2 are the Damköhler numbers of the CHMO and the ADH systems respectively as a result of combining the terms given by;

$$Da_1 = \frac{^1V_{max}}{\tau_1 C_{s,in}}$$

and

$$Da_2 = \frac{^2V_{max}}{\tau_2 C_{s,in}}$$

where τ_1 and τ_2 are given by;

$$\tau_1 = \frac{F_{s,in}}{V_T}, \quad \tau_2 = \frac{F_{gly,in}}{V_T}$$

The term Γ is a constant formed when;

$$C_{s,in} \neq C_{gly,in}$$

such that

$$\Gamma = \frac{C_{gly,in}}{C_{s,in}}$$

and the term T is the combination of the dimensionless times τ_1 and τ_2, where;

$$T = \frac{\tau_2}{\tau_1}$$

However, the amount of the oxidised cofactor, $NADP^+$ could not be determined using the wavelength detection via spectrophotometer, therefore, the initial condition of $\dot{x_4}$ could not be easily set. In order to avoid such complication, a dependent parameter, φ was introduced, where;

$$\varphi = x_3 + x_4 \tag{6.13}$$

Substitution of equation (6.13) into system (6.12) reduces the 6–dimensional system of differen-

tial equations into 5 and they are given by system (6.14) below;

$$\begin{aligned}
\dot{x_1} &= -x_1 + \frac{Da_1(1-x_1)x_3}{\mathscr{A}} \\
\dot{x_2} &= -x_2 + \frac{Da_1(1-x_1)x_3}{\mathscr{A}} \\
\dot{x_3} &= -\frac{Da_1(1-x_1)x_3}{\mathscr{A}} + \frac{Da_2(\Gamma-x_4)(\varphi-x_3)T}{\mathscr{B}} + \left(\frac{\varphi-2x_3}{2}\right)(1+T) \\
\dot{x_4} &= -Tx_4 + \frac{Da_2(\Gamma-x_4)(\varphi-x_3)T}{\mathscr{B}} \\
\dot{x_5} &= -Tx_5 + \frac{Da_2(\Gamma-x_4)(\varphi-x_3)T}{\mathscr{B}}
\end{aligned} \tag{6.14}$$

The system of 5–dimensional ordinary differential equations from (6.14) describes the cofactor regeneration of a coupled enzyme–catalysed reactions. The total amount of the available cofactor governs both the CHMO and the ADH enzyme systems. A number of numerical simulations at different parameter values were carried out using the model system. The curves resulted from the combination of parameters were than compared. However, before carrying out these simulations, the significance of varying these parameters need to be understood. The two Damköhler numbers, Da_1 and Da_2 represent the speed of each reaction which are originally defined by the values of ${}^1V_{max}$ and ${}^2V_{max}$. The ratio of the two dilution rates of substrates from both systems are given by the term T and finally the term Γ defines the ratio of the initial concentrations of glycerol and ketone.

The first numerical simulation of the effect of the rate of reaction is shown in the next 4 graphical plots (*Figures 6.3* to *6.6*). All parameters used in the simulation are the same (Da_2=1.5×10^{-1}, T=0.1, Γ=2 and φ=1.0×10^{-5}), except for Da_1. *Figure 6.3* shows the different rate of consumptions of ketone and glycerol during the reaction. The curves stayed at the same trajectory even when the value of Da_1 was varied. On the other hand, the amount of product formation gave a major different if the rate of reaction of one of the systems was changed. Obviously, at a different rate of reaction, there would be a competition between the two systems; the CHMO system that requires the substrate produced from the ADH system and that the ADH-catalysed reaction which depends on the oxidised cofactor to complete the reaction. The system nevertheless attained its steady-state right after the start of the reaction

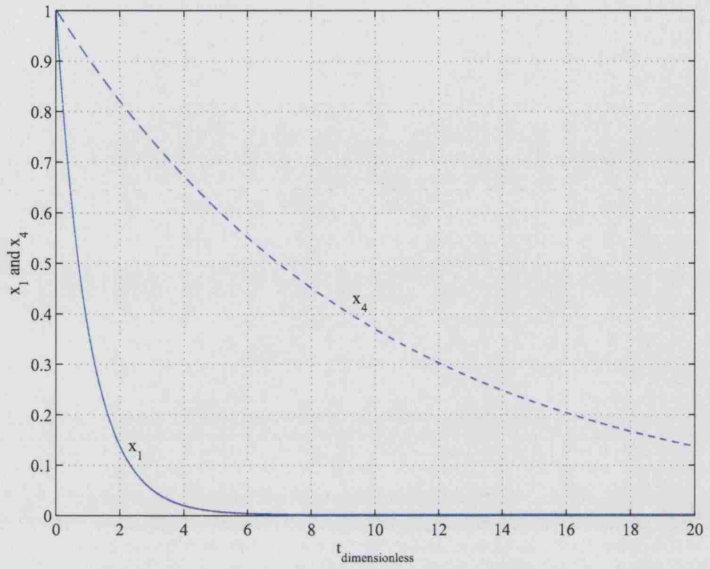

Figure 6.3: The depletion of ketone and glycerol at Da_1=1.5×10^{-2}, Da_1=1.5×10^{-1} and Da_1=1.5 with the same Da_2=1.5×10^{-1}.

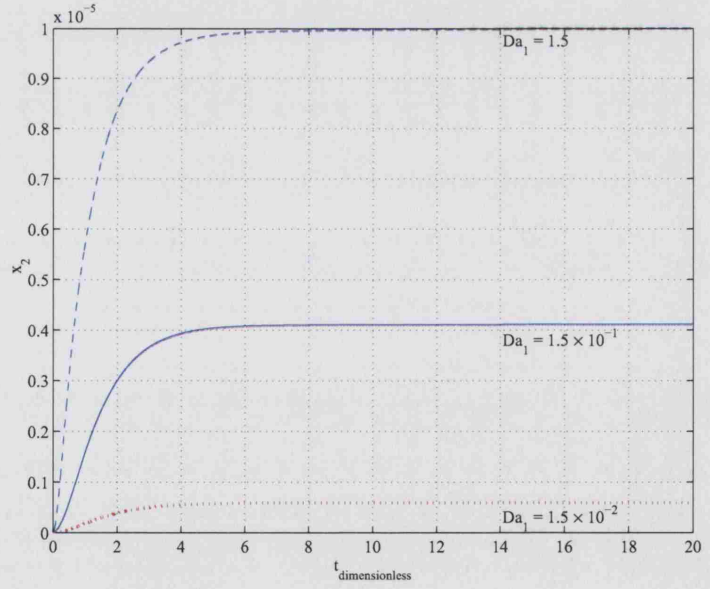

Figure 6.4: The effect of different Da_1's with the same Da_2 for product formation.

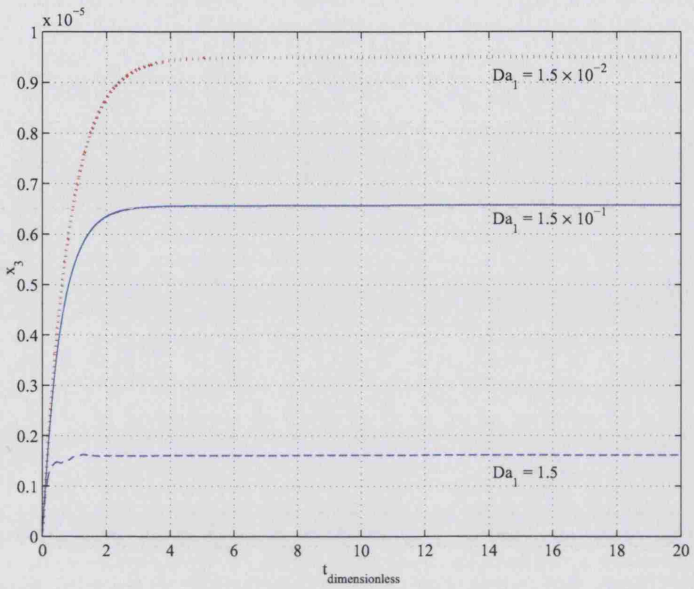

Figure 6.5: The amount of regenerated cofactor from the different rate of consumption and formation of the main systems (Da_2=1.5×10^{-1}).

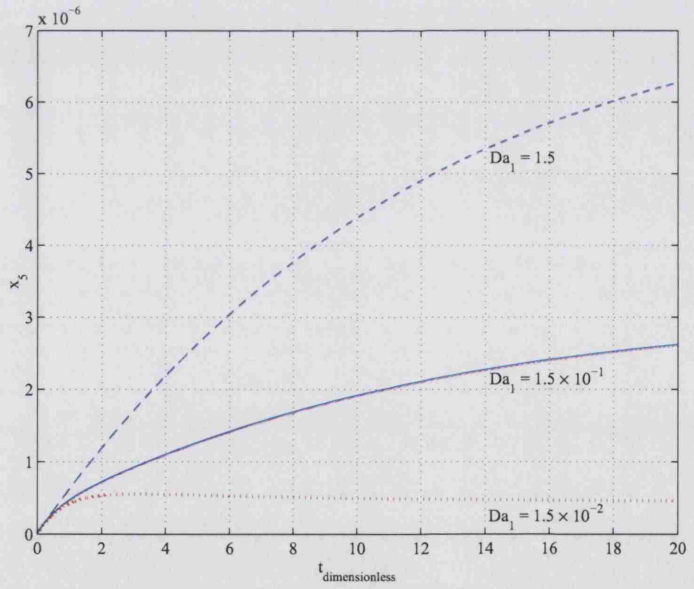

Figure 6.6: The amount of side-product (dihydroxyacetone) formed from the different rate of reactions defined by Da_1 and Da_2.

and remained at this condition as the time increased. Such a condition will be further discussed in Section 6.4. The different amount of lactone formed at the different reaction rates is shown in *Figure 6.4*. The lines clearly illustrate that at a higher rate of reaction of the CHMO system compared to that of the ADH system, a higher amount of product was formed, and that at a lower rate of reaction, resulted in a lower product formed. An opposite result was observed in the plot of the cofactor formation. An increase of Da_1 by 10 folds led to a low cofactor formation. However, an opposite result was obtained if the value was differed 10 times that of Da_2, which is clearly shown in *Figure 6.5*. The plot of x_5 that represents the amount of product (dihydroxyacetone) generated from the reaction catalysed by ADH, resembles that of the lactone formation, however such a value is by far smaller than that of the lactone formed. This is due to the ratio given by the value of T, which suggested that the feeding rate of glycerol is slower than that of ketone.

In the next numerical simulation, the ratio of the initial glycerol concentration to the initial concentration of ketone, Γ was changed to 0.1. This means that a higher concentration of ketone was used compared to that of glycerol used previously. The results from the highly nonlinear system are given in *Figures 6.7* to *6.9*. Such results are believed could only be observed theoretically since the instability only occurs in a range of 1 unit of time. By referring to *Figure 6.7*, there is a sudden *jump* in the lactone formation at the beginning of the reaction when Da_1=1.5. This value is 10 times higher than the value of Da_2, which shows that the rate of formation of lactone is faster compared to the rate of formation of cofactor it consumed during the conversion. Furthermore, in order to initiate the reaction, a sufficient amount of cofactor is required, and this is obtained from the total cofactor given by φ. With such a fast rate of reaction, the available amount of cofactor will be used up and the first conversion of product reaches a peak for a period of 2 units of time before it stabilises and reaches a steady-state. This observation is closely related to the small amount of Γ where the low concentration of glycerol could not compensate the high demand of cofactor requirement to balance out the system. The system however started to stabilise as the reaction rate of the CHMO enzyme-catalysed reaction equalises or lower than that of the ADH system. This is clearly shown from the other curves in *Figure 6.7*.

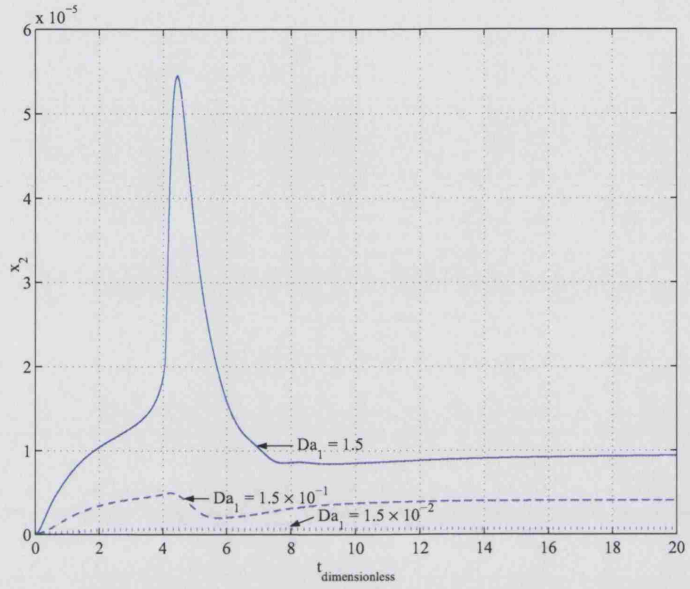

Figure 6.7: Lactone formation at different values of Da_1 with Da_2=1.5×10^{-1}.

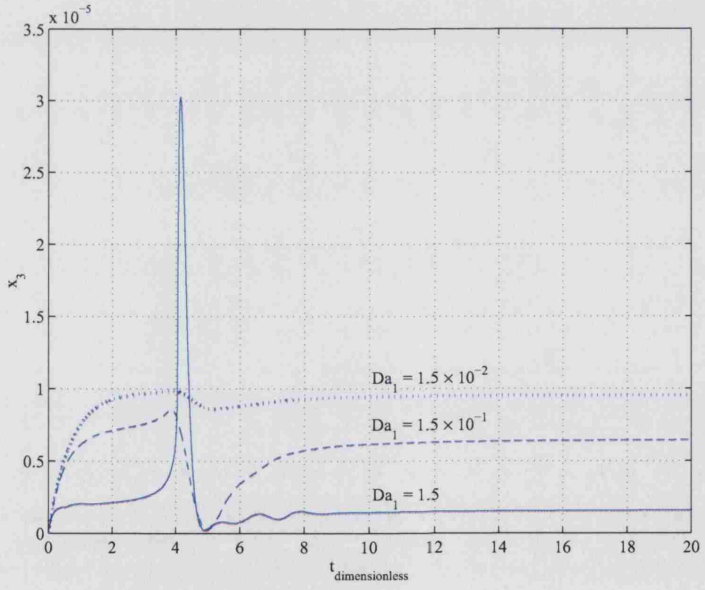

Figure 6.8: The amount of cofactor formed at low concentration of glycerol.

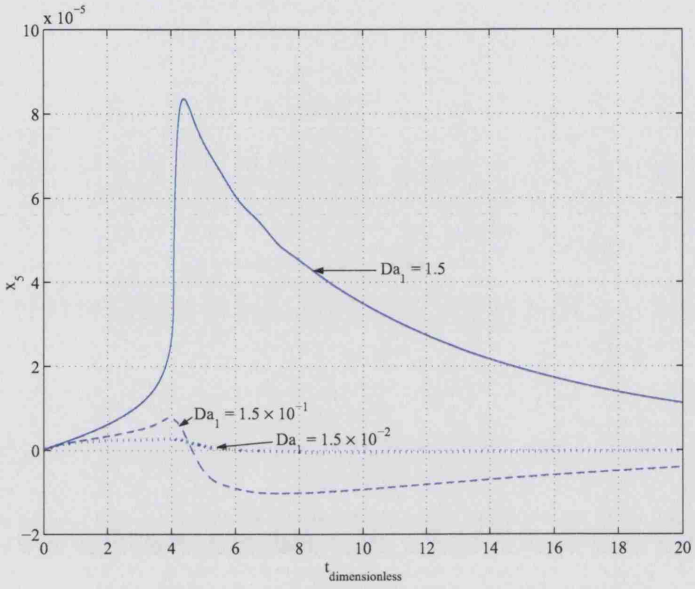

Figure 6.9: Dihydroxyacetone formation at different Da_1's.

A similar result was also observed during the formation of cofactor. The curve that represents a higher Da_1 in *Figure 6.8* also reached a peak at the same time the product was formed. It was then attained a steady-state condition as the time was prolonged. The formation of the side-product however differed from the previous two observations. At Da_1=1.5, the peak was observed in between 4 and 5 units of time, and it gradually decreased towards an equilibrium steady-state.

The model system describing the cofactor recycling in the bioconversion system was theoretically discussed. An accurate model can be obtained by thoroughly analysing the individual rate expression of CHMO and ADH enzyme-catalysed systems. In observing, as well as kinetically studying the coupled system, the reactions should be initially carried out using the isolated enzymes. Prior to the whole-cell system, such reaction is important in determining the kinetic constants of both systems. Similar analysis has been utilised in the study of the UNI–UNI mechanism of the CHMO enzyme-catalysed reaction in *Chapter 3*. The kinetic information from the isolated enzyme reaction can then be used for reactions in the whole cell system. The study of the ADH enzyme for cofactor regeneration was previously given by Pereira *et al.* (1994),

however, an error was found in the derived rate expression of the particular system. Correction of the rate equation from the work of Pereira *et al.* (1994) is given by equation (6.2). In order to give a clear view of the important of the secondary reaction system (ADH enzyme-catalysed reaction), a number of experimental work were carried out using different values of the glycerol feeding rates as well as the effect of its absent during a bioconversion. A detail experimental work is given in the following section.

6.3 Experimental Validation

6.3.1 Materials and Method

Chemicals and Whole-Cell Biocatalyst

The purified substrate, (bicyclo[3.2.0]hept-2-en-6-one) and products, ((-)1(S)5(R)2-oxabicyclo-[3.3.0]oct-6-en-3-one and (-)1(R)5(S)3-oxabicyclo[3.3.0]-oct-6-en-2-one) were received from Fluka (Buchs, Switzerland). All other chemicals were purchased from Sigma Chemical Co. (Poole, Dorset, UK), while the fermentation media were ordered from Fluka (Buchs, Switzerland) or otherwise from Sigma Chemical Co (Poole, Dorset, UK). The bacterial cell of *Escherichia coli* TOP10[pQR239] was obtained from 5–litre (working volume) fermentation using the 7–litre fermenter. Fermentation process of *Escherichia coli* as a source of biocatalyst has been described in detail in *Chapter 3.*

Fed-Batch Substrate and Glycerol Reactions in Cofactor Regeneration System

The bioconversion reaction of bicyclo[3.2.0]hept-2-en-6-one was carried out in the same bioreactor used to grow the bacterial cell. This avoids the transfer of a bulk biocatalyst from one bioreactor to another. Two different pumps were set to deliver the substrate (101 U/R, Watson–Marlow Limited, Falmouth, Cornwall, UK) and glycerol (505*Du*–Digital, Watson-Marlow Limited, Falmouth, Cornwall, UK) into the bioreactor which formed a fed-batch bioconversion system. Such a configuration controls the feeding rate of the substrate as well as the carbon source (glycerol) for growth of the cell. This would lead to the understanding of the important of glycerol in providing the "substrate" for cofactor regeneration in the secondary system described in the previous section.

The experiment was initially performed in the absence of glycerol within the reaction medium. It was assumed that only a small trace of glycerol remained in the medium after the cell fermentation. This small amount of glycerol would only last less than an hour after the start of the reaction. The growth of the biocatalyst was followed during the reaction as well as the amount of glycerol that present in the media.

In order to obtain the rate of glycerol consumption during the reaction, a batch glycerol experiment is required. A known amount of pure glycerol was added into the reaction medium which consisted of the complex media and the active cell. The feeding rate of substrate was maintained at $0.5 g \cdot l^{-1} h^{-1}$ below the inhibition point. Results from this work will be a benchmark for the next three fed-batch experiments; below, at and above the rate of glycerol consumptions. Detail results and discussion of the experimental work are explained in Section 6.3.2.

Glycerol Assay

The amount of glycerol in the reaction medium was determined using the Glycerol Assay Kit® purchased from R–Biopharm (Roche) AG, Darmstadt, Germany. The kit contains 3 reagents; reagent 1 contains approximately 2g coenzyme/buffer mixture consists of glycylglycine buffer at pH approximately 7.4, NADH approximately 7mg, 22mg of ATP, PEP–CHA approximately 11mg and magnesium sulphate. The second reagent (reagent 2) with 0.4ml volume comprises of a mixture of pyruvate kinase approximately 240U and L–lactate dehydrogenase approximately 220U and finally reagent 3 with total volume of 0.4ml consists of glycerokinase suspension approximately 34U.

The solid form of reagent 1 was dissolved with 11ml distilled or reverse osmosis (RO) water and allowed to stand for approximately 10min at 20–25°C. The other 2 reagents (reagent 2 and 3) were left undiluted. The analysis was divided into two; reaction with blank sample (without glycerol sample) and reaction with sample solution. For a blank sample, a mixture of 1ml of reagent 1, 2ml of RO water and 0.01ml of reagent 2 was prepared and thoroughly mixed. It was then left for pre–reaction (reaction between ADP in ATP and pyruvate in phosphoenolpyruvate (PEP)) for approximately 5 to 7min. The absorbance of the mixture was then read and marked as reading A_1. The mixture was then added with 0.01ml reagent 3 and the reaction was left for completion for another 5 to 10min. The second absorbance A_2 was then taken. For the sample

reaction, a similar procedure was followed but the volume of the first 3 solutions of 1ml, 0.1ml and 1.9ml of reagent 1, glycerol sample solution and RO water respectively were consecutively added. Readings A_1 and A_2 were noted following the similar procedure as the blank sample. The glycerol absorbance, ΔA was determined according to the following absorbance different;

$$\Delta A = (A_1 - A_2)_{sample} - (A_1 - A_2)_{blank}$$

and the total glycerol concentration from a sample solution was calculated using;

$$c = \frac{2.781 \Delta A}{\varepsilon} \left(\frac{g_{glycerol}}{l_{sample\ solution}}\right)$$

6.3.2 Results and Discussion

From the theoretical analysis given in the previous section, it was found that the glycerol that existed in the reaction medium provided the basis for both the cellular growth and the substrate bioconversion. A further kinetic analysis is still required if the model system is to be accurately compared to the experimental data. This final work however, does not intend to give a detail analysis of the system but only to explain the coupled enzyme reaction in the cofactor regeneration system using a theoretical analysis. The experimental data obtained from varying the glycerol feeding rates would provide a preliminary proof of such an effect.

Figures 6.10 and *6.11* were plotted from the reaction with the remaining glycerol from the fermentation of biocatalyst. The fermentation profile showed an increase of cell density for approximately 6 hours. The growth of the cell could be further explained from the low dissolved oxygen tension in the reaction medium. This shows that almost all molecular oxygen sparged into the media was completely consumed by the cell in order to maintain the growth. After 6 hours of fermentation, when the cell density reached $13 g_{dcw} l^{-1}$, the substrate ketone was fed into the fermenter (bioreactor). At the same time the optical densities of the cell were continuously analysed.

The effect of insufficient carbon source can be seen in the profile given in *Figure 6.10.* After about 2 hours of bioconversion reaction, the dissolved oxygen tension started to rise and the

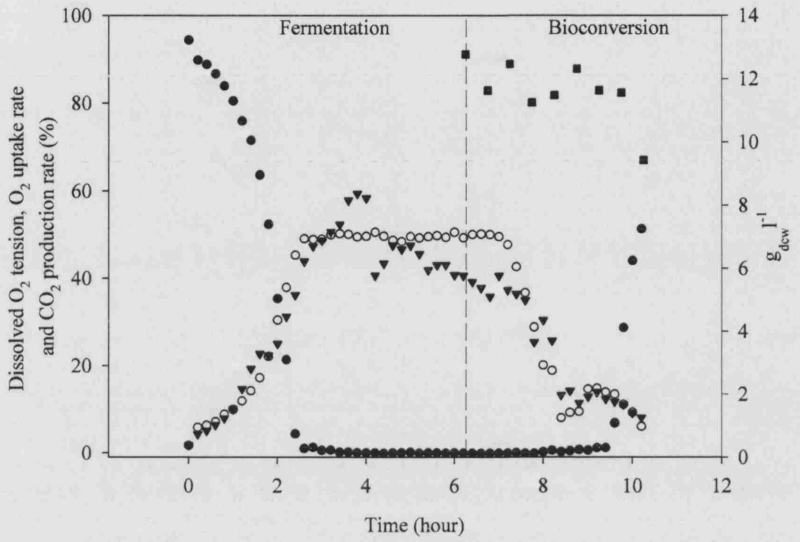

Figure 6.10: Fermentation and bioconversion profiles; DOT, '●', OUR, '○', CPR, '▼' and dry cell weight, '■'.

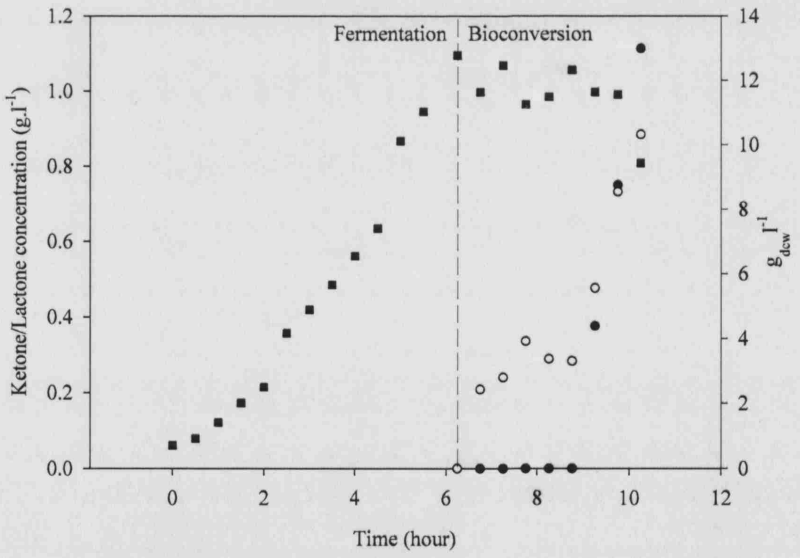

Figure 6.11: Amount of substrate consumed, '●' and product formed, '○' and biocatalyst (cell) growth, '■' during bioconversion.

molecular carbon dioxide formed began to cease as well as the uptake of oxygen in the vessel. The growth of the cell then gradually decreased and reached a plateau for approximately 3 hour and it was then started to lyse.

The substrate bioconversion was also affected from the lack of glycerol in the medium. The reaction proceeded normally for a period of 3 hours before the concentration of substrate in the bioreactor began to increase. Nevertheless, the concentration of product continued to rise. Such a result is observed due to the remaining free enzyme that exists in the medium from the lysed cells. A steady amount of product formed should be expected if the reaction was prolonged for another 5 hours until the enzyme lost its activity from the effect of increasing of pH in the medium.

The rate of glycerol consumption during the bioconversion of substrate could only be determined by adding a known amount of pure glycerol before a reaction starts. This would replenish the remaining glycerol in the vessel from the cell fermentation. $10g{\cdot}l^{-1}$ of glycerol was added in this experiment and the reaction proceeded by feeding the substrate into the bioreactor. *Figure 6.12* shows the profile of the biocatalyst fermentation, and after about 6 hours, it captured the profile for the bioconversion of ketone. A sudden drop was observed for the oxygen uptake rate and the rate of production of carbon dioxide. However the dissolved oxygen tension in the vessel remained at a very low value during the fermentation and it remained until the end of the bioconversion. The cell growth was also increased during both processes, where the value increased by $4g_{dcw}l^{-1}$ from the previous experiment.

In addition to the plot of substrate and product concentrations from the reaction shown in *Figure 6.13*, the activity of the CHMO enzyme during the reaction is also included. The plot clearly shows the effect of the substrate and product towards the enzyme. As depicted in the figure, the CHMO activity began to decrease right after the feeding of substrate into the bioreactor. Such results imply that the stability of CHMO-enzyme is affected by the presence of both substrate and product, where in most biocatalytic reactions, the enzyme or rather the biocatalyst should remain stable in a longer period of time in order to achieve a considerable yield from the reaction. However, in the whole-cell biocatalytic system, where enzyme is believed to be protected by the cellular membrane, the statement could not be the only reason that can

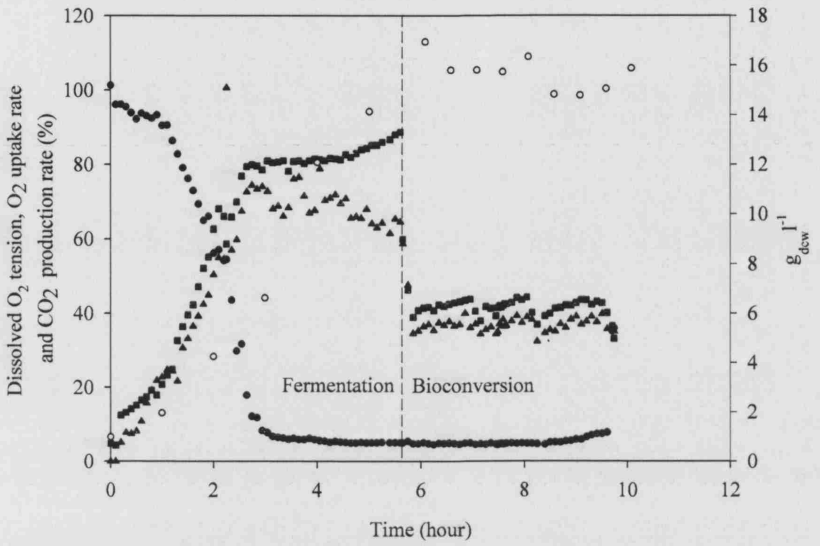

Figure 6.12: Fermentation and bioconversion profiles; DOT, '•', OUR, '■', CPR, '▲' and dry cell weight, '○' with $10g{\cdot}l^{-1}$ added glycerol.

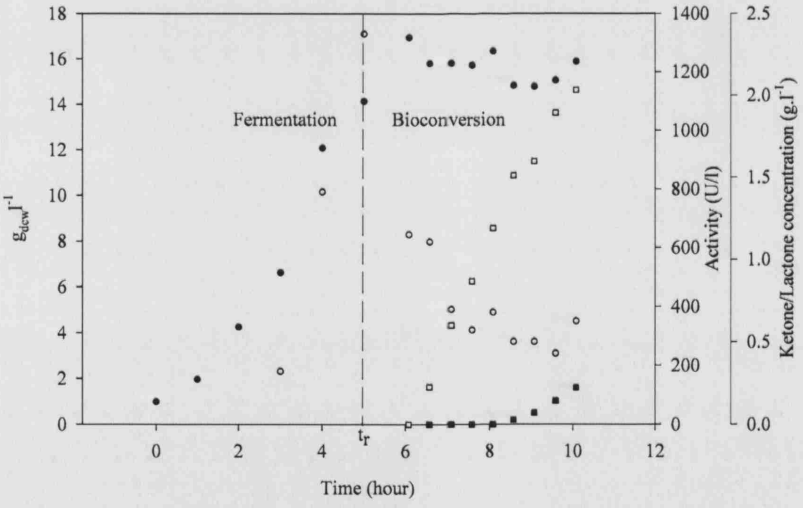

Figure 6.13: Bioconversion of substrate '■' with the added glycerol (cell density '•', product concentration '□' and enzyme activity '○').

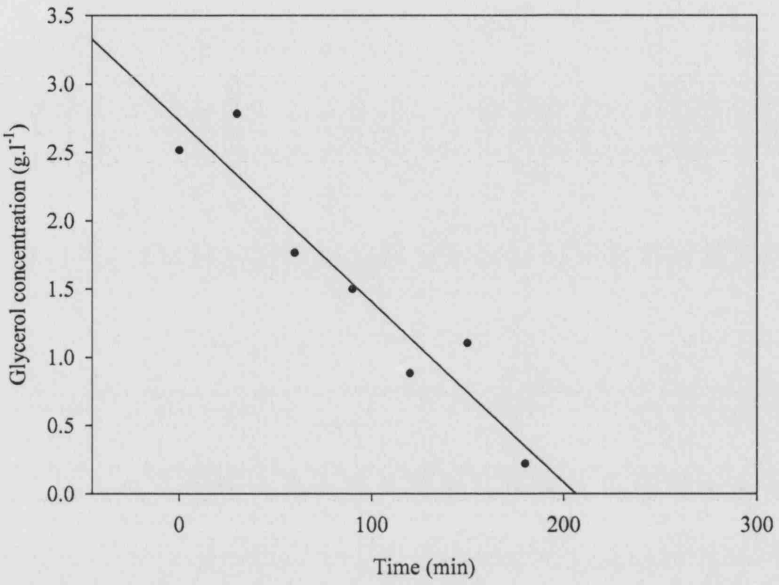

Figure 6.14: Rate of glycerol consumption during substrate bioconversion.

describe the low value of activity of the particular enzyme. In a living organism, where the source of carbon is an important component used to maintain the growth, lacking of such a component could only lead to the cell "*starvation*" and consequently death. This however would not give a direct impact to the enzyme, instead, the system that generates the cofactor for the bioconversion reaction will first be affected. This consequently restricts the enzyme-substrate binding and thus, reduction in enzyme's activity as the reaction progresses.

When the enzyme has no catalytic reaction towards the substrate, the component began to accumulate in the bioreactor. The gradually fed substrate remained at lower values for almost 2 hours before it started to increase. The product however, maintained at its rate of formation throughout the reaction from the remaining cofactor and the substrate-bound enzyme until the amount of glycerol completely disappeared from the media. The plot of glycerol consumption is given in *Figure 6.14* and the rate of $3g{\cdot}l^{-1}h^{-1}$ was determined.

With the value of the rate of glycerol consumption, three other experiments were conducted. These include, the bioconversion of ketone at the feeding rate of glycerol below the given value;

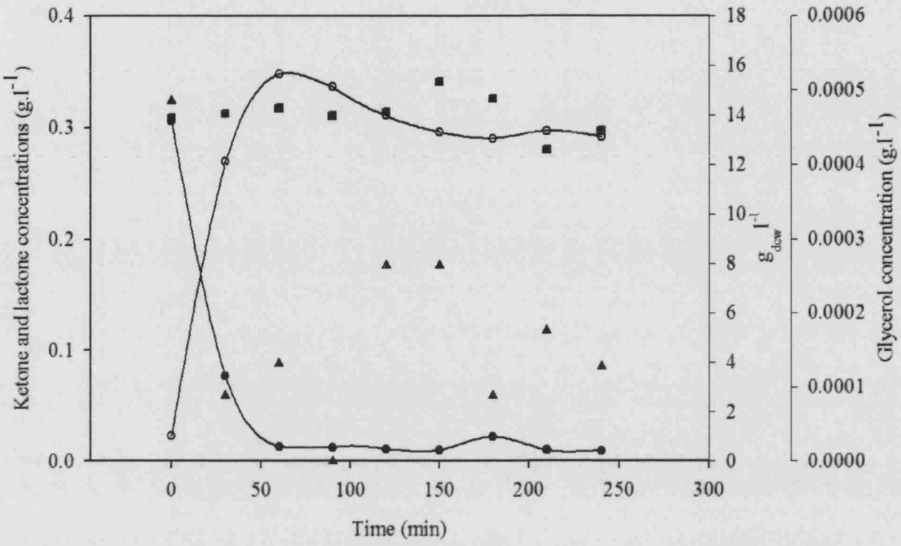

Figure 6.15: Plot of bioconversion; substrate, '•', product, '○', cell growth, '■' and glycerol concentration, '▲' below the rate of glycerol consumption.

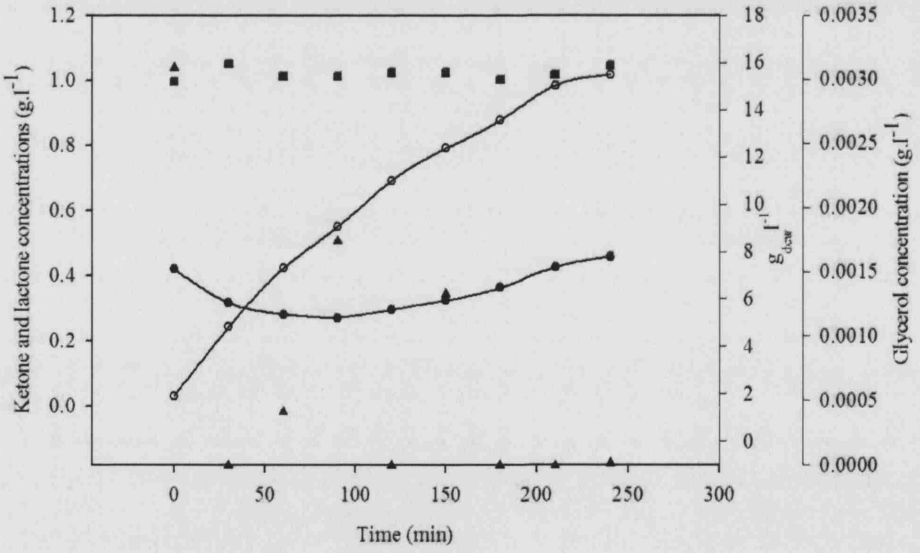

Figure 6.16: Plot of bioconversion; substrate, '•', product, '○', cell growth, '■' and glycerol concentration, '▲' at the rate of glycerol consumption.

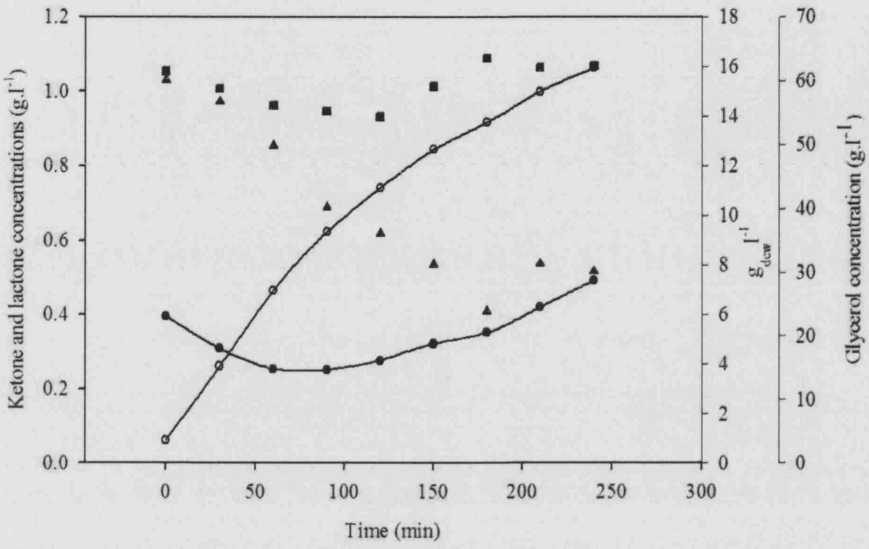

Figure 6.17: Plot of bioconversion; substrate, '•', product, '○', cell growth, '■' and glycerol concentration, '▲' higher than the rate of glycerol consumption.

at the value it is consumed during a bioconversion and finally at a higher rate than the rate it is consumed during a bioconversion. This will provide a complete outcome between the amount of product formed from the reaction and the condition of the cell throughout the process. The relationship between the main Baeyer-Villiger reaction mechanism and the cofactor regeneration system can then be confirmed.

Figure 6.15 shows the result of the first experimental data with glycerol feeding rate below the rate it is consumed. This suggested that the cell was under "*starvation*" during the entire reaction. Lack of glycerol as the carbon source during the reaction does not only affect the growth of the cell, but also the rate of substrate consumption. In order to avoid the effect of substrate inhibition, the rate of substrate feeding was kept below the inhibition point. The figure clearly shows a decrease of substrate to nearly $0g{\cdot}l^{-1}$ from its original batched concentration at the start of the reaction. The product was formed right after the introduction of the substrate into the vessel to a point where it started to level off around $0.3g{\cdot}l^{-1}$. A similar observation was also obtained for the density of the cell in the reaction medium. The initial density of $14g_{dcw}l^{-1}$

remained constant for about 120min of reaction and it started to decrease towards the end of the reaction.

The result obtained from the first experimental data confirmed the connection between the main Baeyer-Villiger reaction and the cofactor regeneration system. It is apparent that the cell utilises the glycerol for two separate purposes; maintaining its growth and behaves as the second substrate in the ADH-enzyme system. Since the amount of glycerol fed into the bioreactor is such that below the rate of it being consumed in a *rich* glycerol reaction, therefore, a balanced system could not be achieved. The reaction also produced a rather small amount of product during the entire process and it reached the steady-state after about 150min of reaction.

The graph plotted in *Figure 6.16* shows the result of reaction performed by feeding the glycerol at its consumption rate. A major different particularly in the amount of product formed can be seen from this plot compared to the plot given in the previous figure. Almost all glycerol fed into the vessel was consumed during the reaction. A sufficient amount of glycerol resulted in a stable cell density throughout the reaction and this provided a steady increase of product to nearly $1.0 g \cdot l^{-1}$. The experiment clearly shows that a good yield of product can be achieved only when a sufficient amount of glycerol is provided for the reaction.

With the two experiments described above, a conclusion can be made regarding the effect of glycerol in Baeyer-Villiger reaction. But there is another problem that one might ask about the state of the cell. Since the rate of glycerol in the second experiment is only sufficient for the reaction, therefore, the cell can only maintain at the same density for certain period of time. No further growth was observed from the condition specified in the second experiment. Therefore, in order to change the behaviour of the cell so that it can continuously produce new cells for bioconversion, an excess amount of glycerol was used in the third experiment.

Figure 6.17 shows a slight increase of the cell density for the reaction in an excess glycerol concentration. $10 g \cdot l^{-1} h^{-1}$ of glycerol feeding rate was used in the bioconversion reaction and with such a high concentration, its gradual depletion could be clearly observed from the same plot. Product formation appeared to be similar to that of the second experimental result, however, towards the end of the 250min reaction, the product seemed to show a further increase compared to that of the second reaction.

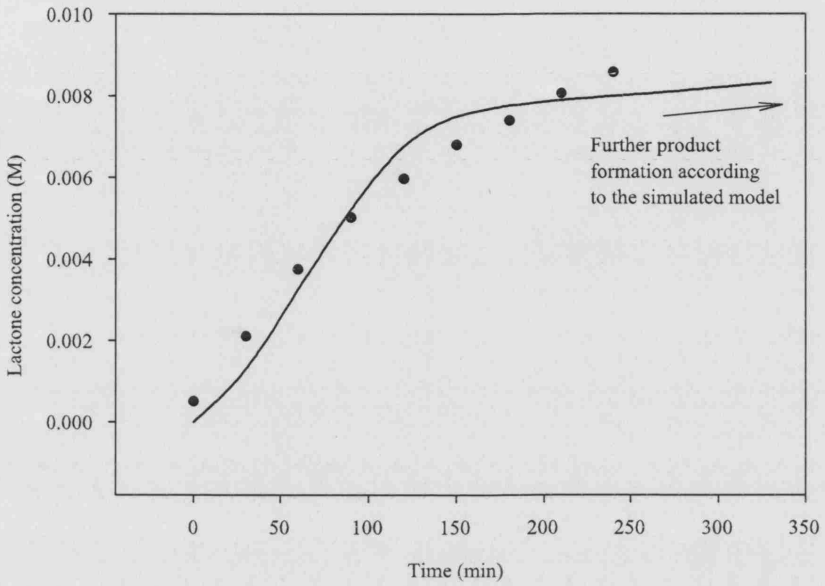

Figure 6.18: Comparing the shape of the experimental data with the simulated model of bienzymatic reaction; data point, '•' and simulated line, '–' for reaction with excess glycerol.

Form the results of the three experiments discussed above, it is apparent that the cofactor regeneration system is entirely governed by the amount of carbon source supplied during the reaction. Insufficient amount of such a component will gradually terminate the reaction, which result has been investigated in this work in order to closely link the termination of the ADH enzyme-catalysed system with the main Baeyer-Villiger reaction. However, a close comparison between the experimental data and the simulated lines still could not be made. This is entirely due to the unavailability of the pure form of CHMO enzyme and the pure form of the enzymatic-lactone ((-)1(R)5(S)3-oxabicyclo[3.3.0]-oct-6-en-2-one) to undergo the isolated enzyme reaction. The data is important for curve fittings of equations (6.1) and (6.2). Comparisons can only be based on the shape of curves of such studies which is plotted in *Figure 6.18.*

6.4 Stability Analysis

The stability of an enzyme-catalysed system has been clearly defined in *Chapter 2.* A similar analysis was carried out using the system of cofactor regeneration in the Baeyer-Villiger reaction. There are two main objectives of this theoretical work; firstly, to look at the interaction of the coupled reaction and secondly, to investigate the multiplicity of the steady-state conditions which could lead to system's instability and bifurcation.

The system described by the ordinary differential equations (6.14) is found to be highly nonlinear and multiple steady states could exist as a result of the nonlinearity. A flowchart that explains the stability study of the system is shown in *Figure 6.19.* The first three main boxes from the left hand corner of the diagram have been completely defined and studied. The remaining 2 will be analysed in this particular section. Due to its high nonlinearity, the trivial solution of the 5–dimensional equations is not possible. The method of linearisation explained by Verhulst (1985) was applied to the system where the final equations were analysed in the neighbourhood of an equilibrium solution. The system was initially expanded via Taylor series expansion and only linear variables from the expansion were considered.

A general Taylor expansion of 5–dimensional ordinary differential equations is given below;

$$\dot{X}_i = f(\dot{x}_i) = f(\dot{x}_0) + \frac{(\dot{x}_i - \dot{x}_0)}{1!} f'(\dot{x}_0) + \frac{(\dot{x}_i - \dot{x}_0)^2}{2!} f''(\dot{x}_0) + \ldots + O_n \dot{x}_0^n \qquad (6.15)$$

$$i = 1, 2, \ldots, n, \text{ with } n = 5$$

where O_n is the higher order terms, and the full linearised coupled enzyme-catalysed system is listed in the system of equations (6.16);

$$\begin{aligned} \dot{X}_1 &= -x_1 + \frac{Da_1 x_3}{km_{co} + \frac{km_{co}\varphi}{k_{ico_+}} + km_s k_{ico}} \\ \dot{X}_2 &= -x_2 + \frac{Da_1 x_3}{km_{co} + \frac{km_{co}\varphi}{k_{ico_+}} + km_s k_{ico}} \end{aligned}$$

$$
\begin{aligned}
\dot{X}_3 &= \left(\tfrac{1}{2}+\tfrac{T}{2}+\tfrac{T\Gamma Da_2}{\mathscr{M}}\right) \\
&- \left(1+T+\frac{Da_1}{km_{co}+\frac{km_{co}\varphi}{ki_{co_+}}+km_s ki_{co}}-\tfrac{T\Gamma}{\mathscr{M}^2}(\Gamma\varphi Da_2+km_{gly}\varphi Da_2-Da_2\mathscr{M})-\frac{T\Gamma km_{gly}k'_{i_{co+}}\varphi Da_2}{k'_{i_{co}}}\right)x_3 \\
&+ \tfrac{T}{\mathscr{M}^2}\left(\Gamma k'_{m_{co+}}\varphi Da_2+\Gamma\varphi^2 Da_2-\varphi Da_2\mathscr{M}\right)x_4 \\
&- \tfrac{T\Gamma}{ki_{dha}\mathscr{M}}(ki_{gly}k'_{m_{co+}}\varphi Da_2+km_{gly}\varphi^2 Da_2)x_5 \\
\dot{X}_4 &= \tfrac{T\Gamma\varphi Da_2}{\mathscr{M}}+\tfrac{T\Gamma}{\mathscr{M}^2}\left(\Gamma\varphi Da_2+km_{gly}\varphi Da_2-Da_2\mathscr{M}-\frac{km_{gly}k'_{i_{co+}}\varphi Da_2}{k'_{i_{co}}}\right)x_3 \\
&- T\left(1-\tfrac{1}{\mathscr{M}^2}\left[\Gamma k'_{m_{co+}}\varphi Da_2+\Gamma\varphi^2 Da_2-\varphi Da_2\mathscr{M}\right]\right)x_4 \\
&- \tfrac{T\Gamma}{ki_{dha}\mathscr{M}}\left(ki_{gly}k'_{m_{co+}}\varphi Da_2+km_{gly}\varphi^2 Da_2\right)x_5 \\
\dot{X}_5 &= \tfrac{T\Gamma\varphi Da_2}{\mathscr{M}}+\tfrac{T\Gamma}{\mathscr{M}^2}\left(\Gamma\varphi Da_2+km_{gly}\varphi Da_2-Da_2\mathscr{M}-\frac{km_{gly}k'_{i_{co+}}\varphi Da_2}{k'_{i_{co}}}\right)x_3 \\
&+ \tfrac{T}{\mathscr{M}^2}\left(\Gamma k'_{m_{co+}}\varphi Da_2+\Gamma\varphi^2 Da_2-\varphi Da_2\mathscr{M}\right)x_4 \\
&- \tfrac{T\Gamma}{ki_{dha}\mathscr{M}}\left(1+ki_{gly}k'_{m_{co+}}\varphi Da_2+km_{gly}\varphi^2 Da_2\right)x_5
\end{aligned}
\tag{6.16}
$$

where $\mathscr{M}$ represents the terms given by;

$$\mathscr{M} = \Gamma(k'_{m_{co+}}+\varphi)+km_{gly}(k'_{i_{co+}}+\varphi)$$

The lower case k defines the non-dimensional kinetic constants and k' represents the difference between the constants for the cofactor used in the CHMO system and that used in the ADH system. The equations given by system (6.16) are highly complicated, however, the variables involved in the system have been reduced into a linear form.

The stability of this linear system was analysed by determining its eigenvalues. This was carried out by constructing a Jacobian matrix from system (6.16) which generally made up of;

$$
\begin{pmatrix}
\partial_{x_1}\dot{X}_1 & \partial_{x_2}\dot{X}_1 & \partial_{x_3}\dot{X}_1 & \partial_{x_4}\dot{X}_1 & \partial_{x_5}\dot{X}_1 \\
\partial_{x_1}\dot{X}_2 & \partial_{x_2}\dot{X}_2 & \partial_{x_3}\dot{X}_2 & \partial_{x_4}\dot{X}_2 & \partial_{x_5}\dot{X}_2 \\
\partial_{x_1}\dot{X}_3 & \partial_{x_2}\dot{X}_3 & \partial_{x_3}\dot{X}_3 & \partial_{x_4}\dot{X}_3 & \partial_{x_5}\dot{X}_3 \\
\partial_{x_1}\dot{X}_4 & \partial_{x_2}\dot{X}_4 & \partial_{x_3}\dot{X}_4 & \partial_{x_4}\dot{X}_4 & \partial_{x_5}\dot{X}_4 \\
\partial_{x_1}\dot{X}_5 & \partial_{x_2}\dot{X}_5 & \partial_{x_3}\dot{X}_5 & \partial_{x_4}\dot{X}_5 & \partial_{x_5}\dot{X}_5
\end{pmatrix}
\tag{6.17}
$$

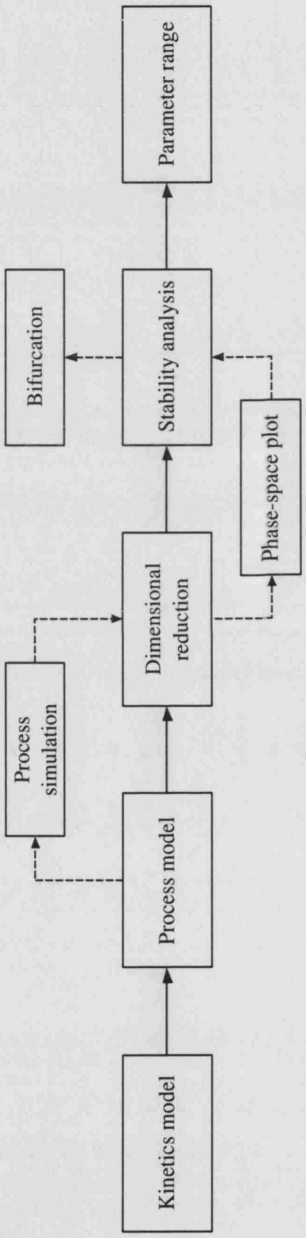

Figure 6.19: Flowchart of stability analysis of CHMO enzyme-catalysed Baeyer-Villiger reaction.

Upon solving the steady-state of system (6.16), solutions of x_1 to x_5 are obtained. With these solutions, the eigenvalues were then determined using the Jacobian matrix given by (6.17). The eigenvalues with the magnitudes of;

$$\lambda_1 < \lambda_2 < \lambda_3 < \lambda_4 < \lambda_5 < 0$$

were obtained, which concludes that around the neighbourhood of this equilibrium point, the system is locally asymptotically stable. The solutions of the trace and determinant of the matrix with the given equilibrium point also obeyed the sufficient conditions for the existence of such a stable behaviour.

The stability of this steady-state can be plotted at different parameter conditions such as the Damköhler numbers of the given system. This will determine whether the system will maintain the stability as the parameter changes. Such a plot will also provide a graphical view of the curve if bifurcation should arise. Two separate plots showing variation of Damköhler numbers of the CHMO system and that of the ADH system are depicted in *Figures 6.20* and *6.21* respectively. These plots were also varied with the dimensionless amount of cofactor, φ available at the beginning of the reaction. The effect could be clearly observed from both figures. *Figure 6.20* shows the four different conditions of φ and their effects toward the product formation as Da_1 gradually increases. At a very low φ, the steady-state values lay around the line of $x = 0$ even when $Da_1 \rightarrow \infty$. This explains that the amount of product formed is highly dependent on the amount of cofactor available at the start of the reaction. As φ increases up to the value of 1.0, the steady-state of x_2 also increases remarkably.

The next plot examines the variation of Da_2 to the steady-state of x_2. Different values of φ were also used in order to observe the effect of different amount of cofactor that existed in each reaction. An obvious different could be seen from *Figure 6.21* when the steady-state points of x_2 started at different values as φ varies. This is due to the high Damköhler number used for the CHMO system, (Da_1). Higher value of Da_1 represents a higher rate of reaction of a system compared to the other, therefore, the reaction tends to go to completion faster compared to that of the second reaction. Both plots also appear to give smooth lines for every condition applied, in other words, the steady-state points reached a plateau as the parameter

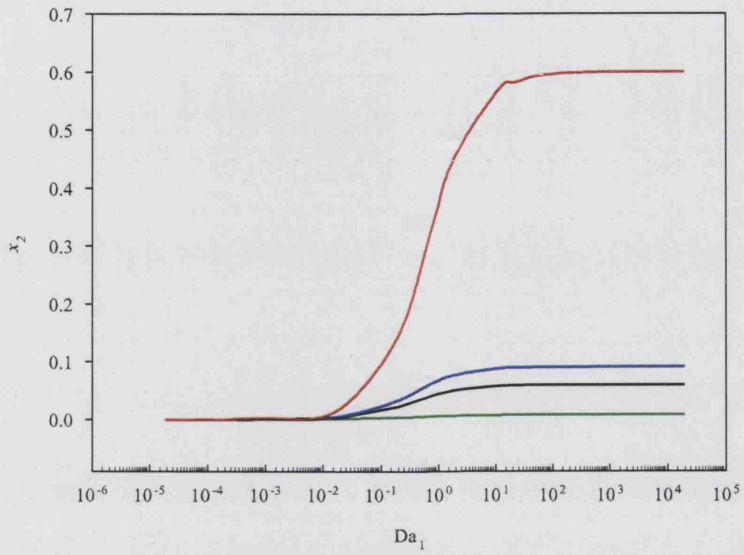

Figure 6.20: Effect of varying Da_1 and φ at constant Da_2 towards product formation (Da_2=1.5×10^{-4}, φ=0.01, '–', φ=0.1, '–', φ=0.15, '–', φ=1.0, '–').

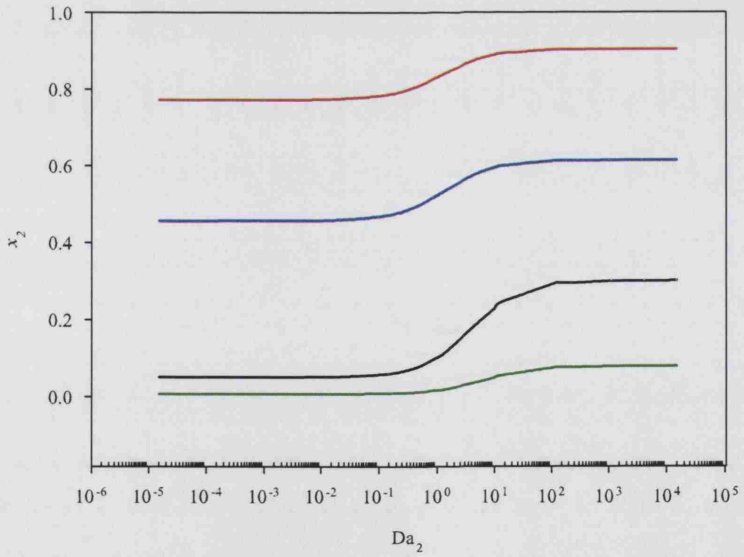

Figure 6.21: Effect of varying Da_2 and φ at constant Da_1 towards product formation (Da_1=1.89, φ=0.01, '–', φ=0.1, '–', φ=1.0, '–', φ=1.89, '–').

was increases. Therefore, it can be concluded that the cofactor regeneration system of enzyme-catalysed Baeyer-Villiger reaction is locally asymptotically stable in spite of its highly nonlinear terms.

6.5 Summary and Conclusion

A theoretical model of the cofactor regeneration system has been completely constructed for reactions involving the CHMO and ADH enzymes catalysing the Baeyer-Villiger reaction. Preliminary experimental work was also performed in order to verify the numerical analysis (which leads to graphical simulations) of the model system. In addition to the modelling work, the system was also analysed for its stability. The analysis was carried out based on the nonlinearity of the system. Generally, a set of nonlinear equations could lead to system's instability, however, the system of coupled Baeyer-Villiger reaction proved otherwise (Hayashi and Sakamoto, 1986).

This study also showed that the whole-cell bioconversion reaction could be maintained as long as there is enough supply of substrate (glycerol) for the cell growth, which at the same time preserves the cofactor recycling. This could be an additional explanation to the complete study by Walton and Stewart (2002, 2004) on the bioconversion using the non-growing *E. coli* cells. However, the key limitation in the whole-cell reaction is the toxicity of the substrate and product. If the cells are exposed too long to either of these components, it could result in cell death and subsequently termination of the oxidation reaction (OShitu, 2005).

Moreover, with this complete model, a reaction involving the membrane diffusion and a detailed bioconversion reaction within the cellular ensemble can then be devised. The method following the work of Sokolichin *et al.* (1997) and Lapin *et al.* (2004) which incorporate the cellular growth with a complete metabolic reaction can be introduced in bioconversion system. The model which was described using the Euler-Lagrange technique could visualise the fluid/substrate motion within a bioreactor. A similar model describing an enzyme-catalysed reaction would be an advantage if the reaction as well as the cell population could be monitored.

Chapter 7

Conclusions and Future Work

This chapter summarises the conclusions that were drawn from the work presented in this thesis and based thereupon some suggestions for future investigations. Critical discussion of the findings and comparison with the initial objectives are also highlighted.

7.1 Conclusions

The kinetics of enzyme-catalysed reaction is entirely based upon the mechanistic route of a particular reaction. Therefore, a thorough analysis on the steps it takes to carry out the reaction is particularly important.

1. A simple mechanism of an enzyme-catalysed reaction was used to perform the analysis, this had led to the suggestion of the new conditions for the validity of the standard quasi steady-state approximation. Upon identifying the reaction mechanism, a kinetic rate expression could be obtained. The form of rate expression however changed when the enzyme was affected by the substrate and product concentrations. A similar analysis on the substrate and product inhibitions failed to give the appropriate results since the set of differential equations resulted in a singular form which led to the incomplete solution. The equations were simplified into a 3–dimensional form and with an aid of bifurcation theory, the change of initial substrate and product concentrations had resulted in different steady-state behaviours of each species involved. These analysis explained the effect of increasing the concentration of substrate towards the formation of product. The effect of product inhibition was also performed as part of the analysis which solutions give rise to bifurcation phenomena. The occurrence of branching of solutions was in the fourth

quadrant in the plot of bifurcation diagram, therefore, such an effect could generally be ignored.

2. Results from the above analysis clearly explained the mechanism of enzyme-catalysed Baeyer-Villiger reaction. The route of the enzyme-catalysed reaction was found to follow the mechanism of the chemical-based conversion. The mechanism was also studied based on the structure of phenylacetone monooxygenase enzyme. The active-sites of this enzyme reflect the active-sites of the cyclohexanone monooxygenase enzyme used in the bioconversion of bicyclic-ketone to chiral lactones. The study concluded with the derivation of cyclohexanone monooxygenase enzyme-catalysed rate expression. The rate expression was found to exhibit a non–competitive type inhibition; a combination of a competitive inhibition with respect to the product concentration and that an un-competitive inhibition with respect to the substrate concentration.

3. A complete rate expression of the reaction was then used to estimate the kinetic parameters that governed the equation. The equation was found to obtain two variables which upon changing these variables resulted in the change of the rate of reaction. Therefore, the normal fitting was not possible. Instead, the method of following the progress curve of the reaction was used. The kinetic parameters; V_{max}, $K_{m_{[Bicyclo]}}$, $K_{m_{[OxaBicyclo]}}$ $K_{i_{[Bicyclo]}}$ and $K_{i_{[OxaBicyclo]}}$ were estimated with the integrated rate expression and the progress curve experimental data.

4. One of the main objectives of this work was to construct a model system of bioconversion of Baeyer-Villiger reaction. This was clearly described in the two different bioreactor configurations; batch and fed-batch bioreactors. Comparison between the model simulations and the appropriate experimental data were made. The discrepancy between the two curves was initially assumed to be due to the effect of diffusion of substrate and product. This was led to the construction of mathematical model with diffusion terms. Characterisation of diffusion based on the Thiele modulus, Φ_s had shown that the effect of diffusion was incredibly small such that the plot of the effectiveness factor lay on the region of the diffusion free reaction. This again conflicted with the proposed unstructured model

of biotransformation of bicyclic-ketone. Such a result is believed to be due to the initial investigation of the kinetics of the reaction. The work based on the enzyme extracted from the lysed *E. coli* cell could be the main cause of such disagreement since the free enzyme was very sensitive to the temperature change, and for monooxygenase enzyme in particular, excess air (oxygen) could lead to the enzyme degradation and lost of activity. These effects would consequently lead to the decrease in the rate of enzyme-catalysed reaction.

5. The final work looked into the effect of cofactor regeneration in the enzyme-catalysed Baeyer-Villiger reaction. The relationship between the main reaction and the reaction that produced the cofactor resulted in a coupled reaction. A set of ordinary differential equations describing the system was constructed and simulated by means of numerical integration. Results shown that the reaction basically depended on the amount of initial cofactor concentration. However, the reaction always returned to the steady-state condition at various amounts of cofactor.

Form the conclusions listed above, it can be summarised that the study of biocatalytic reaction based on the whole-cell catalysis should begin with the analysis of the kinetics of the actual enzyme itself. One should be aware that the kinetics obtained from the whole-cell reaction would not describe the kinetics of the actual enzyme during a reaction. If a reaction involves a substrate that is highly toxic to the cell, the decrease of the rate of reaction is in fact due to the cell death rather than the inhibitory effect of the substrate of a particular enzyme. The kinetic information based on such a system could not be used to describe either the enzyme efficiency or comparing the values to other enzyme-catalysed reactions. A proposed route to achieve a complete model of the whole-cell biocatalysis is given in *Figure 7.1.* The findings obtained from this work are also tabulated and compared between different techniques used.

The comparison presented in the given table could perhaps provide a guidance to further investigate factors such as

- the un-permeated product that was trapped within the membrane cell
- the hydrophobicity characteristic between the substrate and the cell as a result of different molecular charges

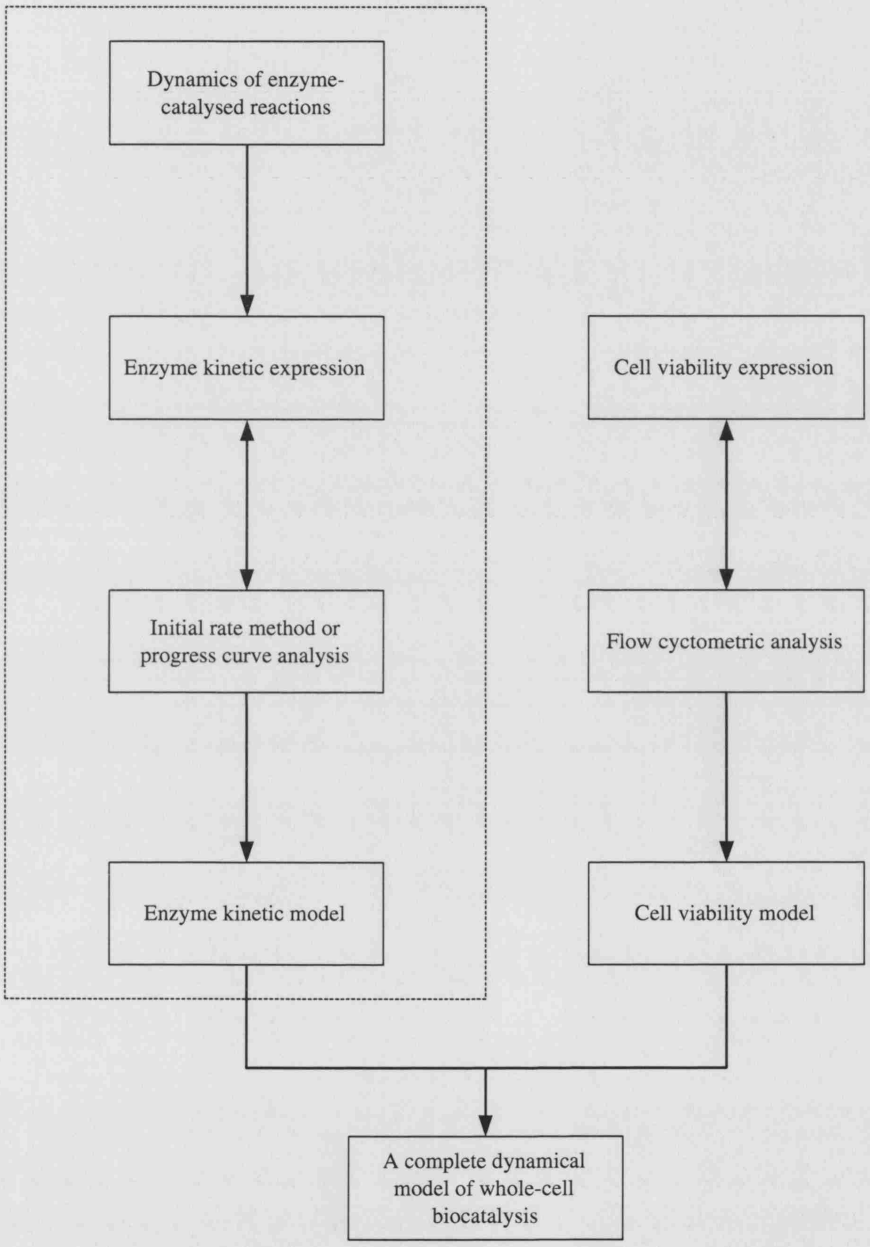

Figure 7.1: Proposed route for modelling of the whole-cell biocatalysis. The dotted box represents the work carried out in this thesis.

Problem	Conditions	Comments
Reaction rate derivation	sQSSA	For $\frac{[E]_T}{[S]_0} \ll 1$, hence, $\frac{d[ES]}{dt} \approx 0$ and for $\frac{[E]_T}{[S]_0} \gg 1$, thus, $\frac{d[ES]}{dt} \neq 0$, and $[ES] < \frac{K_m+[S]_0+[E]_T}{2}$.
	tQSSA	For $\frac{[E]_T}{[S]_0} \ll 1$, hence, $\frac{d[ES]}{dt} \approx 0$ and for $\frac{[E]_T}{[S]_0} \gg 1$, thus, $\frac{d[ES]}{dt} \approx 0$, and $[ES] > \frac{K_m+[S]_0+[E]_T}{3}$.
Enzyme kinetic analysis	Initial rate method	Only applicable for simple one variable rate expressions.
	Progress curve analysis	Applicable for various type of rate expressions up to two variables functions.
Types of modelling techniques	Structured model	Ability to connect different systems within a cellular structure. Important in modelling. of metabolic pathways.
	Unstructured model	Focusing only on a particular reaction. Mainly used to simplify the model of cellular growth. Can be applied for modelling of biochemical reaction. *Black box*[†] type model.
Reaction-diffusion type model	Model incorporating permeability terms of substrate and product	Modelling with ordinary differential equations that described the dynamics of substrate consumption and product formation.
	Model incorporating diffusion terms of substrate and product	3–dimensional type modelling describing both the space and time of substrate and product behaviours. This type of model also relates the diffusion constant to the Thiele modulus which characterises the reaction-diffusion system.

[†]The definition of the *black box* model has been described in Section 4.1.1.

Table 7.1: Summary of the possible problems investigated in modelling of enzyme-catalysed systems.

- insufficient carbon source to regenerate the cofactor as part of the components during bioconversion
- inactive cell (cell death) due to substrate's toxicity which led to the reaction termination

Yet, the present model could not give a detail description of the (whole-cell) CHMO enzyme-catalysed Baeyer-Villiger reaction without considering the above factors. Further improvement of the analytical assay, the kinetic analysis and monitoring of cells viability together with the refinement of the model system should be made in order to obtain a more robust and sensitive system of equations.

7.2 Future Work

Some suggestions for future investigations based on the presented results are made in this section. The main factor that governs the kinetics of industrial-scale biocatalytic reaction has been carefully discussed in this work. Industrial-scale in this context means that the range of substrate concentrations used in a particular bioconversion is by far higher than that in a lab-scale reaction. This has resulted in a different type of Michaelis-Menten model which was termed as the non-Michaelian-typed by Bobe *et al.* (2004) compared to that of the normal hyperbolic curve. The original form of the enzyme-catalysed Baeyer-Villiger rate expression with TER–BI mechanism (cofactor, bicyclic–ketone and molecular oxygen as the *substrates* and the two chiral lactones as the main *products*) could be further studied for a detail kinetics of the system. The analysis however required different assays for each of the substrate participated in the reaction. The result of this study could then explain the effect of the cofactor availability, the substrate toxicity and most importantly, the dissolved molecular oxygen as the main oxidising agent in the reaction.

The experimental set-up during this analysis could however raise some interesting questions. The isolated enzyme used in the kinetic analysis was obtained from the cell lysate, therefore, the reaction could also be affected by other type of enzymes during the course of reaction. A more accurate study of the kinetics of cyclohexanone monooxygenase enzyme could be carried out using a pure enzyme. This should require a thorough investigation on the purification of enzymes to be used in chemical bioconversions so that the results would describe an exact kinetics of the particular reaction.

Finally, the work on the particular cell itself should be undertaken so that a relationship between the effect of substrate and/or product and the cellular system is obtained. The steps are clearly shown on the right hand boxes of *Figure 7.1.* A mathematical function could only be found from the results observed using the flow cytometric technique and these steps should be carried out so that a system of differential equations relating the cellular growth and the amount of substrate used is obtained. A complete model of an industrial-scale whole-cell bioconversion could then be described by integrating these two effects of the enzyme kinetics analysis and the cell viability as shown in *Figure 7.1.*

Bibliography

Agrawal, P., Lee, C., Lim, H. C. and Ramkrishna, D. (1982) Theoretical Investigations of Dynamic Behaviour of Isothermal Continuous Stirred Tank Biological Reactors. *Chemical Engineering Science*, **37**(3), 453–462.

Ahmed, F., Stein, A. and Lye, G. J. (2001) *In situ* Product Removal to Enhance the Yield of Biocatalytic Reactions with Competing Equilibria: α-Glucosidase Catalysed Synthesis of Disaccharides. *Journal of Chemical Technology and Biotechnology*, **76**(9), 971–977.

Ainsworth, S. (1977) *Steady-State Enzyme Kinetics.* The MacMillan Press Ltd. London.

Alphand, V. and Furstoss, R. (1992) Microbiological Transformation 22. Microbiologically Mediated Baeyer-Villiger Reaction: A Unique Route to Several Bicyclic -Lactones in High Enantiomeric Purity. *Journal of Organic Chemistry*, **57**(4), 1306–1309.

Amaral, L. A. N. and Ottino, J. M. (2004) Complex Systems and Networks: Challenges and Opportunities for Chemical and Biological Engineers. *Chemical Engineering Science*, **59**(8–9), 1653–1666.

Aris, R. (1975) *The Mathematical Theory of Diffusion and Reaction in Permeable Catalysts: The Theory of The Steady-State.* Vol. 1 Oxford University Press. London.

Aris, R. and Keller, K. H. (1972) Asymmetries Generated by Diffusion and Reaction, and their Bearing on Active Transport Through Membranes. *Proceedings of National Academy of Sciences of the United States of America*, **69**(4), 777–779.

Aris, Rutherford (1993) Ends and Beginnings in The Mathematical Modelling of Chemical Engineering Systems. *Chemical Engineering Science*, **48**(14), 2507–2517.

Asprey, S. P. (2001) Dynamic Behaviour of Process Systems (Lecture Notes). Technical report Department of Chemical Engineering and Chemical Technology, Imperial College of Science, Technology and Medicine.

Asprey, S. P. and Macchietto, S. (2000) Statistical Tools for Optimal Dynamic Model Building. *Computers & Chemical Engineering*, **24**(2–7), 1261–1267.

Ataai, M. M. and Shuler, M. L. (1985*a*) Simulation of CFSTR Through Development of a Mathematical Model for Anaerobic Growth of *Escherichia coli* Cell Population. *Biotechnology & Bioengineering*, **27**(7), 1051–1055.

Ataai, M. M. and Shuler, M. L. (1985*b*) Simulation of the Growth Pattern of a Single Cell of *Escherichia coli* Under Anaerobic Conditions. *Biotechnology & Bioengineering*, **27**(7), 1027–1035.

Bailey, J. E. (1998) Mathematical Modeling and Analysis in Biochemical Engineering: Past Accomplishments and Future Opportunities. *Biotechnology Progress*, **14**(1), 8–20.

Bailey, J. E. and Ollis, D. F. (1986) *Biochemical Engineering Fundamentals.* second edn McGraw-Hill International Editions.

Baker, J. R. (1966) *Cytological Technique.* fifth edn Wiley & Sons, New York.

Baldwin, C. V. F. and Woodley, J. M. (2005) Oxygen Limitations in a Whole-Cell Biocatalytic Baeyer-Villiger Oxidation Process. *Biotechnology & Bioengineering*, **Submitted.**

Bard, Y. (1974) *Nonlinear Parameter Estimation.* Academic Press Inc. Ltd. London.

Bates, D. J. and Frieden, C. (1973*a*) Full Time Course Studies on the Oxidation of Reduced Coenzyme by Bovine Liver Glutamate Dehydrogenase. Use of Computer Simulation to Obtain Rate and Dissociation Constants. *Journal of Biological Chemistry*, **248**(22), 7885–7890.

Bates, D. J. and Frieden, C. (1973*b*) Treatment of Enzyme Kinetic Data. III. The Use of the Full Time Course of a Reaction, as Examined by Computer Simulation, in Defining Enzyme Mechanisms. *Journal of Biological Chemistry*, **248**(22), 7878–7884.

Beck, J. V. and Arnold, K. J. (1977) *Parameter Estimation in Engineering and Science.* John Wiley & Sons Inc.

Bishop, S. R. and Clifford, M. J. (1996) The Use of Manifold Tangencies to Predict Orbits, Bifurcations and Estimate Escape in Driven Systems. *Chaos Solitons & Fractals*, **7**(10), 1537–1553.

Bobe, I. M., Abdelmoez, W., Ogino, H., Yasuda, M., Ishimi, K. and Ishikawa, H. (2004) Kinetics and Mechanism of a Reaction Catalysed by PST-01 Protease from *Pseudomonas aeruginosa* PST-01. *Biotechnology & Bioengineering*, **86**(3), 365–373.

Boeker, E. A. (1984) Integrated Rate Equations for Enzyme-Catalysed First-Order and Second-Order Reactions. *Biochemical Journal*, **223**(1), 15–22.

Boeker, E. A. (1987) Analytical Methods for Fitting Integrated Rate Equations. A Discontinuous Assay. *Biochemical Journal*, **245**(1), 67–74.

Borghans, J. A. M., DeBoer, R. J. and Segel, L. A. (1996) Extending the Quasi-Steady State Approximation by Changing Variables. *Bulletin of Mathematical Biology*, **58**(1), 43–63.

Bruns, D. D., Bailey, J. E. and Luss, D. (1973) Steady-State Multiplicity and Stability of Enzymatic Reaction Systems. *Biotechnology & Bioengineering*, **15**(6), 1131–1145.

Brusch, L., Cuniberti, G. and Bertau, M. (2004) Model Evaluation for Glycolytic Oscillations in Yeast Biotransformations of Xenobiotics. *Biophysical Chemistry*, **109**(3), 413–426.

Bulmus, V., Kesenci, K. and Piskin, E. (1998) Poly(EGDMA/AAm) Copolymer Beads: A Novel Carrier for Enzyme Immobilization. *Reactive & Functional Polymers*, **38**, 1–9.

Cabral, J. M. S., Aires-Barros, M. R., Pinheiro, H. and Prazeres, D. M. F. (1997) Biotransformation in Organic Media by Enzymes and Whole Cells. *Journal of Biotechnology*, **81**(1), 133–143.

Carbonell, R. G. and Kostin, M. D. (1972) Enzyme Kinetics and Engineering. *AIChE Journal*, **18**(1), 1–12.

Cha, S. (1970) Kinetic Behavior at High Enzyme Concentrations. Magnitude of Errors of Michaelis-Menten and Other Approximations. *Journal of Biological Chemistry*, **245**(18), 4814–4818.

Chang, K. W. and Howes, F. A. (1984) *Nonlinear Singular Perturbation Phenomena: Theory and Applications.* Vol. 56 of *Applied Mathematical Sciences* Springer-Verlag New York.

Chen, A. and Vincent, T. M. (2000) Cross-Linking of Cell Surface Receptors Enhances Cooperativity of Molecular Adhesion. *Biophysical Journal*, **78**, 2814–2820.

Chen, B. H., Doig, S. D., Lye, G. J. and Woodley, J. M. (2002) Modelling of the Baeyer-Villiger Monooxygenase Catalysed Synthesis of Optically Pure Lactones. *Food and Bioproducts Processing*, **80**(C1), 51–55.

Chen, B. H. and Woodley, J. M. (2002) Wavelet Shringkage Data Processing for Neural Networks in Bioprocess Modeling. *Computers & Chemical Engineering*, **26**(11), 1611–1620.

Chen, B. J., Lim, H. C. and Tsao, G. T. (1976) A Model for Bacterial Growth on Methanol. *Biotechnology & Bioengineering*, **18**(11), 1629–1633.

Chen, K-C., Wu, J-Y., Yang, W-B. and Hwang, S-C. J. (2003) Evaluation of Effective Diffusion Coefficient and Instrinsic Kinetic Parameters on Azo Dye Biodegradation Using PVA–Immobilized Cell Beads. *Biotechnology & Bioengineering*, **83**(7), 821–832.

Chow, S. N. and Hale, J. K. (1996) *Methods of Bifurcation Theory.* second edn Springer-Verlag New York.

Chu, C. and Hougen, O. A. (1962) The Effect of Adsorption on the Effectiveness Factor of Catalyst Pellets. *Chemical Engineering Science*, **17**(3), 167–176.

Cleland, W. W. (1963*a*) The Kinetics of Enzyme-Catalysed Reactions with Two or More Substrates or Products: I. Nomenclature and Rate Equations. *Biochimica et Biophysica Acta*, **67**, 104–137.

Cleland, W. W. (1963*b*) The Kinetics of Enzyme-Catalysed Reactions with Two or More Substrates or Products: II. Inhibition: Nomenclature and Theory. *Biochimica et Biophysica Acta*, **67**, 173–187.

Cleland, W. W. (1982) An Analysis of Haldane Relationships. *Methods in Enzymology*, **87**, 366–369.

Cohen, D. S. and Alexander, R. (1986) Chemical Reactor Theory and Problems in Diffusion. *Physica D*, **20**(1), 122–141.

Cornish-Bowden, A. (1995) *Fundamentals of Enzyme Kinetics.* revised edn Portland Press.

Cornish-Bowden, A. and Eisenthal, R. (1974) Statistical Considerations in the Estimation of Enzyme Kinetic Parameters by the Direct Linear Plot and Other Methods. *Biochemical Journal*, **139**(3), 721–730.

Crank, J. (1975) *The Mathematics of Diffusion.* Claradon Press, Oxford.

Crawford, J. D. (1991) Introduction to Bifurcation-Theory. *Reviews of Modern Physics*, **63**(4), 991–1037.

Criegee, V. R. (1948) Die Umlagerung der Dekalin–peroxydester als Folge von Kationischem Sanerstoff. *Justus Liebigs Annals Chem*, **560**(3), 127–135.

Crooke, P. S., Tanner, R. D. and Aris, R. (1979) The Role of Dimensionless Parameters in the Brigg-Haldane and Michaelis-Menten Approximations. *Chemical Engineering Science*, **34**(11), 1354–1357.

Curtis, H. and Barnes, S. N. (1989) *Biology.* fifth edn Worth Publishers, New York.

da Silva, T. L., Reis, A., Kent, C. A., Kosseva, M., Roseiro, J. C. and Hewitt, C. J. (2005) Stress-Induced Physiological Responses to Starvation Periods as Well as Glucose and Lactose Pulses in *Bacillus licheniformis* CCMI 1034 Continuous Aerobic Fermentation Processes as Measured by Multi-Parameter Flow Cytometry. *Biochemical Engineering Journal*, **24**(1), 31–41.

Daniel, R. M., Dunn, R. V., Finney, J. L. and Smith, J. C. (2003) The Role of Dynamics in Enzyme Activity. *Annual Review of Biophysics and Biomolecular Structure*, **32**, 69–92.

Dhooge, A., Govaerts, W. and Kuznetsov, Y. A. (2003) MATCONT: A MATLAB® Package for Numerical Bifurcation Analysis of ODE's. *ACM Transaction on Mathematical Software*, **29**(2), 141–164.

Dilthey, W., Inckel, M. and Stephan, H. (1940) Die Oxydation der Ketone mit Perhydrol. *Journal Praktical Chemistry*, **154**(6–10), 219–237.

Doering, W. v. E. and Dorfman, E. (1953) Mechanism of the Peracid Ketone-Ester Conversion. Analysis of Organic Compounds for Oxygen-18. *Journal of American Chemical Society*, **75**, 5595–5598.

Doering, W. v. E. and Speers, L. (1950) Baeyer-Villiger Reaction Mechanism II. *Journal of American Chemical Society*, **72**, 5515–5518.

Doig, S. D., Avenell, P. J., Bird, P. A., Gallati, P., Lander, K. S., Lye, G. J., Wohlgemuth, R. and Woodley, J. M. (2002) Reactor Operation and Scale-Up of Whole Cell Baeyer-Villiger Catalysed Lactone Synthesis. *Biotechnology Progress*, **18**(5), 1039 – 1046.

Doig, S. D., O'Sullivan, L. M., Patel, S., Ward, J. M. and Woodley, J. M. (2001) Large Scale Production of Cyclohexanone Monooxygenase from *Escherichia coli* TOP10[pQR239]. *Enzyme and Microbial Technology*, **28**, 265–274.

Duggleby, R. G. (1995) Analysis of Enzyme Progress Curve by Nonlinear Regression. *Method in Enzymology*, **249**, 61–90.

Duggleby, R. G. (2001) Quantitative Analysis of the Time Courses of Enzyme-Catalysed Reactions. *Methods*, **24**, 168–174.

Duggleby, R. G. and Morrison, J. F. (1977) The Analysis of Progress Curves for Enzyme-Catalysed Reactions by Non-Linear Regression. *Biochimica et Biophysica Acta*, **481**, 297–312.

Duggleby, R. G. and Morrison, J. F. (1978) Progress Curve Analysis in Enzyme Kinetics Model Discrimination and Parameter Estimation. *Biochimica et Biophysica Acta*, **526**, 398–409.

Duggleby, R. G. and Wood, C. (1989) Analysis of Progress Curve for Enzyme-Catalysed Reactions: Automatic Construction of Computer Programs for Fitting Integrated Rate Equations. *Biochemical Journal*, **258**(2), 397–402.

Dunn, I. J., Heinzle, E., Ingham, J. and Prenosil, J. E. (1992) *Biological Reaction Engineering: Principles, Applications and Modelling with PC Simulation.* VCH Verlagsgesellschaft mbH Germany.

Dunn, I. J. and Mor, J. R. (1975) Variable Volume Continuous Cultivation. *Biotechnology & Bioengineering*, **17**, 1805–1822.

Eckstein, M., Daußmann, T. and Kragl, U. (2004) Recent Developments in NAD(P)H Regeneration for Enzymatic Reductions in One– and Two–Phase Systems. *Biocatalysis and Biotransformation*, **22**(2), 89–96.

Eisenthal, R. and Cornish-Bowden, A. (1974) A New Graphical Procedure for Estimating Enzyme Kinetic Parameters. *Biochemical Journal*, **139**(3), 715–720.

Epstein, I. R. (1984) Complex Dynamical Behaviour in "Simple" Chemical Systems. *Journal of Physical Chemistry*, **88**(1), 187–198.

Esterl, S., Özmutlu, Ö., Hartmann, C. and Delgado, A. (2003) Three–Dimensional Numerical Approach to Investigate the Substrate Transport and Conversion in an Immobilized Enzyme Reactor. *Biotechnology & Bioengineering*, **83**(7), 780–789.

Fernley, H. N. (1974) Statistical Estimations in Enzyme Kinetics: The Integrated Michaelis Equation. *European Journal of Biochemistry*, **43**, 377–378.

Fraser, S. J. (1988) The Steady-State and Equilibrium Approximations: A Geometrical Picture. *Journal of Chemical Physics*, **88**(8), 4732–4738.

Frieden, C. (1994) Analysis of Kinetic Data: Practical Applications of Computer Simulation and Fitting Programs. *Methods in Enzymology*, **240**, 311–322.

Fritsch, F. N., Shafer, R. E. and Crowley, W. P. (1973) Solution of the Transcendental Equation $\omega e^{\omega} = x$. *Communications of the ACM*, **16**(2), 123–124.

Garcia, T., Coteron, A., Martinez, M. and Aracil, J. (1996) Kinetic Modelling of Esterification Reactions Catalysed by Immobilised Lipases. *Chemical Engineering Science*, **51**(11), 2841–2846.

Gerlich, D., Beaudouin, J., Gebhard, M., Ellenberg, J. and Eils, R. (2001) Four-Dimensional Imaging and Quantitative Reconstruction to Analyse Complex Spatiotemporal Processes in Live Cells. *Nature: Cell Biology, Macmillan Magazine Ltd.*, **3**, 852–855.

Gheber, L. A. and Edidin, M. (1999) A Model for Membrane Patchiness: Lateral Diffusion in the Presence of Barriers and Vesicle Traffic. *Biophysical Journal*, **77**(6), 3163–3175.

Goudar, C. T., Sonnad, J. R. and Duggleby, R. G. (1999) Parameter Estimation Using a Direct Solution of the Integrated Michaelis-Menten Equation. *Biochimica et Biophysica Acta*, **1429**, 377–383.

Gu, Z. M., Nefedov, N. N. and Omalley, R. E. (1989) On Singular Singularly Perturbed Initial-Value Problems. *Siam Journal on Applied Mathematics*, **49**(1), 1–25.

Guckenheimer, J. and Holmes, P. (2002) *Nonlinear Oscillations, Dynamical Systems, and Bifurcations of Vector Fields*. Vol. 42 of *Applied Mathematical Sciences* seventh edn Springer-Verlag New York Inc. New York.

Halling, P. J., Wilson, S. K., Jacobs, R., McKee, S. and Coles, C. W. (2003) Modeling the Kinetics of Enzymic Reactions in Mainly Solid Reaction Mixtures. *Biotechnology Progress*, **19**(4), 1228–1237.

Hatzimanikatis, Vassily and Bailey, James E. (1997) Studies on Glycolysis – I. Multiple Steady-States in Bacterial Glycolysis. *Chemical Engineering Science*, **52**(15), 2579–2588.

Hayashi, K. and Sakamoto, N. (1986) *Dynamic Analysis of Enzyme Systems: An Introduction*. Japan Scientific Societies Press and Springer-Verlag.

Heineken, F. G., Tsuchiya, H. M. and Aris, R. (1967) On the Mathematical Status of the Pseudo-Steady State Hypothesis of Biochemical Kinetics. *Mathematical Bioscience*, **1**(1), 95–113.

Hewitt, C. and Petit, P. X. (2004) Scientific Tutorial III. Cytometric Measurements of Micro-Organisms. *Cytometry Part A*, **59A**(1), 27–27.

Higgins, J. (1967) The Theory of Oscillating Reactions. *Industrial and Engineering Chemistry*, **59**(5), 18–62.

Hogan, M. C. and Woodley, J. M. (2000) Modelling of Two Enzyme Reactions in a Linked Cofactor Recycle System for Chiral Lactone Synthesis. *Chemical Engineering Science*, **55**(11), 2001–2008.

Hogben, C. A. M. (1960) Movement of Material Across Cell Membranes. *The Physiologist*, **3**(4), 56–62.

Hölzel, R. (1999) Non-invasive Determination of Bacterial Single Cell Properties by Electrorotation. *Biochimica et Biophysica Acta*, **1450**, 53–60.

Howard, M., Rutenberg, A. D. and de Vet, S. (2001) Dynamic Compartmentalization of Bacteria: Accurate Division in *E coli*. *Physical Review Letters*, **87**(27), 1–4.

Keener, J. and Sneyd, J. (1998) *Mathematical Physiology* Vol. 8 of *Interdisciplinary Applied Mathematics*. Springer-Verlag. New York.

Keller, H. B. and Dunn, I. J. (1978*a*) Fed–Batch Microbial Culture: Models, Errors and Applications. *Journal of Applied Chemistry and Biotechnology.*, **28**(7), 508–514.

Keller, R. and Dunn, I. J. (1978*b*) Computer Simulations of the Biomass Production Rate of Cyclic Fed Batch Continuous Culture. *Journal of Applied Chemistry and Biotechnology.*, **28**(11), 784–790.

Kelly, D. R. (1996) A Proposal for The Origin of Stereoselectivity in Enzyme Catalysed Baeyer-Villiger Reactions. *Tetrahedron: Asymmetry*, **7**(4), 1149–1152.

King, E. L. and Altman, C. (1956) A Schematic Method of Deriving the Rate Laws for Enzyme-Catalysed Reactions. *Journal of Physical Chemistry*, **60**(10), 1375–1378.

Kuchel, P. W. and Gregory, B. R. (1988) *Theory and Problems of Biochemistry*. Schaum's Series, McGraw-Hill Publishers, New York.

Kurtanjek, Z. (1994) Modeling And Control by Artificial Neural Networks in Biotechnology. *Computers & Chemical Engineering*, **18**(Suppl.), S627–S631.

Ladero, M., Santos, A., Garcia, J. L. and Garcia-Ochoa, F. (2001) Activity Over Lactose and ONPG of a Genetically Engineered β-Galactosidase From *Escherichia coli* in Solution and Immobilised: Kinetic Modelling. *Enzyme and Microbial Technology*, **29**, 181–193.

Lapin, A., Muller, D. and Reuss, M. (2004) Dynamic Behavior of Microbial Populations in Stirred Bioreactors Simulated with Euler-Lagrange Methods: Traveling Along the Lifelines of Single Cells. *Industrial & Engineering Chemistry Research*, **43**(16), 4647–4656.

Lee, D-C., Park, J-H., Kim, G-J. and Kim, H-S. (1999) Modeling, Simulation, and Kinetic Analysis of a Heterogeneous Reaction System for the Enzymatic Conversion of Poorly Soluble Substrate. *Biotechnology & Bioengineering*, **64**(3), 272–283.

Lewis, G., Taylor, I. W., Nienow, A. W. and Hewitt, C. J. (2004) The Application of Multi-Parameter Flow Cytometry to the Study of Recombinant *Escherichia coli* Batch Fermentation Processes. *Journal of Industrial Microbiology & Biotechnology*, **31**(7), 311–322.

Liese, A. and Filho, M. V. (1999) Production of Fine Chemicals Using Biocatalysis. *Current Opinion in Biotechnology*, **10**(6), 595–603.

Lim, H. C. (1973) On Kinetic Behaviour at High Enzyme Concentrations. *AIChE Journal*, **19**(3), 659–661.

Lyberatos, G., Kuszta, B. and Bailey, J. E. (1985*a*) Bifurcation From the Potential Field Analog of Some Chemical Systems. *Chemical Engineering Science*, **40**(9), 1679–1687.

Lyberatos, G., Kuszta, B. and Bailey, J. E. (1985*b*) Normal Forms for Chemical Reaction Systems via the Affine Transformation. *Chemical Engineering Science*, **40**(2), 199–208.

Lyberatos, G., Kuszta, B. and Bailey, J. E. (1985*c*) Versal Matrix Families, Normal Forms and Higher Order Bifurcations in Dynamic Chemical Systems. *Chemical Engineering Science*, **40**(7), 1177–1189.

Lye, G. J. and Woodley, J. M. (1999) Application of *In situ* Product–Removal Techniques to Biocatalytic Processes. *Trends in Biotechnology*, **17**(10), 395–402.

Malito, E., Alfieri, A., Fraaije, M. W. and Mattevi, A. (2004) Crystal Structure of a Baeyer-Villiger Monooxygenase. *Proceeding of the National Academy of Science of the United States of America*, **101**(36), 13157–13162.

Marquardt, D. W. (1963) An Algorithm for Least-Squares Estimation of Non-Linear Parameters. *Journal of The Society for Industrial and Applied Mathematics*, **11**(2), 431–441.

Martinez, M. B., Schendel, F. J., Flickinger, M. C. and Nelsestuen, G. L. (1992) Kinetic Properties of Enzyme Populations in Vivo: Alkaline Phosphatase of the Escherichia coli Periplasm. *Biochemistry*, **31**(46), 11500–11509.

Marx, A., Hewitt, C. J., Grewal, R., Scheer, S., Vandre, K., Pfefferle, W., Kossmann, B., Ottersbach, P., Beimfohr, C., Snaidr, J., Auge, C. and Reuss, M. (2003) Use of Cytometry of Biotechnology. *Chemie Ingenieur Technik*, **75**(5), 608–614.

MathWorks, Inc. (1993–2001) *Optimization Toolbox User's Guide for MATLAB®*. Vol. Version 3 The MathWorks Inc. Massachusetts.

Michaelis, L. and Menten, M. (1913) Die Kinetik der Invertinwirkung. *Biochem. Z.*, **49**, 333–369.

Montague, G. and Morris, J. (1994) Neural-Network Contributions in Biotechnology. *Trends in Biotechnology*, **12**(8), 312–324.

Murray, J. D. (2002) *Mathematical Biology*. Vol. 17 of *Interdisciplinary Applied Mathematics*. third edn Springer-Verlag. Berlin.

Nelder, J.A. and Mead, R. (1965) A Simplex Method for Function Minimisation. *Computing Journal*, **7**, 308–313.

Nguyen, A. N. and Fraser, S. J. (1989) Geometrical Picture of Reaction in Enzyme Kinetics. *Journal of Chemical Physics*, **91**(1), 186–193.

Nielsen, Jens and Villadsen, John (1992) Modelling of microbial kinetics. *Chemical Engineering Science*, **47**(17-18), 4225–4270.

Nikaido, H. and Rosenberg, E. Y. (1981) Effect of Solute Size on Diffusion Rates through the Transmembrane Pores of the Outer Membrane of *Escherichia coli*. *Journal of General Physiology*, **77**(2), 121–135.

Nimmo, I. A. and Atkins, G. L. (1974) A Comparison of Two Methods for Fitting the Integrated Michaelis-Menten Equation. *Biochemical Journal*, **141**(1), 913–914.

Ochoa, J. A., Stroeve, P. and Whitaker, S. (1986) Diffusion and Reaction in Cellular Media. *Chemical Engineering Science*, **41**(12), 2999–3013.

Ochoa, J. A., Whitaker, S. and Stroeve, P. (1987) Determination of Cell Membrane Permeability in Concentrated Cell Ensembles. *Biophysical Journal*, **52**(5), 763–774.

Ocone, R. and Kummer, A. (2002) When the Curves don't Fit. *The Chemical Engineers*, (729), 38–39.

OShitu, J. (2005) The Use of Multiparameter Flow Cyctometry to Examine the State of *Escherichia coli* During a Bioprocess. PhD thesis University College London.

Ottolina, G., Carrea, G., Colonna, S. and Ruckemann, A. (1996) A Predictive Active Site Model for Cyclohexanone Monooxygenase Catalysed Baeyer-Villiger Oxidations. *Tetrahedron: Asymmetry*, **7**(4), 1123–1136.

Palsson, B. O. (1987) On the Dynamics of the Irreversible Michaelis-Menten Reaction Mechanism. *Chemical Engineering Science*, **42**(3), 447–458.

Pereira, D. A., Pinto, G. F. and Oestreicher, E. G. (1994) Kinetic Mechanism of the Oxidation of 2-propanol Catalysed by *Thermoanaerobium brockii* Alcohol Dehydrogenase. *Journal of Biotechnology*, **34**(1), 43–50.

Perry, R. H. and Chilton, C. H. (1993) *Chemical Engineers' Handbook* seventh edn McGraw-Hill New York.

Peters, R. and Kubitscheck, U. (1999) Scanning Microphotolysis: Three-Dimensional Diffusion Measurement and Optical Single-Transporter Recording. *Methods*, **18**(4), 508–517.

Phair, R. D. and Misteli, T. (2001) Kinetic Modelling Approaches to *in vivo* Imaging. *Nature Reviews: Molecular Cell Biology, Macmillan Magazine Ltd.*, **2**, 898–907.

Plimpton, S. J. and Slepoy, A. (2005) Microbial Cell Modelling via Reacting Diffusive Particles. *Journal of Physics: Conference Series*, **16**, 305–309.

Renkin, E. M. (1954) Filtration, Diffusion and Molecular Sieving Through Porous Cellulose Membrane. *Journal of General Physiology*, **38**, 225–243.

Renz, M. and Meunier, B. (1999) 100 Years of Baeyer-Villiger Oxidations. *European Journal of Organic Chemistry*, (4), 737–750.

Robert, H. (1999) *Membrane: The Facts on File Dictionary of Biology.* third edn Checkmark, New York.

Roberts, G. W. and Satterfield, C. N. (1965) Effectiveness Factor for Porous Catalysts: Langmuir-Hinshelwood Kinetic Expressions. *Industrial & Chemistry Engineering (Fundamentals).*, **4**(3), 288–293.

Roberts, G. W. and Satterfield, C. N. (1966) Effectiveness Factor for Porous Catalysts: Langmuir-Hinshelwood Kinetic Expressions for Bimolecular Surface Reactions. *Industrial & Chemistry Engineering (Fundamentals).*, **5**(3), 317–325.

Rodriguez-Lopez, J. N., Fenoll, L. G., Garcia-Ruiz, P. A., Varon, R., Tuleda, J., Thorneley, R. N. F. and Garcia-Canovas, F. (2000) Stopped-Flow and Steady-State Study of the Diphenolase Activity of Mushroom Tyrosinase. *Biochemistry*, **39**(34), 10497–10506.

Roussel, M. R. and Fraser, S. J. (1990) Geometry of the Steady-State Approximation: Perturbation and Accelerated Convergence Methods. *Journal of Chemical Physics*, **93**(2), 1072–1081.

Roussel, M. R. and Fraser, S. J. (1991) On the Geometry of Transient Relaxation. *Journal of Chemical Physics*, **94**(11), 7106–7113.

Roussel, M. R. and Fraser, S. J. (1993) Global Analysis of Enzyme Inhibition Kinetics. *Journal of Physical Chemistry*, **97**(31), 8316–8327.

Roux, J-C. (1993) Dynamical System Theory Illustrated: Chaotic Behaviour in the Belousov–Zhabotinsky Reaction. *in* R. J.Field and L.Györgyi, eds, 'Chaos in Chemistry and Biochemistry' World Scientific pp. 21–46.

Rozzell, J. D. (1999) Commercial Scale Biocatalysis: Myths and Realities. *Bioorganic & Medicinal Chemistry*, **7**, 2253–2261.

Ruzicka, L. and Stoll, M. (1928) Über die Oxydation der 13–bis 17–gliedrigen Monocyclischen Ketone mit Caro'scher Säure zu den 14–bis 18–gliedrigen Lactonen. *Helvetica Chimie Acta*, **11**(1), 1159–1173.

Ryerson, C. C., Ballou, D. P. and Walsh, C. (1982) Mechanistic Studies on Cyclohexanone Oxygenase. *Biochemistry*, **21**(11), 2644–2655.

Santoyo, A. B., Carrasco, J. L. G., Gomez, E. G., Rodriguez, J. B. and Morales, E. M. (1993) Transient Stirred-Tank Reactors Operating with Immobilised Enzyme System: Analysis and Simulation Models and Their Experimental Checking. *Biotechnology Progress*, **9**(2), 166–173.

Schmid, A., Dordick, J. S., Hauer, B., Keiner, A., Wubbolts, M. and Witholt, B. (2001) Industrial Biocatalysis Today and Tomorrow (Insight Review Article) *Nature, Macmillan Magazine Ltd.*, **409**, 258–268.

Schneider, K. R. and Wilhelm, T. (2000) Model Reduction by Extended Quasi-Steady-State Approximation. *Journal of Mathematical Biology*, **40**(5), 443–450.

Schneider, P. and Mitschka, P. (1966) Effect of Internal Diffusion on Catalytic Reactions. *Chemical Engineering Science*, **21**(5), 455–463.

Schnell, S. and Maini, P. K. (2000) Enzyme Kinetics at High Enzyme Concentration. *Bulletin of Mathematical Biology*, **62**(3), 483–499.

Schnell, S. and Maini, P. K. (2002) Enzyme Kinetics Far From the Standard Quasi-Steady-State and Equilibrium Approximations. *Mathematical and Computer Modelling*, **35**(1-2), 137–144.

Schnell, S. and Maini, P. K. (2003) A Century of Enzyme Kinetics: Reliability of the K_m and v_{max} Estimates. *Comments on Theoretical Biology*, **8**(2-3), 169–187.

Schnell, S. and Mendoza, C. (1997) Closed Form Solution for Time-Dependent Enzyme Kinetics. *Journal of Theoretical Biology*, **187**(2), 207–212.

Schroën, C. G. P. H., Fretz, C. B., DeBruin, V. H., Berendsen, W., Moody, H. M., Roos, E. C., VanRoon, P. J., Strubel, M., Janssen, A. E. M. and Tramper, J. (2002) Modelling of the Enzymatic Kinetically Controlled Synthesis of Cephalexin, Influence of Diffusion Limitation. *Biotechnology & Bioengineering*, **80**(3), 331–340.

Schultz, S. G. and Solomon, A. K. (1961) Determination of the Effective Hydrodynamic Radii of Small Molecules by Viscometry. *Journal of General Physiology*, **44**, 1189–1199.

Schulze, B. and Wubbolts, M. G. (1999) Biocatalysis for Industrial Production of Fine Chemicals. *Current Opinion in Biotechnology*, **10**(6), 609–615.

Schwab, J. M. (1981) Stereochemistry of an Enzymatic Baeyer-Villiger Reaction. Application of Deuterium NMR. *Journal of American Chemical Society*, **103**(7), 1876–1878.

Schwab, J. M., Li, W. B. and Thomas, L. P. (1983) Cyclohexanone Oxygenase: Stereochemistry, Enantioselectivity, and Regioselectivity of an Enzyme-Catalysed Baeyer-Villiger Reaction. *Journal of American Chemical Society*, **105**(14), 4800–4808.

Segel, I. H. (1993) *Behaviour and Analysis of Rapid Equilibrium and Steady-State Enzyme Systems. (Wiley Classic Library Edition)* A Wiley Interscience Publication, John Wiley & Sons, Inc.

Segel, L. A. (1988) On the Validity of the Steady-State Assumption of Enzyme-Kinetics. *Bulletin of Mathematical Biology*, **50**(6), 579–593.

Segel, L. A. and Slemrod, M. (1989) The Quasi Steady-State Assumption: A Case Study in Perturbation. *Siam Review*, **31**(3), 446–477.

Shene, C., Andrews, A. and Asenjo, J. A. (1999) Fedbatch Fermentations of *Bacillus subtilis* ToC46 (pPFF1) for the Synthesis of a Recombinant b-1,3-Glucanase: Experimental Study and Modelling. *Enzyme and Microbial Technology*, **24**(5 - 9), 247–254.

Sheng, D., Ballou, D. P. and Massey, V. (2001) Mechanistic Studies of Cyclohexanone Monooxygenase: Chemical Properties of Intermediates Involved in Catalysis. *Biochemistry*, **40**(37), 11156–11167.

Siggia, E. D., Lippincott-Schwartz, J. and Bekiranov, S. (2000) Diffusion in Inhomogeneous Media: Theory and Simulations Applied to Whole Cell Photobleach Recovery. *Biophysical Journal*, **79**(4), 1761–1770.

Sokolichin, A., Eigenberger, G., Lapin, A. and Lubert, A. (1997) Dynamic Numerical Simulation of Gas-Liquid Two-Phase Flows Euler/Euler versus Euler/Lagrange. *Chemical Engineering Science*, **52**(4), 611–626.

Steinmeyer, D. E. and Shuler, M. L. (1989) Structured Model for *Saccharomyces cerevisiae*. *Chemical Engineering Science*, **44**(9), 2017–2030.

Stewart, J. D. (1998) Cyclohexanone Monooxygenase: A Useful Reagent for Asymmetric Baeyer-Villiger Reaction. *Current Organic Chemistry*, **2**, 195–216.

Straathof, A. J. J. (2001) Development of a Computer Program for Analysis of Enzyme Kinetics by Progress Curve Fitting. *Journal of Molecular Catalysis B: Enzymatic*, **11**, 991–998.

Tanojo, H., Reomele, P. E. H., van Veen, G. H., Stieltjes, H., Junginger, E. and Bodde, H. E. (1997) New Design of a Flow-Through Permeation Cell for Studying *in-vitro* Permeation Studies Across Biological Membranes. *Journal of Controlled Release*, **45**, 41–47.

Thayer, A. M. and McCoy, M. (2001) Cover Story: Biocatalysis. *Chemical & Engineering News*, pp. 27–43.

Thompson, J. M. T. and Stewart, H. B. (2002) *Nonlinear Dynamics and Chaos*. second edn John Wiley and Sons Ltd. Chichester.

Tzafriri, A. R. (2003) Michaelis-Menten Kinetics at High Enzyme Concentrations. *Bulletin of Mathematical Biology*, **65**(6), 1111–1129.

Uppal, A., Ray, W. H. and Poore, A. B. (1974) On the Dynamic Behaviour of Continuous Stirred Tank Reactors. *Chemical Engineering Science*, **29**(4), 967–985.

Ussing, H. H. (1949) The Distinction by Means of Tracers between Active Transport and Diffusion - the Transfer of Iodide Across the Isolated Frog Skin. *Acta Physiologica Scandinavica*, **19**(1), 43–56.

Van Slyke, D. D. and Cullen, G. E. (1914) The Mode of Action of Urease and of Enzymes in General. *Journal of Biological Chemistry*, **19**(2), 141–180.

Van Slyke, D. D. and Cullen, G. E. (1917) Studies of Acidosis. I. The Bicarbonate Concentration of the Blood Plasma; Its Significance, and its Determination as a Measure of Acidosis. *Journal of Biological Chemistry*, **30**(2), 289–346.

Vasic-Racki, D., Kragl, U. and Liese, A. (2003) Benefits of Enzyme Kinetics Modelling. *Chemical end Biochemical Engineering Quarterly*, **17**(1), 7–18.

Verhulst, F. (1985) *Nonlinear Differential Equations and Dynamical Systems*. Universitext second edn Springer–Verlag, Berlin.

Villadsen, J. (1989) Simulation of Biochemical Reactions. *Computers & Chemical Engineering*, **13**(4–5), 385–395.

Villadsen, J. and Sorensen, J. P. (1969) Solution of Parabolic Partial Differential Equations by a Double Collocation Method. *Chemical Engineering Science*, **24**(8), 1337–1349.

Wakao, N. and Smith, J. M. (1964) Diffusion and Reaction in Porous Catalysts. *Journal of Industrial and Engineering Chemistry (Fundamental)*, **3**(2), 123–127.

Wallberg, F., Sundstrom, H., Ledung, E., Hewitt, C. J. and Enfors, S. O. (2005) Monitoring and Quantification of Inclusion Body Formation in *Escherichia coli* by Multi-Parameter Flow Cytometry. *Biotechnology Letters*, **27**(13), 919–926.

Walton, A. Z. and Stewart, J. D. (2002) An Efficient Enzymatic Baeyer-Villiger Oxidation by Engineered *Escherichia coli* Cells Under Non-Growing Conditions. *Biotechnology Progress*, **18**(2), 262–268.

Walton, A. Z. and Stewart, J. D. (2004) Understanding and Improving NADPH-Dependent Reactions by Nongrowing *Escherichia coli* Cells. *Biotechnology Progress*, **20**(2), 403–411.

Warshel, A. (2003) Computer Simulations of Enzyme Catalysis. *Annual Review of Biophysics and Biomolecular Structure*, **32**, 425–443.

Whitaker, S. (1986) Transient Diffusion, Adsorption and Reaction in Porous Catalysts: The Reaction Controlled, Quasi–Steady Catalytic Surface. *Chemical Engineering Science*, **41**(12), 3015–3022.

Wiggins, S. (1990) *Introduction to Applied Nonlinear Dynamical Systems and Chaos.* Texts in Applied Mathematics 2. second edn Springer–Verlag. New York.

Willetts, A. (1997) Structural Studies and Synthetic Application of Baeyer-Villiger Monooxygenases. *Trends in Biotechnology*, **15**(2), 55–62.

Wolf, J. and Heinrich, R. (2000) Effect of Cellular Interaction on Glycolytic Oscillations in Yeast: A Theoretical Investigation. *Biochemistry Journal*, **345**(2), 321–334.

Zambianchi, F., Pasta, P., Carrea, G., Colonna, S., Gaggero, N. and Woodley, J. M. (2002) Use of Isolated Cyclohexanone Monooxygenase from Recombinant *Escherichia coli* as a Biocatalyst for Baeyer-Villiger and Sulphide Oxidations. *Biotechnology & Bioengineering*, **78**(5), 489–496.

Zambianchi, F., Pasta, P., Ottolina, G., Carrea, G., Colonna, S., Gaggero, N. and Ward, J. M. (2000) Effect of Substrate Concentration on the Enantioselectivity of Cyclohexanone Monooxygenase from *Acinetobacter calcoaceticus* and its Rationalisation. *Tetrahedron: Asymmetry*, **11**, 3653–3657.

Zhang, F., Crise, B., Su, B., Hou, Y., Rose, J. K., Bothwell, A. and Jacobson, K. (1991) Lateral Diffusion of Membrane-Spanning and Glycosylphosphatidylinositol-Linked Proteins - Toward Establishing Rules Governing the Lateral Mobility of Membrane-Proteins. *Journal of Cell Biology*, **115**(1), 75–84.

Zhao, H. and van der Donk, W. A. (2003) Regeneration of Cofactors for Use in Biocatalysis. *Current Opinion in Biotechnology*, **14**, 583–589.

Appendices

A Derivation of the Enzyme-Catalysed Baeyer-Villiger Monooxygenase Rate Expression

In *Chapter 3*, the Baeyer-Villiger rate expression was derived using the method described by King and Altman. In order to check the work, the usual algebraic method was set up and it was then solved using Mathematica®. The symbols used in Mathematica® are given in the table below.

Symbols	Definition
ENZ	$[E_{CHMO}]$
X1	$[E_{CHMO}Co^{+}H]$
X2	$[E_{CHMO}Co^{+}HOO]$
X3	$[E_{CHMO}Co^{+}HOOS] \rightleftharpoons [E_{CHMO}Co^{+}(H_2O)P]$
X4	$[E_{CHMO}Co^{+}P]$
X5	$[E_{CHMO}Co^{+}]$
dS1dt	Rate of cofactor consumption
dS2dt	Rate of molecular oxygen consumption
dS3dt	Rate of substrate consumption
dP1dt	Rate of product formation
dP2dt	Rate of oxidised cofactor formation

The system of ordinary differential equations was input into Mathematica® by applying the `FullSimplify` and the `Solve` functions simultaneously;

```
FullSimplify[Solve[{dS1dt == -k1 * ENZ * S1 + k-1 * X1,
   dS2dt == -k2 * X1 * S2 + k-2 * X2,
   dS3dt == -k3 * X2 * S3 + k-3 * X3,
   k1 * ENZ * S1 - k-1 * X1 - k2 * X1 * S2 + k-2 * X2 == 0,
   k2 * X1 * S2 - k-2 * X2 - k3 * X2 * S3 + k-3 * X3 == 0,
   k3 * X2 * S3 - k-3 * X3 - k4 * X3 + k-4 * X4 == 0,
   k4 * X3 - k-4 * X4 - k5 * X4 + k-5 * X5 * P1 == 0,
   k5 * X4 - k-5 * X5 * P1 - k6 * X5 + k-6 * ENZ * P2 == 0,
   dP1dt == k5 * X4 - k-5 * X5 * P1,
   dP2dt == k6 * X5 - k-6 * ENZ * P2,
   EnT == ENZ + X1 + X2 + X3 + X4 + X5},
  {dS1dt, dS3dt, dS2dt, dP1dt, dP2dt, X1, X2, X3, X4, X5, ENZ}]]
```

which leads to the solutions of the rate of substrate consumption and product formation given by dS3dt and dP1dt respectively;

```
dS3dt → (EnT (P1 P2 k-6 k-5 k-4 k-3 k-2 k-1 - S1 S2 S3 k1 k2 k3 k4 k5 k6)) /
  (P1 k-5 (k-4 (k-3 (k-2 (k-1 + S1 k1) + S1 S2 k1 k2) + S1 S2 S3 k1 k2 k3) +
       S1 S2 S3 k1 k2 k3 k4) + S1 S2 S3 k1 k2 k3 k4 k5 +
    P2 k-6 (k-4 k-3 k-2 k-1 + P1 k-5 (k-3 k-2 k-1 + k-4 (k-2 k-1 + k-3 (k-2 + k-1 + S2 k2) +
          S3 (k-1 + S2 k2) k3) + (k-2 k-1 + S3 (k-1 + S2 k2) k3) k4) +
       (k-3 k-2 k-1 + (k-2 k-1 + S3 (k-1 + S2 k2) k3) k4) k5) + k-4 k-3 k-2 k-1 k6 +
    (S1 k1 (k-4 (k-3 (k-2 + S2 k2) + S2 S3 k2 k3) + S2 S3 k2 k3 k4) +
       (k-3 (k-2 (k-1 + S1 k1) + S1 S2 k1 k2) + S1 S2 S3 k1 k2 k3 +
          (k-2 (k-1 + S1 k1) + S1 S2 k1 k2 + S3 (k-1 + S1 k1 + S2 k2) k3) k4) k5) k6)

dP1dt → -(EnT (P1 P2 k-6 k-5 k-4 k-3 k-2 k-1 - S1 S2 S3 k1 k2 k3 k4 k5 k6)) /
  (P1 k-5 (k-4 (k-3 (k-2 (k-1 + S1 k1) + S1 S2 k1 k2) + S1 S2 S3 k1 k2 k3) +
       S1 S2 S3 k1 k2 k3 k4) + S1 S2 S3 k1 k2 k3 k4 k5 +
    P2 k-6 (k-4 k-3 k-2 k-1 + P1 k-5 (k-3 k-2 k-1 + k-4 (k-2 k-1 + k-3 (k-2 + k-1 + S2 k2) +
          S3 (k-1 + S2 k2) k3) + (k-2 k-1 + S3 (k-1 + S2 k2) k3) k4) +
       (k-3 k-2 k-1 + (k-2 k-1 + S3 (k-1 + S2 k2) k3) k4) k5) + k-4 k-3 k-2 k-1 k6 +
    (S1 k1 (k-4 (k-3 (k-2 + S2 k2) + S2 S3 k2 k3) + S2 S3 k2 k3 k4) +
       (k-3 (k-2 (k-1 + S1 k1) + S1 S2 k1 k2) + S1 S2 S3 k1 k2 k3 +
          (k-2 (k-1 + S1 k1) + S1 S2 k1 k2 + S3 (k-1 + S1 k1 + S2 k2) k3) k4) k5) k6)
```

B Gauss-Newton Procedure for the Progress Curve Analysis

The method of progress curve is closely related to the fitting of data via nonlinear regression technique. A number of algorithms can be applied in order to fit an experimental data to a particular rate expression. This supplementary section provides the simplest technique of using nonlinear regression to fit a set of data. The principles of Gauss-Newton method is discussed in detail and applied to the function obtained from the rate expression of enzyme-catalysed Baeyer-Villiger reaction.

The rate expression that described the reaction is given by;

$$\frac{d[P_{OxaBicyclo}]}{dt}=\frac{V_{max}[S_{Bicyclo}]}{K_{m_{[Bicyclo]}}\left(1+\frac{[P_{OxaBicyclo}]}{K_{m_{[OxaBicyclo]}}}\right)+[S_{Bicyclo}]\left(1+\frac{[S_{Bicyclo}]}{K_{i_{[Bicyclo]}}}+\frac{[P_{OxaBicyclo}]}{K_{i_{[OxaBicyclo]}}}\right)} \tag{B.1}$$

this is then transformed into the integrated rate expression in the form of an objective function;

$$\begin{aligned}\Phi(t,z) &= \ln(z)\left[K_{m_{[Bicyclo]}}+\frac{K_{m_{[Bicyclo]}}[S_{Bicyclo}]_0}{K_{m_{[OxaBicyclo]}}}\right] \\ &+ z\left[1-\frac{K_{m_{[Bicyclo]}}}{K_{m_{[OxaBicyclo]}}}+\frac{[S_{Bicyclo}]_0}{K_{i_{[OxaBicyclo]}}}\right] \\ &+ z^2\left[\frac{1}{2K_{i_{[Bicyclo]}}}-\frac{1}{2K_{i_{[OxaBicyclo]}}}\right] \\ &+ V_{max}t\end{aligned} \tag{B.2}$$

Equation (B.2) signifies that the function is governed by two independent variables, t and z with 5 nonlinear parameters associated with the function. This can be stated as;

$$\Phi = f(t,z;K_{m_{[Bicyclo]}},K_{m_{[OxaBicyclo]}},K_{i_{[Bicyclo]}},K_{i_{[OxaBicyclo]}},V_{max}). \tag{B.3}$$

Let this function generally denoted as z_i for the variables and that θ_j for the parameters. Thus;

$$\Phi = f(z_1,z_2;\theta_1,\theta_2,\theta_3,\theta_4,\theta_5) \tag{B.4}$$

The first step of Gauss-Newton procedure is to get the initial estimates of all the parameters, θ_j^0. For the purpose of obtaining these estimates, the model equation should be transformed into a

set of linear parameters θ_j^l, therefore, a set of experimental data can be fitted to this linear form and values of θ_j^0 can be easily obtained. These initial estimates are then needed to be refined using the first-order approximation of a Taylor series expansion in the form of

$$(\Phi - \hat{\Phi}) = \delta\theta_1 \left(\frac{\partial\Phi}{\partial\theta_1}\right) + \delta\theta_2 \left(\frac{\partial\Phi}{\partial\theta_2}\right) + \ldots + \delta\theta_j \left(\frac{\partial\Phi}{\partial\theta_j}\right) \tag{B.5}$$

where $\hat{\Phi}$ is the expected values of Φ for all $\theta = \theta_0$ and $\frac{\partial\Phi}{\partial\theta_j}$ is the partial derivative of the function with respect to the appropriate parameter in the objective function. The term $\delta\theta_j$ in (B.5) refers to the correction terms from the regression and iteratively used as;

$$\theta^1 = \theta^0 + \delta\theta$$

These refined estimates are then used in the second iteration to obtain θ^2 and so on, until $\delta\theta$ becomes negligible. At this point, the iteration is terminated and the standard errors of the parameters are determined from the variance of $\delta\theta$.

There is another obstacle needed to be resolved with the objective function given by (B.2), i.e. it is in the form of a closed function or normally known as the transcendental type equation (Fritsch *et al.*, 1973; Goudar *et al.*, 1999), therefore the iteration cannot be dealt in a straight forward manner. The method of estimating the root of a function via Newton-Raphson procedure is used, and it is given in the form of;

$$z_{n+1} = z_n - \left(\frac{\Phi(z)}{\Phi'(z)}\right)_{z=z_n} \tag{B.6}$$

where $\Phi(z)$ is the objective function given previously and that $\Phi'(z)$ is its first derivative with respect to z which is given by;

$$\Phi'(z) = f(z) \tag{B.7}$$

where $f(z)$ is the denominator of equation (B.1) which can be written in terms of z as;

$$\frac{dz}{dt} = -\frac{V_{max}}{\frac{K_{m_{[Bicyclo]}}}{z}\left[1 + \frac{([S]_T - z)}{K_{m_{[OxaBicyclo]}}}\right] + \left(1 + \frac{z}{K_{i_{[Bicyclo]}}} + \frac{([S]_T - z)}{K_{i_{[OxaBicyclo]}}}\right)} \tag{B.8}$$

The equivalence given by (B.7) can be proven by differentiating the integrated form of (B.8) with respect to the variable z;

$$\frac{d}{dz}\Phi(z) = \frac{d}{dz}\int_0^z f(z)dz + \frac{d}{dz}V_{max}\int_0^t dt \tag{B.9}$$

since

$$\frac{d}{dz}\int_0^z f(z)dz = f(z)$$

and

$$\frac{d}{dz}V_{max}\int_0^t dt = \frac{d}{dz}V_{max}t = 0$$

thus

$$\frac{d}{dz}\Phi(z) = f(z) \tag{B.10}$$

which simplifies to (B.7) with

$$\frac{d}{dz}\Phi(z) = \Phi'(z).$$

Let the denominator of equation (B.8) being Γ, thus the equation reduces into;

$$\frac{dz}{dt} = \frac{V_{max}}{\Gamma} \tag{B.11}$$

and rearranging Γ into the form that separates the parameters and variable z, leads to;

$$\begin{aligned}\Gamma &= 1+\left(\frac{[S]_T}{K_{i_{[OxaBicyclo]}}} - \frac{Km_{[Bicyclo]}}{Km_{[OxaBicyclo]}}\right) \\ &+ \frac{1}{z}\left[\left(K_{m_{[Bicyclo]}} + \frac{Km_{[Bicyclo]}[S]_T}{Km_{[OxaBicyclo]}}\right) + z^2\left(\frac{1}{K_{i_{[Bicyclo]}}} - \frac{1}{K_{i_{[OxaBicyclo]}}}\right)\right]\end{aligned} \tag{B.12}$$

The function can then be represented by,

$$\Gamma = f(z) = g_z(z) + f_z(z).f_\theta^1(\theta) + h_z(z).f_\theta^2(\theta)$$

thus, (B.11) simplifies into,

$$\frac{dz}{dt} = \frac{V_{max}}{g_z(z) + f_z(z).f_\theta^1(\theta) + h_z(z).f_\theta^2(\theta)} \tag{B.13}$$

where $g_z(z)$, $h_z(z)$ and $f_z(z)$ are functions consist only of variable z while $f_\theta^1(\theta)$ and $f_\theta^2(\theta)$ are functions consist of only the parameter terms. Using this form of equation, the derivatives of the objective function with respect to each parameter can be easily obtained. Consider the derivative of the objective function with respect to the parameter, V_{max};

$$\begin{aligned}
\frac{\partial \Phi}{\partial V_{max}} &= \frac{d}{dV_{max}}\left(\int_0^z f(z)dz\right) + \frac{d}{dV_{max}} V_{max} t \\
&= \frac{d}{dV_{max}} \int_0^z f(z)dz + t \\
&= f(z)\frac{dz}{dV_{max}} + t
\end{aligned} \tag{B.14}$$

Using the same procedure to the other parameters, θ_j in the function, the general solution of the partial derivative with respect to a given parameter can be generally found by differentiating equation (B.2) with the presence of denominator function defined by Γ;

$$\begin{aligned}
\frac{\partial \Phi}{\partial \theta_j} &= \frac{d}{d\theta_j}\left(\int_0^z g_z(z)dz + f_\theta^1(\theta)\int_0^z f_z(z)dz + f_\theta^2(\theta)\int_0^z h_z(z)dz + V_{max}t\right) \\
&= \frac{d}{d\theta_j}\int_0^z g_z(z)dz + \frac{d}{d\theta_j}\left(f_\theta^1(\theta)\int_0^z f_z(z)dz\right) \\
&+ \frac{d}{d\theta_j}\left(f_\theta^2(\theta)\int_0^z h_z(z)dz\right) + \frac{d}{d\theta_j} V_{max} t \\
&= \left(g_z(z) + f_\theta^1(\theta) f_z(z) + f_\theta^2(\theta) h_z(z)\right)\frac{dz}{d\theta_j} \\
&+ \frac{f_\theta^1(\theta)}{d\theta_j}\int_0^z f_z(z)dz + \frac{f_\theta^2(\theta)}{d\theta_j}\int_0^z h_z(z)dz
\end{aligned} \tag{B.15}$$

C Treatment of the Integrated Rate Expression with Lambert's ω–Function

Definition: Lambert's ω–function is an exponential type function given by;

$$x = \omega(x)e^{\omega(x)} \tag{C.1}$$

and it can be considered as a sort of "Golden Ratio" of the exponential when $x = 1$, hence;

$$\begin{aligned} \omega(1) &= e^{-\omega(1)} \\ \ln\left[\frac{1}{\omega(1)}\right] &= \omega(1) \end{aligned} \tag{C.2}$$

The function $\omega(x)$ can be represented in a series expansion of the form;

$$\omega(x) = \sum_{n=1}^{\infty} \frac{(-1)^{n-1}n^{n-2}}{(n-1)!}x^n = x - x^2 + \frac{3}{2}x^3 - \frac{8}{3}x^4 + \ldots \tag{C.3}$$

Finding values of the above function seems to be a rather longwinded task, however an accurate algorithm has been implemented and one would not have any problem using equation (C.3) for the fitting of the rate expression.

The Function Applied to the Enzyme-Catalysed Rate Expression

The application of Lambert's ω–function to the integrated enzyme-catalysed rate expression is shown here. A simple Michaelis-Menten kinetics is used as a model equation. Given that an enzyme, [E] catalyses a substrate, [S] following a model equation in the form of;

$$\frac{d[S]}{dt} = -\frac{V_{max}[S]}{K_m + [S]} \tag{C.4}$$

Integrating this leads to,

$$K_m\left(\frac{[S]_0}{z}\right) + ([S]_0 - z) = V_{max}t \tag{C.5}$$

Equation (C.5) is rearranged such that the variable z (concentration of substrate at time t) and all other constants are separated on the left and right hand side respectively,

$$K_m \ln(z) + z = K_m \ln([S]_0) + [S]_0 - V_{max}t \tag{C.6}$$

Let $\phi = \frac{z}{K_m}$, thus,

$$\begin{aligned} \phi K_m + K_m \ln(\phi K_m) &= [S]_0 + K_m \ln([S]_0) - V_{max}t \\ \phi + \ln(\phi) &= \frac{[S]_0}{K_m} + \ln\left(\frac{[S]_0}{K_m}\right) - \frac{V_{max}t}{K_m} \end{aligned} \tag{C.7}$$

Treating equation (C.1) in the same manner by taking log_e on both sides gives,

$$\ln(x) = \omega(x) + \ln(\omega(x)) \tag{C.8}$$

comparing the terms on the left hand side of equation (C.7) and that on the right hand side of equation (C.8), results in;

$$\ln(x) = \frac{[S]_0}{K_m} + \ln\left(\frac{[S]_0}{K_m}\right) - \frac{V_{max}t}{K_m} \tag{C.9}$$

and the term x is now obtained with further arrangement gives;

$$\begin{aligned} \ln\left[\frac{x}{\left(\frac{[S]_0}{K_m}\right)}\right] &= \frac{[S]_0 - V_{max}t}{K_m} \\ x &= \left(\frac{[S]_0}{K_m}\right) e^{\left\{\frac{[S]_0 - V_{max}t}{K_m}\right\}} \end{aligned} \tag{C.10}$$

Again, comparing the term ϕ to the general transcendental equation (C.8) gives,

$$\phi = \omega(x)$$

hence,

$$\phi = \omega\left[\left(\frac{[S]_0}{K_m}\right) e^{\left\{\frac{[S]_0 - V_{max}t}{K_m}\right\}}\right] \tag{C.11}$$

A non-dimensional form of equation can be obtained from the above function by defining, $\bar{S}_0 = \frac{[S]_0}{K_m}$ and $\kappa = \frac{V_{max}}{K_m}$ which lead to,

$$\phi = \omega \bar{S}_0 e^{\{\bar{S}_0 - \kappa t\}} \tag{C.12}$$

The above dimensionless parameters especially κ apparently represents the first order rate constant of a particular reaction which defined the approximate fraction of substrate being converted to product at a unit time. If the equation is left in its normal form with $\phi = \frac{z}{K_m}$, thus,

$$z = K_m \omega \left[\left(\frac{[S]_0}{K_m} \right) e^{\left\{ \frac{[S]_0 - V_{max} t}{K_m} \right\}} \right] \tag{C.13}$$

The integrated rate equation is now set in terms of substrate as a function of time, [S](t) where the nonlinear regression can then be applied in a normal way.

D Theorem and Proof

Theorem 1. *Cramer's Rule (Solution of linear system by determinants)*

For system of 2 equations and 2 unknowns, of the form

$$ax + by = e \tag{D.1}$$

$$cx + dy = f \tag{D.2}$$

it has a unique solution only if

$$\Delta = \begin{vmatrix} a & b \\ c & d \end{vmatrix} \neq 0,$$

namely $x = \frac{\Delta_1}{\Delta}$ *and* $y = \frac{\Delta_2}{\Delta}$ *where*

$$\Delta_1 = \begin{vmatrix} e & b \\ f & d \end{vmatrix}$$

and

$$\Delta_2 = \begin{vmatrix} a & e \\ c & f \end{vmatrix}.$$

Proof 1. *Suppose that* $\Delta \neq 0$. *Then,* $A = \begin{vmatrix} a & b \\ c & d \end{vmatrix}$ *has an inverse of the form;*

$$A^{-1} = \Delta^{-1} \begin{bmatrix} d & -b \\ -c & a \end{bmatrix}$$

and also it is known that

$$A \begin{bmatrix} x \\ y \end{bmatrix} = \begin{bmatrix} e \\ f \end{bmatrix}$$

has a unique solution of the form

$$\begin{bmatrix} x \\ y \end{bmatrix} = A^{-1} \begin{bmatrix} e \\ f \end{bmatrix} = \frac{1}{\Delta} \begin{bmatrix} d & -b \\ -c & a \end{bmatrix} \begin{bmatrix} e \\ f \end{bmatrix}$$
$$= \frac{1}{\Delta} \begin{bmatrix} de & -bf \\ -ce & af \end{bmatrix}$$
$$= \frac{1}{\Delta} \begin{bmatrix} \Delta_1 \\ \Delta_2 \end{bmatrix} = \begin{bmatrix} \frac{\Delta_1}{\Delta} \\ \frac{\Delta_2}{\Delta} \end{bmatrix}$$

Theorem 2. *(Poincaré Bendixson Theorem)*
For a system describes by

$$\dot{x} = f(x) \tag{D.3}$$

in $\mathbb{R}^2$ *and assume that* γ^+ *is a bounded, positive orbit and that* $\omega(\gamma^+)$ *contains ordinary point only. Then,* $\omega(\gamma^+)$ *is a periodic orbit. If* $\omega(\gamma^+) \neq \gamma^+$ *the periodic orbit is called a limit cycle. an analogous result is valid for a bounded, negative orbit.*

Theorem 3. *(Stable Manifold Theorem for a Fixed Point)*
Suppose that a function is given by,

$$\dot{y} = f(y) \tag{D.4}$$

has a hyperbolic fixed point $\bar{y}$*. Then there exist local stable and unstable manifolds* $W^s_{loc}(\bar{y})$*,* $W^u_{loc}(\bar{y})$*, of the same dimension,* n_s*,* n_u *as those of the eigenspaces* E^s*,* E^u *of the linearised system*

$$\dot{\gamma} = Df(\bar{y})\gamma \tag{D.5}$$

and tangent to E^s*,* E^u *at* $\bar{y}$*.* $W^s_{loc}(\bar{y})$*,* $W^u_{loc}(\bar{y})$ *are as smooth as the function* f*.*

E Numerical Technique for Solving the System of Nonlinear Partial Differential Equations

```
function celldiffuse(N)

% Solving nonhomogeneous nonlinear partial differential
% equations via finite element method.
if nargin<1
    N = 30;
end

Lstep = 0.05;
tspan = [0:Lstep:5];

y0 =[repmat(1,1,N);repmat(0,1,N)];
h = 0.5;
x = (1:N)/(N+1);

options = odeset('Vectorized','on','JPattern',jpattern(N));

[t,y] = ode15s(@f,tspan,y0,options,N,h);

u1 = y(:,1:2:end);
u2 = y(:,2:2:end);
figure(1)
surf(x,t,u1);
xlabel('y^{*}');
ylabel('t^{*}');
zlabel('C_{s}^{*}');

%title(['The Reaction-Diffusion reaction for N = ' num2str(N)]);
figure(2)
surf(x,t,u2);
xlabel('y^{*}');
ylabel('t^{*}');
zlabel('C_{p}^{*}');

%title(['The Reaction-Diffusion reaction for N = ' num2str(N)]);
function dydt = f(t,y,N,h,k)
PHI1 = 5.97e-1;
PHI2 = 5.83e-0;
```

```
Kms = 0.016;
Kmp = 5.9401/Kms;
Kis = 640.7911/Kms;

Kip = 799.7945/Kms;
k=(N:-1:1);

dydt = zeros(2*N,size(y,2));

% preallocate dy/dt
% Evaluate the two components of the function at one edge of
% the grid (with edge conditions).
for j = 1:length(k) i = 1;
dydt(i,:) =
(1/PHI1.^2)*((1./(h.*k(j)))*(y(i+2,:))+(1./h.^2).*(y(i+2,:)-2*y(i,:)+0))...
-(y(i,:)./((1+(y(i+1,:)./Kmp))+y(i,:).*(1+(y(i+1,:)./Kip)+(y(i,:)./Kis))));
dydt(i+1,:) =
(1/PHI2.^2)*((1./(h.*k(j)))*(y(i+3,:)-1)+(1/h.^2).*(1-2*y(i+1,:)+y(i+3,:)))...
+(y(i,:)./((1+(y(i+1,:)./Kmp))+y(i,:).*(1+(y(i+1,:)./Kip)+(y(i,:)./Kis))));

% Evaluate the two components of the function at all interior
% grid points.
i = 3:2:2*N-3;
dydt(i,:) =
(1/PHI1.^2)*((1./(h.*k(j)))*(y(i+2,:)-y(i-2,:))+(1./h.^2).*(y(i+2,:)...
-2*y(i,:)+y(i-2,:)))-(y(i,:)./((1+(y(i+1,:)./Kmp))+y(i,:).*(1+(y(i+1,:)...
./Kip)+(y(i,:)/Kis))));
dydt(i+1,:) =
(1/PHI2.^2)*((1./(h.*k(j)))*(y(i+3,:)-y(i-1,:))+(1./h.^2).*(y(i+3,:)...
-2*y(i+1,:)+y(i-1,:)))+(y(i,:)./((1+(y(i+1,:)./Kmp))+y(i,:).*(1+(y(i+1,:)...
./Kip)+(y(i,:)/Kis))));

% Evaluate the two components of the function at the other edge
% of the grid (with edge conditions).
i = 2*N-1;
dydt(i,:) =
(1/PHI1.^2)*((1./(h.*k(j)))*(-y(i-2,:)+1)+(1./h.^2).*(y(i-2,:)-2*y(i,:)+1))...
-(y(i,:)./((1+(y(i+1,:)./Kmp))+y(i,:).*(1+(y(i+1,:)./Kip)+(y(i,:)./Kis))));
dydt(i+1,:) =
(1/PHI2.^2)*((1./(h.*k(j)))*(0-y(i-1,:))+(1./h.^2).*(y(i-1,:)-2*y(i+1,:)+0))...
+(y(i,:)./((1+(y(i+1,:)./Kmp))+y(i,:).*(1+(y(i+1,:)./Kip)+(y(i,:)./Kis))));
end

function S = jpattern(N)
```

```
B = ones(2*N,5);

B(2:2:2*N,2) = zeros(N,1);
B(1:2:2*N-1,4) = zeros(N,1);

S =spdiags(B,-2:2,2*N,2*N);
```

F Orthogonal Collocation Method for Boundary Value Problem

```
function collFE

% This program runs a code to solve the reaction-diffusion
% problem using the method of orthogonal collocation on finite elements.
global xoc woc aoc boc qinv np ne nt delx Aocfe Bocfe

%set linear to 1 if problem is linear - this avoids
%one unnecessary iteration
linear = 0

%set the type of reaction rate
iwhich = 3

%set Thiele modulus and geometry
%(geometry = 1, 2, 3 for planar, cylindrical, spherical)
phi = 9.5978
phi2 = phi^2
geometry = 3

%np is the total number of collocation points in one finite element
np = 7

%ne is the number of elements in the z-direction
ne = 10

%This can be changed to produce a variable grid
for k=1:ne
    delx(k) = 1/ne;
end delx(1)

%nt is the total number of points
nt = (np-1)*ne + 1

%number of interior points is np-2 per element
nint=(np-2)*ne;

%create the collocation matrices for the fluid
planar(np,0)

%set up the z values for plotting purposes
num=0; xstart = 0.; for k=1:ne
```

```
    for j=1:np-1
        num=num+1;
        x(num)=xstart+delx(k)*xoc(j);
    end
xstart = xstart+delx(k); end x(nt) = 1.

%iterate
tol = 1.e-10; change = 1.0; iter=0;

%initial guess
for i=1:nt
    c(i) = 1;
end c(nt) = 1.;

while change>tol
    iter=iter+1;

%set the matrices to zero
        Bocfe = zeros(nt,1);
        Aocfe = zeros(np,np,ne);

%set the matrices for the differential equation
    for k=1:ne
        for j=2:np-1
            index = (np-1)*(k-1) + j;
            term = (geometry-1)/x(index);
            for i=1:np
                Aocfe(j,i,k) = boc(j,i) + term*delx(k)*aoc(j,i);
            end
            Ans = rate(c(index)); %ans = rate(c(index),iwhich);
            raterxn = Ans(1);
            drate = Ans(2);
            term=phi2*delx(k)*delx(k);
            Aocfe(j,j,k) = Aocfe(j,j,k) - term*drate;
            Bocfe(index) = term*(raterxn - drate*c(index));
        end
    end

%set the continuity conditions
    for k=1:ne-1
        for i=1:np
            Aocfe(np,i,k) = aoc(np,i)/delx(k);
        end
    end
```

```
    for k=2:ne
        for i=1:np
            Aocfe(1,i,k) = -aoc(1,i)/delx(k);
        end
    end
    for k=2:ne
        term = Aocfe(np,np,k-1)+Aocfe(1,1,k);
        Aocfe(np,np,k-1) = term;
        Aocfe(1,1,k) = term;
        Bocfe((np-1)*(k-1)+1) = 0.;
    end
    for i=1:np
        Aocfe(1,i,1) = aoc(1,i);
    end
    Aocfe(np,np,ne) = 1.;
    Bocfe(nt) = 1;

%Solve one iteration.
    OCFElud(np,ne);
    OCFEfas(np,ne,nt);
    c11 = Bocfe;

%Calculate the criterion to stop the iterations.
    sum=0.;
    for i=1:nt
        sum = sum + abs(c11(i) - c(i));
        c(i) = c11(i);
    end
    if linear==1,break,end
    change = sum
end

%Plot the solution.
figure(1) hold on plot(x,c,'-b')

% Find the coefficients
dd1 = c';
xp = 0:0.02:1; %plotting points
nx = 7; cinterp = planar_interp(nx,dd1,xp,0,1); hold off
xlabel('y^{*}') ylabel('C^{*}_{s}') c

sum = 0; for k=1:ne
    for i=1:np
        index = (np-1)*(k-1) + i;
```

```
        Ans = rate(c(index));
        raterxn = Ans(1);
        sum = sum + delx(k)*woc(i)*raterxn*x(index)^(geometry-1);
    end
end efffectiveness = geometry*sum

function planar(nx,kon)
%   this subroutine computes the matrices for collocation without
%   symmetry.
%   input variable
%     nx = number of collocation points, including two end points
%
%   output variables, must be declared global
%     aoc = matrix for first derivative
%     boc = matrix for second derivative
%     qinv = matrix for q inverse
%     xoc = vector of collocations points
%     woc = vector of weights
%

global xoc woc aoc boc qinv if(nx<3)

  nx=3;
  fprintf('\n ************************************** \n')
  fprintf('The number of collocation points must be between \n')
  fprintf('3 and 7 (inclusive).  nx has been changed to %g\n\n',nx)
end if(nx>7)
  nx=7;
  fprintf('\n ************************************** \n')
  fprintf('The number of collocation points must be between \n')
  fprintf('3 and 7 (inclusive).  nx has been changed to %g\n\n',nx)
end
%now 3<=nx<=7
if kon==0
    fprintf('The total number of collocation points is %g\n\n',nx)
end

xoc(1)=0.; if (nx==3)
  xoc(2)=0.5;
  elseif (nx==4)
  xoc(2)=0.21132486540519;
  xoc(3)=1-xoc(2);
  elseif (nx==5)
  xoc(2)=0.11270166537926;
```

```
  xoc(3)=0.5;
  xoc(4)=1-xoc(2);
  elseif (nx==6)
  xoc(2)=0.06943184420297;
  xoc(3)=0.33000947820757;
  xoc(4)=1-xoc(3);
  xoc(5)=1-xoc(2);
  else
  xoc(2)=0.04691007703067;
  xoc(3)=0.23076534494716;
  xoc(4)=0.5;
  xoc(5)=1-xoc(3);
  xoc(6)=1-xoc(2);
end xoc(nx)=1.; format long for i=1:nx,
    r(i,i) = 0.0;
    aoc(i,i) = 0.0;
    s(i) = 1.0;
    boc(i,i) = 0.0 ;
     for j=1:nx,
        if (i~=j)
           r(i,j) = 1.0/(xoc(i)-xoc(j)) ;
           s(i) = s(i)*r(i,j);
        end
     end
     for j=1:nx,
         jx = nx-j+1;
         if (jx<j), break, end
         if (jx==j)
            aoc(i,i) = aoc(i,i)+r(i,j);
         end
         if (jx>j)
            aoc(i,i) = aoc(i,i)+r(i,j)+r(i,jx);
         end
     end
end for i=1:nx
   for j=1:nx
       if (i~=j)
          aoc(i,j) = s(j)*r(i,j)/s(i);
          boc(i,j) = 2.0*aoc(i,j)*(aoc(i,i)-r(i,j));
          boc(i,i) = boc(i,i)+r(i,j)*(aoc(i,i)-r(i,j));
       end
   end
end for i=1:nx
   qinv(1,i) = s(i);
```

```
   k = 1;
   woc(i) = 0.0 ;
   for j=1:nx
      if (j~=i)
         l = k;
         k = k+1;
         qinv(k,i) = qinv(l,i);
         while (l>1)
            m = l-1;
            qinv(l,i) = qinv(m,i)-xoc(j)*qinv(l,i);
            l = m;
         end
           qinv(1,i) = -xoc(j)*qinv(1,i);
      end
   end
   for j=1:nx
      woc(i) = woc(i)+qinv(j,i)/j;
   end
end

if kon == 0
    fprintf('A matrix (aoc) \n')
    disp(aoc)
    fprintf('B matrix (boc) \n')
    disp(boc)
    fprintf('Q matrix (qinv)\n')
    disp(qinv)
    fprintf('Collocation points (xoc) \n') disp(xoc)
    fprintf('W matrix (woc) \n')
    disp(woc)
end

% This subroutine does the LU decomposition for the
% orthogonal collocation method on finite elements.
% This version is for a single unknown, giving a block
% diagonal matrix with a single entry of overlap.
% The matrix Aocfe is stored as Aocfe(np,np,ne), where
% np is the number of collocation points in one element
% and ne is the number of elements.

function OCFElud(np,ne)

global Aocfe
```

```
n1 = np - 1; for l=1:ne
    for k=1:n1
        k1=k+1;
        for i=k1:np
            s = Aocfe(i,k,l)/Aocfe(k,k,l);
            Aocfe(i,k,l) = s;
            for j=k1:np
                Aocfe(i,j,l) = Aocfe(i,j,l) - s*Aocfe(k,j,l);
            end
        end
    end
    if l<ne
        Aocfe(1,1,l+1) = Aocfe(np,np,l);
    end
end

% This subroutine does the fore and aft sweep for the
% orthogonal collocation method on finite elements.
% This version is for a single unknown, giving a block
% diagonal matrix with a single entry of overlap.
% The matrix Aocfe is stored as Aocfe(np,np,ne), where
% np is the number of collocation points in one element
% ne is the number of elements.
% nt is the total number of unknowns, nt = (np-1)*ne + 1

function OCFEfas(np,ne,nt)

global Aocfe Bocfe

np1=np;
%forward sweep
for l=1:ne
    for i=2:np1
        i2=(l-1)*(np-1)+i;
        s = 0.;
        i1=i-1;
        for j=1:i1
            j2=i2-i+j;
            s=s+Aocfe(i,j,l)*Bocfe(j2);
        end
        Bocfe(i2)=Bocfe(i2)-s;
    end
end
%back substitution
```

```
for l1=1:ne
    l=ne-l1+1;
    if (l==ne)
        Bocfe(nt)=Bocfe(nt)/Aocfe(np,np,ne);
    end
    n1 = np-1;
    for k=1:n1
        i=n1+1-k;
        i2=(l-1)*(np-1)+i;
        m=i+1;
        n2=n1+1;
        s=0.;
        for j=m:n2
            j2=(l-1)*(np-1)+j;
            s=s+Aocfe(i,j,l)*Bocfe(j2);
        end
        Bocfe(i2)=(Bocfe(i2) - s)/Aocfe(i,i,l);
    end
end

%calculate the rate and derivative for a given concentration

function Ans = rate(c)

%use for linear reaction
%ans(1) = c;
%ans(2) = 1.;

%use for CHMO-enzyme--catalysed reaction
A = (1 + (0/371.25625));
B = 40049.44375;
C = (0/49987.15625);

Ans(1) = c/(A+((c^2)/B)+(1+C)*c);

Ans(2) = (B*(A*B-c^2))/(A*B+c*(B+B*C+c))^2;
```

G Calibration Curves

Standard calibration curve for bicyclic-ketone (bicyclo[3.2.0]hept-2-en-6-one)

Bicyclic-ketone calibration with $R^2 = 1.00$ at 95% confidence interval and gradient of the straight line = 2683064.07. All data points were normalised using naphthalene standard as described in the analytical assay.

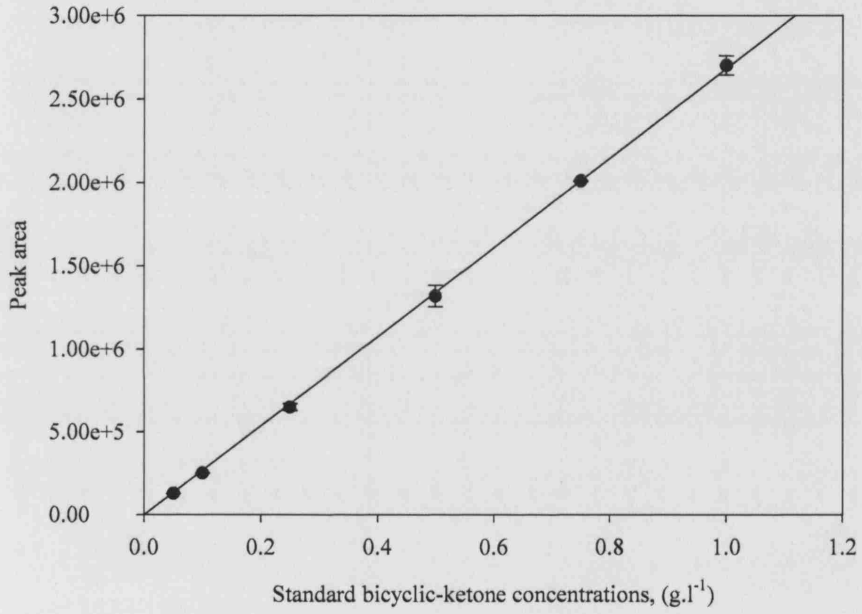

Standard calibration curve for lactone ((-)1(S)5(R)2-oxabicyclo[3.3.0]oct-6-en-3-one)

Lactone calibration with $R^2 = 0.99$ at 95% confidence interval and gradient of the straight line = 2437801.95. All data points were normalised using naphthalene standard as described in the analytical assay.

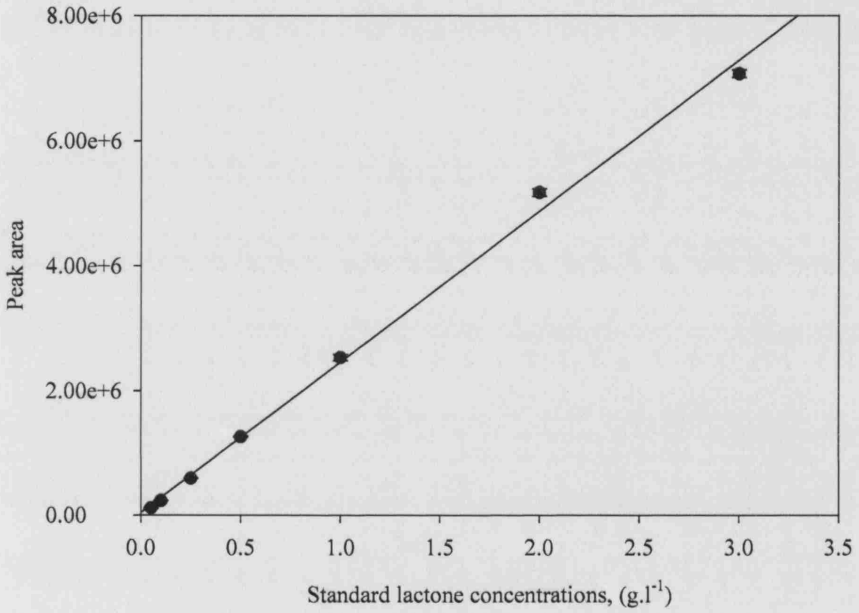

Standard calibration curve for dry cell weight of *E. coli*

Dry cell weight calibration with $R^2 = 0.99$ at 95% confidence interval and gradient of the straight line = 0.7601.

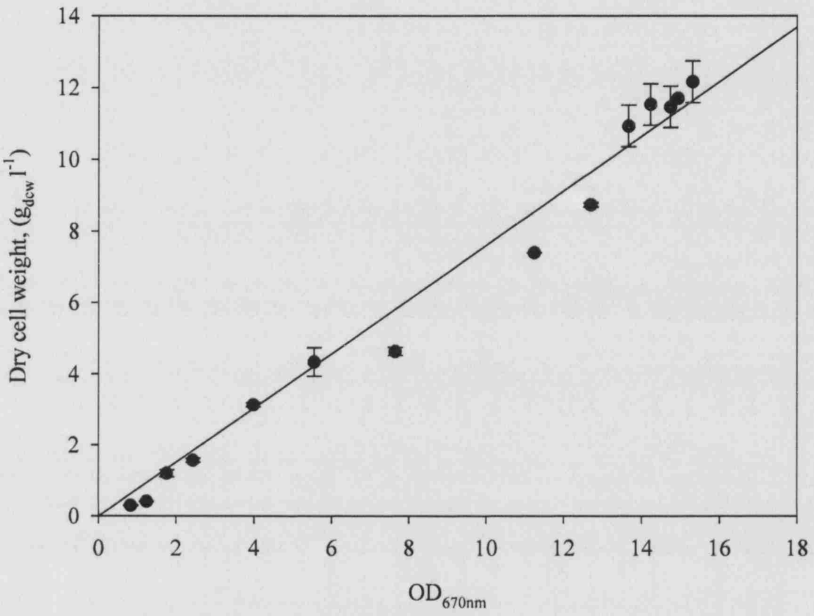

H Method of Initial Rate of Enzyme-Catalysed Reaction

In order to analyse the kinetics of an enzyme-catalysed system, a separate plot of *velocity* against various substrate and product concentrations is required. With these plots, a model system incorporating the effect of substrate and product concentrations can be devised. The reaction was carried out using the whole-cell system in 80ml mini reactors with 60ml working volume. The method of carrying out the experimental work is described in detail in the following paragraphs.

Initial Rate Experiment

The whole cell experiment was carried out in the 80ml mini-reactors previously described in *Chapter 4*. In every reaction, the substrate (bicyclo[3.2.0]hept-2-en-6-one) concentration was varied from $0.5g{\cdot}l^{-1}$ to $5.0g{\cdot}l^{-1}$. Samples were taken every 10 minutes until most of the substrate was converted into products. The samples taken were centrifuged at 13000r.p.m for 1 minute (Biofuge 13, Heraeus Sepatech, Brentwood, Essex) and 1ml of supernatant was thoroughly mixed using vortex mixer with 1ml of ethyl acetate for substrate and products extraction. Gas chromatography (GC) was used to quantify the concentrations of substrate and product in the sample. The GC method is given in the analytical assay section in *Chapter 3*, Section 3.3.1.

Suitable graphs were plotted to determine the initial rate of reaction due to the difference substrate concentrations. During this course of experiment, the activity of the enzyme was measured and plotted separately. A similar set-up was prepared for product ((-)1(S)5(R)2-oxabicyclo[3.3.0]oct-6-en-3-one) inhibition with concentrations varied from $0.5g{\cdot}l^{-1}$ to $5.0g{\cdot}l^{-1}$. Reaction was taken place after the cell was left to incubate with the given amount of product concentrations. A similar plot was devised in order to obtain the initial rate of reaction due to product inhibition.

Initial Rate Analysis: Results and Discussion

In the initial rate experiment, the formation of product during the reaction was plotted against the time for a period of 30 minutes. The gradient of these plots at different substrate(/product) concentrations were determined. These values were then plotted against these two variable concentrations. The above figure shows the effect of increasing the substrate concentration, and

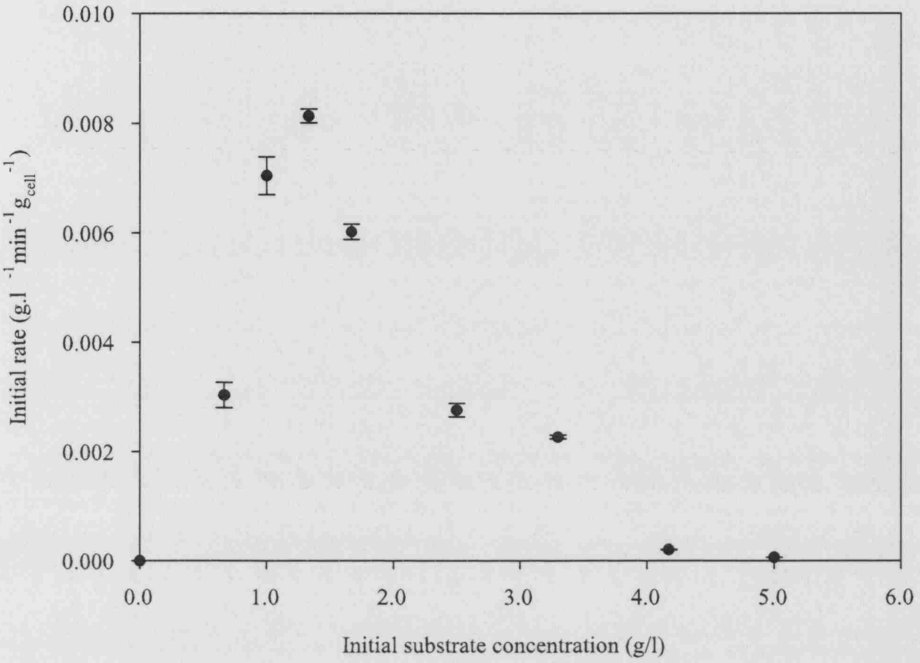

an optimum amount of substrate around $1.5g{\cdot}l^{-1}$ was achieved, however, as the concentration increased, the initial rate of reaction started to decrease until only a small amount of substrate was converted to product.

A similar result was obtained by increasing the amount of product (next figure). The reaction medium without any trace of product gave a high rate of reaction. However, as the amount of initial product was increased and combined that with the amount formed from the bioconversion, the initial rate gradually decreased. With these plots, the effect of substrate and product towards the rate of enzyme-catalysed Baeyer-Villiger reaction can be fully observed.

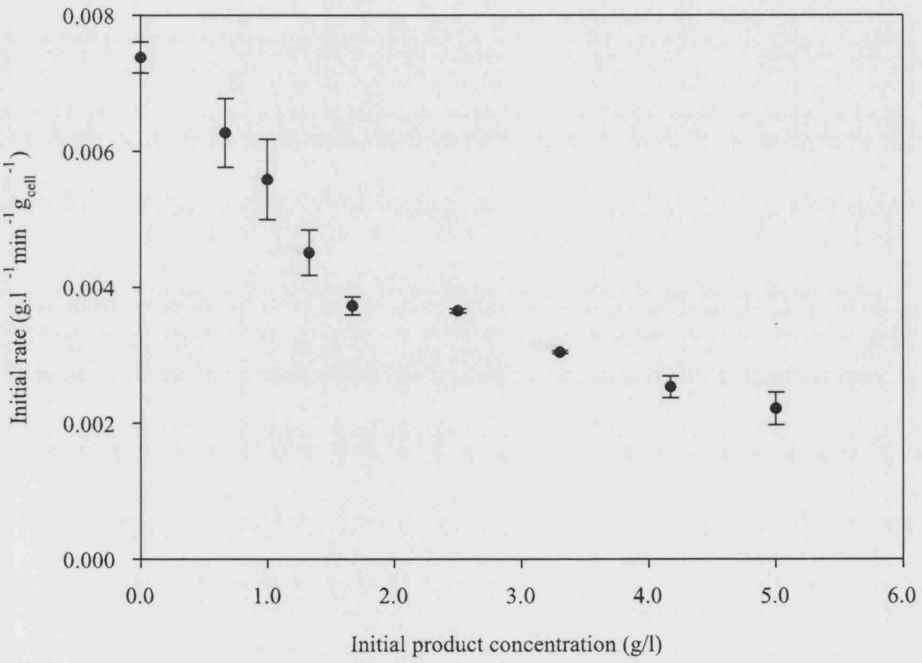
0.008
0.006
0.004
0.002
0.000
Initial rate (g.l $^{-1}$min $^{-1}$ g_{cell} $^{-1}$)
0.0
1.0
2.0
3.0
4.0
5.0
6.0
Initial product concentration (g/l)